

UNCLASSIFIED

AD NUMBER

AD843988

LIMITATION CHANGES

TO:

Approved for public release; distribution is unlimited.

FROM:

Distribution authorized to U.S. Gov't. agencies only; Administrative/Operational Use; 01 SEP 1968. Other requests shall be referred to Office of Naval Research 875 North Randolph Street, Arlington, VA 22203-1995.

AUTHORITY

ONR ltr, 9 nov 1973

THIS PAGE IS UNCLASSIFIED

AD843988

SUBIC



Submarine Integrated Control

OFFICE OF
NAVAL
RESEARCH

GENERAL DYNAMICS CORPORATION
ELECTRIC BOAT DIVISION
GROTON, CONNECTICUT

GENERAL DYNAMICS
Electric Boat Division

PROCESSING OF DATA
FROM SONAR SYSTEMS

Volume VI

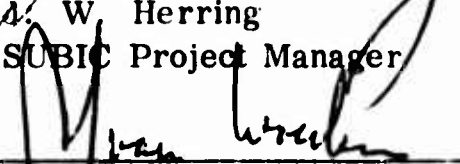
by

Francis S. Hill, Jr.
John B. Lewis
Verne H. MacDonald
Peter M. Schultheiss

Yale University

Examined: 

A. W. Herring
SUBIC Project Manager

Approved: 

Dr. A. J. van Woerkom
Chief Scientist

U417-68-80
September 1, 1968

ABSTRACT

Volume VI deals with the following topics:

1) Optimum Passive Detection

The problem of passive detection and target location by means of a linear array is analyzed from a rather general point of view for the case of stationary Gaussian signals and noises with known statistical properties. Relationships are developed between detector performance indices and such parameters as array dimensions, observation time, signal bandwidth, hydrophone spacing, signal source location and noise model properties. Isotropic and anisotropic near and far field noises are considered. Array gain and directivity measures are treated in detail.

2) Optimum Passive Bearing Estimation

Lower bounds are set on the rms bearing error attainable with a linear array when signal and noise are stationary Gaussian processes with known spectra and the noise is statistically independent from hydrophone to hydrophone. The results are compared with the rms error of a split beam tracker, modified by insertion of an appropriate spectrum-shaping filter into each array half. The split beam tracker reaches the lower bound for a two-element array and comes very close to the lower bound for arrays of arbitrary size. Thus it is a very nearly optimal instrumentation under the given circumstances.

3) Active Sonar Signal Design

The signal design problem is considered for the case of an ideal transmission medium and reverberation modelled as reflections from a series of independent, Poisson distributed scatterers. Primary interest centers on the redesign of the pulse waveshape in accordance with information gained from an earlier return. The results indicate the possibility of some improvements in principle, but the highly idealized nature of the assumption leaves the question of practically important gains open to considerable doubt.

TABLE OF CONTENTS

<u>Report</u>	<u>Title</u>	<u>Page</u>
	Abstract	iii
	Foreword	vii
I	Introduction	1
II	Optimum Passive Detection	1
III	Optimum Passive Bearing Estimation	3
IV	Active Sonar Signal Design	5
35	Optimum Sonar Array Detection	A
36	Adaptive Sonar Signal Design	B
37	Optimum Passive Bearing Estimation in a Spatially Incoherent Noise Environment	C

FOREWORD

This is the sixth in a series of reports describing work performed by Yale University under a subcontract with Electric Boat division of General Dynamics, prime contractor of the SUBIC (SUBmarine Integral Control) Program, contract number NOmr 2512(00). The Office of Naval Research is sponsor of the SUBIC Program; LCDR E. W. Lull is Project Officer for ONR. Mr. J. W. Herring is Project Manager for Electric Boat division under the direction of Dr. A. J. van Woerkom, Chief Scientist of the Applied Sciences Department.

I INTRODUCTION

The following is a summary of work completed under contract 8050-31-55001 between Yale University and Electric Boat division during the period from 1 October 1967 to 30 June 1968. More detailed discussions of the results as well as their derivations are contained in a series of three progress reports which are appended. Two of the topics, dealing with passive detection and bearing estimation, represent continuation of efforts reported in earlier volumes of this series. The third item deals with initial results in a new area, optimum design of active sonar signals.

II OPTIMUM PASSIVE DETECTION

Report No. 35 contains the most comprehensive and general treatment in this series of the optimum passive detection and target location problem. Signal and noise are assumed to be stationary Gaussian processes with known statistical properties. The receiving array is assumed to be linear and uniform hydrophone spacing is postulated whenever specific computations are carried out. The basic analytical procedure follows initially the familiar technique of representing the observed time function at each point in space by a Fourier series. Then, following a basic suggestion by Vanderkulk, the spatial structure of the data is treated by projecting the Fourier coefficients onto the spatial Eigenfunctions of the noise. Thus, each Fourier coefficient is represented by an orthogonal expansion whose coefficients are statistically independent in the absence of signal. This approach produces particularly simple versions of the primary performance indices. Thus, one finds that the single frequency on target array gain G_0 of the optimum detector for a plane wave signal is given by a sum of the form

$$G_0 = \sum_k \frac{|h_k|^2}{\lambda_k}$$

where the λ_k are the normalized Eigenvalues of the noise and h_k is the projection of the signal on the k^{th} Eigenfunction of the noise. The corresponding expression for the conventional power detector assumes the form

$$G_c = \frac{L}{\sum_k |h_k|^2} \lambda_k$$

where L is the array length. Straightforward comparisons of optimal and conventional detector performance are now possible.

In the above formulation, the noise field is completely described by its Eigenvalues λ_k . When the noise originates in a region remote from the array compared with the array dimensions, the spatial correlation function (which generates the λ_k) becomes stationary and is therefore specified completely by a spatial spectrum. Spatial spectra are derived for various forms of sea noise, self noise, and interfering targets. Their study sheds considerable light on the relative magnitudes of the Eigenvalues and on the nature of the detection process. One finds, as expected from Vanderkulk's results, that the linear array has a much higher array gain in the endfire direction than in the broadside direction when the noise consists predominately of spherically isotropic sea noise. The effect is much less pronounced when the noise is circularly isotropic, a fact readily explained by the concentration of noise power at spatial frequencies associated with the endfire direction. The advantage of the endfire direction in either case is drastically diminished by the presence of even a small amount of self-noise (whose spatial spectrum is white, whereas the spectra of all far field noises cut off sharply at a spatial frequency of $2\pi/\lambda$ rad/ft, λ being the acoustic wavelength). For noises of a generally isotropic type, the advantage of the optimum detector over the conventional detector is largely due to decreases in hydrophone spacing below a half wavelength. This may be interpreted loosely as oversampling the spatial spectrum, thus permitting recovery of signal energy shifted to frequencies outside of the basic noise band by passage through the finite spatial window of the array. The presence of self-noise beyond the basic cutoff frequency of $2\pi/\lambda$ clearly does much to offset that advantage. On the other hand, spatially concentrated noise such as interference from a point source remote from the target yields a spatial spectrum largely disjoint from the signal spectrum, so that the optimal processor can eliminate most of the interference. As a result, one finds a high array gain in all directions except in the immediate vicinity of the interference bearing. If the interference originates very close to the array, the array gain is high even in the interference direction, because one can now utilize the different attenuation rates of signal and interference across the array to achieve the necessary discrimination.

Report No. 35 also discusses the directivity of the optimal and suboptimal detectors, using as a criterion the ratio of the array gain off target by a certain angle to the array gain on target. As one would expect, the sensitivity curve is considerably broader for endfire than for broadside targets. A less obvious conclusion is that the sensitivity curve of the conventional detector does not, in general, peak at the true target bearing, even if the noise is isotropic. The magnitude and even the sign of this bias varies with noise field geometry. The directivity curve of the optimum detector, on the other hand, always exhibits a peak at the true target. Finally, the report discusses the error in estimated target location resulting from the use of optimum or conventional detectors. A convenient figure of merit is closely related

to the likelihood function of the target location. Since the true likelihood function varies randomly with the observed data, an average version is employed. For the optimal detector this figure of merit always peaks at the true target location, whereas the conventional detector exhibits the bias phenomenon mentioned earlier. At low signal-to-noise ratios the bias effect can be quite appreciable. The modified likelihood function is plotted as a function of bearing and range. It permits not only comparisons of different detector types, but also allows study of the effect of parameters such as observation time, frequency band and target bearing on the target-locating ability of a given receiver. As one might anticipate, the range discriminating ability of the array is small except at very short ranges.

III OPTIMUM PASSIVE BEARING ESTIMATION

Report No. 37 generalizes the results given in Report No. 32 (Volume V), with regard to array size and spectral properties of signal and noise. The earlier report used the Cramer-Rao technique to set a lower bound on the rms bearing error attainable with a two-element array when signal and noise were stationary Gaussian processes with spectra of the same shape and the noises received at the two hydrophones were statistically independent. Report No. 37 allows an arbitrary number of hydrophones arbitrarily spaced on a linear array (the final comparison with a split beam tracker is only carried out for equally spaced hydrophones). It also allows arbitrary signal and noise spectra. All other assumptions of the earlier analysis (notably that of noise independence from hydrophone to hydrophone) are retained.

For an array of M equally spaced hydrophones, one finds a lower bound

$D(\theta)$ on rms error given by

$$D(\theta) \geq \frac{2\sqrt{3}\pi c}{d\sqrt{T} \cos \theta M\sqrt{M^2-1}} \left[\int_0^{\omega_{\max}} d\omega \omega^2 \frac{\frac{S^2(\omega)}{N^2(\omega)}}{1 + M \frac{S(\omega)}{N(\omega)}} \right]^{1/2}$$

$S(\omega)$ and $N(\omega)$ are the signal and noise spectra respectively, d is the spacing between the hydrophones, T the observation time, θ the bearing angle relative to broadside, ω_{\max} the upper end of the processed frequency range, and c the velocity of sound.

If $M S(\omega) / N(\omega)$, the signal-to-noise ratio after beamforming, is large over the entire processed frequency range, the lower bound varies as $(S/N)^{1/2}$. For $M S(\omega)/N(\omega) \ll 1$, the lower bound varies as $(S/N)^{-1}$. The former is a type of behavior often associated with coherent systems, whereas the latter is generally identified with incoherent processors. Qualitative physical justification for these conclusions is furnished by

where L is the array length. Straightforward comparisons of optimal and conventional detector performance are now possible.

In the above formulation, the noise field is completely described by its Eigenvalues λ_k . When the noise originates in a region remote from the array compared with the array dimensions, the spatial correlation function (which generates the λ_k) becomes stationary and is therefore specified completely by a spatial spectrum. Spatial spectra are derived for various forms of sea noise, self noise, and interfering targets. Their study sheds considerable light on the relative magnitudes of the Eigenvalues and on the nature of the detection process. One finds, as expected from Vanderkulk's results, that the linear array has a much higher array gain in the endfire direction than in the broadside direction when the noise consists predominately of spherically isotropic sea noise. The effect is much less pronounced when the noise is circularly isotropic, a fact readily explained by the concentration of noise power at spatial frequencies associated with the endfire direction. The advantage of the endfire direction in either case is drastically diminished by the presence of even a small amount of self-noise (whose spatial spectrum is white, whereas the spectra of all far field noises cut off sharply at a spatial frequency of $2\pi/\lambda$ rad/ft, λ being the acoustic wavelength). For noises of a generally isotropic type, the advantage of the optimum detector over the conventional detector is largely due to decreases in hydrophone spacing below a half wavelength. This may be interpreted loosely as oversampling the spatial spectrum, thus permitting recovery of signal energy shifted to frequencies outside of the basic noise band by passage through the finite spatial window of the array. The presence of self-noise beyond the basic cutoff frequency of $2\pi/\lambda$ clearly does much to offset that advantage. On the other hand, spatially concentrated noise such as interference from a point source remote from the target yields a spatial spectrum largely disjoint from the signal spectrum, so that the optimal processor can eliminate most of the interference. As a result, one finds a high array gain in all directions except in the immediate vicinity of the interference bearing. If the interference originates very close to the array, the array gain is high even in the interference direction, because one can now utilize the different attenuation rates of signal and interference across the array to achieve the necessary discrimination.

Report No. 35 also discusses the directivity of the optimal and suboptimal detectors, using as a criterion the ratio of the array gain off target by a certain angle to the array gain on target. As one would expect, the sensitivity curve is considerably broader for endfire than for broadside targets. A less obvious conclusion is that the sensitivity curve of the conventional detector does not, in general, peak at the true target bearing, even if the noise is isotropic. The magnitude and even the sign of this bias varies with noise field geometry. The directivity curve of the optimum detector, on the other hand, always exhibits a peak at the true target. Finally, the report discusses the error in estimated target location resulting from the use of optimum or conventional detectors. A convenient figure of merit is closely related

to the likelihood function of the target location. Since the true likelihood function varies randomly with the observed data, an average version is employed. For the optimal detector this figure of merit always peaks at the true target location, whereas the conventional detector exhibits the bias phenomenon mentioned earlier. At low signal-to-noise ratios the bias effect can be quite appreciable. The modified likelihood function is plotted as a function of bearing and range. It permits not only comparisons of different detector types, but also allows study of the effect of parameters such as observation time, frequency band and target bearing on the target-locating ability of a given receiver. As one might anticipate, the range discriminating ability of the array is small except at very short ranges.

III OPTIMUM PASSIVE BEARING ESTIMATION

Report No. 37 generalizes the results given in Report No. 32 (Volume V), with regard to array size and spectral properties of signal and noise. The earlier report used the Cramer-Rao technique to set a lower band on the rms bearing error attainable with a two-element array when signal and noise were stationary Gaussian processes with spectra of the same shape and the noises received at the two hydrophones were statistically independent. Report No. 37 allows an arbitrary number of hydrophones arbitrarily spaced on a linear array (the final comparison with a split beam tracker is only carried out for equally spaced hydrophones). It also allows arbitrary signal and noise spectra. All other assumptions of the earlier analysis (notably that of noise independence from hydrophone to hydrophone) are retained.

For an array of M equally spaced hydrophones, one finds a lower bound

$D(\theta)$ on rms error given by

$$D(\theta) \geq \frac{2\sqrt{3}\pi c}{d\sqrt{T} \cos \theta M\sqrt{M^2-1}} \left[\int_0^{\omega_{\max}} d\omega^2 \frac{\frac{S^2(\omega)}{N^2(\omega)}}{1 + M \frac{S(\omega)}{N(\omega)}} \right]^{1/2}$$

$S(\omega)$ and $N(\omega)$ are the signal and noise spectra respectively, d is the spacing between the hydrophones, T the observation time, θ the bearing angle relative to broadside, ω_{\max} the upper end of the processed frequency range, and c the velocity of sound.

If $M S(\omega) / N(\omega)$, the signal-to-noise ratio after beamforming, is large over the entire processed frequency range, the lower bound varies as $(S/N)^{1/2}$. For $M S(\omega)/N(\omega) \ll 1$, the lower bound varies as $(S/N)^{-1}$. The former is a type of behavior often associated with coherent systems, whereas the latter is generally identified with incoherent processors. Qualitative physical justification for these conclusions is furnished by

the observation that one can obtain a good estimate of the signal waveshape when the post-beamforming signal-to-noise ratio is high. Hence, basically coherent techniques are available in this situation. No such option exists when the post-beamforming signal-to-noise ratio is low.

A second interesting feature of the lower bound is its dependence on the number of hydrophones (M). If $M \gg 1$, one has a dependence on M^{-2} and M^{-1} for low and high post-beamforming signal-to-noise ratios respectively. Since $dM = L$, the length of the array, a more significant observation is perhaps that the lower bound varies as $(LM)^{-1}$ and $L^{-1} M^{-1/2}$ and high post-beamforming signal-to-noise ratios respectively.

Finally, the lower bound exhibits an anomaly which deserves some comment. The dependence on $(\cos \theta)^{-1}$ leads to an infinite lower bound for the endfire direction. In order to understand this phenomenon, we note first that the version of the Cramer-Rao inequality used in the derivation gives the minimum variance unbiased estimate. Secondly, we observe that the basic data furnish information concerning relative signal delay from hydrophone to hydrophone. Since delay is proportional to $\sin \theta$, it is perfectly possible for noise-perturbed estimates of $\sin \theta$ to exceed unity, so that no natural interpretation in terms of θ is available. If one resolves this problem by assigning $\theta = 90^\circ$ to all such cases, one clearly has a finite variance estimate, but one which is now biased. It is clear, therefore, that biased estimates exist whose mean square error is smaller than that of any unbiased estimate for some specific value of θ . This suggests that one should look for a "best" bias function $b(\theta)$. The Cramer-Rao inequality with bias is not significantly more complicated than the unbiased form, so that no serious obstacle exists on that score. However, there is a certain arbitrariness in the use of bias, for one can in principle make the error for any given target bearing as small as one pleases, at the expense of larger errors for other bearings. At best, therefore, one could search for a bias function optimum in an average sense, which in turn implies a priori knowledge concerning the probability of various target bearings. The question is perhaps worthy of some further study. However, if one excludes bearings very close to endfire and if the observation time T is long enough to make the indicated bearing practically useful, any improvements due to bias should be quite small and would probably be outweighed by the practical advantage of working with an unbiased instrumentation. It appears reasonable, therefore, to regard the unbiased figure as a lower bound for most practically interesting situations.

A more significant question concerns the ability to realize the lower bound. The Cramer-Rao inequality gives a value of rms error which cannot be reduced, but which cannot always be reached. In our case, the obvious instrumentation to check against the lower bound is the split beam tracker, which is unbiased for the postulated noise field. If one obtains the required 90° phase shift with a differentiator and if one modifies the conventional instrumentation by inserting into the summed output of each array half a filter with transfer function $H(j\omega)$, satisfying

$$|H(jw)|^2 = \frac{\frac{S(w)}{N^2(w)}}{1 + M \frac{S(w)}{N(w)}}$$

then the rms bearing error $D(\theta)$ assumes a form similar to the lower bound. In fact,

$$\frac{D(\theta)}{\text{Lower bound}} = \sqrt{\frac{4}{3}} \sqrt{1 - \frac{1}{M^2}}$$

This function increases monotonically from 1 to $\sqrt{4/3}$ as M increases from 2 to ∞ . Thus the split beam tracker, with the minor modification described above, is an optimal unbiased bearing estimator for $M=2$ and a very nearly optimal estimator for arbitrary M .

Efforts to extend the above results to noise fields not necessarily independent from hydrophone to hydrophone are now in progress.

IV ACTIVE SONAR SIGNAL DESIGN

Report No. 36 contains the results of the initial study in this series concerned with the design of active sonar signals. Only the most idealized case is considered. The reverberation model is based on independent Poisson distributed scatterers in independent motion. Signals are assumed to remain undistorted in transmission and the target is modeled as a perfect reflector, changing the signal waveshape only by a fixed doppler shift. The target is assumed to be moving on a straight line course at a constant velocity and its bearing is regarded as known (presumably from passive sonar measurements). Thus only range and range rate must be estimated from the active sonar return. The question of ultimate interest is the target position some substantial time after the active sonar return has been received (e.g. at the time of possible intercept). The study deals in particular with the possibility of using information from a first sonar ping to improve the design of a second ping.

In signal design, one is concerned with two distinct but interrelated problems: ambiguity and accuracy. A return is ambiguous if two or more distinct regions in the range-doppler shift plane represent probable locations of the target. The term "accuracy" refers to the dimensions of a single such region of possible target location. The analysis concentrates on the accuracy problem, the assumption being that the signal-to-noise ratio is sufficiently high so that the gross errors of ambiguity cannot occur with any significant probability. However, one cannot ignore the ambiguity problem entirely, for one finds rather generally that signal designs calculated to improve accuracy tend to increase ambiguity. Thus, bounds on attainable accuracy are often set by the maximum tolerable level of ambiguity.

As time elapses after a pulse has been received, the region of uncertainty describing the accuracy problem elongates in the range direction, but retains a fixed dimension in the velocity direction. This is simply due to the fact that the target velocity is fixed by assumption, but that any error in the velocity estimate reflects as a constantly growing error in future range estimates. If there is substantial "wait time" (time between transmission and the instant at which the target position is ultimately required), the error is largely due to this velocity component for any reasonable signal waveshape. One is therefore led to the conclusion that the initial pulse of a two-pulse sequence should seek primarily to establish target velocity, i.e. it should be a narrow band pulse. If the target happens to be moving rapidly enough, this will also improve the signal-to-noise ratio because the reverberation will be spectrally disjoint from the target return. This, however, is merely a fortuitous circumstance, for in the absence of a priori information on target velocity one could not design a first pulse to discriminate against reverberation.

The function of the second pulse is primarily to measure target range. It appears clear on intuitive grounds that this pulse should be sent as late as possible, but there are two conflicting factors affecting the choice of waveform: For a given signal-to-noise ratio, best range accuracy is achieved by a wideband signal, but a wideband signal does not permit spectral separation of signal from reverberation and therefore leads to lower signal-to-noise ratios when the target is moving. If the first pulse return indicates a target moving above the same minimal velocity (depending on rms scatterer motion), some compromise in signal design is clearly indicated. The matter is further complicated by the ambiguity problem mentioned above. The resulting complexity is such that straightforward analytical optimization becomes impractical and one has to resort to numerical procedures instead. The results indicate that substantial improvements in final accuracy can often be made in principle by proper design of the second pulse. However, the required waveshapes tend to be rather complicated and critically dependent on the velocity information gained from the first pulse. Furthermore, if one hopes to extract most of the information coded into the complex waveshape of the second pulse, one cannot relax the postulate of distortion-free transmission appreciably. Thus there is serious doubt whether important gains over the most obvious signal designs can in fact be made in many interesting situations. To resolve this question, one must deal with more realistic transmission models. Studies directed toward this end are now in progress.



OPTIMUM SONAR ARRAY DETECTION

By

John Bayard Lewis

Progress Report No. 35

General Dynamics/Electric Boat Research

(8050-31-55001)

April 1968

DEPARTMENT OF ENGINEERING
AND APPLIED SCIENCE
YALE UNIVERSITY

ABSTRACT

"Optimum" weak signal passive detection is studied for a linear array of hydrophones in a Gaussian noise field. Relationships are developed between the detector performance and the array length, observation time, processing frequency band, hydrophone spacing, signal source location and characteristics, and noise model properties. The basis for the analysis is the eigenfunction expansion introduced by Vanderkulk [3]. The noise models considered are two types of isotropic sea noise, a noise of local origin, interference from a previously detected source, and the self noise in the hydrophones. Particular attention is paid to self noise limitations on endfire detection. The measures used to describe the array performance are the output signal-to-noise ratio, the array gain, and directivity measures that indicate output changes as a function of either steering angle or of noise source location relative to a fixed steering angle. A new measure of the ability to locate a given signal source is also employed. The conventional power detector and one other suboptimum detector are analyzed for comparison with the "optimum" detector. A measure of the weak signal bias in the conventional detector is introduced.

TABLE OF CONTENTS

ABSTRACT	A-1
LIST OF FIGURES AND TABLES	A-iv
LIST OF SYMBOLS	A-ii
CHAPTER 1 INTRODUCTION	
1.1 General Background and Objectives	1
1.2 Description of the Detection Problem	
a) The Received Signal	5
b) An Eigenfunction Expansion for the Received Signal	8
c) The Received Signal Through Discretely Located Hydrophones	14
d) The Detection Problem	17
CHAPTER 2 SIGNAL AND NOISE MODELS	
2.0 Introduction	22
2.1 Sea Noise	23
2.2 Interfering Target Noise and Local Noise	33
2.3 Self Noise	40
2.4 The Signal Covariance Matrix	44
CHAPTER 3 DETECTOR DEFINITIONS	
3.0 Introduction	53
3.1 The b-Detector	54
3.2 The c-Detector	62
3.3 The l-Detector	67
CHAPTER 4 OUTPUT SNR AND ARRAY GAIN	
4.0 Introduction	69
4.1 The Output SNR and Array Gain	70
4.2 The Array Gain for the b and c-Detectors	
a) General Definition	73
b) b-Detector Array Gain	74
c) c-Detector Array Gain	93

4.3 The ℓ -Detector Array Gain	98
CHAPTER 5 DIRECTIVITY MEASURES	
5.0 Introduction	101
5.1 The Normalized SNR	
a) Definition	102
b) The Normalized b-Detector SNR	102
c) The Normalized c-Detector SNR	104
d) The Normalized ℓ -Detector SNR	105
5.2 An Influence Measure \textcircled{H}	
a) Definition	107
b) \textcircled{H} for the b-Detector	108
c) \textcircled{H} for the c-Detector	110
d) \textcircled{H} for the ℓ -Detector	110
5.3 Uncertainty in Signal Source Location	111
5.4 A Bias Measure for the c-Detector	120
APPENDIX A THE "BOXCAR" FUNCTION	127
APPENDIX B DERIVATION OF THE POWER SPECTRUM OF 12 SEA NOISE	129
APPENDIX C OUTPUT STATISTICS FOR THE GENERAL DETECTOR	134
APPENDIX D ℓ -DETECTOR STATISTICS	137
APPENDIX E APPROXIMATE EIGENFUNCTIONS FOR USE IN A PRACTICAL b-DETECTOR	138
a) A Practical Requirement	138
b) Breakup of the Observation Time into Subintervals	139
c) Frequency Dependent Time Intervals	141
d) Time Intervals with Space Dependent Phase	144
e) Breakup of the Array Dimension into Subintervals	144
APPENDIX F THE SIGNAL COVARIANCE MATRIX G	
a) The General Form of G	148
b) Elements of G When $i=1'$	154
c) Upper Bounds on Elements of G When $i \neq 1'$	162
REFERENCES	169

LIST OF FIGURES AND TABLES

Figure 1-1	The Array with a Target Signal Present	6
Figure 1-2	Hydrophone Array Dimensions	15
Figure 2-1	A Power Spectral Density Function for I2 Sea Noise	27
Figure 2-2	A Power Spectral Density Function for I3 Sea Noise	29
Figure 2-3	Spatial Eigenfunctions	30
Figure 2-4	Spatial Eigenvalues	32
Figure 2-5	Spatial Eigenfunctions for I3 and Local Noise	37
Figure 2-6	Eigenvalues for I3 and Local Noise	39
Figure 2-7	Spatial Spectrum of I3 Sea Noise Plus Self Noise	42
Figure 2-8	Relative Spatial Spectra of the Signal in I3 Sea Noise	50
Table 2-1	Relative Spatial Spectra of the Signal in I3 and Local Noise	51
Figure 3-1	An Implementation of the b-Detector	57
Figure 3-2	An Alternative b-Detector Structure	58
Figure 3-3	Implementation of the c-Detector for Plane Wave Detection	64
Figure 3-4	The l-Detector	68
Figure 4-1	The Effect of Self Noise on Channel Factors	77
Figure 4-2	b-Detector Array Gain in I2 and I3 Sea Noise	80
Figure 4-3	High Spatial Frequency Behavior of Signal and Noise Spectra	81
Figure 4-4	b-Detector Array Gain with 2 and 4 Hydrophones	83
Figure 4-5	b-Detector Array Gain with Increasing Numbers of Hydrophones	85

Figure 4-6	Channel Factors with Local and Distant Interference	87
Figure 4-7	b-Detector Array Gain with Local and Distant Interference	88
Figure 4-8	b-Detector Array Gain with Interference and Self Noise	91
Figure 4-9	Characteristics of b and c-Detectors at 75.9° Incidence	95
Figure 4-10	Array Gain Comparison	97
Figure 4-11	b-Detector Array Gain	100
Figure 5-1	Normalized Output SNR for the b-Detector	103
Figure 5-2	Normalized Output SNR for b and c-Detectors in I2 and I3 Sea Noise	106
Figure 5-3	The Influence Measure \textcircled{H} for the b and c-Detectors	109
Figure 5-4	Location Uncertainty Using the b-Detector	117
Figure 5-5	b-Detector Bearing Resolution	119
Figure 5-6	Bias in the c-Detector	124
Figure A-1	The "Boxcar" Function	127
Figure L-1	Frequency-Time Plots for Sinusoidal Time Eigenfunctions	140
Figure E-2	The Spacing Parameter p	143
Figure E-3	The Normalized Spacing	143
Figure E-4	Variable Duration Sinusoids in the Frequency-Time Plane	145
Figure E-5	Subinterval Grid in the Time-Space Domain	147
Figure F-1	The "Triangle" Function Defined by Eq. F-10	151
Figure F-2	The Domain of Integration in the x,y Plane when $l \geq L$	156
Figure F-3	Relative Spatial Spectra of the Signal	159
Figure F-4	The Domain of Integration in the ξ, η Plane when $l \ll L$	161

Figure F-5 Elements of G when $l \ll L$	163
Figure F-6 A Bound on Elements of G when $l \geq L$	167
Figure F-7 A Bound on Elements of G when $l \ll L$	167

LIST OF SYMBOLS

*	complex conjugate	pg. 8
$\langle \rangle$	ensemble average	pg. 7
(f,g)	the inner product of functions f and g	pg. 10
$c c ^2$	quadratic form $c^* C c$	pg. 17
$ c $	"length" of c	pg. 48
'	transpose	pg. 9
α	signal attenuation function	Eq. 2-65
β	angle of incidence of the signal	Fig. 1-1
Δ	subset of consecutive indices	pg. 112
γ	time advance	Eq. 2-59
δ_{ij}	1 when $i=j$ and 0 when $i \neq j$	pg. 10
n	dummy variable	Eq. F-25
\textcircled{H}	boxcar function	App. A
\textcircled{H}	an influence measure	Eq. 5-5
λ	eigenvalue of Q	Eq. 1-15
Λ	noise covariance matrix of \underline{u}	Eq. 1-17
ν	the space frequency	pg. 23
ξ	dummy variable	Eq. F-25
ξ	self noise spectral level	pg. 40
ξ	complex amplitude	pg. 129
ρ	attenuation factor	Eq. 2-60
σ	relative self noise level	Eq. 2-49
τ	time delay	Eq. 2-2
ϕ	time eigenfunction	Eq. 1-24
ϕ	output signal to noise ratio	Eq. 4-1

ϕ	basis function associated with an element of \underline{u}	Eq. 1-8
x	spatial separation	Eq. 2-3
x	exponent function	Eq. 1-55
ψ	space eigenfunction	Eq. 1-29
Ψ	complex sinc function	Eq. A-2
ω	the time frequency	pg. 11
Ω	set of time frequency indices	pg. 11
Ω^+	positive indices in Ω	pg. 60
$A=(a_{ij})$	covariance matrix of \underline{u}	pg. 9
A	an index set	Eq. B-1
b	b-detector output	Eq. 1-54
B	a bias measure	pg. 120
c	c-detector output	Eq. 3-27
c	velocity of propagation	pg. 26
C	channel factor	Eq. 4-31
C	bias term in general detector	Eq. 4-5
δ	Dirac delta function	pg. 14
\hat{D}	normalized SNR	Eq. 5-1
D	an index set	pg. 8
E	transformation from v to \underline{u}	Eq. 1-9
f	shading filter	pg. 56; Fig. 3-2
f	spectral density function	Eq. B-6
f	probability density function	Eq. 5-10
f_0	density function when $\underline{y} \in R$	pg. 17
f_1	density function when $\underline{y} \in R_c$	pg. 17
F	filter	pg. 56; Fig. 3-2

F	signal covariance factor	Eq. 2-72
\mathcal{G}	array gain	Eq. 4-9
g	element of G	Eq. 1-19
G	signal covariance matrix of \underline{u}	Eq. 1-19
G_L and G_U	array gain limits	pgs. 89 and 90
h	hydrophone position index	pg. 14
\underline{h}	relative signal spectrum	pg. 48
\mathcal{H}	location uncertainty	Eq. 5-24
$H(A)$	number of elements in index set A	pg. 98
I_2 or I_3	isotropic in two or three dimensions	pg. 26
i	index in D	pg. 8
i	time eigenfunction index	pgs. 11 and 12
j	$\sqrt{-1}$	Eq. 1-23
j	index in D	Eq. 1-13
J_0	zero order Bessel function	Eq. 2-22
k	space eigenfunction index	pg. 12
K	normalization factor	Eq. 1-56
k	wave observation constant	pg. 47
k	k -detector output	Eq. 1-57
\mathcal{L}	the likelihood ratio	Eq. 1-50
L	array length	pg. 5
m	number of hydrophones	pg. 14
M	attenuation function	Eq. 2-68
M	moment generating function	Eq. C-8
n	time interval index	pg. 141
$n(\omega, \nu)$	power spectral density function on ω and ν	Eq. 2-4

n_1	one dimensional time power spectral density	Eq. 1-36
η	one dimensional time spectral density	Fig. 2-1
N	total average noise power	Eq. 1-35
N	number of oscillation periods	pg. 141
$O(a)$	of the order of "a"	pg. 115
p	subset index	pg. 112
p	spacing parameter	Eq. E-6
P_1	probability that signal is present within \mathcal{R}	Eq. 1-2
P_0	probability that signal is absent from \mathcal{R}	Eq. 1-3
$\text{Pr}(a b)$	probability of "a" given "b"	pg. 5
P	signal process covariance function	Eq. 1-7
P	set of subset indices p	pg. 112
q_1	intermediate form	Eq. 1-20
q_2	intermediate form	pg. 24
Q	noise process covariance function	Eq. 1-6
\mathcal{R}	that portion of the real space within which a signal may be detected	pg. 5
R	process covariance function	Eq. 1-4
R	filter output ratio	Eq. 2-51
s	time	pg. 7
s	signal power spectral density	Eq. 2-57
S	total average signal power	Eq. 2-67
S	bias term	pg. 56; Fig. 3-2
t	time	pg. 5
t	term in c-detector output	Eq. 5-27
\triangle	the triangle function	Eq. F-10; Fig. F-1
T	total time observation interval	pg. 5

$\underline{u}=(u_1)$	an equivalent form for v	pg. 8
v	observed random process	pg. 5
$V(c)$	variance of c	pg. 70
w	scalar product in general detector	Eq. C-3
W	frequency interval	pg. 11
W	term in general detector output	Eq. 4-5
\hat{w}	output of a general detector	pg. 70
x	array axis	pg. 5; Fig. 1-1
\underline{X}	detector steering location vector	pgs. 17-19
y	array axis	pg. 7
Y	random point function	pg. 34
\underline{Y}	target signal location vector	pg. 5
\hat{z}	functional in the general detector	Eq. 4-13
\underline{Z}	functional in the b-detector	Eq. 3-6
\underline{Z}	representative vector in	pgs. 63 and 65
Z	random point function	pg. 44

CHAPTER 1

INTRODUCTION

1.1 General Background and Objectives

Much recent progress has been made in the analysis of passive sonar detection using an array of hydrophones. In 1962 Bryn [1] showed how to calculate the array gain and directivity of an array whose elements are so closely spaced that significant noise dependence exists between neighboring elements. He went on to indicate how optimum (likelihood ratio¹) processing might be implemented using a combination steering and shading filter following each element of the array. This analysis and design are valid for the detection of low level Gaussian plane wave signals in a wideband Gaussian noise field with arbitrary continuous power spectra. Specifically, Bryn discusses the processing characteristics of a cubic array operating in an isotropic noise field. He concludes that "at low frequencies the optimum detector offers marked improvements over the standard delay-square-integrate detector...", and that "the degree to which the improvements can be realized in practice depends largely on the extent to which self noise can be eliminated in the input circuits of the detector."

In 1963 Vanderkulk [3] made a more complete study of the effects on

¹The relationships between this and certain other processing objectives such as the maximization of output signal to noise ratio are the subject of a mathematical comparison by Edelblute, Fisk, and Kinnison [2]. It is shown that Bryn's optimum detector maximizes the output signal to noise ratio.

array performance of self noise and the number of elements composing the array. The low frequency advantage was restated but with the warning that it could be offset by measurement errors in parameters required by the optimum detector. The analysis was carried out for spherical, linear, and ring shaped arrays operating in isotropic noise. It was mentioned that optimum processing might be most useful when the noise process is nonisotropic.

Supporting this study, Vanderkulk introduced the use of an eigenfunction expansion for the single frequency covariance matrix of the noise. The mathematical structure of the detector which results from the use of this expansion provides significant additional insight into array behavior. It is the object of the present study to exploit this expansion in a more extensive and somewhat less restrictive analysis of optimum linear array processing.

Bryn's assumptions regarding the noise field are used here, that is, the noise field is assumed to be Gaussian and ergodic with an arbitrary continuous power spectrum. Model fields of nonisotropic as well as isotropic noise are considered. In particular, the nonisotropic effects of interfering targets and of local noise arising from sources on or near the array are discussed and simple examples presented. The medium surrounding the array is assumed to be homogeneous and nondispersive (so that the velocity of propagation will be constant). Spherical, attenuating signals from the target are included so that the effects of the target range may be studied.

In making these assumptions and particularly in selecting the noise models, no attempt is made to set up special situations in which the

optimum processor could significantly outperform the conventional detector. Such situations do exist, but our aim is to give a somewhat more detailed account of optimum processing under familiar and easily analyzed conditions. Even though optimum processing under these conditions may yield small performance gains over conventional processing, the analysis itself is valuable because it provides an easily calculated and understood upper limit to the performance of any detector. Thus we shall use performance measures defined for the optimum detector to deal with the basic "detectability" (for a fixed array) of the target signals themselves. For example, a new measure is proposed to indicate how well a signal source may be located, given the observation time, the array length, the signal to noise ratio, etc.

In the analysis made here it became convenient to define a detector whose processing includes the eigenfunction expansion used by Vanderkulk. Although not a practical detector from an operational standpoint, it processes optimally as defined by Bryn and provides far more insight into the behavior of an optimum processor under a variety of signal and noise conditions.

The analysis using this detector proceeds through the usual performance measures, the output signal to noise ratio and the array gain. The effects of the significant properties of the noise models are discussed. A rough criterion is given for equivalence between the optimum and conventional detectors (see also [4]). Comparisons are made with a detector that is similar to the conventional detector in [1] and [3] and also with another simple suboptimum detector introduced here.

Since the output of array detectors is commonly shown plotted against steering direction, an account of the directivity properties is also

included. Terms are identified in the optimum detector output which are unimportant when analyzing detection in a single fixed direction but which can be prime factors in a directivity plot. An explanation is offered for bias that develops in the conventional detector display as the observation time is increased.

The representation of the detector in terms of the eigenfunction expansion permits a simple and direct analysis of the behavior mentioned above. The question then arises whether this representation can also lead to a simple and direct processing algorithm for practical detectors. Much further study is required to provide a conclusive answer; some initial thoughts are presented in appendices E and F.

1.2 Description of the Detection Problem

a) The Received Signal

An origin is placed at the center of a straight line array of hydrophones (acoustic transducers) and an x coordinate axis is aligned with this array and centered at the origin (Fig. 1 - 1). A member of the random process observed at the hydrophone outputs at time t (in seconds) and position x (in meters) is denoted by $v(t,x)$. The time interval used for detection is denoted by T and the length of the array by L . Though in practice hydrophones cannot be placed at every x within the interval $(-\frac{L}{2}, \frac{L}{2})$, every x is available to the array; for now, x is allowed to assume all values within $(-\frac{L}{2}, \frac{L}{2})$. Detection thus begins with an observed

$$\begin{aligned} & 0 < t < T \\ & v(t,x) \quad -\frac{L}{2} < x < \frac{L}{2} \end{aligned} \quad 1 - 1$$

The array is surrounded by a homogeneous, nondispersive medium occupying the real space \mathcal{R} . (This may be \mathcal{R}_2 or \mathcal{R}_3 depending upon whether the problem is to detect in a plane or in a volume). Various stationary Gaussian noise processes are assumed to propagate within this medium, and the statistics of the resulting disturbance along the array are assumed known. Now in addition to these noise processes, it is assumed that a low level Gaussian signal process may or may not be emanating from a single point source somewhere within \mathcal{R} . Presence of this signal is expressed by the statement $\underline{Y} \in \mathcal{R}$ where the tip of the vector \underline{Y} is the location of the point source, and the absence of signal is expressed by $\underline{Y} \notin \mathcal{R}$.

The a priori probabilities

$$p_1 \equiv \Pr (\underline{Y} \in \mathcal{R}) \quad 1 - 2$$

$$p_0 \equiv \Pr (\underline{Y} \notin \mathcal{R}) \quad 1 - 3$$

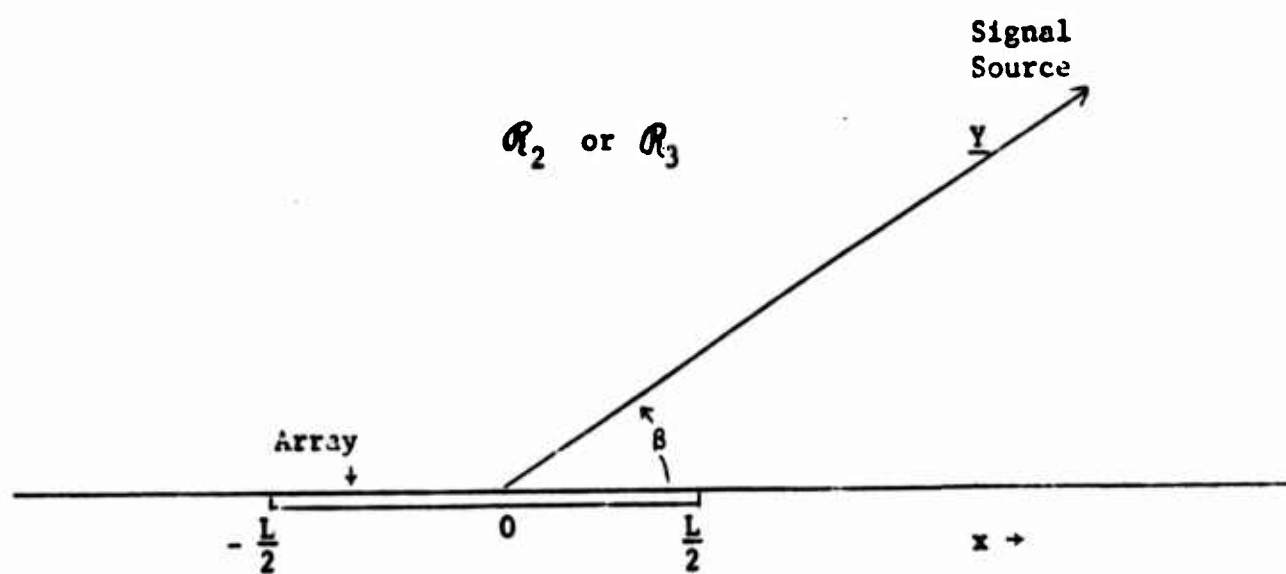


Figure 1 - 1 The Array with a Target Signal Present

are assumed known. The spectrum of the signal process (when $\underline{Y} \in \mathcal{R}$) as observed at the center of the array is assumed known. The detection problem treated here is to decide on the basis of the received signal v whether $\underline{Y} \in \mathcal{R}$. Some of the assumptions made above may be somewhat unrealistic, but at this point they provide the basis for a straightforward analysis. Some of them may later be dropped (complete knowledge of p_1 and p_0) and others may be satisfied approximately by adaptive techniques (knowledge of signal and noise statistics). For a more inclusive hypothesis see [5].

According to the above hypothesis, then, $v(t, x)$ is a member of a Gaussian process; that is, all sets of the random variables

$$\begin{aligned} &v(t_1, x_1), v(t_1, x_2), \dots \\ &\dots, v(t_2, x_1), v(t_2, x_2), \dots \end{aligned}$$

for

$$\begin{aligned} t_1, t_2, \dots &\in (0, T) \\ x_1, x_2, \dots &\in \left(-\frac{L}{2}, \frac{L}{2}\right) \end{aligned}$$

are normally distributed. The mean of this process is assumed to be zero.

The covariance function R is defined by

$$R(t, x, s, y) = \langle v(t, x) v(s, y) \rangle, \quad 1 - 4$$

in which the brackets $\langle \rangle$ denote the ensemble average. Because stationarity is assumed,

$$R(t, x, s, y) = R(t - s; x, y). \quad 1 - 5$$

When no signal source is present,

$$R(t-s; x, y) \equiv Q(t-s; x, y). \quad 1 - 6$$

The signal to be detected is assumed independent of and additive to the noise background so that when a signal source is present,

$$R(t-s; x, y) = Q(t-s; x, y) + P(t-s; x, y) . \quad 1 - 7$$

When the signal source alone is present the covariance function R is equal to P .

b) An Eigenfunction Expansion for the Received Signal

Since $v(t, x)$ is defined for all $t \in (0, T)$ and $x \in (-\frac{L}{2}, \frac{L}{2})$, the member v represents the joint occurrence of events at all points t, x in this interval. To avoid having to consider this infinite dimensional representation, v is replaced by a finite dimensional vector \underline{u} . The vector \underline{u} will not contain all the detection information in v , but by giving \underline{u} a sufficiently large number of properly chosen components, the practically retrievable detection information in v that is left out of \underline{u} may be made arbitrarily small. These components, in fact, are obtained by the projection of v onto a set of orthonormal basis vectors $\{\phi_i\}$, $i \in D$ where D is a finite index set. That is

$$\underline{u} \equiv (u_i) \quad i \in D$$

$$u_i = \int_0^T \int_{-\frac{L}{2}}^{\frac{L}{2}} \phi_i^*(t, x) v(t, x) dx dt \quad 1 - 8$$

in which $*$ denotes the complex conjugate. The resulting transformation is denoted by

$$\underline{u} = E v . \quad 1 - 9$$

Since the rows of E (the basis vectors ϕ_i) are orthogonal, a

pseudoinverse of E is E^* where $'$ denotes transposition. Operation on \underline{u} with E^* produces

$$\hat{v} = E^* \underline{u} \quad 1 - 10$$

and it will be presumed that the set of basis vectors is chosen such that the relation

$$v \approx \hat{v} \quad 1 - 11$$

may be accepted for the purposes of detection. Then

$$v \approx E^* \underline{u} . \quad 1 - 12$$

The covariance matrix of \underline{u} is

$$A = (a_{ij}) \quad i, j \in D \quad 1 - 13$$

where

$$\begin{aligned} a_{ij} &= \langle u_i u_j^* \rangle \\ &= \int_0^T \int_{-\frac{L}{2}}^{\frac{L}{2}} \phi_i^*(t, x) dx \quad dt \int_0^T \int_{-\frac{L}{2}}^{\frac{L}{2}} R(t-s; x, y) \phi_j(s, y) dy ds . \end{aligned} \quad 1 - 14$$

A particularly simple form for A results when the ϕ_i are chosen to be a set of orthonormal eigenfunctions of the 'noise only' covariance function Q . In fact, let the ϕ_i solve the equations

$$\int_0^T \int_{-\frac{L}{2}}^{\frac{L}{2}} Q(t-s; x, y) \phi_i(s, y) ds dy = \lambda_i \phi_i(t, x) \quad 1 - 15$$

and

$$(\phi_i, \phi_j) = \delta_{ij} \quad 1 - 16^1$$

where λ_i is a scalar quantity and $\delta_{ij} = \begin{cases} 1 & i = j \\ 0 & i \neq j \end{cases}$. Then, when no signal source is present,

$$A = \Lambda \equiv (\lambda_i \delta_{ij}), \quad i, j \in D. \quad 1 - 17$$

When a signal source as well as the background noise is present,

$$A = \Lambda + G \quad 1 - 18$$

where

$$G = (g_{ij})$$

$$g_{ij} = \int_0^T \int_{-\frac{L}{2}}^{\frac{L}{2}} \phi_i^*(t, x) dx dt \int_0^T \int_{-\frac{L}{2}}^{\frac{L}{2}} P(t-s; x, y) \phi_j(s, y) dy ds. \quad 1 - 19$$

For the analysis that will be presented here, it is required that the eigenfunctions ϕ defined on t and x be separable into two factors², one dependent only on t and the other only on x . For the separation that will be made here, the following two conditions are assumed - 1) that the noise process is stationary, and 2) that the observation time is at least an order of magnitude greater than the coherence time of the noise process.

¹ (ϕ_i, ϕ_j) stands for the inner product of ϕ_i and ϕ_j .

²See Courant and Hilbert [6], p.56.

Under assumption 1) the covariance function Q may be written

$$Q(t-s; x, y) = \frac{1}{2\pi} \int_{-\infty}^{\infty} q_1(\omega, x, y) e^{j\omega(t-s)} d\omega \quad 1 - 20$$

in which

$$q_1(-\omega, x, y) = q_1^*(\omega, x, y) , \quad 1 - 21$$

$$q_1(\omega, y, x) = q_1^*(\omega, x, y) , \quad 1 - 22$$

and

$$j \equiv \sqrt{-1} . \quad 1 - 23$$

The intermediate form q_1 may be regarded as either a cross power spectral density in the time frequency ω or a single frequency spatial covariance function. Then assumption 2) means that at all pairs of x and y in $(-\frac{L}{2}, \frac{L}{2})$ the cross power spectral density q_1 is relatively constant (smooth) over ω intervals $(\omega - W, \omega + W)$, for W significantly greater than $\frac{2\pi}{T}$. Consequently

$$\int_0^T Q(t-s; x, y) \phi_1(s) ds \approx q_1(\omega, x, y) \phi_1(t) , \quad 0 < t < T \quad 1 - 24$$

in which ϕ_1 belongs to a set of sinusoids. These sinusoids are

$$\phi_1(t) = \frac{e^{j\omega_1 t}}{\sqrt{T}} \quad \textcircled{H}(t; 0, T) , \quad 1 \in \Omega \quad 1 - 25$$

where \textcircled{H} is the "boxcar" function defined by Eq. A-1 (in Appendix A) and pictured in Fig. A-1. The index set Ω contains integers such that the frequencies ω_1 (positive and negative) given by

$$\omega_1 = \frac{2\pi i}{T} \quad 1 - 26$$

are within the frequency band of interest. Note that

$$\phi_{-i} = \phi_i^* \quad 1 - 27$$

and that the ϕ_i form an orthonormal set, i.e.

$$\int_0^T \phi_i^*(t) \phi_{i'}(t) dt = \delta_{ii'} \quad 1 - 28$$

Now for each $i \in \Omega$, a set of eigenfunctions ψ_{ik} , $k \in D_i$ is determined by

$$\int_{-\frac{L}{2}}^{\frac{L}{2}} q_1(\omega_i, x, y) \psi_{ik}(y) dy = \lambda_{ik} \psi_{ik}(x), \quad -\frac{L}{2} < x < \frac{L}{2} \quad 1 - 29$$

and the orthonormality condition

$$\int_{-\frac{L}{2}}^{\frac{L}{2}} \psi_{ik}^*(x) \psi_{i'k'}(x) dx = \delta_{kk'} \quad 1 - 30$$

Also, according to Eq. 1 - 21,

$$\psi_{-ik} = \psi_{ik}^* \quad 1 - 31$$

Though D_i could be infinite in general, it will develop later that only a finite number of ψ_{ik} can serve useful detection purposes. Consider D_i to be composed of the double indices ik of this finite set.

Replacing the indices in D with double indices, the separation of the ϕ_{ik} is achieved by writing

$$\phi_{ik}(t, x) \equiv \phi_i(t) \psi_{ik}(x) \quad 1 - 32$$

$$ik \in D = \bigcup_{i \in \Omega} D_i \quad 1 - 33$$

The function $\phi_1(t)$ will be called a time eigenfunction and $\psi_{1k}(x)$ will be called a space eigenfunction. The eigenvalue associated with ϕ_{1k} in Eq. 1 - 15 is now λ_{1k} . Projection of the received signal v onto this set of time and space eigenfunctions to obtain \underline{u} will be the first major operation in the detection analysis. The result \underline{u} of this projection (Eq. 1 - 8) of the real process v is constrained by

$$\underline{u}_{-1} = \underline{u}_1^* \quad . \quad 1 - 34$$

Since further analysis will begin with \underline{u} it is useful to relate the total average noise power in v to quantities directly associated with \underline{u} . In particular the relations below are useful in normalizing detector performance measures and in calculating absolute noise levels using measurements at a single hydrophone. According to Eq. 1 - 20, the total average noise power N in v is

$$N = \int_{-\frac{L}{2}}^{\frac{L}{2}} Q(0; x, x) dx = \frac{L}{2\pi} \int_{-\infty}^{\infty} n_1(\omega) d\omega \quad 1 - 35$$

where n_1 is defined by

$$n_1(\omega) = \frac{1}{L} \int_{-\frac{L}{2}}^{\frac{L}{2}} q_1(\omega, x, x) dx \quad . \quad 1 - 36$$

The form q_1 is Hermitian (Eq. 1 - 22) and can therefore¹ be expressed

¹Halmos [7], p. 38.

by

$$u_1(\omega_1, x, y) = \sum_{ik \in D_1} \psi_{ik}(x) \lambda_{ik} \psi_{ik}^*(y) \quad 1 - 37$$

Consequently,

$$n_1(\omega_1) = \frac{1}{L} \sum_{ik \in D_1} \lambda_{ik} \quad 1 - 38$$

c) The Received Signal through Discretely Located Hydrophones

The use of hydrophones along the array imposes a sampling function on the space dimension x . For simplicity in approximating the integral form along the array length or "aperture" $(-\frac{L}{2}, \frac{L}{2})$, the m discrete hydrophones will be assumed to be equally spaced at a separation of $\frac{L}{m}$. They will be centered within $(-\frac{L}{2}, \frac{L}{2})$, so that there is an interval $\frac{L}{2m}$ before the first hydrophone and beyond the last one (see Fig. 1 - 2). Strictly speaking, then, the length of the hydrophone array is $L(1 - \frac{1}{m})$ or very nearly L for large m .

With the above convention, spatial sampling may be introduced at the positions x_h , $h = 1, \dots, m$ by replacing the measure dx with

$$\frac{L}{m} \sum_{h=1}^m \delta(x - x_h) dx \quad 1 - 39$$

in which the function δ (the Dirac delta function) is such that

$$\delta(x) = 0, x \neq 0 \quad 1 - 40$$

and

$$\int_{-\epsilon}^{\epsilon} \delta(x) dx = 1, \epsilon \neq 0. \quad 1 - 41$$

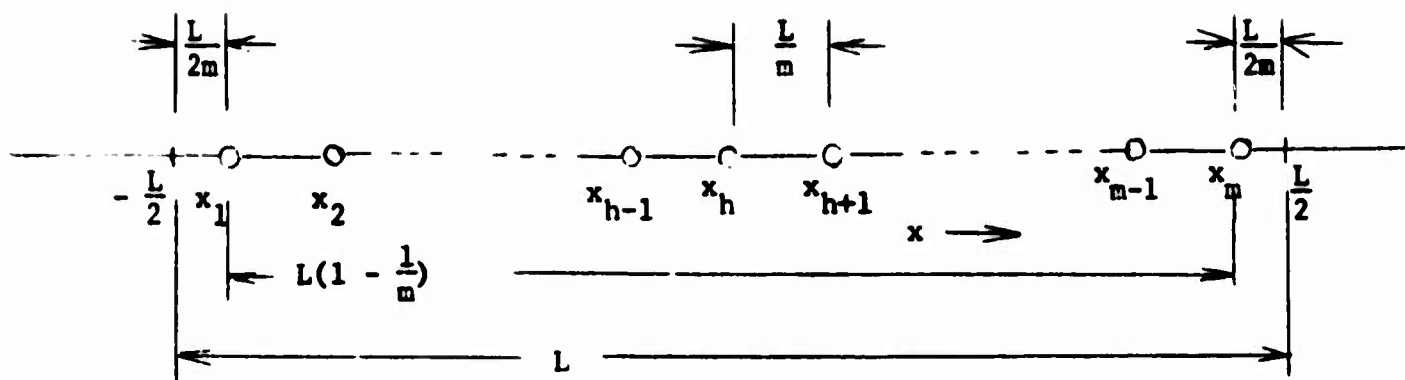


Figure 1 - 2 Hydrophone Array Dimensions

For instance, with hydrophone sampling Eq. 1 - 29 becomes

$$\int_{-\frac{L}{2}}^{\frac{L}{2}} q_1(\omega_1, x_h, y) \psi_{1k}(y) \frac{L}{m} \sum_{h'=1}^m \delta(y - y_{h'}) dy$$

$$= \frac{L}{m} \sum_{h'=1}^m q_1(\omega_1, x_h, y_{h'}) \psi_{1k}(y_{h'}) = \lambda_{1k} \psi_{1k}(x_h), \quad 1 - 42$$

$h = 1, \dots, m.$

The orthonormality condition given in Eq. 1 - 30 becomes

$$\frac{L}{m} \sum_{h=1}^m \psi_{1k}^*(x_h) \psi_{1k'}(x_h) = \delta_{kk'}. \quad 1 - 43$$

As the hydrophones approach a spacing that is small relative to the variation in a particular space eigenfunction defined on the unsampled array dimension, the corresponding space eigenfunction on the sampled dimension becomes proportional at the sample points (hydrophone locations) to this particular eigenfunction. The detection characteristics using the sampled dimension then become the same as those obtained without sampling. On the other hand, if the hydrophone spacing is increased, the array performance will worsen from that obtained without space sampling.

Depending upon the noise model and the time frequency, the received noise from separate hydrophones may become independent as their distance apart increases. With independent hydrophones the simple set

$$\{\psi_k\} \quad k = 1, \dots, m \quad 1 - 44$$

defined by

$$\psi_k(x) = \left(\frac{m}{L}\right)^{1/2} \delta_{kh} \quad x = x_1, \dots, x_m \quad 1 - 45$$

is a valid set of space eigenfunctions. In the analysis to follow, the unsampled integral forms will be preferred for their simplicity. The space dimension will be sampled only when 1) the specific effects of hydrophone spacing are being considered and 2) actual arrays are analyzed for illustration.

d) The Detection Problem

After the transformation from the received signal v to the equivalent finite dimensional vector \underline{u} , the detection problem is to determine from \underline{u} whether $\underline{Y} \in \mathcal{R}$. The best that can be done toward this is to form

$$\Pr(\underline{Y} \in \mathcal{R} | \underline{u}) = \frac{p_1 f_1(\underline{u})}{p_1 f_1(\underline{u}) + p_0 f_0(\underline{u})} \quad 1 - 46$$

where $f_0(\underline{u})$ is the probability density function of \underline{u} when background noise alone is present, and $f_1(\underline{u})$ is the probability density of \underline{u} when a signal is also present somewhere within \mathcal{R} . By hypothesis, f_0 and f_1 are (complex) Gaussian probability density functions.¹ Using the notation $C||\underline{u}||^2$ to denote the quadratic form $\underline{u}^* C \underline{u}$,

$$f_0(\underline{u}) = \frac{1}{\det \pi \Lambda} e^{-\Lambda^{-1} ||\underline{u}||^2} \quad 1 - 47$$

and

$$f_1(\underline{u}) = \int_{\mathcal{R}} f_1(\underline{u} | \underline{x}) f_1(\underline{x}) d\underline{x} \quad 1 - 48$$

¹See Arens [8], p. 205.

where

$$f_1(\underline{u}|\underline{X}) = \frac{1}{\det \pi(\Lambda + G(\underline{X}))} e^{- (\Lambda + G(\underline{X}))^{-1} ||\underline{u}||^2} \quad 1 - 49$$

and $f_1(\underline{X})$ is the a priori probability density function of \underline{X} knowing \underline{Y} is somewhere within \mathcal{R} .

With the likelihood ratio \mathcal{L} defined by

$$\mathcal{L}(\underline{Y} \in \mathcal{R} | \underline{u}) = \frac{p_1 f_1(\underline{u})}{p_0 f_0(\underline{u})} = \frac{p_1}{p_0} \int_{\mathcal{R}} \frac{f_1(\underline{u}|\underline{X}) f_1(\underline{X})}{f_0(\underline{u})} d\underline{X} \quad 1 - 50$$

the detection probability in Eq. 1 - 46 may be written

$$\Pr(\underline{Y} \in \mathcal{R} | \underline{u}) = \frac{1}{1 + \frac{1}{\mathcal{L}(\underline{Y} \in \mathcal{R} | \underline{u})}} \quad 1 - 51$$

Since \mathcal{L} is a monotonic function of $\Pr(\underline{Y} \in \mathcal{R} | \underline{u})$, \mathcal{L} may replace $\Pr(\underline{Y} \in \mathcal{R} | \underline{u})$ as the detection statistic. According to Eq. 1 - 50, this likelihood \mathcal{L} factors into

$$\frac{p_1}{p_0} \text{ and } \int_{\mathcal{R}} \frac{f_1(\underline{u}|\underline{X}) f_1(\underline{X})}{f_0(\underline{u})} d\underline{X} \quad 1 - 52$$

The second factor provides a measure on all possible \underline{u} that allows them to be arranged in order of increasing likelihood that they arose in the presence of a signal source. The factor $\frac{p_1}{p_0}$ is used in setting a detection threshold within this continuum of ordered \underline{u} . Since $\frac{p_1}{p_0}$ is almost always only vaguely known, this threshold will usually be approximate. Furthermore, in practice, not all the steps in processing \underline{u} prescribed by

$\int_{\mathcal{R}} \frac{f_1(\underline{u}|\underline{X}) f_1(\underline{X})}{f_0(\underline{X})} d\underline{X}$ may be implemented, and the ordering itself may be only

approximately realized. In fact, an approximate likelihood ordering of \underline{u} may be performed subjectively by observing the shape of the integrand $\frac{f_1(\underline{u}|\underline{X}) f_1(\underline{X})}{f_0(\underline{u})}$ displayed on a screen as a function of \underline{X} for each \underline{u} that is observed.

For example, for each \underline{u} , the integrand $\frac{f_1(\underline{u}|\underline{X}) f_1(\underline{X})}{f_0(\underline{u})}$ may be displayed at \underline{X} of fixed length (range) and angle of incidence (bearing θ in Fig. 1 - 1) between 0° and 180° . The observer may feel that a shape



is more indicative of signal presence than



Thus $\mathcal{L}(\underline{u}_A)$ would be judged larger than $\mathcal{L}(\underline{u}_B)$. Next, the threshold for deciding that a signal is in fact present is determined from a subjective estimate of $\frac{p_1}{p_0}$, and the cost of errors. In summary, the mathematical processing of the received signal may end in practice with a display of the shape of $\frac{f(\underline{u}|\underline{X}) f_1(\underline{X})}{f_0(\underline{u})}$ versus \underline{X} . An experienced observer may then complete the detection process subjectively.

Under the assumptions made in this study, further mathematical processing of $\frac{f_1(\underline{u}|\underline{X}) f_1(\underline{X})}{f_0(\underline{u})}$ could lead to a decision without an observer; however, this possibility will not be considered here. Instead, only the term $\frac{f_1(\underline{u}|\underline{X}) f_1(\underline{X})}{f_0(\underline{u})}$ in \mathcal{L} (Eq. 1 - 50) will be analyzed. Explicitly, this term is

$$\frac{f_1(\underline{u}|\underline{X}) f_1(\underline{X})}{f_0(\underline{u})} = e^{b(\underline{u},\underline{X})} \quad 1 - 53$$

where

$$b(\underline{u},\underline{X}) = \chi(\underline{u},\underline{X}) - \ln \det (\Lambda + G(\underline{X})) + \ln \det \Lambda + \ln f_1(\underline{X}) \quad 1 - 54$$

and

$$\chi(\underline{u},\underline{X}) = - \left[(\Lambda + G(\underline{X}))^{-1} - \Lambda^{-1} \right] ||\underline{u}||^2. \quad 1 - 55$$

A detector labeled the b-detector will form $b(\underline{u},\underline{X})$ from \underline{u} .

Since the shape of $\frac{f_1(\underline{u}|\underline{X}) f_1(\underline{X})}{f_0(\underline{u})}$ (considered as a function of \underline{X})

is the key to detection by an observer, it is significant to note that the signal source location probability density function $f_1(\underline{X}|\underline{u})$ has the same shape. In fact,

$$f_1(\underline{X}|\underline{u}) = \frac{f_1(\underline{u}|\underline{X}) f_1(\underline{X})}{f_1(\underline{u})} = \frac{e^{b(\underline{u},\underline{X})}}{K(\underline{u})} \quad 1 - 56$$

where $K(\underline{u})$ is independent of \underline{X} . Thus in addition to being a detection statistic, the shape of $e^{b(\underline{u},\underline{X})}$ will also determine the location of the signal source as accurately as possible.

Conditions for deciding that a signal source is present are that $p_0 f_0(\underline{u})$ in Eq. 1 - 50 be small and that $p_1 \int_{\mathcal{R}} f_1(\underline{u}|\underline{X}) f_1(\underline{X}) d\underline{X}$ be large. The first of these conditions alone may in some cases serve as an indication of signal presence. If this approach is used, errors that will be made when both $p_0 f_0(\underline{u})$ and $p_1 \int_{\mathcal{R}} f_1(\underline{u}|\underline{X}) f_1(\underline{X}) d\underline{X}$ are small must be accepted. But, these errors may be infrequent enough for a detector forming $p_0 f_0(\underline{u})$ to perform usefully. Since $f_0(\underline{u})$ is very simple to form and is affected by signal presence over a large region of scan, the following suboptimum detector is proposed. This

detector, labeled the l -detector, will form

$$l(\underline{u}, \underline{X}) = - \ln \left(\frac{f_0(\underline{u})}{f_1(\underline{X})} \right) = \Lambda^{-1} \|\underline{u}\|^2 + \ln \det \pi \Lambda + \ln f_1(\underline{X}) . \quad 1 - 57$$

The a priori probability of signal absence p_0 is assumed close enough to unity to be omitted. To make this detector crudely steerable, the set D of indices of the components of \underline{u} will be made a function of the steering vector \underline{X} . That is,

$$D = D(\underline{X}) . \quad 1 - 58$$

A method for choosing the indices to accomplish the desired steering will be discussed after performance measures have been defined.

This chapter has given a general description of the detection problem and outlined the signal processing procedure. The aims in the remainder of this study are to

- 1) Determine the spatial set $\{\psi_{ik}, \lambda_{ik}\}$, $ik \in D$ (Eq. 1 - 29) and the resulting signal covariance matrix G (Eq. 1 - 19) for specific noise fields.
- 2) Define performance measures for detectors forming b and l (Eqs. 1 - 54 and 1 - 57) and use these to analyze detection in the specific noise fields of 1).

CHAPTER 2

SIGNAL AND NOISE MODELS

2.0 Introduction

This chapter begins with a description of various noise fields and the sets of eigenfunctions and eigenvalues they determine. Then, with the eigenfunctions in mind, characteristics of the signal covariance matrix G are given. The intent is to supplement some of the definitions in the last chapter with examples. The quantities discussed are important in understanding and constructing the detection statistics b and l (Eqs. 1 - 54 and 1 - 57).

The noise fields considered here are the superposition of four possible independent components. These components are

- 1) Sea noise (acoustic background noise) - noise from surface waves, and other noise that is not highly directional.
- 2) Interfering target noise - noise from signal sources that have already been detected and located.
- 3) Local noise - noise generated in the immediate vicinity of the array. The primary source of this noise is the ship or other platform supporting the array.
- 4) Self noise - noise that is generated in the hydrophones composing the array.

Since all the components are assumed Gaussian (with zero mean), they are completely described by their covariance function. This function is given in the following for forms of the noise components that are both typical and easily represented mathematically. Examples of the eigenfunctions and eigenvalues determined by the covariance function are also included.

2.1 Sea Noise

The sea noise observed in time t and in the space dimension x is assumed to be homogeneous.¹ Consequently, the covariance function Q may be written

$$Q(t-s, x, y) = Q(t-s, x-y) = Q(\tau, \chi), \quad 2-1$$

where

$$\tau = t-s \quad 2-2$$

and

$$\chi = x-y. \quad 2-3$$

The Fourier transform of Q yields the power spectrum $n(\omega, \nu)$ in which ω (in radians/second) is called the time frequency and ν (in radians/meter) is called the space frequency. That is,

$$n(\omega, \nu) = \int_{-\infty}^{\infty} \int_{-\infty}^{\infty} e^{-j(\omega\tau + \nu\chi)} Q(\tau, \chi) d\tau d\chi \quad 2-4$$

and inversely,

$$Q(\tau, \chi) = \frac{1}{(2\pi)^2} \int_{-\infty}^{\infty} \int_{-\infty}^{\infty} e^{j(\omega\tau + \nu\chi)} n(\omega, \nu) d\omega d\nu. \quad 2-5$$

Since the noise process is real,

$$n(-\omega, -\nu) = n(\omega, \nu). \quad 2-6$$

The transformation from $Q(\tau, \chi)$ to $n(\omega, \nu)$ may be considered either

¹See Yaglom [9], pp. 81-84.

a transformation from $Q(\tau, \chi)$ to an intermediate form $q_1(\omega, \chi)$ and then to $n(\omega, \nu)$, or a transformation first from $Q(\tau, \chi)$ to an intermediate form $q_2(\tau, \nu)$ and then to $n(\omega, \nu)$. The transform pairs describing the $Q \leftrightarrow q_1 \leftrightarrow n$ transformation are

$$q_1(\omega, \chi) = \int_{-\infty}^{\infty} Q(\tau, \chi) e^{-j\omega\tau} d\tau \quad 2 - 7$$

$$Q(\tau, \chi) = \frac{1}{2\pi} \int_{-\infty}^{\infty} q_1(\omega, \chi) e^{j\omega\tau} d\omega \quad 2 - 8$$

and

$$n(\omega, \nu) = \int_{-\infty}^{\infty} q_1(\omega, \chi) e^{-j\nu\chi} d\chi \quad 2 - 9$$

$$q_1(\omega, \chi) = \frac{1}{2\pi} \int_{-\infty}^{\infty} n(\omega, \nu) e^{j\nu\chi} d\nu \quad 2 - 10$$

The transform pairs describing the $Q \leftrightarrow q_2 \leftrightarrow n$ transformations are

$$q_2(\tau, \nu) = \int_{-\infty}^{\infty} Q(\tau, \chi) e^{-j\nu\chi} d\chi \quad 2 - 11$$

$$Q(\tau, \chi) = \frac{1}{2\pi} \int_{-\infty}^{\infty} q_2(\tau, \nu) e^{j\nu\chi} d\nu \quad 2 - 12$$

and

$$n(\omega, \nu) = \int_{-\infty}^{\infty} q_2(\tau, \nu) e^{-j\omega\tau} d\tau \quad 2 - 13$$

$$q_2(\tau, \nu) = \frac{1}{2\pi} \int_{-\infty}^{\infty} n(\omega, \nu) e^{j\omega\tau} d\omega \quad 2 - 14$$

Eq. 2 - 8 is recognized as Eq. 1 - 20 in the last section. Since

$q_1(\omega, x-x) = q_1(\omega, 0)$, Eq. 1 - 36 for n_1 becomes

$$n_1(\omega) = q_1(\omega, 0) . \quad 2 - 15$$

For sea noise, then, $n_1(\omega)$ is the power spectrum of the time process observed at any point along the array. By Eqs. 2 - 7 and 2 - 10 n_1 is related to Q and n through the equations

$$n_1(\omega) = \frac{1}{2\pi} \int_{-\infty}^{\infty} n(\omega, \nu) d\nu \quad 2 - 16$$

and

$$n_1(\omega) = \int_{-\infty}^{\infty} Q(\tau, 0) e^{-j\omega\tau} d\tau . \quad 2 - 17$$

The relation

$$n_1(-\omega) = n_1(\omega) \quad 2 - 18$$

follows from Eqs. 1 - 21 and 1 - 22 for this two-sided spectrum. The spectral normalization implied by Eqs. 1 - 20 and 2 - 15 is such that the noise power in bands of width $\Delta\omega$ centered at ω_c and $-\omega_c$ is $2 n_1(\omega_c) \Delta\omega/2\pi$ when n_1 is flat over these bands. (This normalization is also employed by Helstrom¹).

A homogeneous Gaussian sea noise field may be constructed by superimposing an infinite number of independent, infinitesimally small single frequency plane waves propagating within a homogeneous

¹[10], pp. 2, 35.

nondispersive medium. The space frequency ν at which power is received from any one of these plane waves is

$$\nu = \frac{\omega}{c} \cos \beta \quad 2 - 19$$

where β is the angle of incidence of the wave (Fig. 1 - 1) and c is the velocity of propagation within the medium. (The quantity $\frac{\omega}{c}$ is recognized as the wavenumber.) Now for any β ,

$$-\frac{\omega}{c} < \nu < \frac{\omega}{c} \quad 2 - 20$$

This band limiting in space frequency is an important characteristic of sea noise.

Two simple examples of sea noise are the following isotropic models.

- 1) When the direction vectors of the infinitesimal wave components are uniformly distributed and confined to a horizontal plane, the total field is isotropic in two dimensions and is labeled I2 sea noise. Physically, this field might approximate noise conditions in an expanse of shallow water.
- 2) When the direction vectors are uniformly distributed in three dimensions, the noise is labeled I3 sea noise. This noise might approximate the noise background in deep water.

The power spectrum of I2 sea noise is (Appendix B)

$$n(\omega, \nu) = \frac{2 n_1(\omega)}{\sqrt{\frac{\omega^2}{c^2} - \nu^2}} \mathbb{H}(\nu; -\frac{\omega}{c}, \frac{\omega}{c}) \quad 2 - 21$$

where \mathbb{H} is the "boxcar" function defined by Eq. A - 1. This spectrum is sketched in Fig. 2 - 1 for the case in which the time power spectrum

$$r(\omega, v) = \frac{2n_1(\omega)}{\sqrt{\frac{\omega_0^2}{c^2} - v^2}} \Theta\left(v; -\frac{c}{\omega_0}, \frac{c}{\omega_0}\right) \quad \eta = \text{Constant}$$

$$n_1(\omega) = \eta \Theta(\omega; -\omega_0, \omega_0)$$

Sections shown at $\omega = \omega_0, \frac{\omega_0}{2}, -\frac{\omega_0}{2}, -\omega_0$ and at $v = 0$

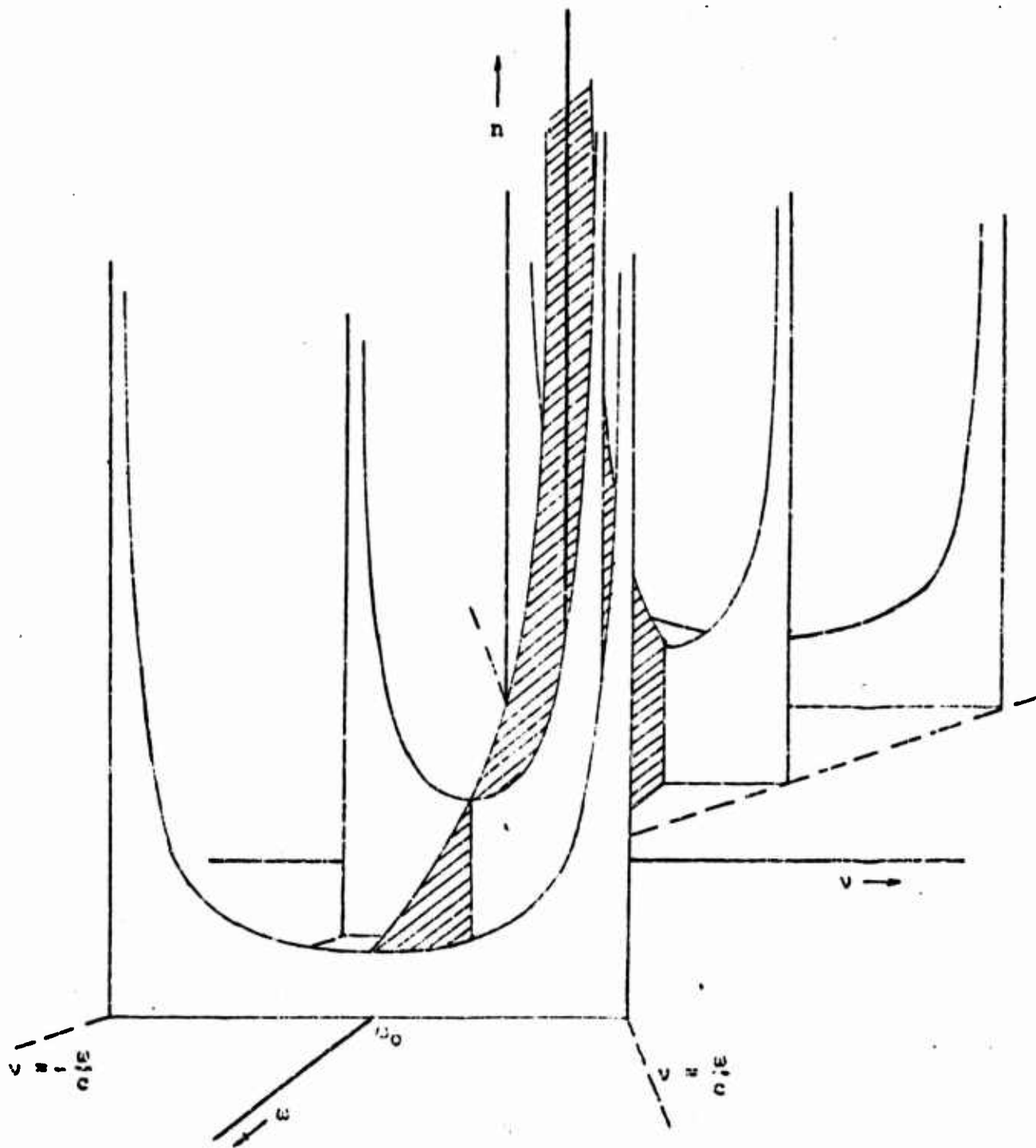


Figure 2-1 A Power Spectral Density Function for I2 Sea Noise

$n_1(\omega)$ is a "boxcar" function (note the spatial frequency bandlimiting). The spatial covariance function q_1 , obtained from n through Eq. 2 - 10, is

$$q_1(\omega, \chi) = n_1(\omega) J_0\left(\frac{\omega\chi}{c}\right) \quad 2 - 22$$

where

$$\chi = x - y.$$

The I3 sea noise power spectrum is

$$n(\omega, \nu) = \frac{\pi c}{\omega} n_1(\omega) \mathcal{H}\left(\nu; -\frac{\omega}{c}, \frac{\omega}{c}\right) \quad 2 - 23$$

and is sketched in Fig. 2 - 2 for the case in which $n_1(\omega)$ is a "boxcar" function. The spatial covariance function q_1 is

$$q_1(\omega, \chi) = n_1(\omega) \text{sinc}\left(\frac{\omega\chi}{c}\right). \quad 2 - 24$$

According to Eq. 1 - 29, the spatial eigenfunctions and eigenvalues associated with the I3 sea noise field solve the equation

$$n_1(\omega_1) \int_{-\frac{L}{2}}^{\frac{L}{2}} \text{sinc}\left[\frac{\omega_1}{c}(x-y)\right] \psi_{1k}(y) dy = \lambda_{1k} \psi_{1k}(x). \quad 2 - 25$$

The eigenfunctions obtained are in fact prolate spheroidal wavefunctions [11].

Examples of these eigenfunctions are given in Fig. 2 - 3 for a time frequency of 40 hz and an array length of 50 meters. Since these eigenfunctions are not periodic, they do not have a frequency in the strict sense. However, some rough space 'frequency' is usually assignable, based on zero crossings or sometimes on sinusoidal appearance. The spectrum $\{\lambda_{1k}\}$ is plotted in Fig. 2 - 4 versus such a 'frequency'

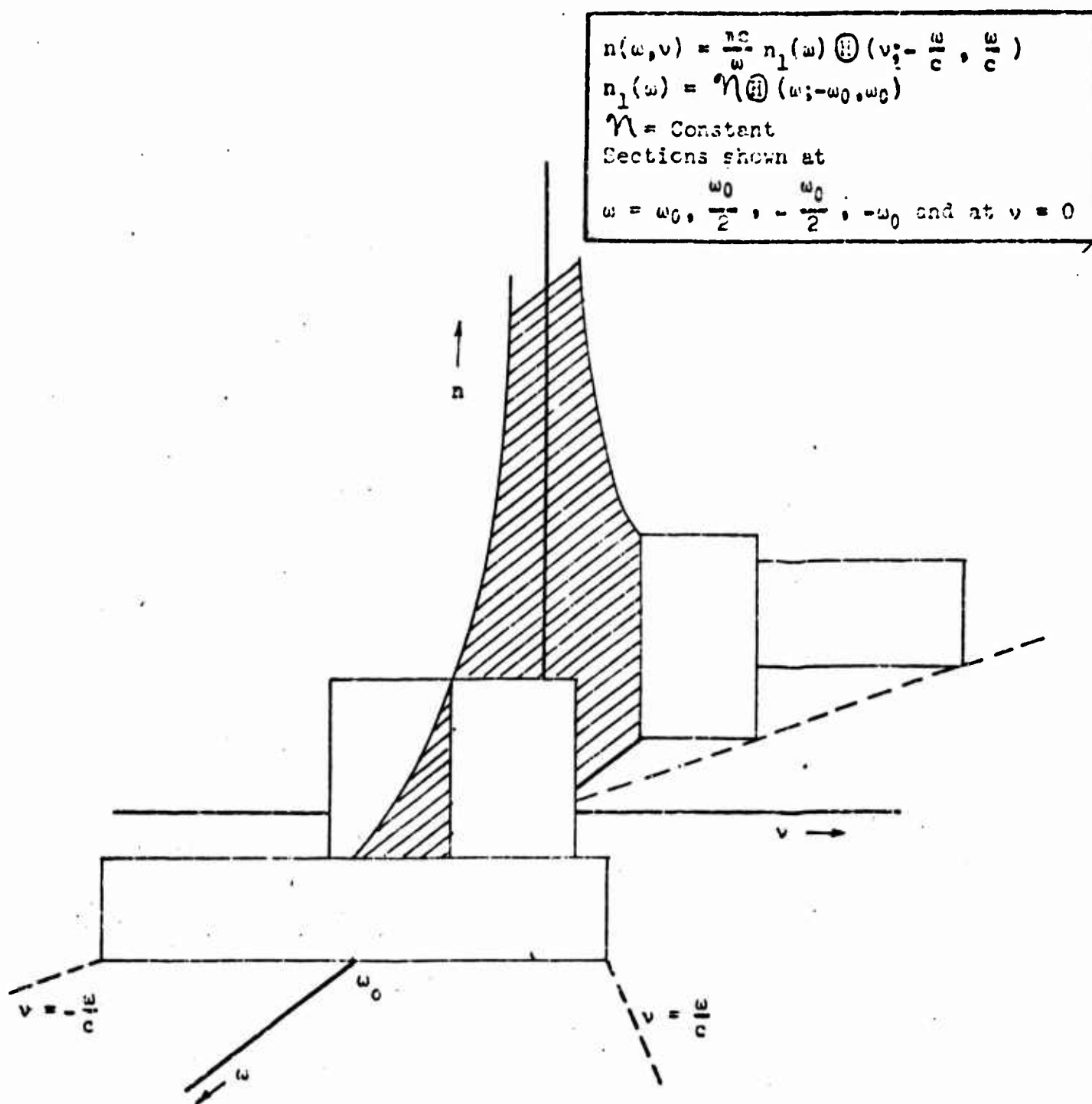


Figure 2-2 A Power Spectral Density Function for 13 Sea Noise

$L = 50$ Meters	Background Noise is
$\omega = 2\pi \times 40 = 251$ RPS	13 Sea Noise
$n = 12$ Hydrophones	$c = 1500$ Meters/Sec

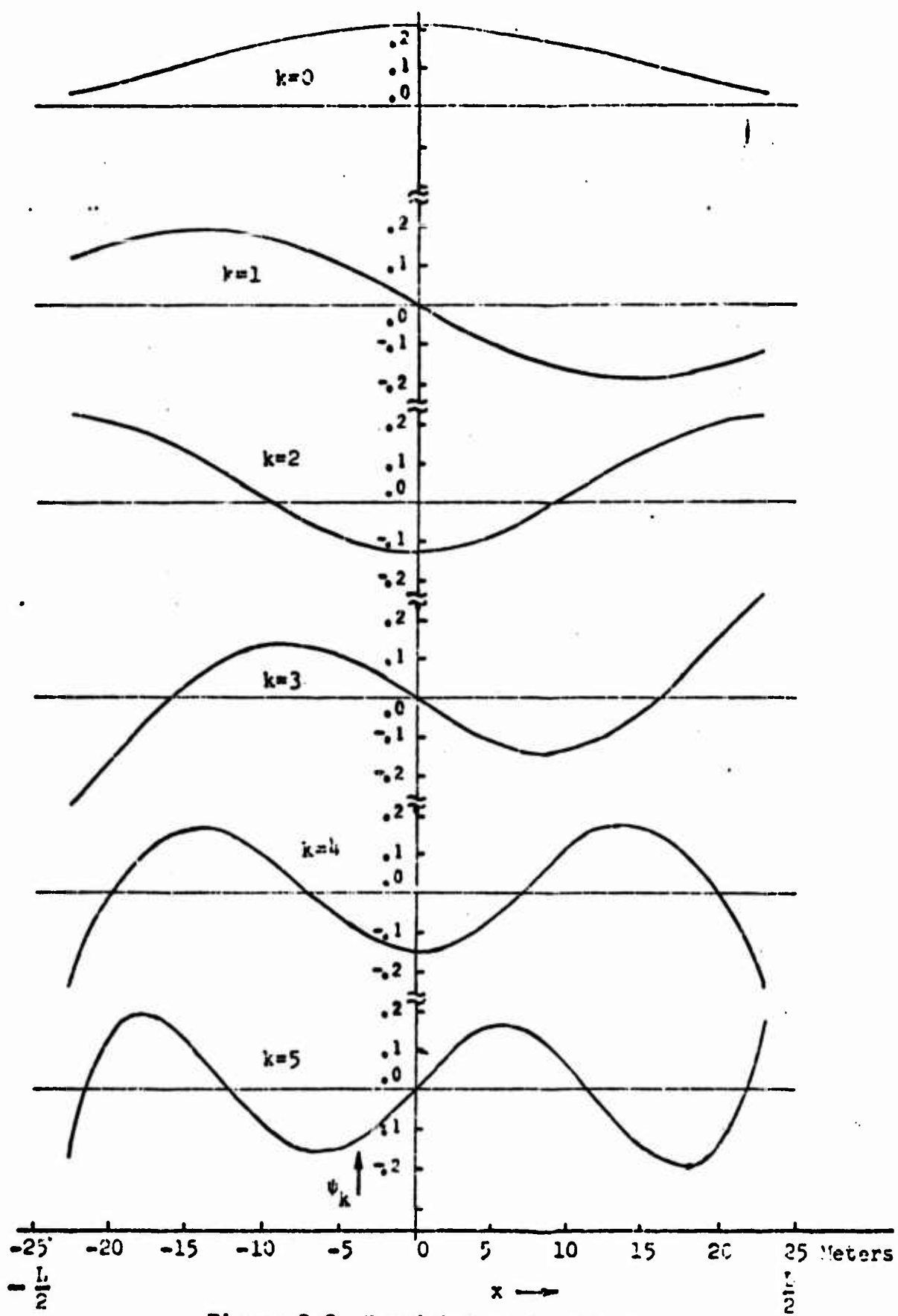


Figure 2-3 Spatial Eigenfunctions

measure. The spatial spectral density function

$$n(\omega, \nu) = \frac{\pi c}{\omega} n_1(\omega) \mathcal{H}(\nu; -\frac{\omega}{c}, \frac{\omega}{c}) \quad 2 - 26$$

given in Eq. 2 - 23 and Fig. 2 - 2 is shown in Fig. 2 - 4 for comparison.

In normalized form, Eq. 2 - 25 is

$$n_1(\omega_1) \int_{-1}^1 \text{sinc} \left[\frac{L\omega_1}{2c} (x' - y') \right] \psi_{1k} \left(\frac{L}{2} y' \right) dy' = \frac{2\lambda_{1k}}{L} \psi_{1k} \left(\frac{L}{2} x' \right) . \quad 2 - 27$$

It is of interest to note that since ω and L appear only in product form in the argument of the sinc function on the left-hand side of this equation, the solutions ψ_{1k} obtained at $\frac{\omega_1}{2\pi} = 40$ hz and $L = 50$ meters are valid at all pairs of ω_1 and L whose product is

$$\omega_1 L = 251 \times 50 .$$

For example, if $\frac{\omega}{2\pi} = 200$ hz and $L = 10$ meters, then

$$\psi'_{1k}(x) = \sqrt{5} \psi_{1k}(5x); \lambda'_{1k} = \frac{\lambda_{1k}}{5} \quad 2 - 28$$

will solve

$$n_1(\omega_1) \int_{-\frac{L}{2}}^{\frac{L}{2}} \text{sinc} \left[\frac{\omega_1}{c} (x-y) \right] \psi'_{1k}(y) dy = \lambda'_{1k} \psi'_{1k}(x) , \quad 2 - 29$$

where ψ_{1k} and λ_{1k} are obtained at $\frac{\omega_1}{2\pi} = 40$ hz and $L = 50$ meters (Figs. 2 - 3 and 2 - 4). This is only characteristic of certain 'special' noise models such as the I2 and I3 sea noise models; less regular dependence on frequency and length may be expected in general.

$L = 50$ Meters
 $\omega = 2\pi \times 40 = 251$ RPS
 Background Noise is
 13 Sea Noise
 $m = 12$ Hydrophones
 $c = 1500$ Meters/Sec

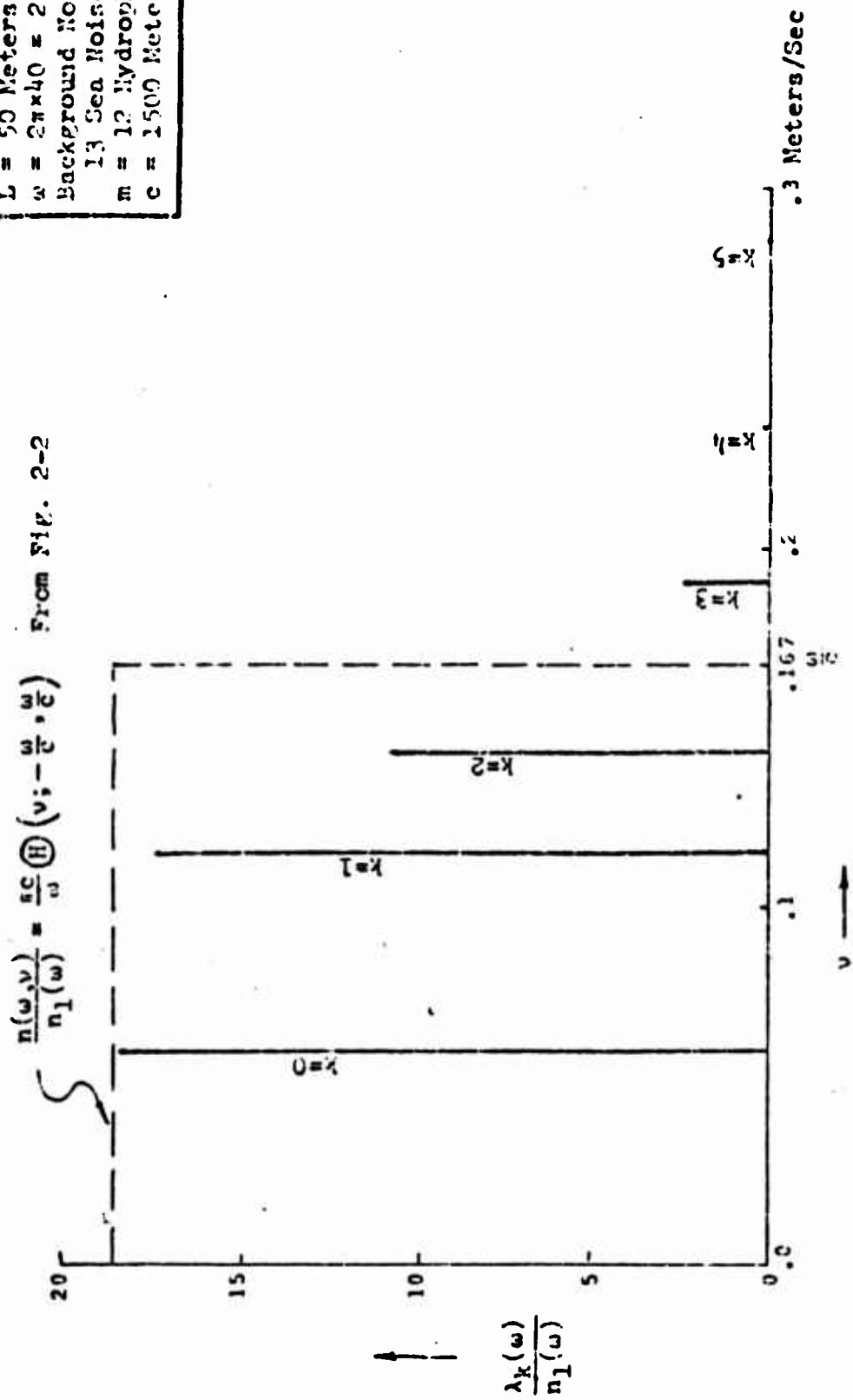


Figure 2-4 Continal Eigenvalues

2.2 Interfering Target Noise and Local Noise

Interference noise and local noise as modeled here are Gaussian processes that are stationary but not homogeneous. Interference originates at some presumably known location or locations, and local noise originates in the vicinity of the receiving array. Interference could be generated by a vessel that has already been detected and located, and local noise could be generated by the vessel or other platform that is supporting the array.

Since these noise processes are not homogeneous, there is no point in defining the process on x beyond the interval $(-\frac{L}{2}, \frac{L}{2})$. The spectral equations of Sect. 2.1 apply directly, describing the transformations $Q \leftrightarrow q_1$. Repeating Eqs. 2 - 7 and 2 - 8 ,

$$q_1(\omega, x, y) = \int_{-\infty}^{\infty} Q(\tau; x, y) e^{-j\omega\tau} d\tau \quad 2 - 30$$

$$Q(\tau; x, y) = \frac{1}{2\pi} \int_{-\infty}^{\infty} q_1(\omega, x, y) e^{j\omega\tau} d\omega \quad 2 - 31$$

The two dimensional spectrum n describing sea noise is not defined for this inhomogeneous noise, and instead, the discrete set $\{\lambda_k(\omega)\}$ contains the spectral information. In fact, composing Eqs. 1 - 29, 1 - 30 and 1 - 37 , the transformation $q_1 \leftrightarrow \lambda$ may be written

$$\lambda_k(\omega) = \int_{-\frac{L}{2}}^{\frac{L}{2}} \psi_k^*(\omega, x) \int_{-\frac{L}{2}}^{\frac{L}{2}} q_1(\omega, x, y) \psi_k(\omega, y) dy dx \quad 2 - 32$$

$$q_1(\omega, x, y) = \sum_{k \in D(\omega)} \psi_k(\omega, x) \lambda_k(\omega) \psi_k^*(\omega, y) \quad 2 - 33$$

A simple example of an inhomogeneous process is the noise generated at a point source, and such a process is now described. Locating the point source one meter beyond the negative end of the array (at $x = -\frac{L}{2} - 1$), a member of this process is

$$v(t, x) = \int_{-\infty}^{\infty} \frac{e^{j\omega(t - \frac{x+L}{2})}}{x + \frac{L}{2} + 1} dY(\omega) \quad 2 - 34$$

where Y is a complex random point function with normally distributed orthogonal increments.¹ In this equation Y is normalized so that

$$\langle dY(\omega) dY^*(\omega) \rangle = \frac{1}{2\pi} q_1(\omega, -\frac{L}{2}, -\frac{L}{2}) d\omega \quad 2 - 35$$

where $q_1(\omega, -\frac{L}{2}, -\frac{L}{2})$ is recognized as the power spectrum of the time process measured at the end of the array $x = -\frac{L}{2}$. Furthermore, since v is real

$$Y(-\omega) = -Y^*(\omega) . \quad 2 - 36$$

Now according to Eqs. 1 - 4, 2 - 34 and 2 - 35

$$\begin{aligned} Q(t-s, x, y) &= \langle v(t, x) v^*(s, y) \rangle \\ &= \frac{1}{2\pi(x + \frac{L}{2} + 1)(y + \frac{L}{2} + 1)} \int_{-\infty}^{\infty} q_1(\omega, -\frac{L}{2}, -\frac{L}{2}) e^{j\left[\omega(t-s) - \frac{\omega}{c}(x-y)\right]} d\omega . \end{aligned} \quad 2 - 37$$

Comparing this with Eq. 2 - 31 in which $\tau = t-s$,

$$q_1(\omega, x, y) = \frac{q_1(\omega, -\frac{L}{2}, -\frac{L}{2}) e^{-j\frac{\omega}{c}(x-y)}}{(x + \frac{L}{2} + 1)(y + \frac{L}{2} + 1)} . \quad 2 - 38$$

¹Yaglom [9], p. 38.

If this noise were present by itself, the set $\{\psi_{1k}, \lambda_{1k}\}$ of spatial eigenfunctions and eigenvalues would follow from Eqs. 1 - 29 and 1 - 30. In fact for each time frequency index 1 there would be one nonzero eigenvalue

$$\lambda_{10} = \frac{L}{1+L} q_1(\omega, -\frac{L}{2}, -\frac{L}{2}) \quad 2 - 39$$

with associated eigenfunction

$$\psi_{10}(x) = \sqrt{1 + \frac{1}{L}} \frac{e^{-j\frac{\omega_1 x}{c}}}{x + \frac{L}{2} + 1} \quad 2 - 40$$

In addition, Eqs. 1 - 29 and 1 - 30 indicate an arbitrarily large number of spatial eigenfunctions with zero eigenvalues. In practice, however, the continuous model discussed here is replaced by a discrete model defined only at the hydrophone locations, so that the total number of spatial eigenfunctions may not exceed m , the number of hydrophones in the array. The total single frequency noise power n_1 defined by Eq. 1 - 38 is

$$n_1(\omega) = \frac{1}{1+L} q_1(\omega, -\frac{L}{2}, -\frac{L}{2}) \quad 2 - 41$$

In an actual detection problem there will always be some sea noise (Sect. 2.3) present along with the interference or local noise. The eigenvalues determined by the composite noise covariance function will be nonzero in general. If the interference (or local noise) is strong, the eigenfunction or eigenfunctions upon which this interference is principally received will be close to those associated with the major nonzero eigenvalues of the interference covariance function by itself.

As an example, consider a process made up of the noise from a point source one meter beyond the negative end of the array (Eqs. 2 - 34

2 - 41) in the presence of -10 db of I3 sea noise. (By -10 db it is meant that n_1 for the sea noise (Eq. 2 - 15) is 10 db below n_1 for the local noise (Eq. 2 - 41). The eigenfunctions are as shown in Fig. 2 - 5 for an array of length $L=50$ meters at a time frequency $\frac{\omega}{2\pi} = 40$ hz .

Because of the nonisotropic component in the noise, some of the eigenfunctions are necessarily complex. Any eigenfunction may be multiplied by a complex scalar of absolute value unity without changing its normalization. The separation into real and imaginary parts, then, is not unique. A separation is chosen here such that the real and imaginary parts are orthogonal and such that the real part has the larger norm.

The spectrum $\{\lambda_k\}$ of the noise power is plotted in Fig. 2 - 6 versus the index k . The sea noise level and local noise power are plotted for reference. According to this spectrum almost all of the local noise appears on the first eigenfunction. The shape of this eigenfunction evidences the attenuation of the local noise due to spreading, and the phase relation between the real and imaginary parts indicates that the noise energy is propagating from the negative end of the array (see Eq. 2 - 40).

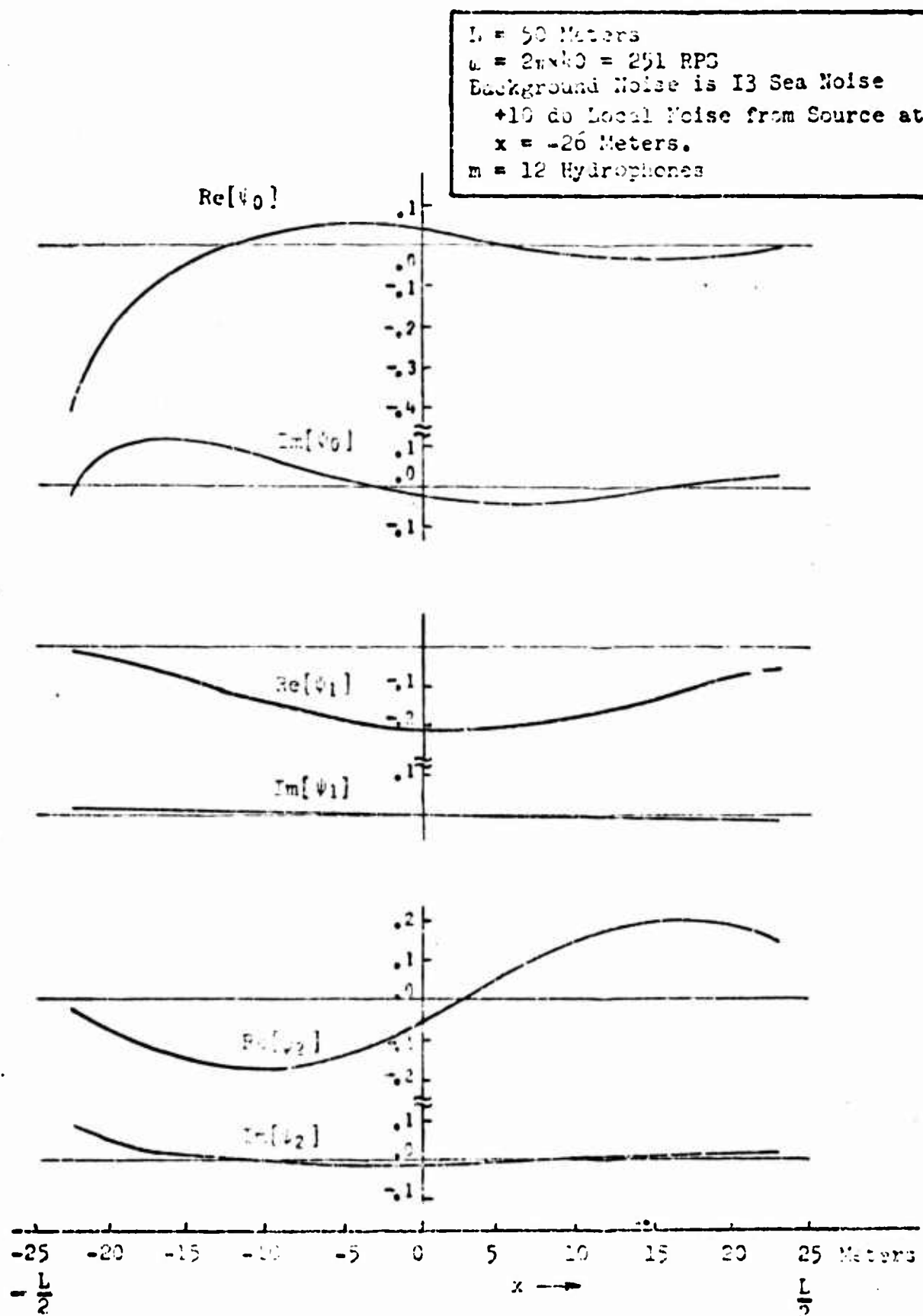


Figure 2-5 Spatial Eigenfunctions for 13 and Local Noise

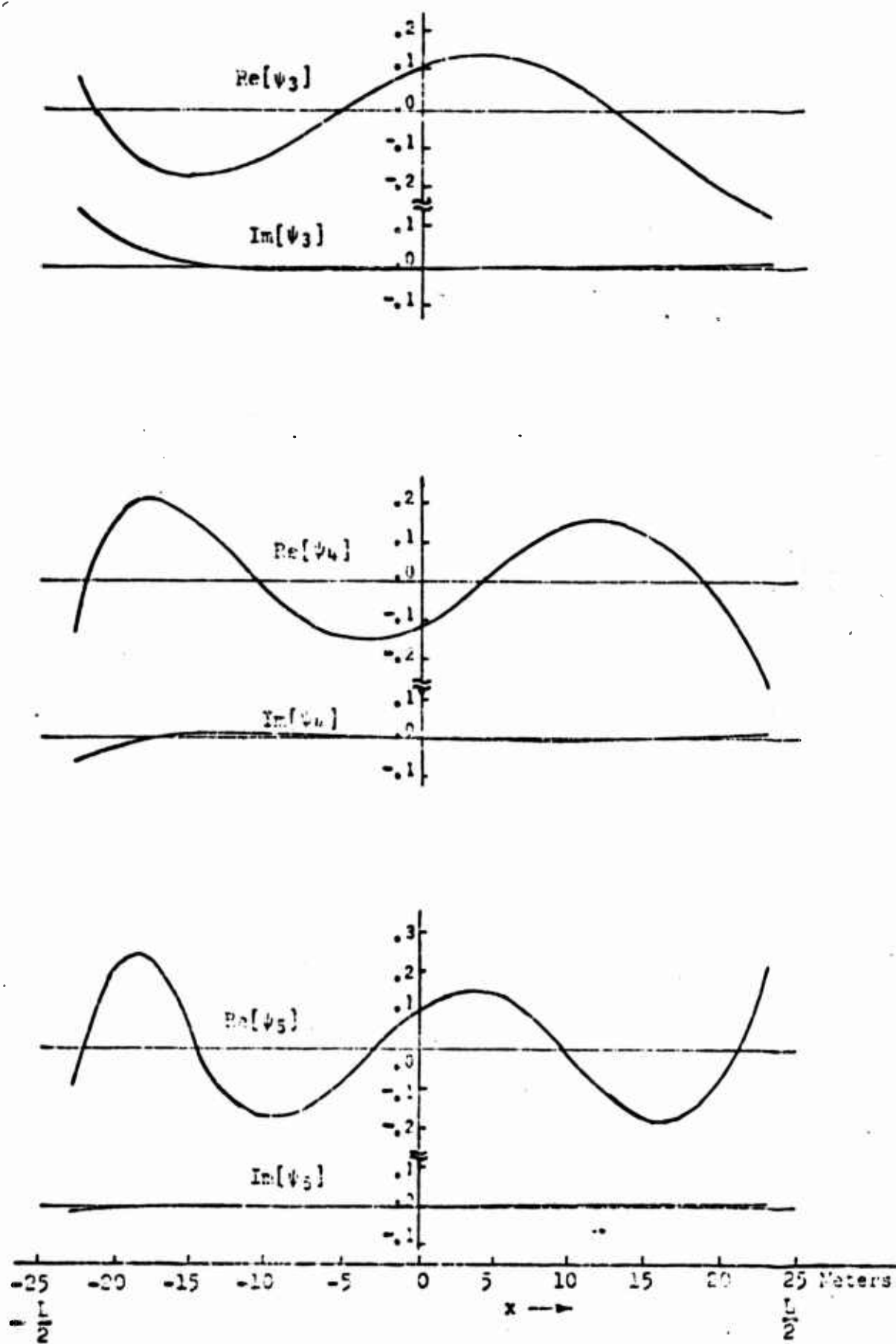
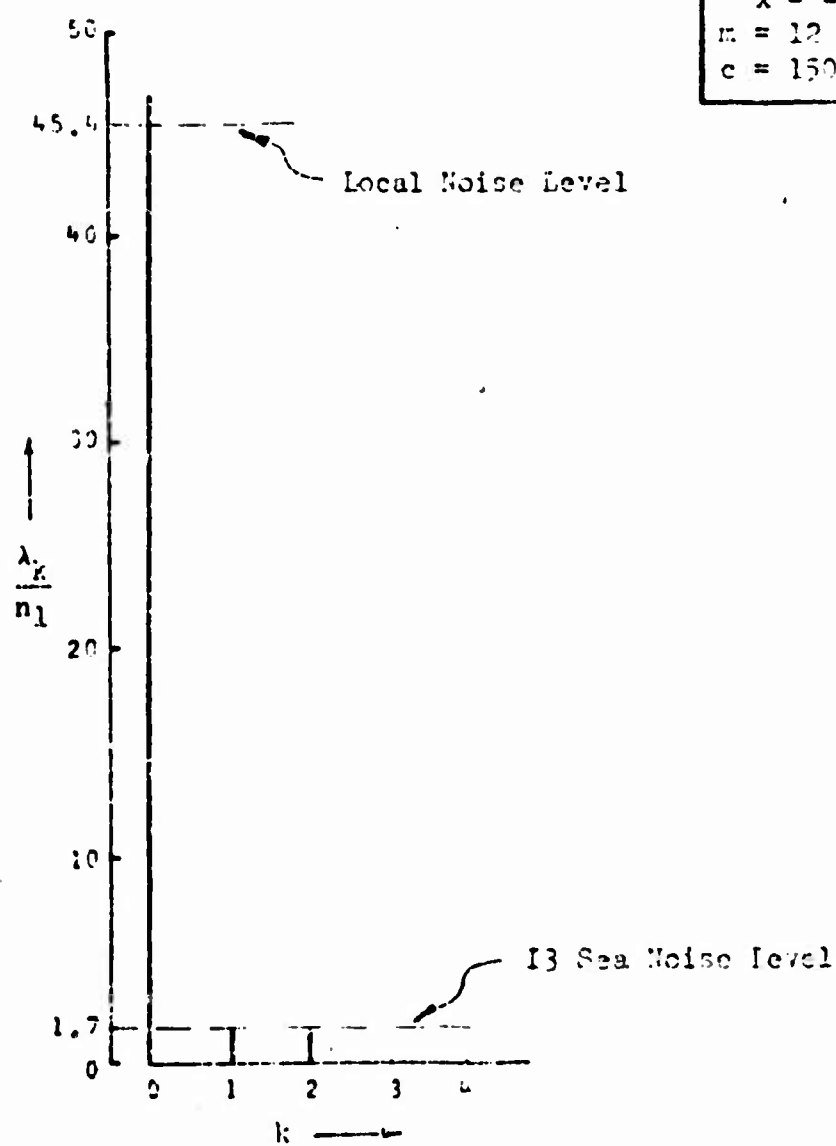


Figure 2-5 Continued



$L = 50$ Meters
 $\omega = 2\pi \times 40 = 251$ RPS
 Background Noise is 13
 Sea Noise + 10 db Local
 Noise from Source at
 $x = -26$ Meters
 $m = 12$ Hydrophones
 $c = 1500$ Meters/Sec

Figure 2-6 Eigenvalues for I3 and Local Noise

2.3 Self Noise

In addition to the acoustic noise just considered, there is always some self noise generated in the transducing elements (hydrophones) of the array [12]. This self noise in any hydrophone is assumed to be stationary and Gaussian with uniform power spectral density η over all frequencies ω of practical interest. Furthermore, the noise at each hydrophone is independent of that at all others, so that

$$q_1(\omega, x_h - y_{h'}) = \eta \delta_{hh'} \quad 2 - 42$$

in which h is the hydrophone position index.

A direct spectral comparison may be made with the sea noise processes defined on the whole array dimension (Sect. 2.1) under the following conditions. 1) The hydrophones are spaced $\frac{L}{m}$ apart over the entire space dimension ($h = -\infty, \dots, \infty$). 2) The space frequency ν is significantly less than the Nyquist cutoff frequency

$$\nu_0 = 2\pi \frac{m}{2L} = \frac{\pi m}{L} \quad 2 - 43$$

Under these conditions a power spectrum is adequately defined by a sampled version $\hat{n}(\omega, \nu)$ of $n(\omega, \nu)$. From Eq. 2 - 9

$$\hat{n}(\omega, \nu) = \frac{L}{m} \sum_{h=-\infty}^{\infty} q_1(\omega, x_h) e^{j\nu x_h} \quad 2 - 44$$

For self noise, since q_1 is $\eta \delta_{hh'}$,

$$\hat{n}(\omega, \nu) = \xi, \quad 2 - 45$$

where

$$\xi = \frac{L}{m} \eta \quad 2 - 46$$

Fig. 2 - 7 shows the shape of the spatial spectrum at fixed time frequency ω of a noise process consisting of 13 sea noise plus self noise ($n = n$ (13 sea noise) + n (self noise)). Note that the spectrum is not bandlimited to $\frac{\omega}{c}$ as it was with sea noise alone (Fig. 2 - 2). Although this spectrum is not defined in the vicinity of ν_0 and beyond, this is a small restriction because m equally spaced hydrophones do not permit effective processing above ν_0 . By increasing m , one decreases the self noise level ξ (Eq. 2 - 46), and extends the effective processing range $(-\nu_0, \nu_0)$ (Eq. 2 - 43).

An important property of the intermediate form q_1 for self noise is that

$$\frac{L}{m} \sum_{h=1}^m q_1(\omega, x_h - y_h) f(y_h) = \frac{\eta L}{m} f(x_h) = \xi f(x_h) \quad 2 - 47$$

for any f defined at the hydrophone positions x_1, \dots, x_m . Now consider another noise process observed at x_1, \dots, x_m whose intermediate form is q'_1 and whose spatial set at ω_1 is

$$\{\psi_{ik}(x_h), \lambda'_{ik}, h = 1, \dots, m\}, ik \in D_1 \quad 2 - 48$$

determined by Eq. 1 - 42. According to Eq. 2 - 47 the addition of self noise to this process (q_1 in Eq. 2 - 42 is added to q'_1) will not change the spatial eigenfunctions. The only change, in fact, is the addition of the constant level ξ to each eigenvalue λ'_{ik} . In any noise model that includes self noise, then, none of the eigenvalues can be less than ξ . Since the self noise is added to the acoustic noise, the effect it will have depends on the ratio of ξ to the eigenvalues λ'_{ik} of the acoustic noise process. The relative self noise

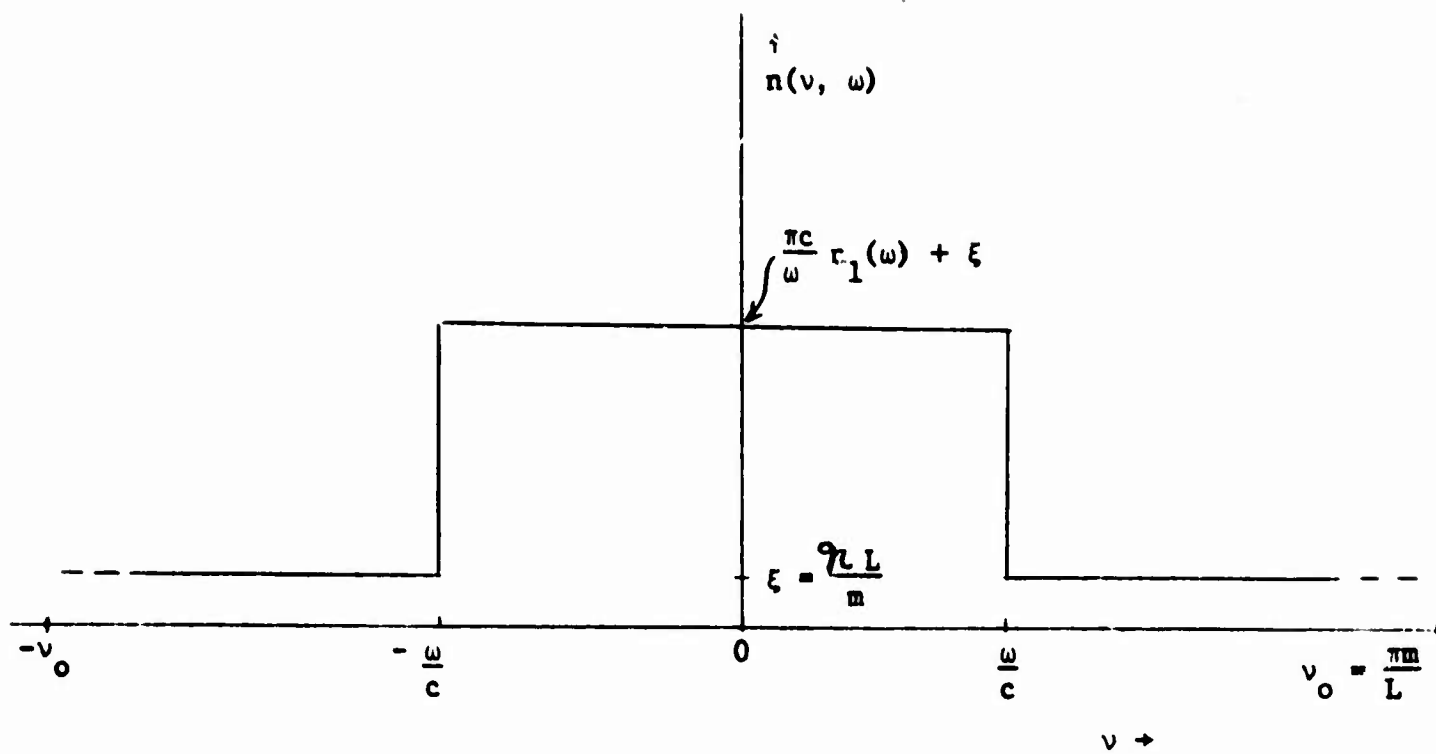


Figure 2 - 7 Spatial Spectrum of I3 Sea Noise plus Self Noise

level, defined by

$$\sigma(\omega) = \frac{\xi}{\sum_{k \in D(\omega)} \lambda_k'(\omega)} \quad 2 - 49$$

expresses this ratio. According to Eqs. 1 - 38 and 2 - 46 this is also

$$\sigma(\omega) = \frac{1}{m} \frac{\eta}{n_1'(\omega)} \quad 2 - 50$$

where η is the time spectral level of the self noise at a single hydrophone and $n_1'(\omega)$ is $n_1(\omega)$ for the acoustic noise process alone. When the acoustic noise is sea (homogeneous) noise, the ratio $\frac{\eta}{n_1'(\omega)}$ may be directly measured at a hydrophone output, using a narrow band filter of center frequency ω . If

$$R = \frac{\text{Filter power output with acoustic noise absent (self noise)}}{\text{Filter power output with acoustic noise present (self noise also present)}} \quad 2 - 51$$

then

$$\frac{\eta}{n_1'(\omega)} = \frac{R}{1 - R} \quad 2 - 52$$

When $\eta \ll n_1'$,

$$\frac{\eta}{n_1'(\omega)} \approx R \quad 2 - 53$$

2.4 The Signal Covariance Matrix

The "signal only" covariance matrix G defined by Eq. 1 - 19 depends upon the eigenfunctions of Q and hence on the prevailing noise conditions. Significant characteristics of the matrix G are presented in the following for the noise fields discussed in the first part of this chapter. To display these characteristics, a relative signal spectrum on the eigenfunctions used will be constructed from principal elements of G .

To derive an explicit form for G according to Eq. 1 - 19, the "signal only" covariance function P is needed. Repeating Eq. 1 - 4,

$$P(t, x, s, y | \underline{Y}) = \left\langle v(t, x | \underline{Y}) v^*(s, y | \underline{Y}) \right\rangle_{\text{signal only}} \quad 2 - 54$$

which depends, as indicated, on the signal source location vector $\underline{Y} \in \mathcal{R}$. Since the signal is assumed to 1) be emanating from a point source at \underline{Y} , 2) be propagating through a homogeneous nondispersive medium and, 3) be a member of a Gaussian process, the signal v received from \underline{Y} in the absence of background noise may be written

$$v(t, x | \underline{Y}) = \int_{-\infty}^{\infty} \rho(x | \underline{Y}) e^{j(t + \gamma(x | \underline{Y}))} dZ(\omega) \quad 2 - 55$$

in which $Z(\omega)$ is a complex Gaussian random point function with orthogonal increments. Furthermore,

$$Z(-\omega) = -Z^*(\omega), \quad 2 - 56$$

$$\left\langle dZ(\omega) dZ^*(\omega) \right\rangle = \frac{s(\omega)}{2\pi} d\omega \quad 2 - 57$$

and

$$s(-\omega) = s(\omega) \quad 2 - 58$$

where $s(\omega)$ is the two-sided signal power spectral density function observed at the center of the array. (For simplicity, the dependence of $s(\omega)$ on \underline{Y} caused by possible range dependent high frequency transmission loss will be omitted from the notation, i.e., $s(\omega) \equiv s(\omega|\underline{Y})$).

The time advance $\gamma(x|\underline{Y})$ along each separate wavefront relative to the center of the array ($\gamma(0|\underline{Y}) = 0$) is

$$\gamma(x|\underline{Y}) = \frac{1}{c} (|\underline{Y}| - \sqrt{|\underline{Y}|^2 + x^2 + 2x|\underline{Y}| \cos \beta}) \quad 2 - 59$$

The signal attenuation $\rho(x|\underline{Y})$, also relative to the array center ($\rho(0|\underline{Y}) = 1$), is

$$\rho(x|\underline{Y}) = \frac{1}{(1 + \frac{x^2}{|\underline{Y}|^2} - 2\frac{x}{|\underline{Y}|} \cos \beta)^{1/2}} \quad 2 - 60$$

where β is the angle of incidence of \underline{Y} (Fig. 1 - 1) and c is the velocity of propagation in the medium. When $|\underline{Y}| \gg L$,

$$\gamma(x|\underline{Y}) \approx \frac{1}{c} (x \cos \beta - \frac{x^2}{2|\underline{Y}|} \sin^2 \beta) \quad 2 - 61$$

and in the limit when the signal may be considered a plane wave,

$$\gamma(x|\underline{Y}) = \frac{1}{c} x \cos \beta \quad 2 - 62$$

and

$$\rho(x|\underline{Y}) = 1 \quad 2 - 63$$

Now the covariance function P (Eq. 2 - 54) is

$$\begin{aligned} P(t, x, s, y|\underline{Y}) &= \frac{1}{2\pi} \rho(x|\underline{Y}) \rho(y|\underline{Y}) \int_{-\infty}^{\infty} e^{j\omega(t-s+\gamma(x|\underline{Y}) - \gamma(y|\underline{Y}))} s(\omega) d\omega \\ &\equiv \frac{1}{2\pi} \alpha(x, y|\underline{Y}) \int_{-\infty}^{\infty} e^{j\omega(t-s-\tau(x, y|\underline{Y}))} s(\omega) d\omega \end{aligned} \quad 2 - 64$$

where

$$\alpha(x, y | \underline{Y}) = \rho(x | \underline{Y}) \rho(y | \underline{Y}) \quad 2 - 65$$

and

$$\tau(x, y | \underline{Y}) = \gamma(y | \underline{Y}) - \gamma(x | \underline{Y}) \quad 2 - 66$$

This covariance function P leads to an explicit form for G through Eq. 1 - 19. However, before leaving the discussion of P itself, it will be useful to obtain the total average signal power S in v . This is

$$S = \int_{-\frac{L}{2}}^{\frac{L}{2}} P(0; x, x) dx = M(\underline{Y}) \frac{L}{2\pi} \int_{-\infty}^{\infty} s(\omega) d\omega \quad 2 - 67$$

where

$$M(\underline{Y}) = \frac{1}{L} \int_{-\frac{L}{2}}^{\frac{L}{2}} \rho^2(x | \underline{Y}) dx \quad 2 - 68$$

For plane wave signals,

$$M(\underline{Y}) = 1 \quad 2 - 69$$

Now writing G according to Eq. 1 - 19 and recalling Eq. 2 - 64,

$$G(\underline{Y}) = (g_{ik} x \hat{i}_k(\underline{Y})) \quad 2 - 70$$

$$\begin{aligned} g_{ik} x \hat{i}_k(\underline{Y}) &= \int_{-\frac{L}{2}}^{\frac{L}{2}} \psi_{ik}^*(x) \int_{-\frac{L}{2}}^{\frac{L}{2}} \int_0^T \phi_1^*(t) \int_0^T P(t, x, s, y | \underline{Y}) \phi_1(s) ds dt \psi_{ik}(y) dy dx \\ &= \int_{-\frac{L}{2}}^{\frac{L}{2}} \psi_{ik}^*(x) \rho(x | \underline{Y}) \int_{-\frac{L}{2}}^{\frac{L}{2}} F_{ixi}(\tau(x, y | \underline{Y})) \psi_{ik}(y) \rho(y | \underline{Y}) dy dx \quad 2 - 71 \end{aligned}$$

where

$$F_{ixi}(\tau) \equiv \int_0^T \phi_i^*(t) \int_0^T \frac{1}{2\pi} \int_{-\infty}^{\infty} e^{j\omega(t-s-\tau)} s(\omega) d\omega \phi_i(s) ds dt . \quad 2 - 72$$

When

$$\phi_i(t) = \frac{1}{\sqrt{T}} e^{j\omega t} \textcircled{H} (t; 0, T) \quad 2 - 73$$

F assumes the simple form

$$F_{ixi}(\tau) \equiv \begin{cases} s_i e^{-j\omega_i \tau} & i = \hat{i} \\ 0 & i \neq \hat{i} \end{cases} \quad 2 - 74$$

$$(s_i \equiv s(\omega_i)) \quad 2 - 75$$

under the following conditions.

1. The signal power spectral density $s(\omega)$ is smooth over intervals $\Delta\omega = \frac{2\pi}{T}$ in ω .
2. The constant l defined by $l = \frac{cT}{\cos\theta}$ is very much greater than the array length L .

In this analysis it is supposed that these conditions hold well enough so that

$$g_{ik \times ik}^{(Y)} = \begin{cases} g_{k \times k}^{(Y)} & i = \hat{i} \\ 0 & i \neq \hat{i} \end{cases} \quad 2 - 76$$

$$g_{k \times k}^{(Y)} = \int_{-\frac{L}{2}}^{\frac{L}{2}} \psi_{ik}^*(x) \rho(x|Y) s_i \int_{-\frac{L}{2}}^{\frac{L}{2}} e^{-j\omega_i \tau(x,y|Y)} \psi_{ik}(y) \rho(y|Y) dy dx \quad 2 - 77$$

with negligible error.

Continuing with the nonzero elements of G , Eq. 2 - 66 indicates that

$$g_{kxk}^1(\underline{Y}) = s_1 h_{1k}(\underline{Y}) h_{1k}^*(\underline{Y}) \quad 2 - 78$$

in which

$$h_{1k}(\underline{Y}) \equiv \int_{-\frac{L}{2}}^{\frac{L}{2}} \psi_{1k}^*(x) e^{j\omega_1 Y(x|\underline{Y})} \rho(x|\underline{Y}) dx . \quad 2 - 79$$

Consequently with

$$\underline{h}_1(\underline{Y}) \equiv (h_{1k}(\underline{Y})), \quad 1k \in D_1, \quad 2 - 80$$

the single frequency (ω_1) submatrix G_1 of G defined by

$$G_1 \equiv (g_{kxk}^1) \quad 2 - 81$$

may be written

$$G_1(\underline{Y}) = s_1 \underline{h}_1(\underline{Y}) \underline{h}_1^*(\underline{Y}) . \quad 2 - 82$$

This result will be of primary importance to the detection analysis in the next chapter.

For the present note that

$$\underline{h}_{-1} = \underline{h}_1^* \quad 2 - 83$$

and, for normalization purposes, that

$$||\underline{h}_1(\underline{Y})||^2 = L M(\underline{Y}) . \quad 2 - 84$$

In particular, for plane waves,

$$||\underline{h}_1(\underline{Y})||^2 = L . \quad 2 - 85$$

In describing the nature of G_1 for different noise backgrounds, it is sufficient to consider \underline{h}_1 . For instance, the relative spatial

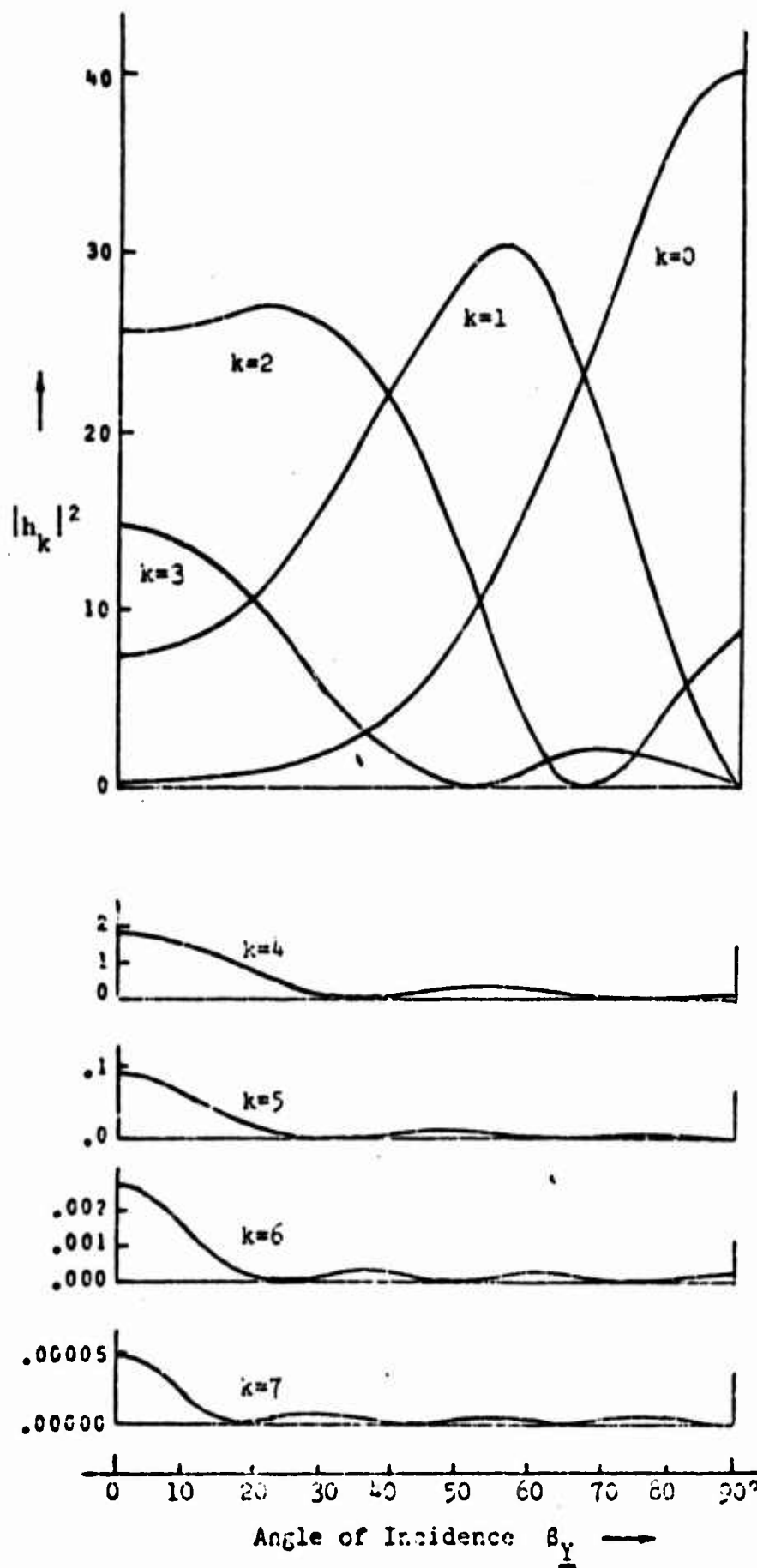
spectrum of the signal $\{|h_{1k}|^2\}$, $1k \in D_1$ shows how signal power is distributed within G_1 , or equivalently, how it is distributed on the spatial eigenfunctions $\{\psi_{1k}\}$, $1k \in D_1$. This spectrum is now plotted in two examples using the eigenfunctions shown in Figs. 2 - 3 and 2 - 5.

As a first example, the relative spatial spectrum of the signal $\{|h_k(\omega)|^2\}$, $k \in D(\omega)$ is given in Fig. 2 - 8 for plane wave signals incident between 0° and 90° . The spatial eigenfunctions used are those obtained for I3 sea noise at $\frac{\omega}{2\pi} = 40$ hz with an array length of 50 meters (see Fig. 2 - 3).

At 90° (broadside) incidence most of the average signal energy is received on ψ_0 . At 55° incidence most of the average signal energy is received on ψ_1 , and at 0° (endfire) incidence, on ψ_2 . When $k \geq 3$ the spectral component is a maximum for endfire signals. It is of interest to note that the angular interval in the endfire region over which the spectral component is large decreases as k increases. That is, the space eigenfunctions become more selective over incidence angle as k is increased.

As a second example, the spectrum $\{|h_k(\omega)|^2\}$, $k \in D(\omega)$ is obtained using the eigenfunctions for I3 sea noise plus 10 db of local noise (see Fig. 2 - 5). In table 2 - 1, which contains the results, the $k = 0$ element in the spectra of 0° incident and 180° incident signals shows that endfire signals from the negative end of the array have a large average power component on ψ_0 in Fig. 2 - 5, whereas endfire signals from the positive end of the array do not. This situation is reversed for ψ_2 and ψ_3 .

In this chapter, noise models for sea noise, local noise, interference and self noise were introduced. Examples were then given of spatial



$L = 50$ Meters
 $\omega = 2\pi \times 40 = 251$ RPS
 $c = 1500$ Meters/Sec
 Background Noise is
 13 Sea Noise
 $m = 12$ Hydrophones

Figure 2-3 Relative Spatial Spectra of the Signal in 13 Sea Noise

$ h_k(\omega, \theta) ^2$			
$k \backslash \theta$	0.0°	90.0°	180.0°
0	2.61	5.28	21.8
1	.624	39.5	.611
2	13.1	.592	7.37
3	27.8	4.54	14.3
4	5.40	.0902	5.32
5	.396	.0409	.514
6	.0186	.0000141	.0192
7	.000491	.0000453	.000472

$L = 50$ Meters
 $\omega = 2\pi \times 40$
 $= 251$ Rads/Sec
 $c = 1500$ Meters/Sec
 Background Noise is
 I3 Sea Noise
 + 10 db of Local Noise
 from Source
 at $x = -26$ Meters
 $m = 12$ Hydrophones

Relative Spatial Spectra of the Signal in I3 and Local Noise

Table 2 - 1

eigenfunctions fitting these models according to the definitions in the first chapter. Finally, G was expressed by its nonzero submatrices $(G_1 = s_1 \underline{h}_1 \underline{h}_1^*)$ and its characteristics were illustrated by two examples. Overall, it was the objective of this chapter to provide a familiarization with the elements λ , ψ , and \underline{h} which will be used in later descriptions of detector behavior.

CHAPTER 3

DETECTOR DEFINITIONS

3.0 Introduction

The three detectors whose behavior is analyzed in chapter 4 are the following:

1. The b-detector defined on page 20 - essentially the "optimum" detector of [1] and [3].
2. The c-detector - essentially the "conventional" or "power" detector. This detector will be derived by abbreviating the realization of the b-detector.
3. The ℓ -detector - the suboptimum detector introduced on page 21.

It should be remembered that analysis alone is the object here and that the equations and structures describing these detectors are not necessarily directly realizable in a practical detection system. The adaptation of the b-detector equations to practical realization is discussed in Appendix E.

Throughout the analysis to follow, Condition 1 on the smoothness of $s(\omega)$ and Condition 2 that $\ell \gg L$ on page 47 are presumed.

eigenfunctions fitting these models according to the definitions in the first chapter. Finally, G was expressed by its nonzero submatrices $\{G_1 = s_{1-1-1} \underline{h} \underline{h}^*\}$ and its characteristics were illustrated by two examples. Overall, it was the objective of this chapter to provide a familiarization with the elements λ , ψ , and \underline{h} which will be used in later descriptions of detector behavior.

CHAPTER 3

DETECTOR DEFINITIONS

3.0 Introduction

The three detectors whose behavior is analyzed in chapter 4 are the following:

1. The b-detector defined on page 20 - essentially the "optimum" detector of [1] and [3].
2. The c-detector - essentially the "conventional" or "power" detector. This detector will be derived by abbreviating the realization of the b-detector.
3. The ℓ -detector - the suboptimum detector introduced on page 21.

It should be remembered that analysis alone is the object here and that the equations and structures describing these detectors are not necessarily directly realizable in a practical detection system. The adaptation of the b-detector equations to practical realization is discussed in Appendix E.

Throughout the analysis to follow, Condition 1 on the smoothness of $s(\omega)$ and Condition 2 that $\ell \gg L$ on page 47 are presumed.

3.1 The b-Detector

The b-detector output, recalled from its definition on page 20 is

$$b(\underline{u}, \underline{X}) = \chi(\underline{u}, \underline{X}) - \ln \det(\Lambda + G(\underline{X})) + \ln \det \Lambda + \ln f_1(\underline{X}) . \quad 3 - 1$$

Now according to Eq. 2 - 76 and 2 - 82, the function χ (Eq. 1 - 55) may be expanded as follows.¹

$$\begin{aligned} \chi(\underline{u}, \underline{X}) &= - \left[(\Lambda + G(\underline{X}))^{-1} - \Lambda^{-1} \right] ||\underline{u}||^2 \\ &= - \sum_{i \in \Omega} \left[(\Lambda_i + G_i(\underline{X}))^{-1} - \Lambda_i^{-1} \right] ||\underline{u}_i||^2 \\ &= - \sum_{i \in \Omega} \left[(\Lambda_i + s_i \underline{h}_i(\underline{X}) \underline{h}_i^*(\underline{X}))^{-1} - \Lambda_i^{-1} \right] ||\underline{u}_i||^2 \\ &= \sum_{i \in \Omega} \frac{s_i |\underline{h}_i^*(\underline{X}) \Lambda_i^{-1} \underline{u}_i|^2}{1 + s_i \Lambda_i^{-1} ||\underline{h}_i(\underline{X})||^2} . \end{aligned} \quad 3 - 2$$

Similarly,

$$\begin{aligned} \ln \det(\Lambda + G(\underline{X})) &= \ln \det \Lambda \\ &= \sum_{i \in \Omega} \ln \frac{\det(\Lambda_i + s_i \underline{h}_i(\underline{X}) \underline{h}_i^*(\underline{X}))}{\det \Lambda_i} \\ &= \sum_{i \in \Omega} \ln \det(I + s_i \Lambda_i^{-1} \underline{h}_i(\underline{X}) \underline{h}_i^*(\underline{X})) . \end{aligned} \quad 3 - 3$$

Since the non-zero eigenvalue of the rank one matrix $\Lambda_i^{-1} \underline{h}_i \underline{h}_i^*$ is

¹The notation $C ||\underline{c}||^2$ denotes the quadratic form $\underline{c}^* C \underline{c}$.

$\Lambda_1^{-1} ||\underline{h}_1||^2$, the above determinant may be expressed in the following polynomial form.¹

$$\det(I + s_1 \Lambda_1^{-1} \underline{h}_1(\underline{X}) \underline{h}_1^*(\underline{X})) = 1 + s_1 \Lambda_1^{-1} ||\underline{h}_1(\underline{X})||^2. \quad 3 - 4$$

These relations (Eqs. 3 - 2, 3 - 3 and 3 - 4) allow the output of the b-detector as given by Eq. 3 - 1 to be written

$$b(\underline{u}, \underline{X}) = \sum_{i \in \Omega} \left[|\underline{z}_i^*(\underline{X}) \underline{u}_i|^2 - \ln(1 + s_1 \Lambda_1^{-1} ||\underline{h}_1(\underline{X})||^2) \right] + \ln f_1(\underline{X}) \quad 3 - 5$$

with the functional \underline{z}_1 defined by

$$\underline{z}_1(\underline{X}) = \sqrt{\frac{s_1}{1 + s_1 \Lambda_1^{-1} ||\underline{h}_1(\underline{X})||^2}} \Lambda_1^{-1} \underline{h}_1(\underline{X}). \quad 3 - 6$$

But $\underline{u}_{-1} = \underline{u}_1^*$ (Eq. 1 - 34) and

$$\underline{z}_{-1} = \underline{z}_1^* \quad 3 - 7$$

because $\underline{h}_{-1} = \underline{h}_1^*$ (Eq. 2 - 83) so that

$$|\underline{z}_{-1}^* \underline{u}_{-1}| = |\underline{z}_1^* \underline{u}_1| = |\underline{z}_1^* \underline{u}_1|. \quad 3 - 8$$

Consequently, if Ω^+ is the set of all positive indices in Ω ,

$$b(\underline{u}, \underline{X}) = 2 \sum_{i \in \Omega^+} \left[|\underline{z}_i^*(\underline{X}) \underline{u}_i|^2 - \ln(1 + s_1 \Lambda_1^{-1} ||\underline{h}_1(\underline{X})||^2) \right] + \ln f_1(\underline{X}). \quad 3 - 9$$

¹See Middleton [13], pp. 724, 725.

The processing of the received signal v to obtain \underline{u} and then $b(\underline{u}, \underline{X})$ is shown schematically in Fig. 3 - 1. The conversion from v to \underline{u} and subsequent noise weighting by Λ^{-1} is independent of the steering vector \underline{X} and takes place before steering is effected. Thus processing logically separates into the production of the weighted components $\frac{u_{1k}}{\lambda_{1k}}$ and the steering of the array according to \underline{X} .

Alternatively, the same result may be obtained starting with v and processing as shown in Fig. 3 - 2 (see [1]). The exact definitions of f , \mathcal{F} and S are left until after the following general explanation.

First, the received signal is delayed and attenuated along the array to match the delay $-\gamma(x|\underline{X})$ and the attenuation $\rho(x|\underline{X})$ along a wavefront arriving from the location at which the array is steered. Consider the received signal to be represented by (Eqs. 1 - 12 and 1 - 32)

$$v(t, x) = \sum_{1k \in D} u_{1k} \phi_1(t) \psi_{1k}(x) . \quad 3 - 10$$

Then since $\phi_1(t)$ is sinusoidal, the form

$$\sum_{1k \in D_1} u_{1k} \psi_{1k}(x) \quad 3 - 11$$

is the time frequency domain representation of $v(t, x)$, and the delayed and attenuated version in the frequency domain is

$$e^{-j \omega_1 \gamma(x|\underline{X})} \rho(x|\underline{X}) \sum_{1k \in D_1} u_{1k} \psi_{1k}(x) . \quad 3 - 12$$

Next, filters $f(\omega, x|\underline{X})$ accomplish shading along the array. In general, this shading is dependent on the time frequency ω and the steering vector \underline{X} . After shading the results are summed along

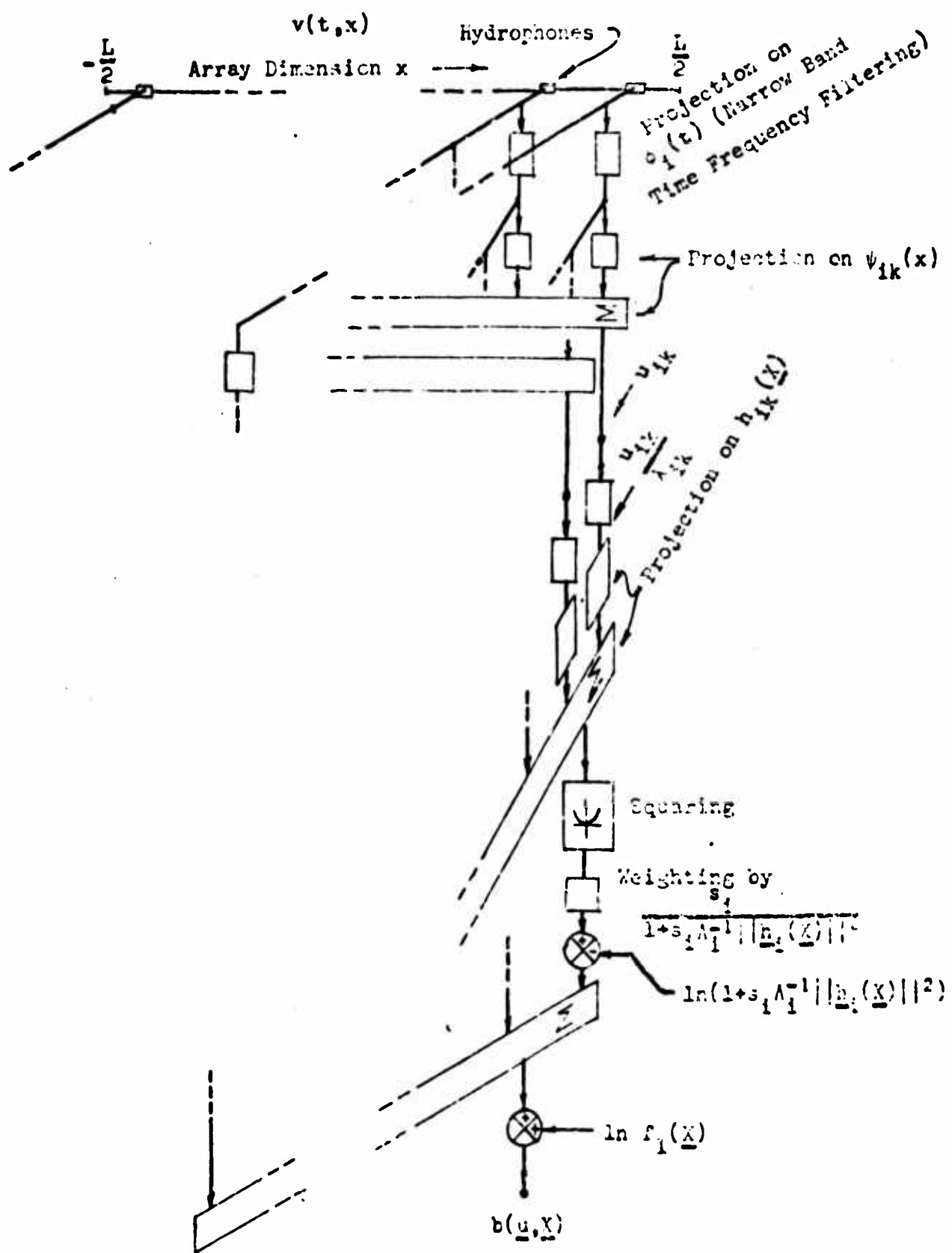


Figure 3-1 An Implementation of the b-Detector

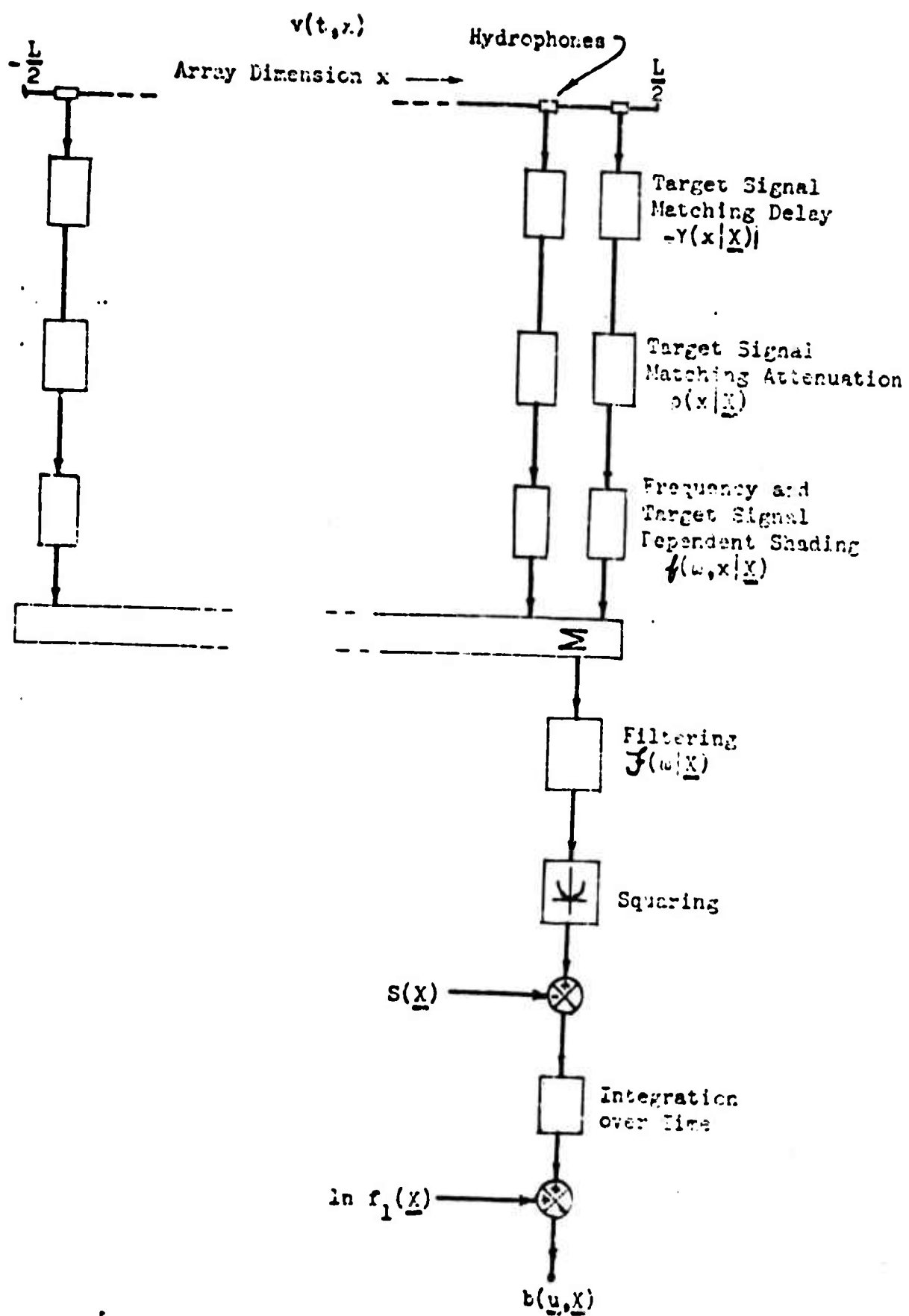


Figure 3-2 An Alternative b-Detector Structure

$x \in (-\frac{L}{2}, \frac{L}{2})$ and then the result is filtered according to $\mathcal{F}(\omega|\underline{X})$.

These operations yield

$$\mathcal{F}(\omega_1|\underline{X}) \sum_{1k \in D_1} u_{1k} \int_{-\frac{L}{2}}^{\frac{L}{2}} e^{-j\omega_1 \gamma(x|\underline{X})} \rho(x|\underline{X}) \phi(\omega_1, x|\underline{X}) \psi_{1k}(x) dx \quad 3 - 13$$

in the time frequency domain.

Returning to the time domain through multiplication by $\phi_1(t)$ followed by summation over the time frequency index set Ω , the expression

$$\sum_{1 \in \Omega} \phi_1(t) \mathcal{F}(\omega_1|\underline{X}) \sum_{1k \in D_1} u_{1k} \int_{-\frac{L}{2}}^{\frac{L}{2}} e^{-j\omega_1 \gamma(x|\underline{X})} \rho(x|\underline{X}) \phi(\omega_1, x|\underline{X}) \psi_{1k}(x) dx \quad 3 - 14$$

is obtained. This is now squared and unbiased by subtracting a term $S(\underline{X})$. And finally, the results are integrated over the observation interval $(0, T)$ and then weighted by adding $\ln f_1(\underline{X})$. The overall result is

$$\int_0^T \left| \sum_{1 \in \Omega} \phi_1(t) \mathcal{F}(\omega_1|\underline{X}) \sum_{1k \in D_1} u_{1k} \int_{-\frac{L}{2}}^{\frac{L}{2}} e^{-j\omega_1 \gamma(x|\underline{X})} \rho(x|\underline{X}) \phi(\omega_1, x|\underline{X}) \psi_{1k}(x) dx \right|^2 - S(\underline{X}) dt + \ln f_1(\underline{X}) \quad 3 - 15$$

When the square in the integrand is written explicitly, the integration over time may be performed over the product pairs $\phi_1(t) \phi_1^*(t)$. The orthogonality of the $\{\phi_1\}$ then reduces the above to

$$\sum_{1 \in \Omega} \left| \mathcal{F}(\omega_1|\underline{X}) \sum_{1k \in D_1} u_{1k} \int_{-\frac{L}{2}}^{\frac{L}{2}} e^{-j\omega_1 \gamma(x|\underline{X})} \rho(x|\underline{X}) \phi(\omega_1, x|\underline{X}) \psi_{1k}(x) dx \right|^2 - TS(\underline{X}) + \ln f_1(\underline{X}) \quad 3 - 16$$

This detector output is seen to be in a form similar to that in Eq. 3 - 9. Hence if the above is equated with the right-hand side of this equation, it is apparent that the total index set Ω may be replaced with Ω^+ , the set of all positive indices in Ω , and that

$$\begin{aligned}
 |\mathcal{F}(\omega_1|\underline{X})| &= \int_{-\frac{L}{2}}^{\frac{L}{2}} e^{-j\omega_1\gamma(x|\underline{X})} \rho(x|\underline{X}) \phi(\omega_1, x|\underline{X}) \psi_{1k}(x) dx \\
 &= \sqrt{\frac{2 s_1}{1+s_1\Lambda_1^{-1}||\underline{h}_1(\underline{X})||^2}} \frac{1}{\lambda_{1k}} \int_{-\frac{L}{2}}^{\frac{L}{2}} \psi_{1k}(x) e^{-j\omega_1\gamma(x|\underline{X})} \rho(x|\underline{X}) dx \quad 3 - 17
 \end{aligned}$$

and

$$\begin{aligned}
 S(\underline{X}) &= \frac{2}{T} \sum_{1 \in \Omega^+} \ln(1 + s_1 \Lambda_1^{-1} ||\underline{h}_1(\underline{X})||^2) \\
 &= \frac{1}{\pi} \int_0^\infty \ln(1+s(\omega) \Lambda^{-1}(\omega) ||\underline{h}(\omega, \underline{X})||^2) d\omega . \quad 3 - 18
 \end{aligned}$$

The phase of $\mathcal{F}(\omega|\underline{X})$ is arbitrary. For each $1 \in D_1$ the two sides of Eq. 3 - 17 may be regarded as elements of a vector relative to the basis $\{\psi_{1k}\}$. Returning to the space domain one obtains the following expression for $\mathcal{F}(\omega_1|\underline{X}) \phi(\omega, y|\underline{X})$,

$$|\mathcal{F}(\omega_1|\underline{X})| \sum_{1k \in D_1} \int_{-\frac{L}{2}}^{\frac{L}{2}} e^{-j\omega_1 \gamma(x|\underline{X})} \rho(x|\underline{X}) f(\omega_1, x|\underline{X}) \psi_{1k}(x) dx \psi_{1k}^*(y)$$

$$= |\mathcal{F}(\omega_1|\underline{X})| \rho(y|\underline{X}) e^{-j\omega_1 \gamma(y|\underline{X})} f(\omega_1, y|\underline{X})$$

3 - 19

$$= \sqrt{\frac{2 s_1}{1+s_1 \Lambda_1^{-1} ||\underline{h}_1(\underline{X})||^2}} \sum_{1k \in D_1} \frac{\int_{-\frac{L}{2}}^{\frac{L}{2}} \psi_{1k}(x) e^{-j\omega_1 \gamma(x|\underline{X})} \rho(x|\underline{X}) dx}{\lambda_{1k}} \psi_{1k}^*(y)$$

so that

$$|\mathcal{F}(\omega_1|\underline{X})| f(\omega_1, y|\underline{X}) =$$

$$\sqrt{\frac{2 s_1}{1+s_1 \Lambda_1^{-1} ||\underline{h}_1(\underline{X})||^2}} \frac{e^{j\omega_1 \gamma(y|\underline{X})}}{\rho(y|\underline{X})} \sum_{1k \in D_1} \frac{\int_{-\frac{L}{2}}^{\frac{L}{2}} \psi_{1k}(x) e^{-j\omega_1 \gamma(x|\underline{X})} \rho(x|\underline{X}) dx}{\lambda_{1k}} \psi_{1k}^*(y)$$

$$= \sqrt{\frac{2 s_1}{1+s_1 \Lambda_1^{-1} ||\underline{h}_1(\underline{X})||^2}} \frac{e^{j\omega_1 \gamma(y|\underline{X})}}{\rho(y|\underline{X})} \sum_{1k \in D_1} \frac{h_{1k}^*(\underline{X})}{\lambda_{1k}} \psi_{1k}^*(y) .$$

3 - 20

The magnitude of the space independent factor \mathcal{F} may be separated from this. The phase of \mathcal{F} may be assigned as is most convenient in the design of the actual filters \mathcal{F} and f .

3.2 The c-Detector

For signals from within a given region \mathcal{R} , h_{1k} is appreciable only for the set D_1 of indices $1k$. If λ_{1k} is constant over this set, the b-detector implementation may be simplified considerably. The resulting detector, labeled the c-detector, is similar to the "standard" or "conventional" detector. Without changing its structure, the definition of the c-detector is extended to cover conditions under which the λ_{1k} are unequal. The c-detector is then considered a separate detector and its characteristics compared with the unsimplified b-detector. In the next chapter quantitative measures will establish typical physical conditions for the c-detector to be equivalent to the b-detector. When it is not equivalent, the c-detector will not perform as well as the b-detector. The specific differences will also be discussed in the next chapter.

The mathematical definition of the c-detector follows from two relations derived from the condition that the significant $\lambda_{1k} \in D_1$ all be the same. These relations are

$$\begin{aligned} \sum_{1k \in D_1} \frac{h_{1k}}{\lambda_{1k}} \psi_{1k}^*(y) &= \frac{1}{\lambda_1} \sum_{1k \in D_1} \int_{-\frac{L}{2}}^{\frac{L}{2}} \psi_{1k}(x) e^{-j\omega_1 \gamma(x|X)} \rho(x|X) dx \psi_{1k}^*(y) \\ &= \frac{1}{\lambda_1} e^{-j\omega_1 \gamma(y|X)} \rho(y|X) \end{aligned} \quad 3 - 21$$

and

$$s_1 \lambda_1^{-1} ||\underline{h}_1(X)||^2 = \frac{s_1}{\lambda_1} ||\underline{h}_1(X)||^2 = \frac{s_1}{\lambda_1} LM(X) \quad 3 - 22$$

in which $\lambda_1 = \lambda_{1k}$ for all $1k \in D_1$. If the first relation is placed in Eq. 3 - 20, it is observed that the shading $f(\omega, x|X)$ for the

c-detector is uniform in x along the array. In virtue of the two relations, in fact, the assignments

$$f(\omega, x|\underline{X}) = 1 \quad 3 - 23$$

and

$$\begin{aligned} |\mathcal{F}(\omega|\underline{X})|^2 &= \frac{s(\omega)}{\lambda^2(\omega)} \frac{1}{1+s(\omega)\Lambda^{-1}(\omega) ||\underline{h}(\omega, \underline{X})||^2} \\ &= \frac{s(\omega)}{\lambda^2(\omega)} \frac{1}{1+\frac{s(\omega)}{\lambda(\omega)} LM(\underline{X})} \end{aligned} \quad 3 - 24$$

may be made. Also

$$S(\underline{X}) = \frac{1}{\pi} \int_0^\infty \ln\left(1+\frac{s(\omega)}{\lambda(\omega)} LM(\underline{X})\right) d\omega. \quad 3 - 25$$

If the signals to be detected are plane waves, then $M(\underline{X}) = 1$ and the second relation shows that the term $s_1 \Lambda_1^{-1} ||\underline{h}_1(\underline{X})||^2$ does not vary with the steering direction \underline{X} . Hence, for plane wave signals, \mathcal{F} and S are independent of the steering direction \underline{X} , and the particularly simple schematic shown in Fig. 3 - 3 results.

In these assignments, when the significant $\lambda_k(\omega) \in D(\omega)$ are unequal, $\lambda(\omega)$ is undefined. A definition for $\lambda(\omega)$ that is consistent when the significant $\lambda_k(\omega)$ are equal and which also defines $\lambda(\omega)$ in a reasonable way when the $\lambda_k(\omega)$ are unequal is as follows.

$$\lambda(\omega) \equiv \lambda(\omega, \underline{Z})$$

$$\begin{aligned} &= \frac{1}{\int_{-\frac{L}{2}}^{\frac{L}{2}} \rho(x|\underline{Z})^2 dx} \sum_{k \in D(\omega)} \lambda_k(\omega) \left| \int_{-\frac{L}{2}}^{\frac{L}{2}} \psi_k(\omega, x) e^{-j\omega\gamma(x|\underline{Z})} \rho(x|\underline{Z}) dx \right|^2 \\ &= \frac{1}{LM(\underline{Z})} \Lambda(\omega) ||\underline{h}(\omega, \underline{Z})||^2. \end{aligned}$$

3 - 26

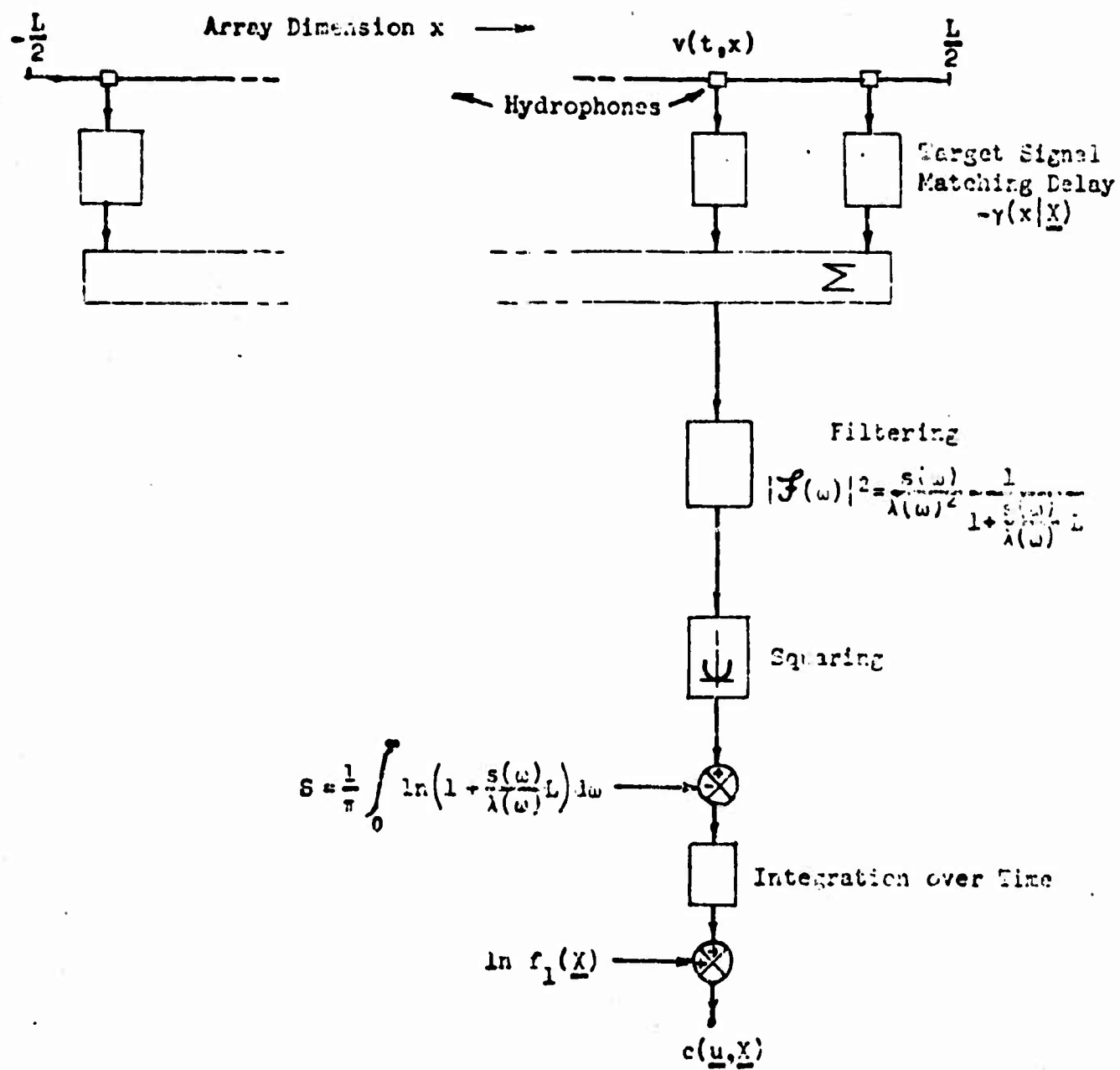


Figure 3-3 Implementation of the c-Detector for Plane Wave Detection

The vector \underline{z} is some representative vector in \mathcal{R} . This definition leaves the structure of the c-detector unchanged for all detection situations within \mathcal{R} , and it can always be compared with the b-detector. To facilitate this comparison, the output of the c-detector $c(\underline{u}, \underline{X})$ is expressed in the form of Eq. 3 - 9 as follows. According to Eqs. 3 - 16 and 3 - 23,

$$c(\underline{u}, \underline{X}) = 2 \sum_{1 \in \Omega+} \left\{ \left| \mathcal{F}(\omega_1 | \underline{X}) \sum_{1k \in D_1} u_{1k} \int_{-\frac{L}{2}}^{\frac{L}{2}} \psi_{1k}(x) e^{-j\omega_1 \gamma(x | \underline{X})} \rho(x | \underline{X}) dx \right|^2 - \ln \left(1 + \frac{s_1}{\lambda_1} LM(\underline{X}) \right) \right\} + \ln f_1(\underline{X})$$

$$= 2 \sum_{1 \in \Omega+} \left\{ \left| \mathcal{F}(\omega_1 | \underline{X}) \underline{h}_1^{*'}(\underline{X}) \underline{u}_1 \right|^2 - \ln \left(1 + \frac{s_1}{\lambda_1} LM(\underline{X}) \right) \right\} + \ln f_1(\underline{X}) . \quad 3 - 27$$

As demonstrated above, this c-detector is equivalent to the b-detector whenever the λ_{1k} are the same over the significant indices $1k \in D_1$. In the first example on page 49, h_{1k} (Fig. 2 - 8) for broadside signals ($\beta = 90^\circ$) is relatively insignificant when $k \neq 0$. In this example, then, the b and c-detectors may be expected to be approximately equivalent when detecting broadside signals. According to Figs. 2 - 4 and 2 - 2 and Eq. 3 - 24, the filter \mathcal{F} would be described by

$$|\mathcal{F}(\omega, \underline{X})|^2 \cong \frac{s(\omega)}{n_1(\omega)^2} \frac{\omega^2}{\pi^2 c^2} \frac{1}{1 + \frac{s(\omega)}{n_1(\omega)} \frac{\omega}{\pi c} LM(\underline{X})} \quad 3 - 28$$

for detection in an I3 sea noise background. And according to Fig. 2 - 1, \mathcal{F} would be described by

$$|\mathcal{F}(\omega | \underline{X})|^2 \cong \frac{s(\omega)}{n_1(\omega)^2} \frac{\omega^2}{4c^2} \frac{1}{1 + \frac{s(\omega)}{n_1(\omega)} \frac{\omega}{2c} LM(\underline{X})} \quad 3 - 29$$

\underline{X} in a near broadside direction

for detection in an I2 sea noise background.

A quantitative comparison of the b and c-detectors is made once performance measures are defined. It will be shown that broadside signal incidence and high time frequency generally favor equivalence.

3.3 The ℓ -Detector

The output of the ℓ -detector defined on page 21 is written

$$\begin{aligned} \ell(\underline{u}, \underline{X}) &= \Lambda^{-1} \|\underline{u}\|^2 + \ln \det \pi \Lambda + \ln f_1(\underline{X}) \\ &= 2 \sum_{i \in \Omega} \left\{ \Lambda_i^{-1} \|\underline{u}_i\|^2 + \ln \det \pi \Lambda_i \right\} + \ln f_1(\underline{X}) \\ &= 2 \sum_{i \in \Omega} \sum_{ik \in D_i(\underline{X})} \left\{ \frac{|\underline{u}_{ik}|^2}{\lambda_{ik}} + \ln \pi \lambda_{ik} \right\} + \ln f_1(\underline{X}) . \end{aligned} \quad 3 - 30$$

(The index set D_i in this expression is allowed to vary with \underline{X} to provide a crude form of steering.) In the processing indicated above, the quantities \underline{u}_{ik} may be generated as in the first stages of the processing shown in Fig. 3 - 1. From this point on, however, the processing is simple compared with the b-detector. Following Fig. 3 - 4, the elements $\frac{|\underline{u}_{ik}|^2}{\lambda_{ik}} + \ln \pi \lambda_{ik}$ formed without regard to the steering vector \underline{X} are included or not included in a summation, depending upon whether the index ik is contained in $D_i(\underline{X})$. Summation over time frequency and weighting by the a priori probability density function $f_1(\underline{X})$ then complete the ℓ -detector processing.

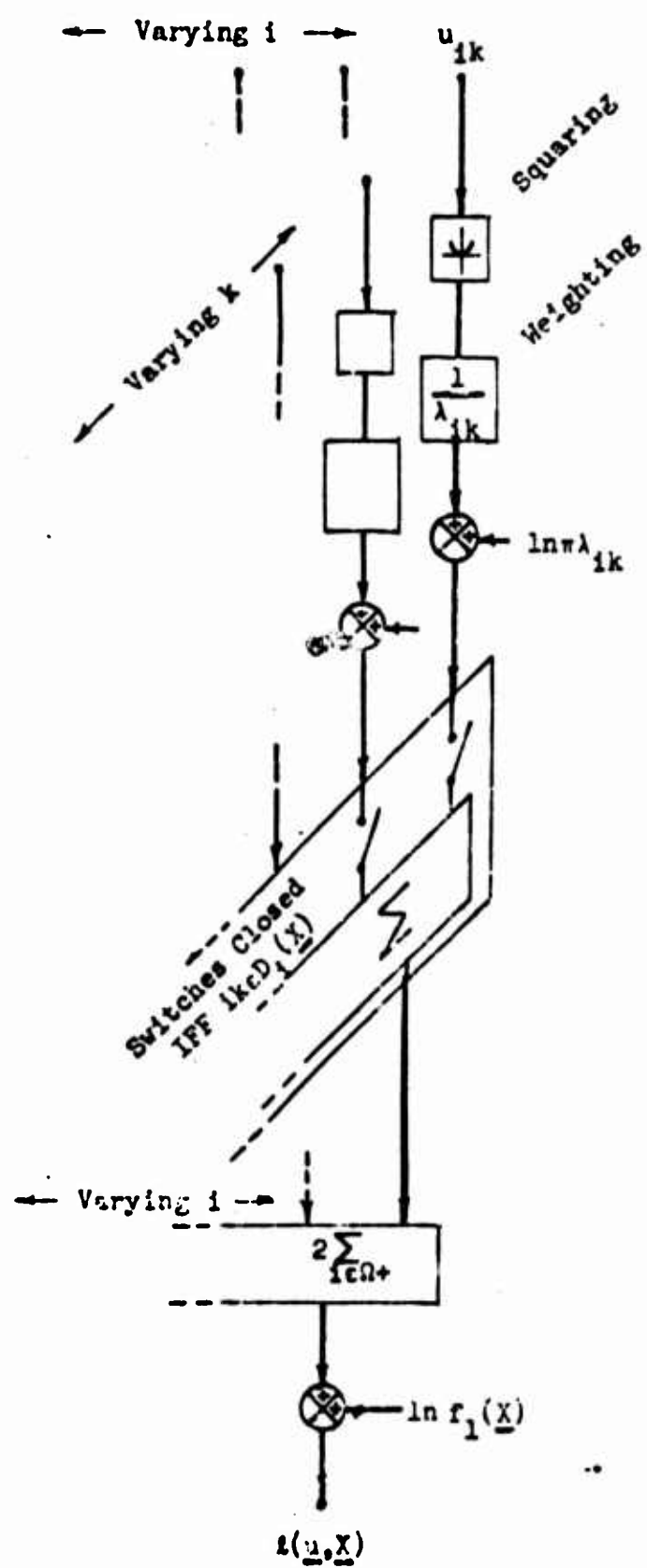


Figure 3-4 The l -Detector

CHAPTER 4

OUTPUT SNR AND ARRAY GAIN

4.0 Introduction

Now that the b , c , and l -detectors have been explicitly defined, performance measures may be employed to describe their behavior and relate it to the specifications of the array and the characteristics of the noise field. The performance measures used are 1. the output signal to noise ratio [14], 2. the array gain [1, 3], which is related to the output signal to noise ratio, and 3. directivity measures (to include measures of the ability of the detector to locate the signal source). Measures 1 and 2 are treated in this chapter and 3 is the subject of chapter 5. Each of these performance measures is first defined in general and then in particular for the b , c , and l -detectors (where applicable).

4.1 The Output SNR and Array Gain

The output signal to noise ratio ϕ for a detector steered toward \underline{X} in the presence of a signal source at \underline{Y} is defined by

$$\phi(\underline{X}|\underline{Y}) = \frac{\text{increase in average detector output due to the presence of signal}}{\text{standard deviation of the detector output when signal and noise are present}} \quad 4 - 1$$

If $\mathcal{H}(\underline{u}, \underline{X})$ is the output of a detector focused on \underline{X} , and the subscript $S(\underline{Y})$ denotes the presence of a signal source at \underline{Y} , and N denotes the presence of a noise background, then the above may be written

$$\phi(\underline{X}|\underline{Y}) = \frac{\langle \mathcal{H}(\underline{u}, \underline{X}) \rangle_{S(\underline{Y})+N} - \langle \mathcal{H}(\underline{u}, \underline{X}) \rangle_N}{\sqrt{V(\mathcal{H}(\underline{u}, \underline{X}))_{S(\underline{Y})+N}}} \quad 4 - 2$$

At the low input signal to noise ratios assumed here

$$V(\mathcal{H}(\underline{u}, \underline{X}))_{S+N} \approx V(\mathcal{H}(\underline{u}, \underline{X}))_N \quad 4 - 3$$

so that the equation

$$\phi(\underline{X}|\underline{Y}) = \frac{\langle \mathcal{H}(\underline{u}, \underline{X}) \rangle_{S(\underline{Y})+N} - \langle \mathcal{H}(\underline{u}, \underline{X}) \rangle_N}{\sqrt{V(\mathcal{H}(\underline{u}, \underline{X}))_N}} \quad 4 - 4$$

may replace Eq. 4 - 2 with negligible error. For simplicity, this replacement is made throughout the following text.

The output \mathcal{H} of all three detectors considered here may be written in the form

$$\mathcal{H}(\underline{u}, \underline{X}) = 2 \sum_{i \in \Omega^+} W_i(\underline{u}_i, \underline{X}) + C(\underline{X}) \quad 4 - 5$$

in which C is a bias term and in which it is reasonable to regard \underline{u}_i independent of $\underline{u}_{i'}$ for i and $i' \in \Omega^+$ whenever $i \neq i'$ (see

Eqs. 1 - 17 and 2 - 76). Consequently the output signal to noise ratio for a detector of the form of Eq. 4 - 5 is expressed by

$$\phi(\underline{X}|\underline{Y}) = \frac{\sum_{i \in \Omega+} [\langle W_1(\underline{u}_1, \underline{X}) \rangle_{S(\underline{Y})+N} - \langle W_1(\underline{u}_1, \underline{X}) \rangle_N]}{\sqrt{\sum_{i \in \Omega+} V[W_1(\underline{u}_1, \underline{X})]_N}} \quad 4 - 6$$

Since a long observation time is assumed, the above summations may be replaced by integrals, the argument ω now corresponding to the time frequency index i . In fact, with negligible error

$$\phi(\underline{X}|\underline{Y}) = \frac{\sqrt{\frac{T}{2\pi}} \int_0^\infty [\langle W(\underline{u}(\omega), \omega, \underline{X}) \rangle_{S(\underline{Y})+N} - \langle W(\underline{u}(\omega), \omega, \underline{X}) \rangle_N] d\omega}{\sqrt{\int_0^\infty V[W(\underline{u}(\omega), \omega, \underline{X})]_N d\omega}} \quad 4 - 7$$

In a sufficiently narrow time frequency band of width $\Delta\omega$ about a frequency ω , the output signal to noise ratio is

$$\phi(\omega, \underline{X}|\underline{Y}) = \sqrt{\frac{T\Delta\omega}{2\pi}} \frac{\langle W(\underline{u}(\omega), \omega, \underline{X}) \rangle_{S(\underline{Y})+N} - \langle W(\underline{u}(\omega), \omega, \underline{X}) \rangle_N}{\sqrt{V[W(\underline{u}(\omega), \omega, \underline{X})]_N}} \quad 4 - 8$$

The array gain \mathcal{G} is obtained from this narrowband output signal to noise ratio by dividing out the dependence on the input signal to noise ratio, the observation time and the bandwidth. In fact,

$$\mathcal{G}(\omega, \underline{X}|\underline{Y}) = \frac{\phi(\omega, \underline{X}|\underline{Y})}{\frac{S}{N} \sqrt{\frac{T\Delta\omega}{2\pi}}} \quad 4 - 9$$

where S is the average signal power in \underline{u} , and N the total average noise power in \underline{u} . The self noise is thus included in N . Toward a

more explicit form for the above, it is noted that (see Eqs. 1 - 35 and 2 - 67)

$$\frac{S}{N} = M(\underline{Y}) \frac{s(\omega)}{n_1(\omega)} \quad 4 - 10$$

over a band that is narrow relative to variations in $s(\omega)$ and $n_1(\omega)$. Thus

$$\mathcal{G}(\omega, \underline{X}|\underline{Y}) = \frac{\phi(\omega, \underline{X}|\underline{Y})}{\frac{s(\omega)}{n_1(\omega)} M(\underline{Y}) \sqrt{\frac{T\Delta\omega}{2\pi}}} \quad 4 - 11$$

If this definition of the array gain (Eq. 4 - 11) is inverted, the relation

$$\phi(\omega, \underline{X}|\underline{Y}) = \frac{s(\omega)}{n_1(\omega)} M(\underline{Y}) \sqrt{\frac{T}{2\pi}\Delta\omega} \mathcal{G}(\omega, \underline{X}|\underline{Y}) \quad 4 - 12$$

is obtained. It is apparent from this that the array gain is as significant as the output signal to noise ratio in evaluating the narrow band performance of detectors of the type described by Eq. 4 - 5. Since the array gain does not depend upon the observation time, the bandwidth, or the input signal to noise ratio, it is a much simpler performance measure to use in comparing detectors. In addition, if the detector is known to detect as well as possible, the array gain may be used as a direct measure of the detectability of given signals.

4.2 The Array Gain for the b and c-Detectors

a) General Definition

For both the b and c-detectors the single frequency output W in Eq. 4 - 5 may be written

$$W(\underline{u}(\omega), \omega, \underline{X}) = |\underline{z}(\omega, \underline{X})^* \underline{u}(\omega)|^2 \quad 4 - 13$$

where

$$\underline{z}(\omega) = (\underline{z}_k(\omega)), k \in D(\omega) \quad 4 - 14$$

is a linear functional. The signal and noise being additive and independent, the average $\langle W \rangle_{S+N}$ in the numerator of Eq. 4 - 8 may be written

$$\langle W \rangle_{S+N} = \langle W \rangle_S + \langle W \rangle_N. \quad 4 - 15$$

Furthermore, the variance in the denominator may be written (Eq. C-18)

$$V(W) = \langle W \rangle_N^2 \quad 4 - 16$$

so that finally

$$\phi(\omega, \underline{X}|\underline{Y}) = \sqrt{\frac{T\Delta\omega}{2\pi}} \frac{\langle W(\underline{u}(\omega), \omega, \underline{X}) \rangle_{S(\underline{Y})}}{\langle W(\underline{u}(\omega), \omega, \underline{X}) \rangle_N}. \quad 4 - 17$$

The array gain for the b and c-detectors may now be written (Eq. 4 - 11)

$$\mathcal{G}(\omega, \underline{X}|\underline{Y}) = \frac{\langle W(\underline{u}(\omega), \omega, \underline{X}) \rangle_{S(\underline{Y})}}{\langle W(\underline{u}(\omega), \omega, \underline{X}) \rangle_N} \bigg/ \frac{s(\omega)}{n_1(\omega)} M(\underline{Y}). \quad 4 - 18$$

In words, this expression is

array gain for	average detector output when	
narrow band b or c-	input is a signal from \underline{Y}	
detector operating about	(no self or background noise)	
ω and steered at \underline{X}	average detector output when	4 - 19
	input is "noise only"	
	input signal to noise ratio	

An explicit form for the single frequency array gain is obtained from Eqs. C - 17, 1 - 17, 1 - 18, and 2 - 82.

$$\begin{aligned} \langle W(\underline{u}(\omega), \omega, \underline{X}) \rangle_{S(\underline{Y})} &= G(\omega, \underline{Y}) ||\underline{z}(\omega, \underline{X})||^2 \\ &= s(\omega) \underline{h}(\omega, \underline{Y}) \underline{h}^{*'}(\omega, \underline{Y}) ||\underline{z}(\omega, \underline{X})||^2 = s(\omega) \underline{z}^{*'}(\omega, \underline{X}) \underline{h}(\omega, \underline{Y})^2 \end{aligned} \quad 4 - 20$$

and

$$\langle W(\underline{u}(\omega), \omega, \underline{X}) \rangle_N = \Lambda(\omega) ||\underline{z}(\omega, \underline{X})||^2 \quad 4 - 21$$

Thus

$$\mathcal{G}(\omega, \underline{X}|\underline{Y}) = \frac{n_1(\omega) |\underline{z}^{*'}(\omega, \underline{X}) \underline{h}(\omega, \underline{Y})|^2}{M(\underline{Y}) \Lambda(\omega) ||\underline{z}(\omega, \underline{X})||^2} \quad 4 - 22$$

b) b-Detector Array Gain

In single frequency notation, the functional \underline{z} in Eq. 4 - 13 is

$$\underline{z}(\omega, \underline{X}) = \underline{z}(\omega, \underline{X}) = \sqrt{\frac{s(\omega)}{1+s(\omega)\Lambda^{-1}(\omega) ||\underline{h}(\omega, \underline{X})||^2}} \Lambda^{-1}(\omega) \underline{h}(\omega, \underline{X}) \quad 4 - 23$$

The array gain $\mathcal{G}^{(b)}$, then, for this detector is

$$\mathcal{G}^{(b)}(\omega, \underline{X}|\underline{Y}) = \frac{n_1(\omega) |\underline{h}^{*'}(\omega, \underline{X}) \Lambda^{-1}(\omega) \underline{h}(\omega, \underline{Y})|^2}{M(\underline{Y}) \Lambda^{-1}(\omega) ||\underline{h}(\omega, \underline{X})||^2} \quad 4 - 24$$

Since the form

$$\frac{|\underline{h}^{*'}(\omega, \underline{X}) \Lambda^{-1}(\omega) \underline{h}(\omega, \underline{Y})|^2}{\Lambda^{-1}(\omega) ||\underline{h}(\omega, \underline{X})||^2 \Lambda^{-1}(\omega) ||\underline{h}(\omega, \underline{Y})||^2} \quad 4 - 25$$

has a maximum over $\underline{X} \in \mathcal{Q}$ at $\underline{X} = \underline{Y}$, it follows that $\mathcal{G}^{(b)}(\omega, \underline{X}|\underline{Y})$ is also a maximum at $\underline{X} = \underline{Y}$. That is,

$$\mathcal{G}^{(b)}(\omega, \underline{Y}|\underline{Y}) \geq \mathcal{G}^{(b)}(\omega, \underline{X}|\underline{Y}) \quad 4 - 26$$

It will be said that the b-detector is "focused" on \underline{Y} when $\underline{X} = \underline{Y}$.

In that case the array gain simplifies to

$$\mathcal{J}^{(b)}(\omega, \underline{Y}|\underline{Y}) = \frac{n_1(\omega)}{M(\underline{Y})} \Lambda^{-1}(\omega) ||\underline{h}(\omega, \underline{Y})||^2 \quad 4 - 27$$

In explicit form this is

$$\mathcal{J}^{(b)}(\omega, \underline{Y}|\underline{Y}) = \sum_{k \in D(\omega)} \frac{|h_k(\omega, \underline{Y})|^2}{\lambda_k(\omega)} \frac{n_1(\omega)}{M(\underline{Y})} \quad 4 - 28$$

It is apparent from Eqs. 1 - 38 and 2 - 84 that

$$\mathcal{J}^{(b)} \geq 1 \quad 4 - 29$$

For if $\mathcal{J}^{(b)}$ were less than one, then all the terms in the summation would have to be less than one because all the terms are positive. But this would imply that

$$\frac{1}{M(\underline{Y})L} \sum_{k \in D(\omega)} |h_k(\omega, \underline{Y})|^2 < \frac{1}{\sum_{k \in D(\omega)} \lambda_k(\omega)} \sum_{k \in D(\omega)} \lambda_k(\omega) \quad 4 - 30$$

which is not true.

Equation 4-28 also indicates that $\mathcal{J}^{(b)}$ is the sum of individual 'channel factors' defined by

$$\mathcal{C}_k(\omega, \underline{Y}) = \frac{n_1(\omega)}{M(\underline{Y})} \frac{|h_k(\omega, \underline{Y})|^2}{\lambda_k(\omega)} \quad 4 - 31$$

Since

$$\mathcal{J}^{(b)}(\omega, \underline{Y}|\underline{Y}) = \sum_{k \in D(\omega)} \mathcal{C}_k(\omega, \underline{Y}) \quad 4 - 32$$

the relative size of $\mathcal{C}_k(\omega, \underline{Y})$ may be used as a measure of the relative significance to detection at time frequency ω of the projection of \underline{v}

on the eigenfunction $\phi(\omega)\psi_k(\omega)$. When designing an actual detector, this information is used to determine the elements that the index set $D(\omega)$ will contain.

If the overall noise process is sufficiently isotropic, the observed processes at distinct hydrophones will become independent as the hydrophone separation is increased (see page 16). Supposing that the noise observations at the hydrophones are independent and in addition that the overall external noise process is homogeneous, the eigenvalues (corresponding to the eigenfunctions given in Eqs. 1 - 44 and 1 - 45) in the expression (Eq. 4 - 28) for the array gain will all be equal. Since

$$n_1(\omega) = \frac{1}{L} \sum_{k \in D(\omega)} \lambda_k(\omega) \quad 4 - 33$$

(Eq. 1 - 38), their value must be

$$\lambda_k(\omega) = \frac{n_1(\omega) L}{m} \quad 4 - 34$$

where m is the number of hydrophones. Finally, placing this in the right-hand side of Eq. 4 - 28 and referring to Eq. 2 - 84, the b-detector array gain equation

$$\mathcal{G}^{(b)}(\omega, \underline{Y}|\underline{Y}) = m \quad 4 - 35$$

is obtained for independent hydrophones in a homogeneous noise field.

(Plotting this on polar coordinates, a circular pattern results.)

When there is only one hydrophone in the array, the array gain attains its lower limit of unity (Eq. 4 - 29) regardless of the noise field.

The channel factors are plotted in Fig. 4 - 1 for the 13 sea noise example given on pages 26 and 49. The time frequency is 40 Hz, the array length is 50 meters and the incident signals are plane waves

$L = 50$ Meters
 $\omega = 2\pi \times 40 = 251$ RPS
 $m = 12$ Hydrophones

Background Noise
 is 13 Sea Noise
 $c = 1500$ Meters/Sec

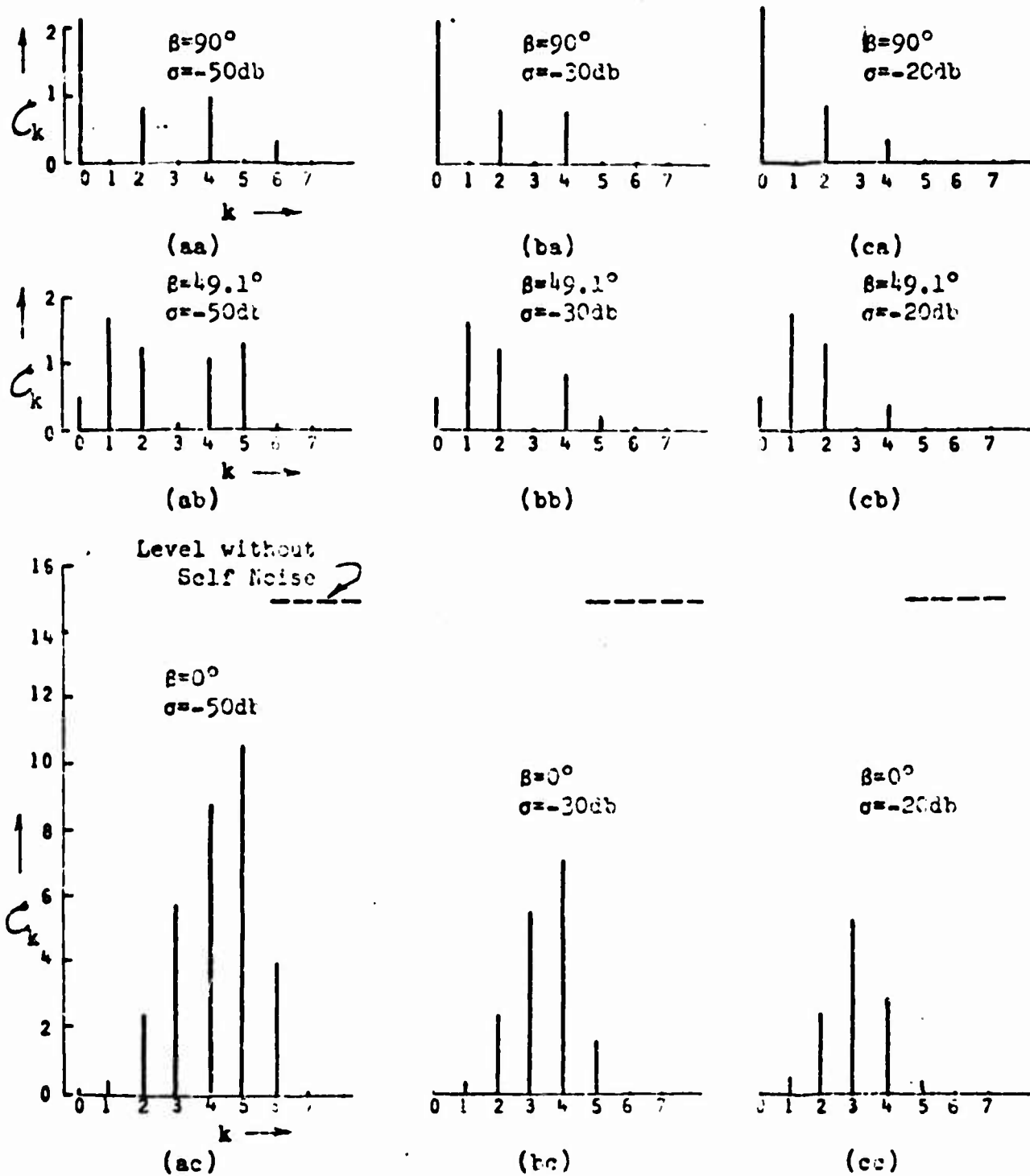


Figure 4-3 The Effect of Self Noise on Channel Factors

($M(Y) = 1$) . The channel factors are plotted at three levels of self noise: 50 db, 30 db, and 20 db below the sea noise.

Recalling Sect. 2.3, self noise does not change the eigenfunctions, but adds a scalar constant ξ to all the eigenvalues. For instance, if $\{\lambda_k'(\omega)\}$, $k \in D(\omega)$ is the set of eigenvalues for sea noise alone, then the set $\{\lambda_k(\omega)\}$, $k \in D(\omega)$ with self noise included is

$$\{\lambda_k(\omega)\} = \{\lambda_k'(\omega) + \xi\}, k \in D(\omega) . \quad 4 - 36$$

When the relative self noise level σ is -50 db, for instance, then (Eqs. 2 - 49 and 2 - 50)

$$\sigma(\omega) = \frac{\xi}{\sum_{k \in D(\omega)} \lambda_k'(\omega)} = \frac{1}{m} \frac{\mathcal{N}}{n_1'(\omega)} = 10^{-5} \quad 4 - 37$$

where \mathcal{N} is the time spectral level of the self noise at a single hydrophone and $n_1'(\omega)$ is $n_1(\omega)$ for the sea noise process alone. In this example the number of hydrophones m is 12 so that

$$\frac{\mathcal{N}}{n_1(\omega)} = 1.2 \times 10^{-4} \quad \left[\begin{array}{l} \sigma = 50 \text{ db} \\ m = 12 \end{array} \right] . \quad 4 - 38$$

This may be related to a physical measurement through Eqs. 2 - 51 and 2 - 52.

Figs. 4 - 1 (aa), (ab) and (ac) show that in this example, the highest channel factors for detection of broadside signals tend to concentrate closer to the left-hand end of the sequence of factors than for the endfire condition. In these figures, the eigenvalues decrease from left to right. Therefore, the addition of self noise affects the sequence of channel factors from the right, meaning that the endfire channels are most sensitive to self noise.

In Eq. 4 - 31, as the self noise increases, $\lambda_k(\omega)$ and $n_1(\omega)$

increase (see page 41 and Eq. 1 - 38). The increase in $\lambda_k(\omega)$ decreases the channel factors at the right, while the increase in $n_1(\omega)$ increases those at the left. The increase due to the increase in $n_1(\omega)$ is usually small. Physically, these changes are due to a change in the proportions of sea noise and self noise in the total received noise energy, the latter being a fixed quantity.

The array gain $\mathcal{G}^{(b)}$, which is the sum of the channel factors, is plotted in Fig. 4 - 2 versus the angle of incidence of the signal. An array of 12 equally spaced hydrophones is assumed. For comparison, the array gain obtained with I2 instead of I3 sea noise is also shown. The larger amount of I2 sea noise in the endfire region (Fig. 2 - 1) results in poorer endfire detection. Since less noise power is present in the broadside region, broadside detection is better when I2 sea noise is present.

In both cases, the endfire detection is markedly affected by the level of self noise. In fact, if k is increased indefinitely, the endfire detection is limited only by the amount of self noise.¹ To show this, the numerator $|h_k(\omega, \underline{Y})|^2$ (the factor $M(\underline{Y})$ is omitted since it is unity in this example) and denominator $\lambda_k(\omega)/n_1(\omega)$ of the channel factors $\mathcal{C}(\omega, \underline{Y})$ (Eq. 4 - 31) are plotted in Fig. 4 - 3 versus k . In both the I2 and I3 sea noise cases, the ratio of the numerator to the denominator approaches a nonzero constant as k is increased. In the I2 sea noise case, this constant is 2.2, and in the I3 noise case, it is 14. Therefore, without self noise,

¹But note that $k \rightarrow \infty$ implies that an infinite number of hydrophones is available.

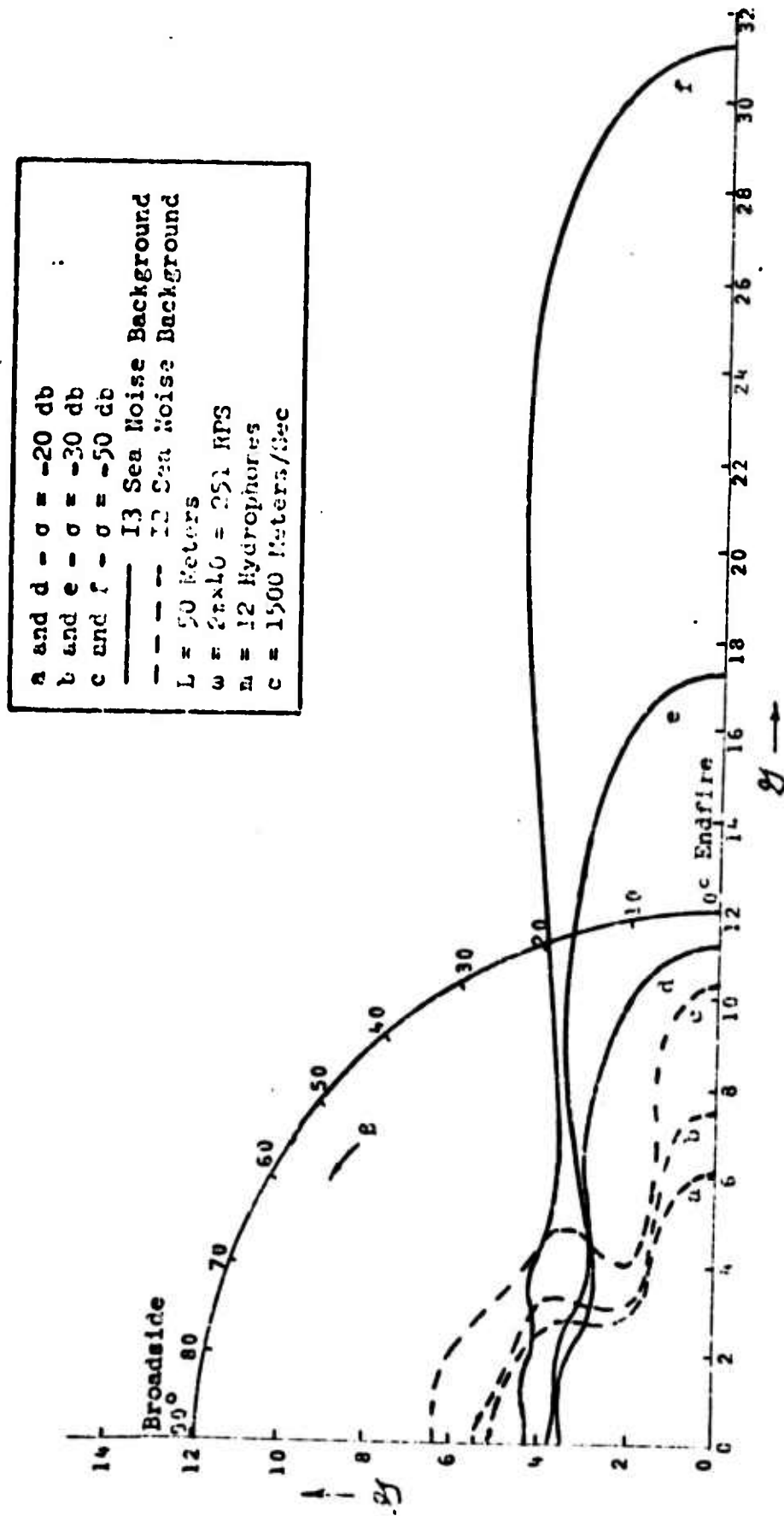


Figure L-2 b-Detector Array Gain in I2 and I3 Sea Noise

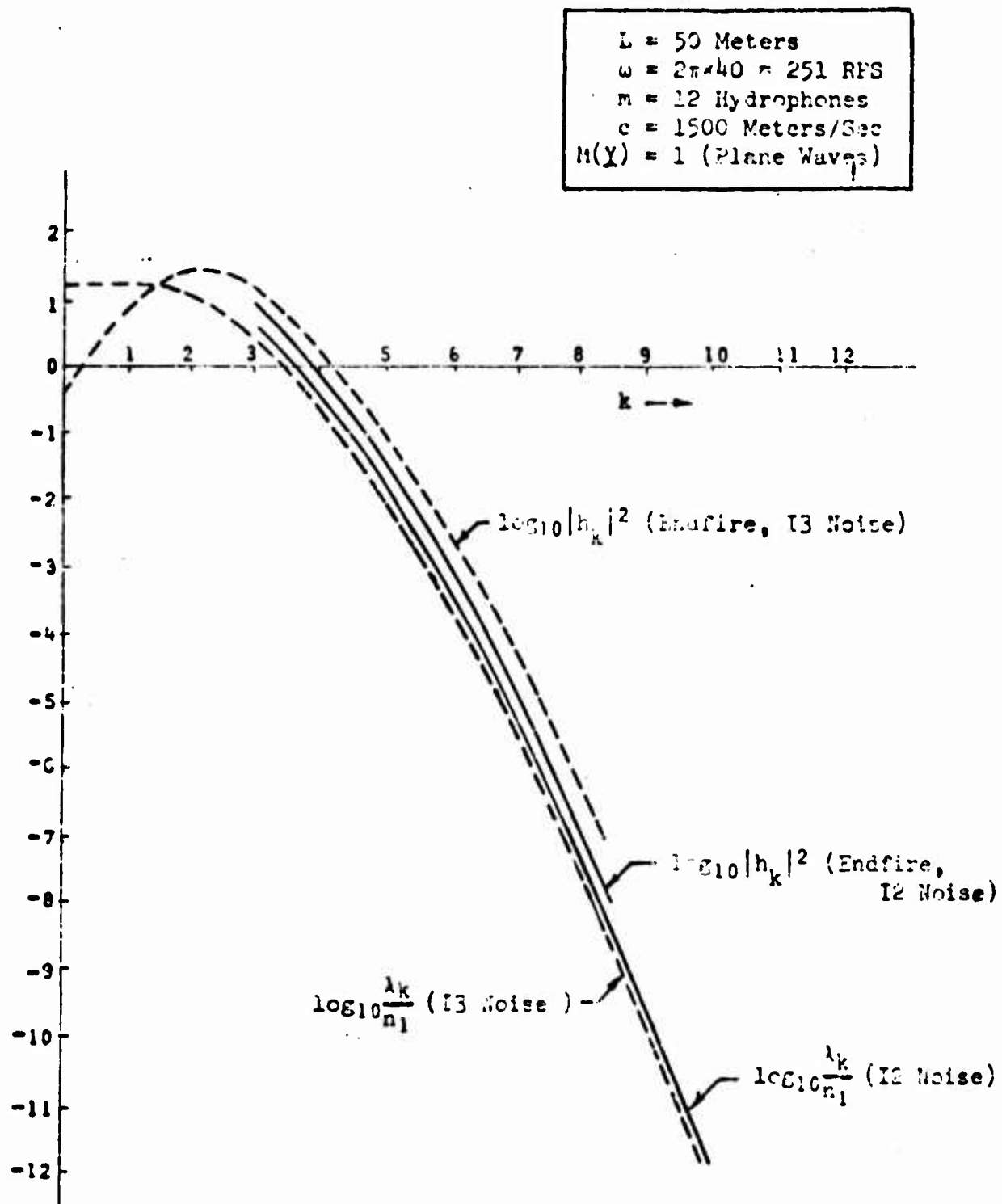


Figure 4-3 High Spatial Frequency Behavior of Signal and Noise Spectra

the array gain (Eq. 4 - 32) will diverge as k is increased. Self noise, however, adds a constant to the denominator so that as the numerator $|h_k(\omega, \underline{Y})|^2$ becomes small (Fig. 4 - 3), the channel factors approach zero, and the array gain converges. To achieve a large endfire array gain, the self noise level must be small. The number of hydrophones m affects the level of relative self noise according to Eq. 2 - 50. The relative self noise may be made arbitrarily small by increasing the number of hydrophones. Specifically, if the number of hydrophones is increased by a factor of ten, the relative self noise level σ is reduced by 10 db. The cost in hydrophones of reducing relative self noise quickly limits the practical reduction that can be obtained.

The number of hydrophones also limits the number of available space eigenfunctions or channels. If m eigenfunctions are desired, at least m hydrophones are required. In qualitative terms, if m hydrophones are used, the noise power on eigenfunctions (channels) of index k greater than $m-1$ is received on the existing eigenfunctions. This can seriously impair detection at all incidences. If in this example m were to equal 2, for instance, then the noise power $\frac{1}{L} \sum_{\substack{k \in D(\omega) \\ k \geq 2}} \lambda_k(\omega)$ would be received

on $\psi_0(\omega)$ and $\psi_1(\omega)$. From Fig. 2 - 4 the added noise is roughly $\frac{1}{4}$ of the total noise. A noise increase of roughly 25% on $\psi_0(\omega)$ and $\psi_1(\omega)$ would decrease the broadside detection by roughly the same amount.

Even worse, the endfire detection would be practically eliminated because the eigenfunctions ψ_2, ψ_3, \dots which are the principal endfire channels would not be defined. Fig. 4 - 4 shows the array gain for $m = 4$ and 2, i.e. with and without ψ_2 and ψ_3 .

In the example discussed above, the noise processes received at separate hydrophones are dependent. However, if the time frequency is

$L = 50$ Meters
 $\omega = 2\pi \times 40 = 251$ RPS
 Background Noise is
 13 Sea Noise
 $\frac{n}{n_1} = m = -30$ db
 $c = 1500$ Meters/Sec

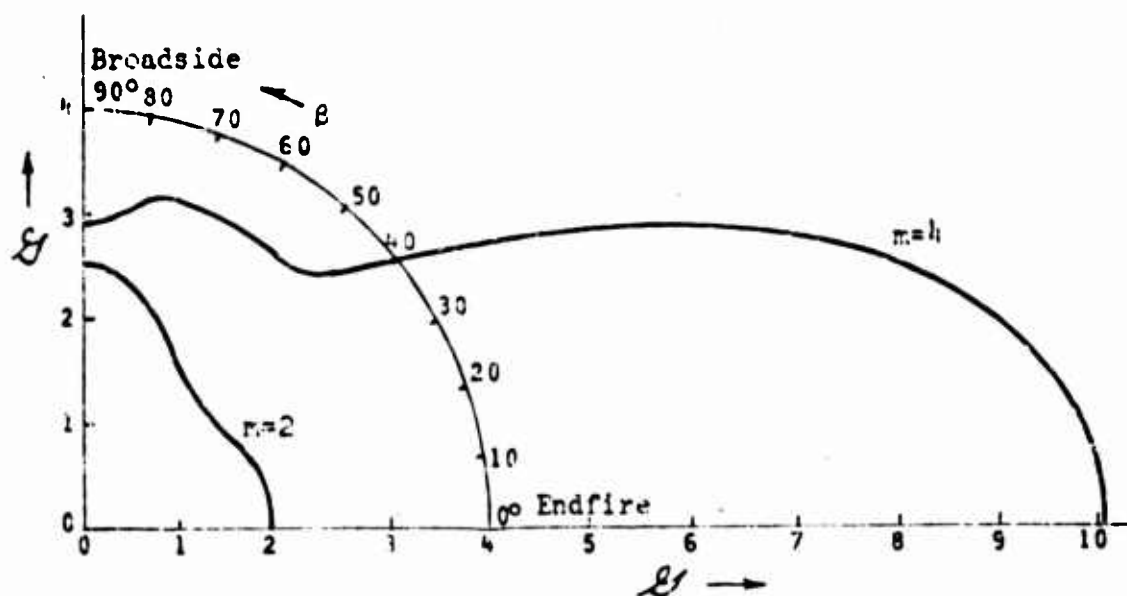


Figure 4-4 b-Detector Array Gain with 2 and 4 Hydrophones

raised from 40 to 60 hz, the hydrophones become essentially independent for $m \leq 4$. The result is the circular array gain patterns pictured in Fig. 4 - 5 for $m \leq 4$. The principal endfire channels in this example are ψ_3 and ψ_4 . Therefore when m is increased beyond 4, the array gain pattern goes almost immediately from circular to lobed toward endfire and never does exhibit the endfire deficiency shown in Fig. 4 - 4.

When $m > 4$, eigenfunctions are defined to receive most of the noise at its normal incidence. Beyond this, more hydrophones have little effect on broadside detection. Endfire detection, however, is significantly improved as more hydrophones are added. At first the added hydrophones define new endfire channels that are not self noise limited. After this, further hydrophones define self noise limited channels, one or two of which may provide significant detection. Beyond this point, adding hydrophones will improve the detection on the self noise limited channels by decreasing the relative self noise level. As mentioned before, however, it takes a large number of extra hydrophones to reduce the relative self noise level significantly. The patterns in Fig. 4 - 5 illustrate this development of the array gain as m is increased.

In the remainder of this section some examples are given to illustrate the behavior of the array in the presence of local noise and interfering target noise. The first example is of detection in the presence of local noise from a point source located one meter beyond the negative end of the array (pages 34 and 49), and the second is of detection in the presence of an interfering target located 75 meters off the negative end of the array ($x = -100$ meters). Both the local and the interfering target noises are 10 db above a background of 13 sea noise. The self noise is 50 db below the total external noise. The array length is 50 meters, and the

$L = 50$ Meters
 $\omega = 2\pi \times 60 = 377$ RPS
 Background Noise is
 13 Sea Noise
 $M_{h,1} = m_0 = -30$ db
 $c = 1500$ Meters/Sec

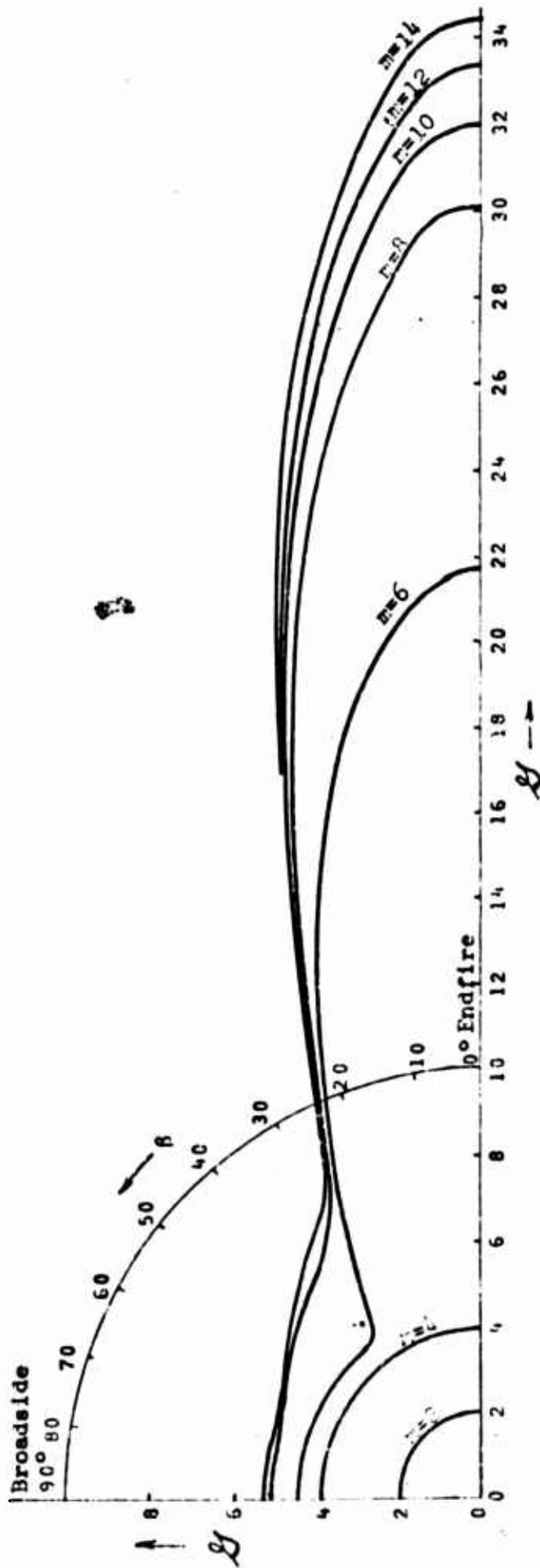


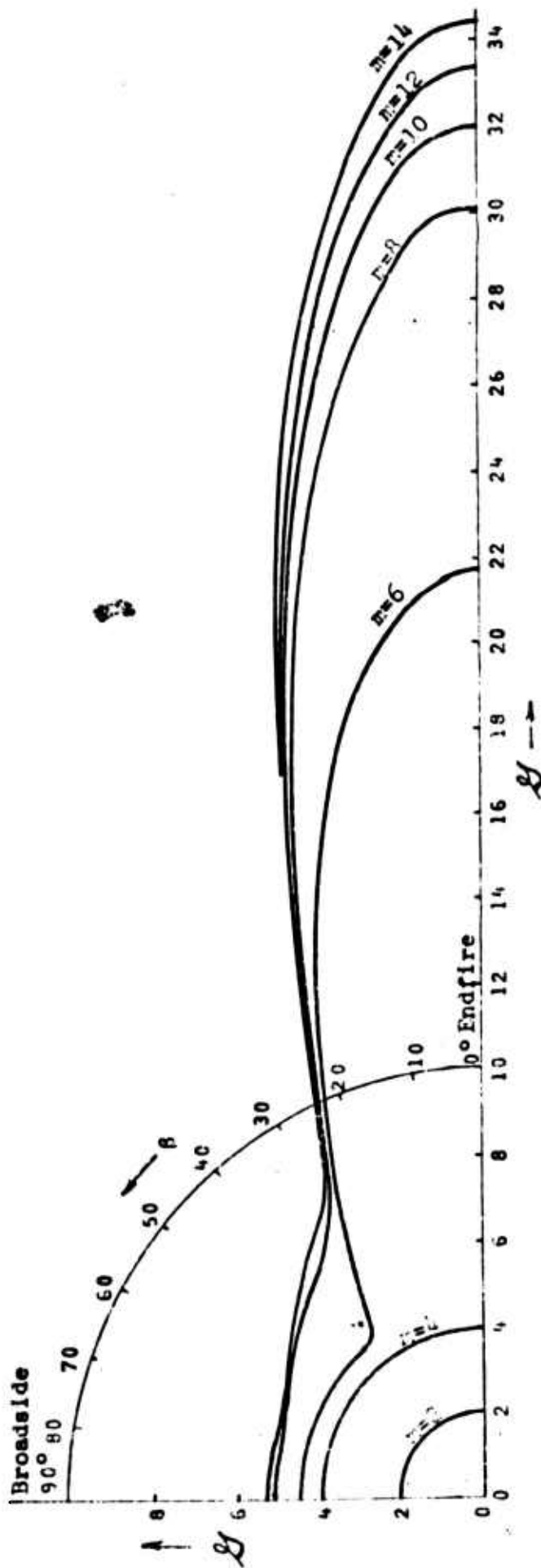
Figure 4-5 b-Detector Array Gain with Increasing Numbers of Hydrophones

raised from 40 to 60 Hz, the hydrophones become essentially independent for $m \leq 4$. The result is the circular array gain patterns pictured in Fig. 4 - 3 for $m \leq 4$. The principal endfire channels in this example are ψ_3 and ψ_4 . Therefore when m is increased beyond 4, the array gain pattern goes almost immediately from circular to lobed toward endfire and never does exhibit the endfire deficiency shown in Fig. 4 - 4.

When $m > 4$, eigenfunctions are defined to receive most of the noise at its normal incidence. Beyond this, more hydrophones have little effect on broadside detection. Endfire detection, however, is significantly improved as more hydrophones are added. At first the added hydrophones define new endfire channels that are not self noise limited. After this, further hydrophones define self noise limited channels, one or two of which may provide significant detection. Beyond this point, adding hydrophones will improve the detection on the self noise limited channels by decreasing the relative self noise level. As mentioned before, however, it takes a large number of extra hydrophones to reduce the relative self noise level significantly. The patterns in Fig. 4 - 5 illustrate this development of the array gain as m is increased.

In the remainder of this section some examples are given to illustrate the behavior of the array in the presence of local noise and interfering target noise. The first example is of detection in the presence of local noise from a point source located one meter beyond the negative end of the array (pages 34 and 49), and the second is of detection in the presence of an interfering target located 75 meters off the negative end of the array ($x = -100$ meters). Both the local and the interfering target noises are 10 db above a background of 13 sea noise. The self noise is 50 db below the total external noise. The array length is 50 meters, and the

$L = 50$ Meters
 $\omega = 2\pi \times 60 = 377$ RPS
 Background Noise is
 13 Sea Noise
 $\bar{M}_{11} = m_0 = -30$ db
 $c = 1500$ Meters/Sec



A-85

Figure 4-5 b-Detector Array Gain with Increasing Numbers of Hydrophones

time frequency is 40 hz.

The channel factors in these two examples are plotted in Fig. 4 - 6. In the local noise case, C_0 is practically zero, because most of the local noise is received on ψ_0 (see Figs. 2 - 5, 2 - 6 and 4 - 6). Since the local noise is attenuating significantly over the array, it is easily distinguishable from 180° signals arriving from a distance so great that they do not attenuate significantly over the array. These 180° signals are principally detected on ψ_3 and ψ_4 . As shown in Fig. 4 - 6, detection in the presence of this local noise is almost as good at 180° as it is at 0° .

For interfering noise at $x = -100$ meters, however, the situation is different. As before, the bulk of the interfering noise is received on ψ_0 , making this channel useless for the detection of signals. But, the interfering noise does not attenuate significantly in this case and therefore is difficult to distinguish from distant signals also incident at 180° . Since the remaining channels do not match the interfering noise, they do not match 180° signals either. This is evident in Fig. 4 - 6 (ba). The array gain for this case is plotted in Fig. 4 - 7, and the detector at 180° is seen to be severely impaired by the presence of the interfering noise.

As a final example, it is assumed that the noise process consists of a single interfering target signal with a source vector $\hat{\underline{y}}$ plus self noise as described in Sect. 2.3. At a frequency ω , the zero order spatial eigenvalue for the total noise process is

$$\lambda_0(\omega) = \lambda_I(\omega) + \epsilon \quad 4 - 39$$

where λ_I is the spatial eigenvalue of the interference alone, and

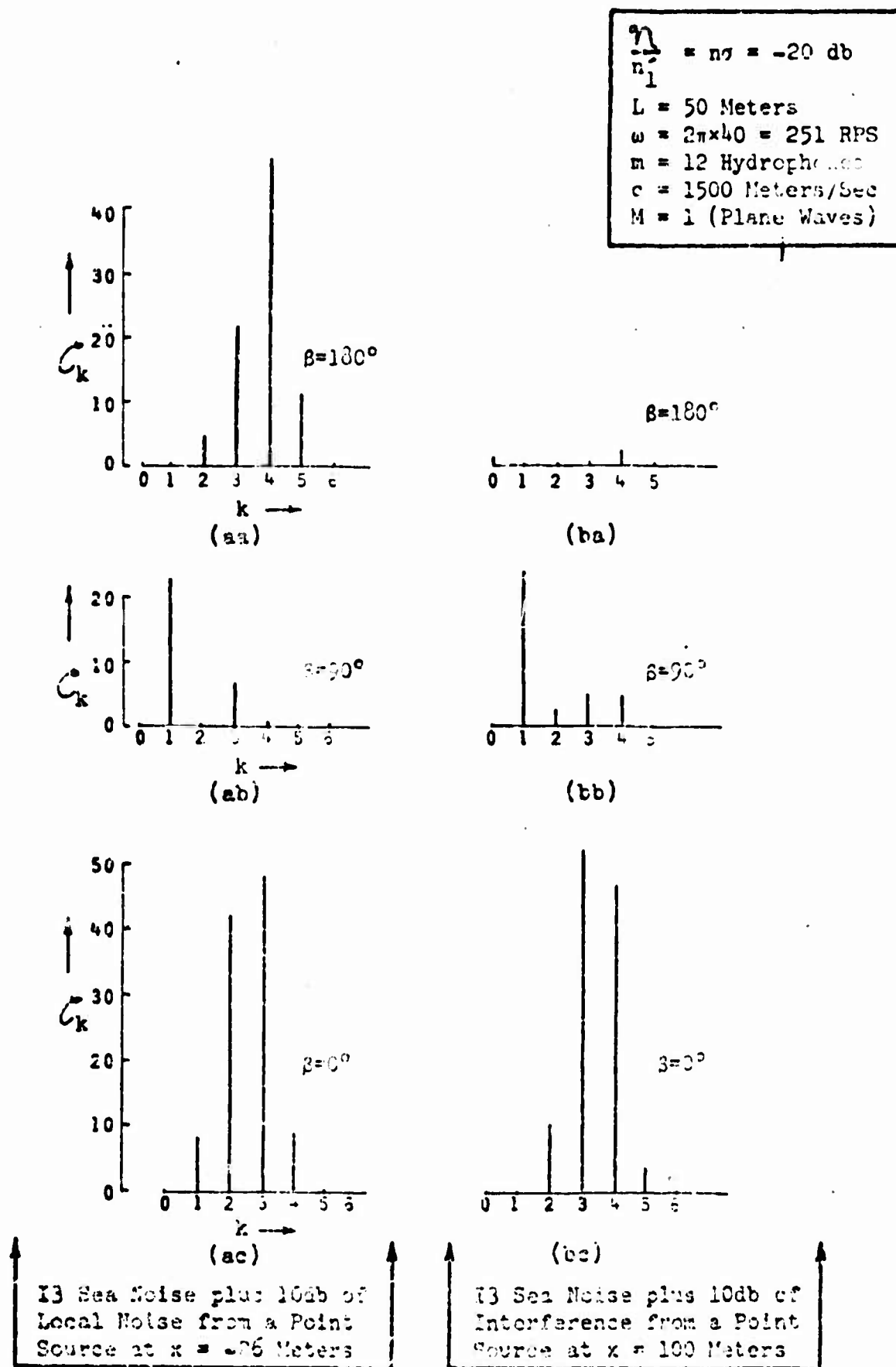


Figure 4-6 Channel Factors with Local and Distant Interference

13 Sea Noise +10 db of Local
 Noise from a Pt. Source at
 $x = -26$ Meters
 13 Sea Noise +10 db of Inter-
 ference from a Pt. Source at
 $x = -100$ Meters
 $M = 1$ (Plane Waves)
 $\mathcal{N}/n_1 = m_1 = -20$ db
 $L = 50$ Meters
 $\omega = 2\pi \times 40 = 251$ RPS
 $m = 12$ Hydrophones
 $c = 1500$ Meters/Sec

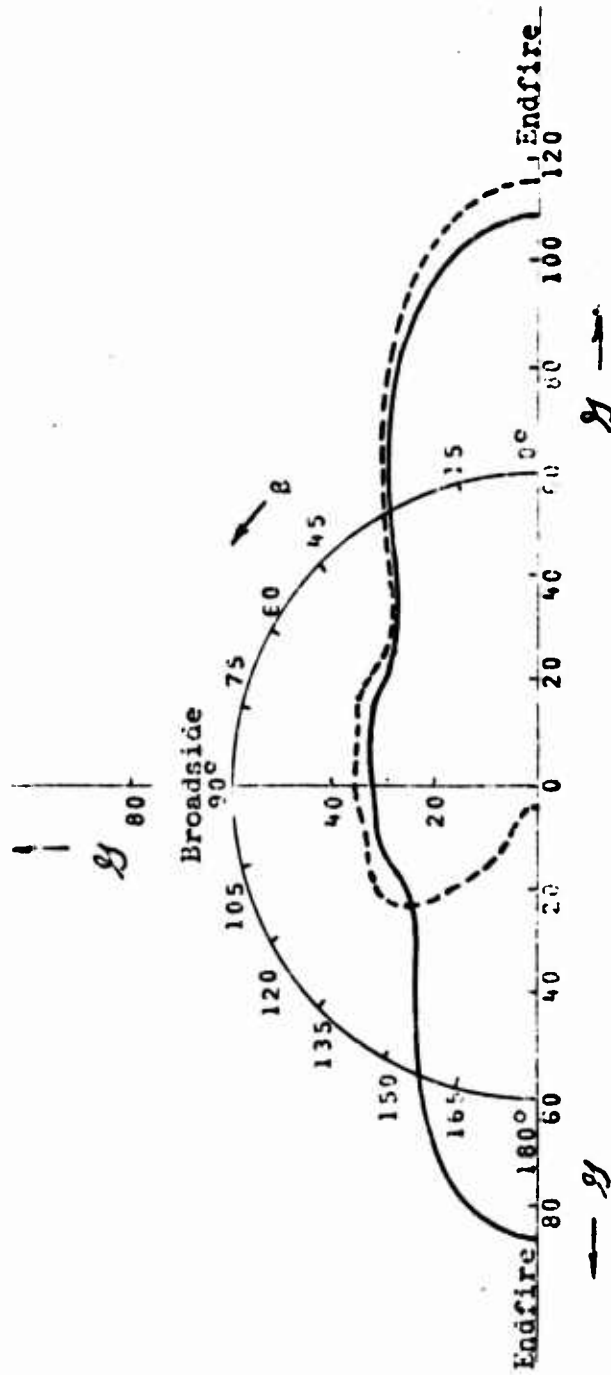


Figure 4-7 b-Detector Array Gain with Local and Distant Interference

ξ is the self noise level (Eq. 2 - 45). As for the remaining eigenvalues,

$$\lambda_k = \xi \quad k = 1, \dots, m-1 \quad 4 - 40$$

in which m is the number of hydrophones in the array. The ratio of the self noise to the interference given by Eq. 2 - 49 is

$$\sigma = \frac{\xi}{\lambda_I} \quad 4 - 41$$

Now Eq. 4 - 28 for the b-detector array gain $\mathcal{G}^{(b)}$ and Eq. 1 - 38 for the total noise n_1 indicate (following a certain amount of algebra) that

$$\mathcal{G}^{(b)}(\omega, \underline{Y}|\underline{Y}) = \frac{1 + m\sigma}{1 + \sigma} \left(1 + \frac{1}{\sigma} \frac{\sum_{k=1}^{m-1} |h_k(\omega, \underline{Y})|^2}{LM(\underline{Y})} \right). \quad 4 - 42$$

The lowest b-detector array gain, labeled $G_L^{(b)}$ is attained when $\underline{Y} = \hat{\underline{Y}}$. Then

$$\sum_{k=1}^{m-1} |h_k(\omega, \hat{\underline{Y}})|^2 = 0 \quad 4 - 43$$

so that

$$G_L^{(b)} = \mathcal{G}^{(b)}(\omega, \hat{\underline{Y}}|\hat{\underline{Y}}) = \frac{1 + m\sigma}{1 + \sigma} \quad 4 - 44$$

Correspondingly if \underline{Y} is such that¹

$$\sum_{k=1}^{m-1} |h_k(\omega, \underline{Y})|^2 = LM(\underline{Y}) \quad 4 - 45^1$$

¹Note from Eq. 2 - 84 that $||h(\omega, \underline{Y})||^2 = LM(\underline{Y})$.

then the array gain is

$$\mathcal{G}^{(b)}(\omega, \underline{y}|\underline{y}) = \frac{1 + m\sigma}{\sigma} \equiv G_U^{(b)} . \quad 4 - 46$$

Suppose that the ratio of self noise to interference is 1/10, that is,

$$\frac{n}{n_1} = m\sigma = \frac{1}{10} \quad 4 - 47$$

in Eq. 2 - 50, suppose further that the array has eight hydrophones. Then the minimum b-detector array gain is

$$G_L^{(b)} = \frac{88}{81} \approx 1.086 . \quad 4 - 48$$

Since the interference power is assumed known, a signal from $\hat{\underline{y}}$ is still slightly detectable by the increase it will make in the power received from $\hat{\underline{y}}$. This is reflected in $G_L^{(b)}$ being slightly above unity, the general minimum for the b-detector array gain (Eq. 4 - 29). The upper limit $G_U^{(b)}$, which is never completely attained, is

$$G_U^{(b)} = 88 . \quad 4 - 49$$

These levels are marked in Fig. 4 - 8 which shows the array gain of a 50 meter array at 60 hz in the presence of an interfering target from a range of two kilometers at an incidence of 49.1° .

In the plot in Fig. 4 - 8 only the shape, and not the scale, may be used in making direct comparisons with other examples in which the interference power is different. If the background or self noise is fixed and the interference is to vary, the array gain may be replaced by an "apparent array gain" defined as follows. Whereas the array gain \mathcal{G} is obtained by normalizing the single frequency output SNR with respect to the total noise n_1 , the "apparent array gain" $\hat{\mathcal{G}}$

$L = 50 \text{ M}$
 $m = 8 \text{ Hydrophobes}$
 $\omega = 2\pi \times 60 = 188 \text{ RPS}$
 $c = 1500 \text{ M/Sec}$



Figure 4-8 b-Detector Array Gain with Interference and Self Noise

will be obtained by normalizing with respect to n_b , the background or self noise without the interference. That is,

$$\tilde{J}(\omega, \underline{X}|\underline{Y}) = \frac{\phi(\omega, \underline{X}|\underline{Y})}{\frac{s(\omega)}{n_b(\omega)} M(\underline{Y}) \sqrt{\frac{T\Delta\omega}{2\pi}}} = \frac{n_b(\omega)}{n_1(\omega)} J(\omega, \underline{X}|\underline{Y}) . \quad 4 - 50$$

In this example,

$$\frac{n_b(\omega)}{n_1(\omega)} = \frac{\frac{1}{L} m \xi}{\frac{1}{L}(m\xi + \lambda_1)} = \frac{m\sigma}{1+m\sigma} \quad 4 - 51$$

so that the new minimum $\tilde{G}_L(b)$ becomes

$$\tilde{G}_L(b) = \frac{m\sigma}{1+m\sigma} G_L(b) = \frac{m\sigma}{1+\sigma} \quad 4 - 52$$

and the new upper limit $\tilde{G}_U(b)$ becomes

$$\tilde{G}_U(b) = \frac{m\sigma}{1+m\sigma} G_U = m . \quad 4 - 53$$

A comparison can now be made with the array gain obtained with no interference at all (with independent noise from hydrophone to hydrophone, such as self noise). According to Eq. 4 - 35 this array gain is m so that it may be concluded from Eq. 4 - 53 that an interference from $\hat{\underline{Y}}$ does not diminish the "apparent array gain" if the signal source location \underline{Y} is far enough from $\hat{\underline{Y}}$ that

$$\tilde{J}(b) \approx \tilde{G}_U(b) = m . \quad 4 - 54$$

(At low frequencies there may not be any $\underline{Y} \in \mathcal{Q}$ for which the above holds).

c) c-Detector Array Gain

For the c-detector, the functional \mathcal{J} in Eq. 4 - 13 is

$$\mathcal{J}(\omega, \underline{X}) = \frac{1}{\lambda(\omega)} \sqrt{\frac{s(\omega)}{1 + \frac{s(\omega)}{\lambda(\omega)} L\mathcal{H}(\underline{X})}} \underline{h}(\omega, \underline{X}) . \quad 4 - 55$$

According to Eq. 4 - 22, then, the c-detector array gain is

$$\mathcal{G}^{(c)}(\omega, \underline{X}|\underline{Y}) = \frac{n_1(\omega) |\underline{h}^*(\omega, \underline{X}) \underline{h}(\omega, \underline{Y})|^2}{M(\underline{Y}) \Lambda(\omega) ||\underline{h}(\omega, \underline{X})||^2} . \quad 4 - 56$$

This is not necessarily a maximum when $\underline{X} = \underline{Y}$, so that steering the c-detector toward \underline{Y} does not necessarily focus it exactly on \underline{Y} .

When the c-detector is steered toward \underline{Y} ,

$$\mathcal{G}^{(c)}(\omega, \underline{Y}|\underline{Y}) = \frac{n_1(\omega) ||\underline{h}(\omega, \underline{Y})||^4}{M(\underline{Y}) \Lambda(\omega) ||\underline{h}(\omega, \underline{Y})||^2} = \frac{n_1(\omega) M(\underline{Y}) L^2}{\Lambda(\omega) ||\underline{h}(\omega, \underline{Y})||^2} . \quad 4 - 57$$

For comparison, the b-detector array gain is

$$\mathcal{G}^{(b)}(\omega, \underline{Y}|\underline{Y}) = \frac{n_1(\omega)}{M(\underline{Y})} \Lambda^{-1}(\omega) ||\underline{h}(\omega, \underline{Y})||^2 . \quad 4 - 58$$

The ratio of the array gains for the two detectors is

$$\begin{aligned} \frac{\mathcal{G}^{(b)}(\omega, \underline{Y}|\underline{Y})}{\mathcal{G}^{(c)}(\omega, \underline{Y}|\underline{Y})} &= \frac{\Lambda^{-1}(\omega) ||\underline{h}(\omega, \underline{Y})||^2 \Lambda(\omega) ||\underline{h}(\omega, \underline{Y})||^2}{M(\underline{Y})^2 L^2} \\ &= \frac{\Lambda^{-1}(\omega) ||\underline{h}(\omega, \underline{Y})||^2 \Lambda(\omega) ||\underline{h}(\omega, \underline{Y})||^2}{||\underline{h}(\omega, \underline{Y})||^4} \\ &= \frac{\sum_{k \in D(\omega)} |h_k(\omega, \underline{Y})|^4 + \sum_{\substack{k, k' \in D(\omega) \\ k < k'}} |h_k(\omega, \underline{Y})|^2 |h_{k'}(\omega, \underline{Y})|^2 \frac{\lambda_k^2(\omega) + \lambda_{k'}^2(\omega)}{\lambda_k(\omega) \lambda_{k'}(\omega)}}{\sum_{k \in D(\omega)} |h_k(\omega, \underline{Y})|^4 + 2 \sum_{\substack{k, k' \in D(\omega) \\ k < k'}} |h_k(\omega, \underline{Y})|^2 |h_{k'}(\omega, \underline{Y})|^2} . \end{aligned} \quad 4 - 59$$

All the terms in this last expression are positive and

$$\frac{\lambda_k^2(\omega) + \lambda_{k'}^2(\omega)}{\lambda_k(\omega) \lambda_{k'}(\omega)} \geq 2 \quad . \quad 4 - 60$$

Therefore,

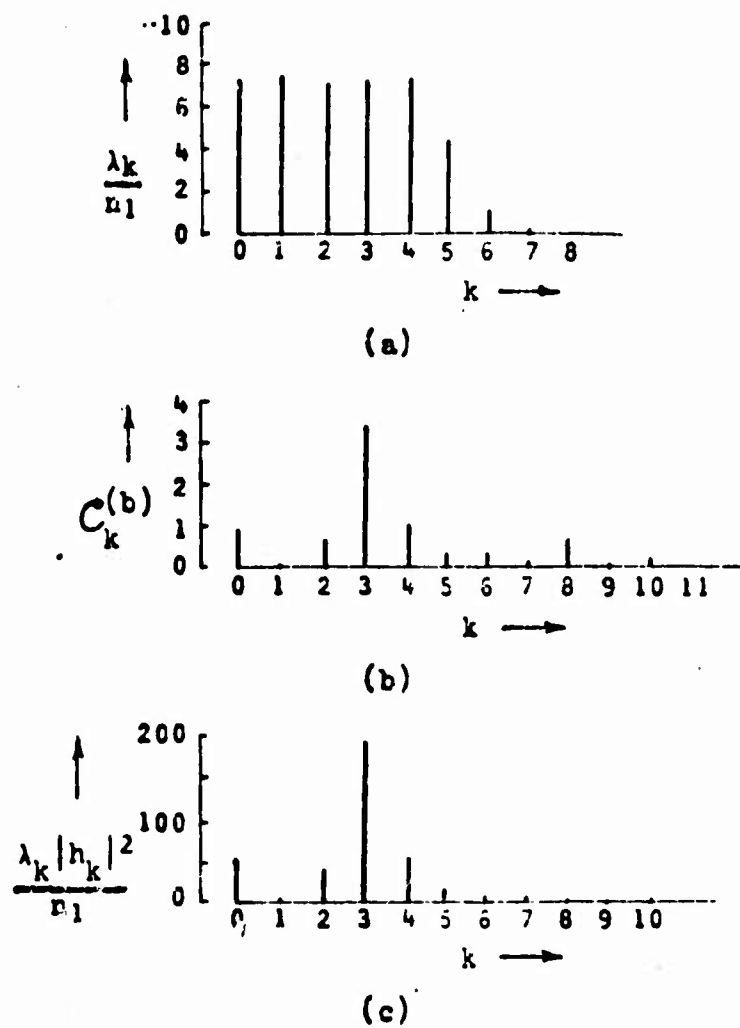
$$\mathcal{J}^{(b)}(\omega, \underline{Y}|\underline{Y}) \geq \mathcal{J}^{(c)}(\omega, \underline{Y}|\underline{Y}) \quad . \quad 4 - 61$$

The equality holds when $\lambda_k(\omega) = \lambda_{k'}(\omega)$ for all k and $k' \in D(\omega)$.

Indeed, it was shown in Sect. 3.2 that when $\lambda_k(\omega) = \lambda_{k'}(\omega)$ for all significant indices k and k' , the b and c -detectors are completely equivalent. Practically, when the average noise energy $\lambda_k(\omega)$ is approximately equal on all b -detector channels for which either $\lambda_k(\omega) |h_k(\omega, \underline{Y})|^2$ or $\frac{|h_k(\omega, \underline{Y})|^2}{\lambda_k(\omega)}$ is relatively significant,

then the c -detector may be expected to have almost the same array gain as the b -detector. This is illustrated in the following example.

Consider a 12 hydrophone, 50 meter array at 100 hz in a background of I3 sea noise. The space spectrum for this array as shown in Fig. 4 - 9 (a) is already approaching the limiting form shown in Fig. 2 - 2. That is, it is practically flat for $k < 5$. Now for a plane wave ($M(\underline{Y}) = 1$) incident at $\beta_{\underline{Y}} = 75.9^\circ$ and a self noise level 50 db below the sea noise, the b -detector channel factors $\mathcal{C}_k(\omega, \underline{Y}) = \frac{n_1(\omega) |h_k(\omega, \underline{Y})|^2}{\lambda_k(\omega)}$ are plotted in Fig. 4 - 9 (b), and the terms $\frac{\lambda_k(\omega)}{n_1(\omega)} |h_k(\omega, \underline{Y})|^2$ in the c -detector array gain (Eq. 4 - 57) are plotted in Fig. 4 - 9 (c). Almost the entire b -detector array gain is on channels whose indices k are less than five, and all of the significant terms $\frac{\lambda_k(\omega)}{n_1(\omega)} |h_k(\omega, \underline{Y})|^2$ in the c -detector array gain have indices $k < 5$. Therefore it is



$\theta = 75.9^\circ$
 $\omega = 2\pi \times 100 = 628 \text{ RPS}$
 $L = 50 \text{ Meters}$
 $M = 1 \text{ (Plane Waves)}$
 $\text{Background Noise is}$
 I3 Sea Noise
 $\sigma = -50 \text{ db}$
 $m = 12 \text{ Hydrophones}$
 $c = 1500 \text{ Meters/Sec}$

Figure 4-9 Characteristics of b and c-Detectors at 75.9° Incidence

expected that the c-detector array gain will be almost equal to the b-detector array gain at the 75.9° signal incidence. This is in fact observed in Fig. 4 - 10. It is also reasonable to expect even greater similarity at incidences nearer broadside. This is also observed in Fig. 4 - 10.

In general, the c-detector array gain will not be very close to the b-detector array gain at endfire or near endfire incidence. At these incidences the spectrum is changing significantly over the channel factors of interest. At broadside and near broadside incidence, the b and c-detectors will have almost the same array gain when the noise model has a smooth spectrum in this incidence region and when the time frequency is high enough so that the significant channel factors and terms in the c-detector array gain occur in this region. Self noise tends to equalize the b and c-detector array gains because it reduces the span in k over which the channel factors are significant.

When the overall noise model is homogeneous and the noise processes received on different hydrophones are independent, the spatial spectrum is constant over all channels at a given time frequency. In this case, then, the c-detector is exactly equivalent to the b-detector. (According to Eq. 4 - 34, $\lambda_k(\omega) = \frac{n_1(\omega)L}{m}$ for all k so that the filter \mathcal{F} (Eq. 3 - 24) in the c-detector is described by

$$|\mathcal{F}(\omega|\underline{X})|^2 = \frac{s(\omega)}{n_1^2(\omega)} \frac{m}{L} \frac{1}{1 + \frac{s(\omega)}{n_1(\omega)} m M(\underline{X})} \quad . \quad 4 - 62$$

This is approximately the Eckart filter [15]).

--- b-Detector
 --- c-Detector
 Background Noise is
 13 Sea Noise
 $\sigma = -50$ db
 $M = 1$ (Plane Waves)
 $\omega = 2\pi \times 100 = 628$ RPS
 $L = 50$ Meters
 $m = 12$ Hydrophones
 $c = 1500$ Meters/Sec

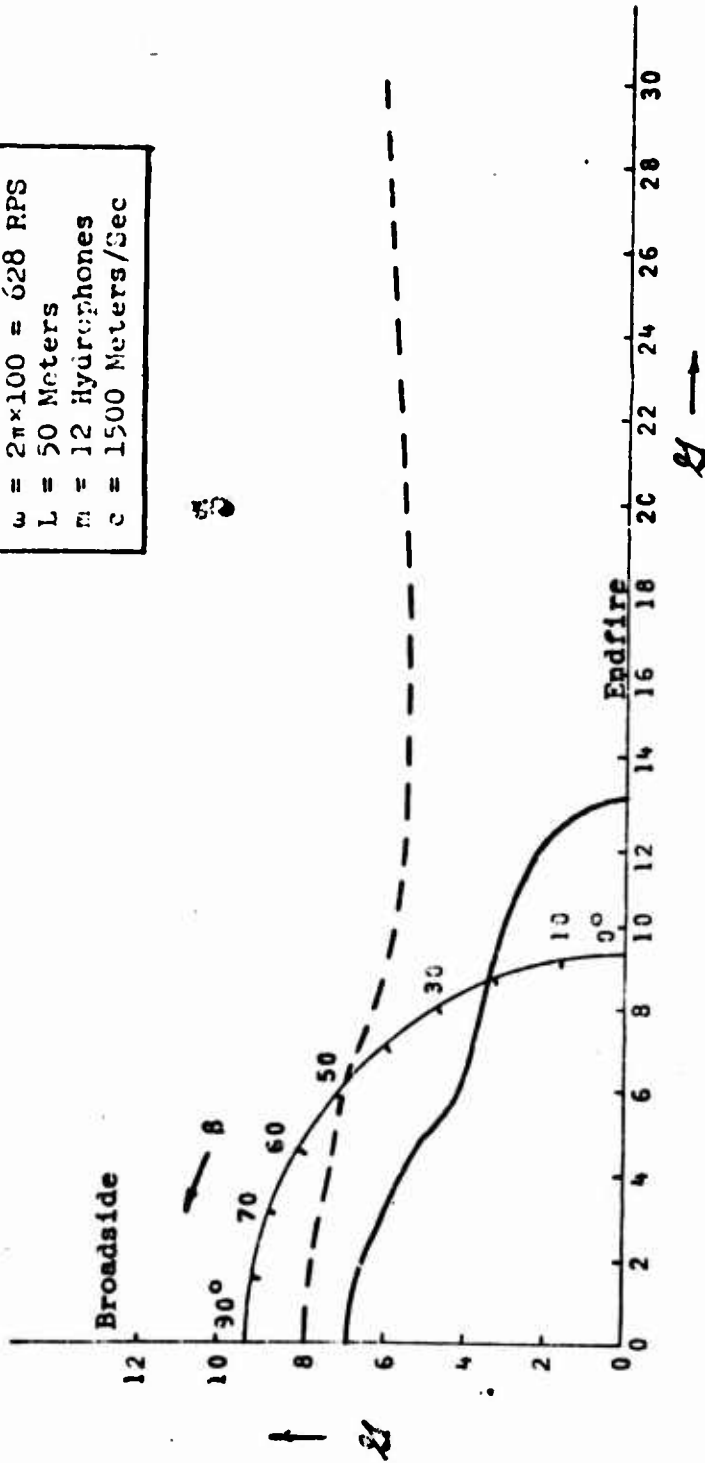


Figure 4-10 Array Gain Comparison

4.3 The ℓ -Detector Array Gain

According to Eq. 4 - 8, the narrowband output signal-to-noise ratio for the ℓ -detector is

$$\phi^{(\ell)}(\omega, \underline{X} | \underline{Y}) = \sqrt{\frac{T\Delta\omega}{2\pi}} \frac{\langle \ell(\underline{u}(\omega), \omega, \underline{X}) \rangle_{S(\underline{Y})+N} - \langle \ell(\underline{u}(\omega), \omega, \underline{X}) \rangle_N}{\sqrt{V[\ell(\underline{u}(\omega), \omega, \underline{X})]_N}} \quad 4 - 63$$

Obtaining the above mean and variance from appendix D,

$$\phi^{(\ell)}(\omega, \underline{X} | \underline{Y}) = \sqrt{\frac{T\Delta\omega}{2\pi}} \frac{\sum_{k \in D(\omega, \underline{X})} \frac{\langle |u_k(\omega)|^2 \rangle_{S(\underline{Y})}}{\lambda_k(\omega)} d\omega}{\sqrt{\sum_{k \in D(\omega, \underline{X})} \left[\frac{\langle |u_k(\omega)|^2 \rangle_N}{\lambda_k(\omega)} \right]^2}} \quad 4 - 64$$

In the numerator of the above

$$\begin{aligned} \frac{\langle |u_k(\omega)|^2 \rangle_{S(\underline{Y})}}{\lambda_k(\omega)} &= \frac{s_{kk}(\omega, \underline{Y})}{\lambda_k(\omega)} \\ &= \frac{s(\omega) |h_k(\omega, \underline{Y})|^2}{\lambda_k(\omega)} = \frac{s(\omega)}{n_1(\omega)} M(\underline{Y}) C_k(\omega, \underline{Y}) \end{aligned} \quad 4 - 65$$

according to Eq. 4 - 31. And in the denominator,

$$\begin{aligned} \sum_{k \in D(\omega, \underline{X})} \frac{\langle |u_k(\omega)|^2 \rangle_N^2}{\lambda_k^2(\omega)} \\ = \sum_{k \in D(\omega, \underline{X})} \frac{\lambda_k^2(\omega)}{\lambda_k^2(\omega)} = H(D(\omega, \underline{X})) \end{aligned} \quad 4 - 66$$

where the function $H(D)$ is the number of elements in the index set

D . Thus

$$\phi^{(l)}(\omega, \underline{X} | \underline{Y}) = \frac{s(\omega)}{n_1(\omega)} M(\underline{Y}) \sqrt{\frac{T \Delta \omega}{2\pi}} \frac{\sum_{k \in D(\omega, \underline{X})} c_k(\omega, \underline{Y})}{\sqrt{H(D(\omega, \underline{X}))}} \quad 4 - 67$$

Referring now to the definition of the array gain given in Eq. 4 - 11, the l -detector array gain $\mathcal{G}^{(l)}$ is

$$\mathcal{G}^{(l)}(\omega, \underline{X} | \underline{Y}) = \frac{\sum_{k \in D(\omega, \underline{X})} c_k(\omega, \underline{Y})}{\sqrt{H(D(\omega, \underline{X}))}} \quad 4 - 68$$

Fig. 4 - 11 shows the array gain for l -detectors with various index sets. This gain is compared with that for the b and c -detectors. The time frequency is 40 hz, the array length is 50 meters and the noise background is I3 sea noise. The data are derived from Fig. 4 - 1 (ba), (bb), and (bc).

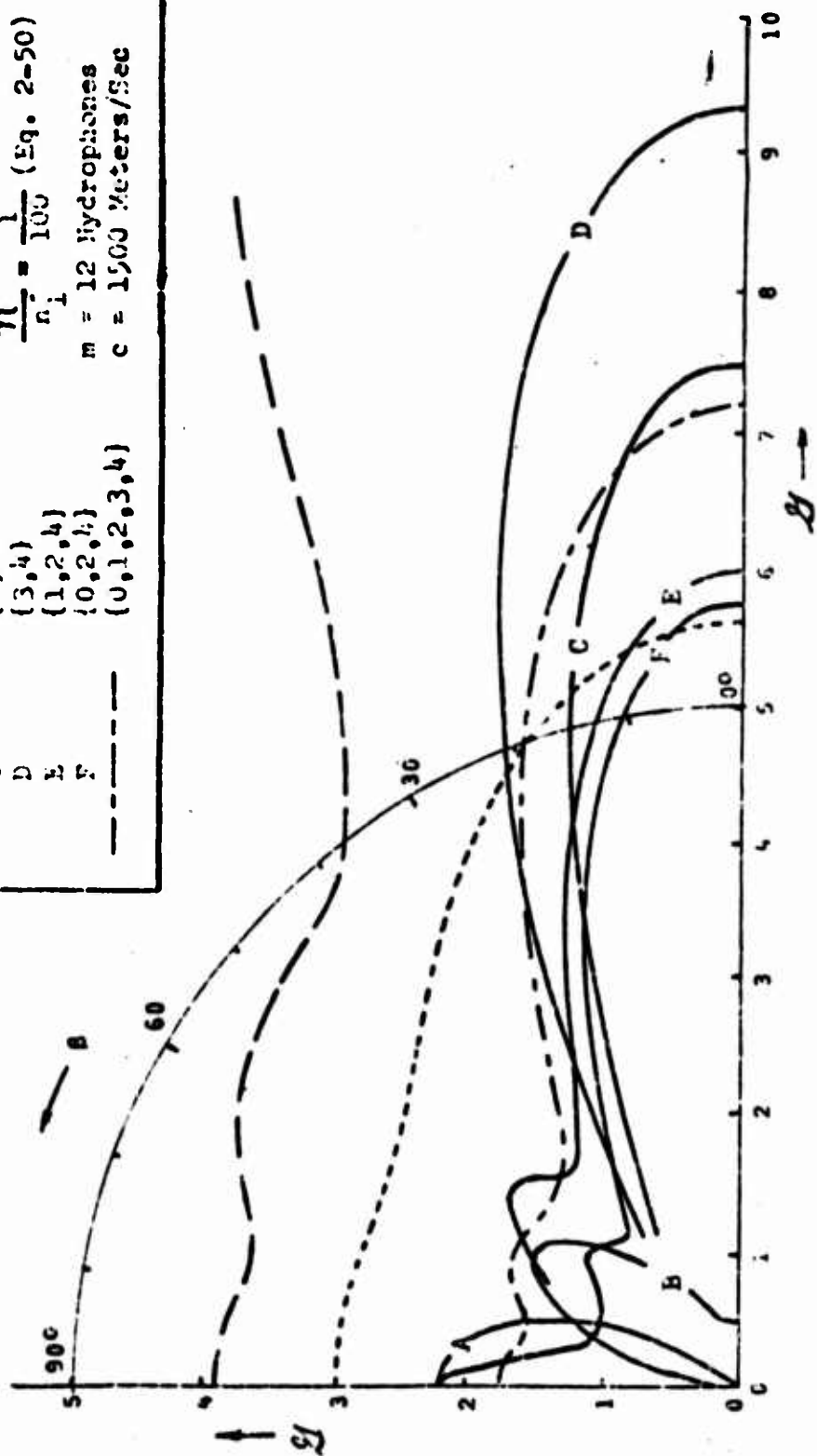
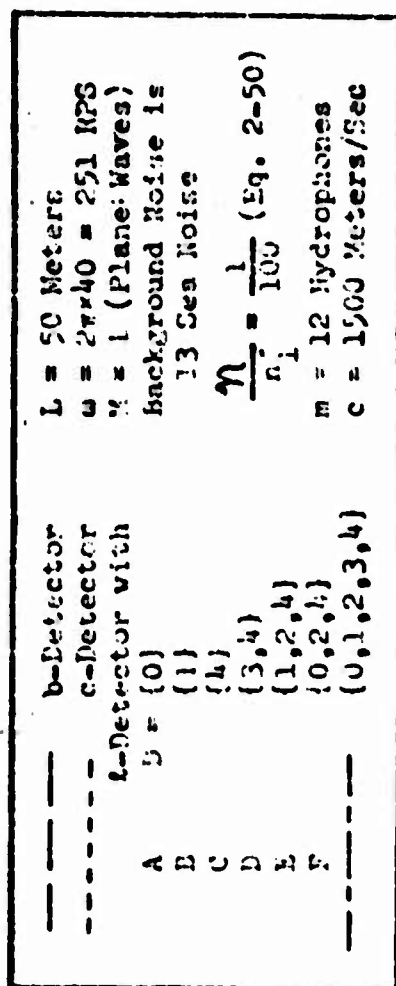


Figure 4-11 L-Detector Array Gain

CHAPTER 5

DIRECTIVITY MEASURES

5.0 Introduction

In detecting a target of fixed but unknown location, the b, c, or ℓ -detector is steered in particular directions. Directivity measures are presented below which will describe specific average relationships between these steering directions, the target location and the detector performance. These measures serve to

1. provide a basis for selecting the steering directions,
2. determine the influence of a signal or noise on a detector steered in some direction, and
3. indicate how well the b-detector may locate a fixed target. (A complete measure of the target locating ability of the c-detector is not given; however, a note on its bias is included.)

As mentioned before, it is assumed that the input signal-to-noise ratio is low and that the observation time is long. The measures derived here under these assumptions are thus strictly asymptotic measures, never exactly representative at finite signal levels and finite times. However, the error will be presumed to be small and the measures treated as though they were exact.

5.1 The Normalized SNR

a) Definition

The first of the directivity measures discussed, the normalized single frequency output signal-to-noise ratio \mathcal{D} , will be useful primarily in making a practical assignment of detector steering directions. It is defined by (see Eq. 4 - 12)

$$\mathcal{D}(\omega, \underline{X}|\underline{Y}) = \frac{\phi(\omega, \underline{X}|\underline{Y})}{\phi(\omega, \underline{Y}|\underline{Y})} = \frac{\mathcal{J}(\omega, \underline{X}|\underline{Y})}{\mathcal{J}(\omega, \underline{Y}|\underline{Y})} \quad 5 - 1$$

This function of \underline{X} is a measure of the change in output signal-to-noise ratio that results from steering the detector toward \underline{X} not coincident with the target signal location \underline{Y} . When \mathcal{D} is close to unity, there is little change.

b) The Normalized b-Detector SNR

The normalized SNR for the b-detector is (Eqs. 5 - 1, 4 - 24 and 4 - 27)

$$\mathcal{D}^{(b)}(\omega, \underline{X}|\underline{Y}) = \frac{\mathcal{J}^{(b)}(\omega, \underline{X}|\underline{Y})}{\mathcal{J}^{(b)}(\omega, \underline{Y}|\underline{Y})} = \frac{|\underline{h}^*(\omega, \underline{X}) \Lambda^{-1}(\omega) \underline{h}(\omega, \underline{Y})|^2}{\Lambda^{-1}(\omega) \|\underline{h}(\omega, \underline{X})\|^2 \Lambda^{-1}(\omega) \|\underline{h}(\omega, \underline{Y})\|^2} \quad 5 - 2$$

This measure is never greater than when the steering vector \underline{X} coincides with the signal location \underline{Y} .

As an example, $\mathcal{D}^{(b)}(\omega, \underline{X}|\underline{Y})$ is plotted in Fig. 5 - 1 for a case in which the time frequency is 40 hz, the array length is 50 meters, and the background noise is 13 sea noise with -20 db of self noise. The postulated array has 12 hydrophones. In Fig. 5 - 1 (a) \mathcal{D} is

$$\omega = 2\pi \times 40 = 251 \text{ RPS}$$

Background Noise is 13 Sea Noise

$$\frac{\gamma}{n_1} = m_0 = -20 \text{ db}$$

$$L = 50 \text{ Meters}$$

$$n = 12 \text{ Hydrophones}$$

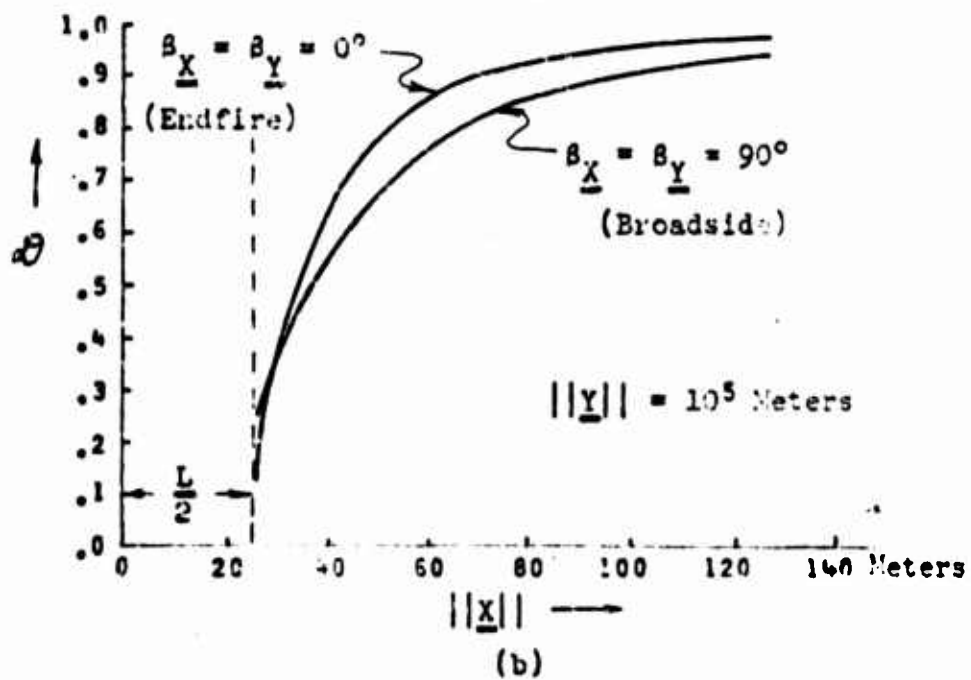
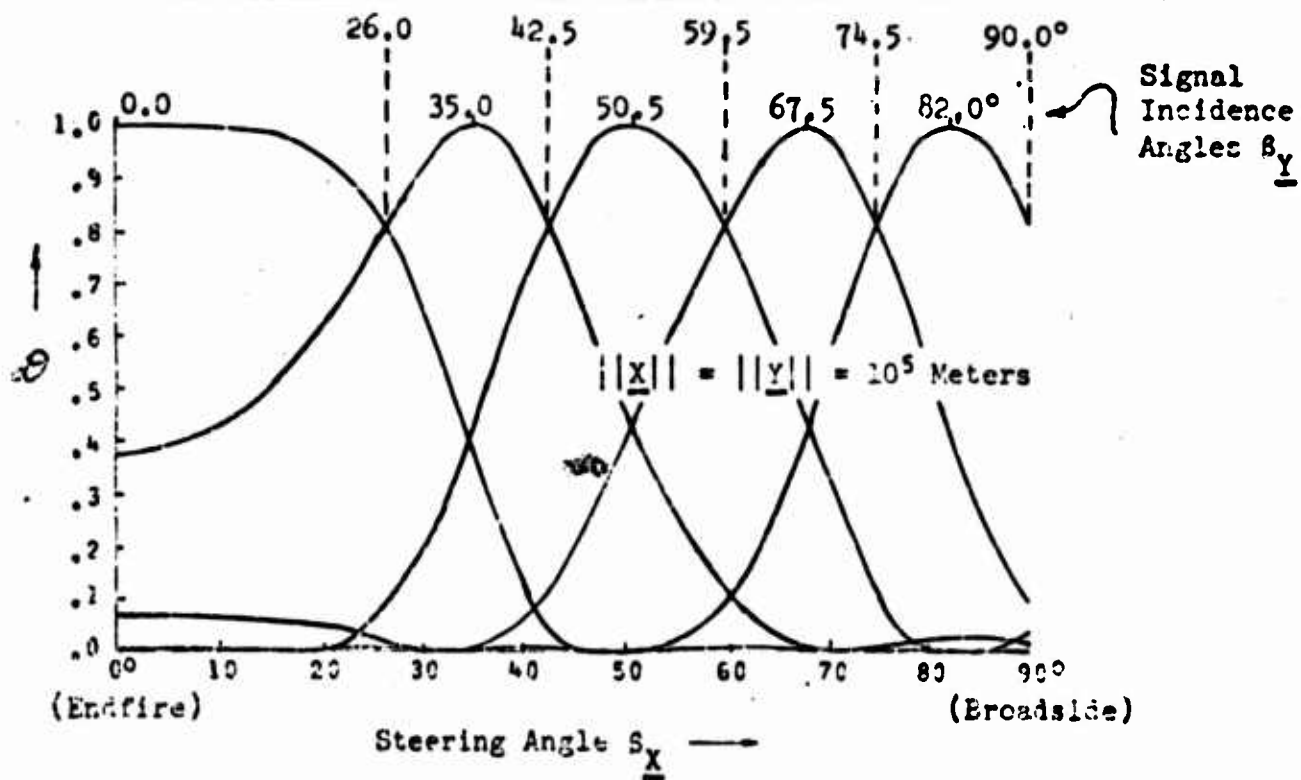


Figure 5-1 Normalized Output SNR for the b-Detector

plotted for signals incident at 0° , 35° , 50.5° , 67.5° , and 82° . The range $||\underline{Y}||$ to the source of these signals is 10^5 meters. Now if the detector is steered at angles 26.0° , 42.5° , 59.5° , 74.5° , and 90.0° at a range of 10^5 meters, it is observed in this figure that the signal-to-noise ratios for signals at the chosen incidences will still be at least 80% of their maximum values. The signal-to-noise ratios for signals at all other incidences should be an even higher percentage of their maximum values.

The outputs of the b-detector steered toward a particular location may be regarded as a sample of its output over the region of possible signal locations. Concerning signals at a range of 10^5 meters, Fig. 5 - 1 (a) indicates that steering the 12 element array toward sampling incidences of 26.0° , 42.5° , ..., 90° will insure that no signal of incidence between these sampling incidences will go undetected.

According to Fig. 5 - 1 (b), the b-detector output signal-to-noise ratio is not appreciably affected by steering range until $||\underline{X}||$ is less than 100 meters.

c) The Normalized c-Detector SNR

Referring to Eqs. 5 - 1, 4 - 56 and 4 - 57, the normalized output SNR for the c-detector is

$$\mathcal{D}^{(c)}(\omega, \underline{X}|\underline{Y}) = \frac{\mathcal{J}^{(c)}(\omega, \underline{X}|\underline{Y})}{\mathcal{J}^{(c)}(\omega, \underline{Y}|\underline{Y})} = \frac{|h^{*'}(\omega, \underline{X})h(\omega, \underline{Y})|^2 \mathcal{J}^{(c)}(\omega, \underline{X}|\underline{X})}{M(\underline{X})M(\underline{Y})L^2 \mathcal{J}^{(c)}(\omega, \underline{Y}|\underline{Y})} \quad 5 - 3$$

This measure \mathcal{D} for the c-detector is not necessarily everywhere less than unity. That is, the output signal-to-noise ratio for the c-detector may be improved in some instances by steering it toward a location \underline{X} other than \underline{Y} , the location of the signal source.

In Fig. 5 - 2, $\mathcal{D}^{(c)}$ is compared with $\mathcal{D}^{(b)}$ in both an I2 and an I3 sea noise background. The c-detector is seen to be unbiased for both endfire and broadside target signals. However, at intermediate incidences the c-detector may be strongly biased. In fact, when a target signal is incident at 50.0° and the background is I2 sea noise, the c-detector exhibits its highest output when steered in a 55° direction. When the background is I3 sea noise the bias is reversed, and the strongest c-detector output occurs at a steering direction of 44° . The measure \mathcal{D} for the b-detector with this signal incidence is unbiased and practically the same in both I2 and I3 sea noise backgrounds.

d) The Normalized l-Detector SNR

The normalized output SNR for the l-detector is (Eqs. 5 - 1 and 4 - 68).

$$\mathcal{D}^{(l)}(\omega, \underline{X}|\underline{Y}) = \frac{\mathcal{J}^{(l)}(\omega, \underline{X}|\underline{Y})}{\mathcal{J}^{(l)}(\omega, \underline{Y}|\underline{Y})}$$

$$= \frac{\sqrt{H(D(\omega, \underline{Y}))} \sum_{k \in D(\omega, \underline{X})} \mathcal{C}_k(\omega, \underline{Y})}{\sqrt{H(D(\omega, \underline{X}))} \sum_{k \in D(\omega, \underline{Y})} \mathcal{C}_k(\omega, \underline{Y})}$$

5 - 4

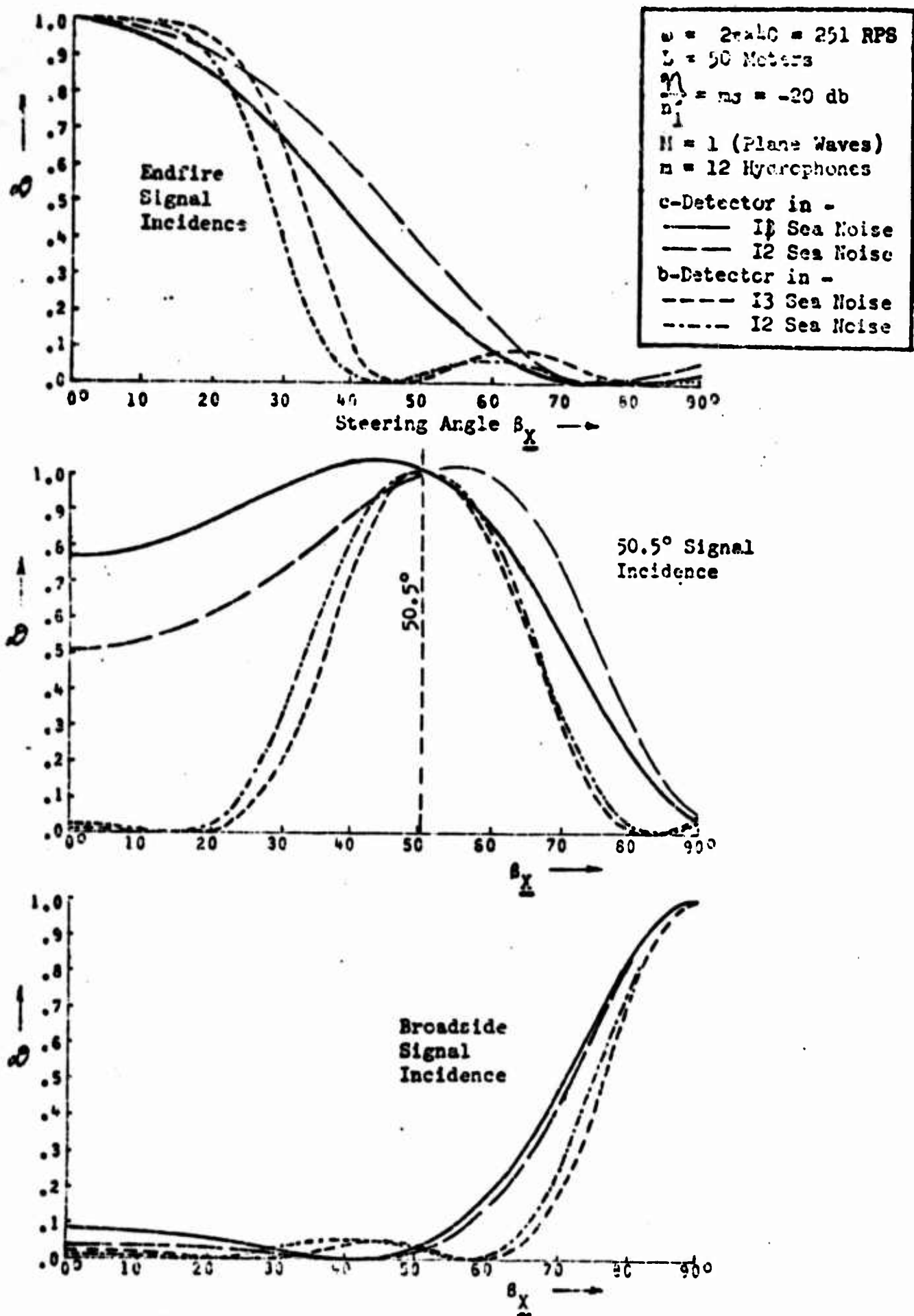


Figure 5-2 Normalized Output SNR for b and c-Detectors in 12 and 13 Sea Noise

5.2 An Influence Measure \mathcal{H}

a) Definition

The measure \mathcal{D} in the previous section provides an indication of the range of steering vectors \underline{X} over which a signal emanating from \underline{Y} has essentially undiminished effect. Turning this around, the question considered below is the change in response of a detector having a fixed steering vector \underline{X} as the signal origin \underline{Y} ranges away from \underline{X} . At a frequency ω , this response change may be viewed through the output signal-to-noise ratio $\phi(\omega, \underline{X}|\underline{Y})$; in fact, a general influence measure $\mathcal{H}(\omega, \underline{Y}|\underline{X})$ on $\underline{Y} \in \mathcal{R}$ is obtained from this by dividing out the implicit dependence on received input signal power $s(\omega|\underline{Y})$ and by normalizing with respect to $\phi(\omega, \underline{X}|\underline{X})$. The result is (see Eq. 4 - 12)

$$\begin{aligned} \mathcal{H}(\omega, \underline{Y}|\underline{X}) &= \frac{\phi(\omega, \underline{X}|\underline{Y})}{\phi(\omega, \underline{X}|\underline{X})} \bigg/ \frac{s(\omega|\underline{Y})}{s(\omega|\underline{X})} \\ &= \frac{M(\underline{Y}) \mathcal{J}(\omega, \underline{X}|\underline{Y})}{M(\underline{X}) \mathcal{J}(\omega, \underline{X}|\underline{X})} . \end{aligned}$$

5 - 5

Since the noise power in the output of the detector is practically independent of the low level signals being considered, this noise power is constant with \underline{Y} for fixed steering vector \underline{X} . For a given \underline{X} , then, \mathcal{H} is the ratio of the average detector output deflection caused by a received signal arriving from \underline{Y} to that caused by a received signal of the same strength arriving from \underline{X} itself. Thus when $\underline{Y} = \underline{X}$, this measure is unity. If the signal from \underline{Y} is not badly out of focus and if the noise field interferes less with the signal from \underline{Y} than with the one from \underline{X} , then the measure \mathcal{H} may be greater than unity.

The quantity \mathcal{H} may be considered a measure of the influence of either signals or noise components. Should the object be to assess the

influence of a noise wave ϕ that is not expressible as a signal emanating from some point \underline{Y} , then $\textcircled{H}(\underline{Y}|\underline{X})$ may be generalized to $\textcircled{H}(\underline{Y}|\phi)$ by replacing $\underline{h}(\omega, \underline{Y})$ (see Eq. 2 - 79) with

$$\underline{h}(\omega, \phi) = \left(\int_{-\frac{L}{2}}^{\frac{L}{2}} \psi_k^*(\omega, x) \phi(x) dx \right). \quad 5 - 6$$

b) \textcircled{H} for the b-Detector

Referring to Eqs. 5 - 5, 4 - 24 and 4 - 27, the influence measure for the b-detector is

$$\textcircled{H}^{(b)}(\omega, \underline{Y}|\underline{X}) = \frac{M(\underline{Y}) \mathcal{J}^{(b)}(\omega, \underline{X}|\underline{Y})}{M(\underline{X}) \mathcal{J}^{(b)}(\omega, \underline{X}|\underline{X})} = \left| \frac{\underline{h}^*(\omega, \underline{X}) \Lambda^{-1}(\omega) \underline{h}(\omega, \underline{Y})}{\Lambda^{-1}(\omega) ||\underline{h}(\omega, \underline{X})||^2} \right|^2. \quad 5 - 7$$

As an illustration, \textcircled{H} is plotted in Fig. 5 - 3 for the b-detector (solid line) steered at a range $||\underline{X}||$ of 5 kilometers and an angle $\beta_{\underline{X}}$ of 40° . Under the circumstances chosen here ($\omega = 2\pi \times 40$, 13 sec noise background, etc.) Fig. 5 - 3 (a) indicates that the b-detector so steered is significantly influenced by signals of incidence $\beta_{\underline{Y}}$ from zero to about seventy degrees ($||\underline{Y}|| = 5$ km). And signals at 35° incidence cause an even larger output deflection in a detector steered at 40° than do signals at the 40° incidence itself. This is of course no paradox since an appropriately steered b-detector in general exhibits appreciably larger sensitivity as the signal incidence approaches endfire. The 35° signal deflection observed at 40° steering is in fact the tail of the entire 35° signal response versus steering angle.

All signals having an incidence of 40° and a range greater than the length of the array show approximately the same influence (Fig. 5 - 3(b)).

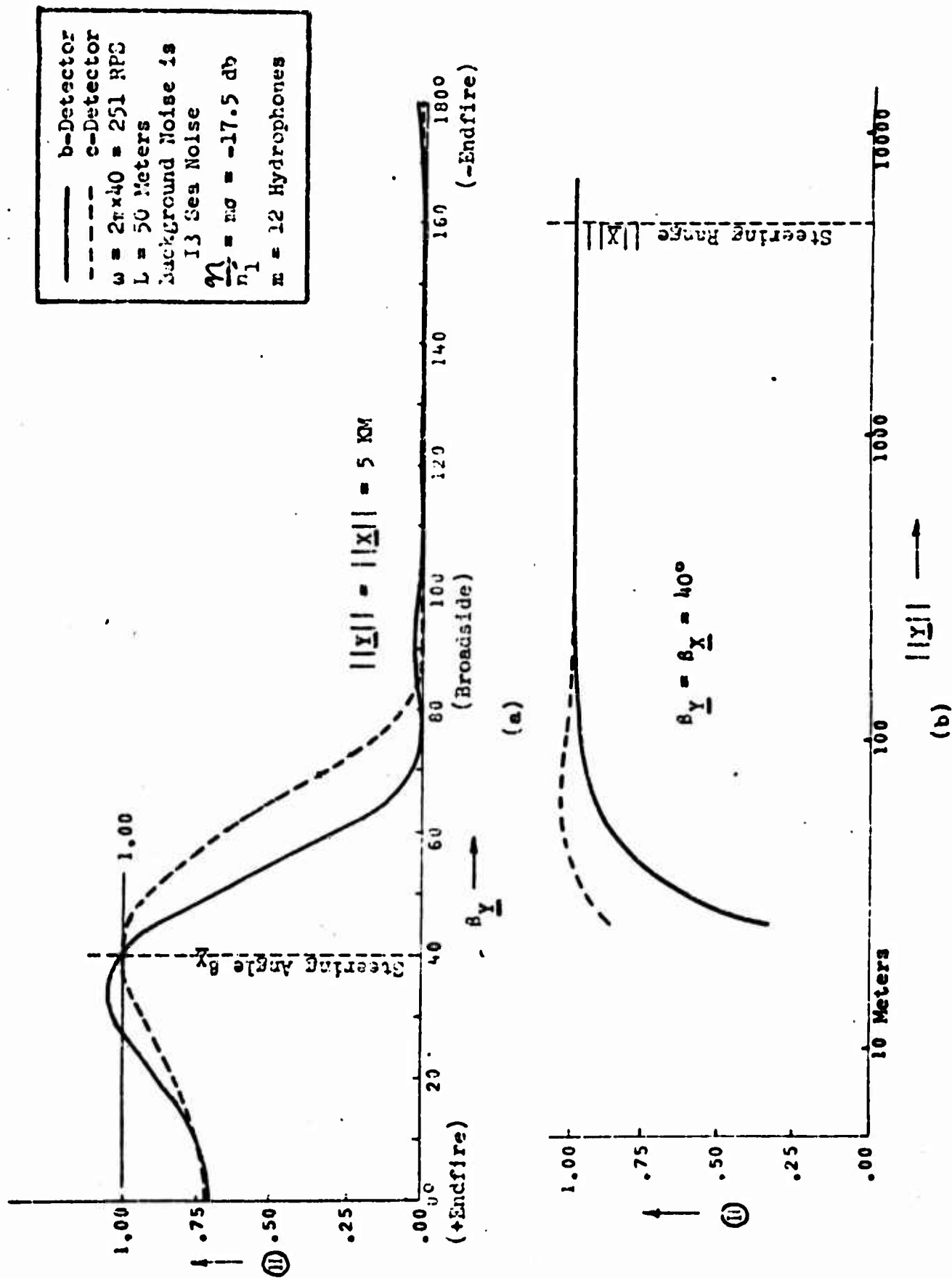


Figure 5-3 The Influence Measure II for the b and c-Detectors

At shorter ranges, the influence of 40° signals is appreciably diminished.

By itself the influence curve in Fig. 5 - 3 (b) describes the variation in the output SNR for signals which produce the same input level at the array. Now since the range varies, this curve does not directly describe the overall variation in the output SNR for signals with the same source strength. To express this new circumstance, the varying input level $s(\omega|Y)$ may be attached as a simple multiplicative factor on \textcircled{H} (see Eq. 5 - 5).

c) \textcircled{H} for the c-Detector

Placing the left-hand sides of Eqs. 4 - 56 and 4 - 57 in the definition of \textcircled{H} (Eq. 5 - 5), the c-detector influence measure becomes

$$\textcircled{H}^{(c)}(\omega, \underline{Y}|\underline{X}) = \frac{M(\underline{Y}) \mathcal{J}^{(c)}(\omega, \underline{X}|\underline{Y})}{M(\underline{X}) \mathcal{J}^{(c)}(\omega, \underline{X}|\underline{X})} = \left| \frac{h^*(\omega, \underline{X}) h(\omega, \underline{Y})}{M(\underline{X})L} \right|^2 \quad 5 - 8$$

This measure is plotted in Fig. 5 - 3 (dashed line) along with the plot of $\textcircled{H}^{(b)}$ discussed in part b. The comparatively uniform response of the c-detector to signals at diverse incidences is reflected in the more regular decay of $\textcircled{H}^{(c)}(\underline{Y})$ away from the steering location \underline{X} .

d) \textcircled{H} for the l-Detector

The measure \textcircled{H} for the l-detector is (Eqs. 5 - 5 and 4 - 68)

$$\textcircled{H}^{(l)}(\omega, \underline{X}|\underline{Y}) = \frac{M(\underline{Y}) \mathcal{J}^{(l)}(\omega, \underline{X}|\underline{Y})}{M(\underline{X}) \mathcal{J}^{(l)}(\omega, \underline{X}|\underline{X})}$$

$$= \frac{M(\underline{Y}) \sum_{k \in D(\omega, \underline{X})} c_k(\omega, \underline{Y})}{M(\underline{X}) \sum_{k \in D(\omega, \underline{X})} c_k(\omega, \underline{X})} = \frac{\sum_{k \in D(\omega, \underline{X})} \frac{|h_k(\omega, \underline{Y})|^2}{\lambda_k(\omega)}}{\sum_{k \in D(\omega, \underline{X})} \frac{|h_k(\omega, \underline{X})|^2}{\lambda_k(\omega)}} \quad 5 - 9$$

5.3 Uncertainty in Signal Source Location

A new measure is proposed below that will indicate how well a detector can determine the location of a target signal source. This measure will quantitatively illustrate how the uncertainty in the signal source location depends upon the observation time, the signal-to-noise ratio, the noise model, the location of the signal, and the geometry of the array.

The basis for this measure is the location equation (Eq. 1 - 56)

$$f(\underline{X}|\underline{u}, \underline{Y} \in \mathcal{R}) = \frac{e^{b(\underline{u}, \underline{X})}}{K(\underline{u})} \quad . \quad 5 - 10$$

The term $b(\underline{u}, \underline{X})$ is the output of the b-detector and $K(\underline{u})$ is a constant independent of the scanning vector \underline{X} . The proposed statistic is to be a measure of the shape of $f(\underline{X}|\underline{u}, \underline{Y} \in \mathcal{R})$ considered as a function of \underline{X} ; therefore it need not contain $K(\underline{u})$. In fact, the ratio

$$\frac{e^{b(\underline{u}, \underline{X})}}{e^{b(\underline{u}, \underline{Y})}} \quad 5 - 11$$

will serve as well as $f(\underline{X}|\underline{u}, \underline{Y} \in \mathcal{R})$ itself, where \underline{Y} is the location of a test signal. If this test signal is sent to the detector, this ratio should be a measure of the ability of the b-detector to determine the location of the test source. That is, when this test signal is present, the above ratio will contain all the significant shape information in $f(\underline{X}|\underline{u}, \underline{Y} \in \mathcal{R})$. This ratio, however, is still somewhat random because of the randomness of \underline{u} . Since this randomness tends to mask the variations due to changes in the physical circumstances (observation time, etc.) the measure proposed below is not this ratio, but a nonrandom description of it. The measure is in fact obtained by

setting the sample variance of $\underline{h}_1^{*'}(\underline{X})\Lambda_1^{-1}\underline{u}_1$ equal to its variance. For long observation times, $b(\underline{u}, \underline{X})$ is the sum of a large set of independent components, many of which have approximately the same variance. The sample variances obtained in forming $b(\underline{u}, \underline{X})$ are therefore expected to be quite close to actual variances at long observation times.

Specifically, the index set Ω^+ of the positive time frequency indices may be partitioned into subsets Δ_p of consecutive indices such that

$$\Omega = \{\Delta_p\} \quad 5 - 12$$

and

$$\Delta_p \cap \Delta_{p'} = 0 \quad 5 - 13$$

when $p \neq p'$. As the observation time T is extended, the indices in any Δ_p denote frequencies that become closer together. If the observed process is smooth relative to the frequency spacing (the reciprocal of the observation time), the signal and noise variances will be approximately the same over many consecutive discrete time frequencies. Each Δ_p will be taken small enough that the same variance may be assigned to all components whose indices are within it. The set of all p 's will be labeled P .

With this notation, the output of the b -detector may be written

$$\begin{aligned} b(\underline{u}, \underline{X}) &= 2 \sum_{i \in \Omega^+} \left(|\underline{z}_1^{*'}(\underline{X})\underline{u}_1|^2 - \ln(1 + \underline{s}_1\Lambda_1^{-1}||\underline{h}_1(\underline{X})||^2) \right) + \ln f_1(\underline{X}) \\ &\approx 2 \sum_{p \in P} \sum_{i \in \Delta_p} |\underline{z}_1^{*'}(\underline{X})\underline{u}_1|^2 - 2 \sum_{i \in \Omega^+} \ln(1 + \underline{s}_1\Lambda_1^{-1}||\underline{h}_1(\underline{X})||^2) + \ln f_1(\underline{X}) \end{aligned} \quad 5 - 14$$

in which

$$\underline{g}_1(\underline{x}) = \sqrt{\frac{s_1}{1 + s_1 \Lambda_1^{-1} ||\underline{h}_1(\underline{x})||^2}} \Lambda_1^{-1} \underline{h}_1(\underline{x}) . \quad 5 - 15$$

Over the set of consecutive indices i in Δ_p , the inner product term in Eq. 5 - 14 may then be written

$$\begin{aligned} & \sum_{i \in \Delta_p} |\underline{g}_i^*(\underline{x}) \underline{u}_i|^2 \\ &= \sum_{i \in \Delta_p} \frac{s_1}{1 + s_1 \Lambda_1^{-1} ||\underline{h}_1(\underline{x})||^2} |\underline{h}_1^*(\underline{x}) \Lambda_1^{-1} \underline{u}_i|^2 \\ &= \frac{s_{1(p)}}{1 + s_{1(p)} \Lambda_{1(p)}^{-1} ||\underline{h}_{1(p)}(\underline{x})||^2} \sum_{i \in \Delta_p} |\underline{h}_1^*(\underline{x}) \Lambda_1^{-1} \underline{u}_i|^2 \end{aligned} \quad 5 - 16$$

where $i(p)$ is any index i belonging to Δ_p . Now if the frequency band covered by Δ_p is denoted by $\Delta\omega_p$, the number of elements H in Δ_p may be written

$$H(\Delta_p) = \frac{\Delta\omega_p T}{2\pi} . \quad 5 - 17$$

Consequently Eq. 5 - 16 may be written

$$\begin{aligned} & \sum_{i \in \Delta_p} |\underline{g}_i^*(\underline{x}) \underline{u}_i|^2 \\ &= \frac{1}{1 + s_{1(p)} \Lambda_{1(p)}^{-1} ||\underline{h}_{1(p)}(\underline{x})||^2} \frac{\Delta\omega_p T}{2\pi} s_{1(p)} \frac{1}{H(\Delta_p)} \sum_{i \in \Delta_p} |\underline{h}_1^*(\underline{x}) \Lambda_1^{-1} \underline{u}_i|^2 . \end{aligned} \quad 5 - 18$$

For a fixed degree of location uncertainty, the longer the observation time T , the smaller will be the signal power $s_{1(p)}$. This compensation suppresses the absolute size of the random variations in

$$T s_{1(p)} \frac{1}{H(\Delta_p)} \sum_{1 \in \Delta_p} |\underline{h}_1^{*'}(\underline{X}) \Lambda_1^{-1} \underline{u}_1|^2 \quad 5 - 19$$

as T is extended (i.e. as the sample size is increased). For long T , then, it appears reasonable in constructing a non-random measure, to replace the sample variance

$$\frac{1}{H(\Delta_p)} \sum_{1 \in \Delta_p} |\underline{h}_1^{*'}(\underline{X}) \Lambda_1^{-1} \underline{u}_1|^2 \quad 5 - 20$$

with the actual variance

$$V\left(\underline{h}_1^{*'}(\underline{X}) \Lambda_{1(p)}^{-1} \underline{u}_{1(p)}\right) = \Lambda_{1(p)}^{-1} ||\underline{h}_{1(p)}(\underline{X})||^2 + s_{1(p)} |\underline{h}_1^{*'}(\underline{X}) \Lambda_{1(p)}^{-1} \underline{h}_{1(p)}(\underline{Y})|^2. \quad 5 - 21$$

(The actual variances of all components with indices 1 within Δ_p are being assumed to be the same.) Making this substitution in Eq. 5 - 18 and placing the quantity obtained back into the right-hand side of Eq. 5 - 14, the resulting output statistic \hat{b} is defined by

$$\begin{aligned} \hat{b}(\underline{X}|\underline{Y}) = & T \sum_{p \in P} s_{1(p)} \frac{\frac{\Delta \omega_p}{2\pi} \Lambda_{1(p)}^{-1} ||\underline{h}_{1(p)}(\underline{X})||^2 + s_{1(p)} |\underline{h}_1^{*'}(\underline{X}) \Lambda_{1(p)}^{-1} \underline{h}_{1(p)}(\underline{Y})|^2}{1 + s_{1(p)} \Lambda_{1(p)}^{-1} ||\underline{h}_{1(p)}(\underline{X})||^2} \\ & - 2 \sum_{1 \in \Omega+} \ln \left(1 + s_1 \Lambda_1^{-1} ||\underline{h}_1(\underline{X})||^2 \right) + \ln f_1(\underline{X}) \quad 5 - 22 \end{aligned}$$

These summations are approximated by integrals as follows,

$$\hat{b}(\underline{x}|\underline{y}) = \frac{T}{\pi} \int_0^\infty \left[\frac{s(\omega) \Lambda^{-1}(\omega) ||\underline{h}(\omega, \underline{x})||^2 + s(\omega)^2 |\underline{h}^*(\omega, \underline{x}) \Lambda^{-1}(\omega) \underline{h}(\omega, \underline{y})|^2}{1 + s(\omega) \Lambda^{-1}(\omega) ||\underline{h}(\omega, \underline{x})||^2} - \ln[1 + s(\omega) \Lambda^{-1}(\omega) ||\underline{h}(\omega, \underline{x})||^2] \right] d\omega + \ln f_1(\underline{x}) \quad 5 - 23$$

Replacing b in Eq. 5 - 11 with \hat{b} , the definition of the location uncertainty measure \mathcal{H} becomes

$$\mathcal{H}(\underline{x}|\underline{y}) = \frac{e^{\hat{b}(\underline{x}|\underline{y})}}{e^{\hat{b}(\underline{y}|\underline{y})}} \quad 5 - 24$$

Since this measure \mathcal{H} describes the shape of the a posteriori probability density function of the target signal source location, it indicates the best location definition that can be obtained with any detector of the given geometry. Thus it is a fundamental measure of the locatability of a given signal source using a given passive array.

In addition to its use in forming \mathcal{H} , the output statistic \hat{b} is useful in examining the structure of b . For example, it is apparent from \hat{b} that the term $s(\omega) \Lambda^{-1}(\omega) ||\underline{h}(\omega, \underline{x})||^2$, though small compared with unity in the expression $1 + s(\omega) \Lambda^{-1}(\omega) ||\underline{h}(\omega, \underline{x})||^2$, can yet be very significant.¹ Consequently the expression

¹Writing the integrand in Eq. 5 - 23 as

$$I = \frac{a+b}{1+a} - \ln(1+a) \quad b \ll a \ll 1$$

the approximation $1+a \approx 1$ leads to $I \approx a+b$. However, this does not agree with the expansion

$$I = b - \frac{a^2}{2} + O(ab) + O(a^3)$$

so that unity cannot replace $1+a$.

$1 + s(\omega)\Lambda^{-1}(\omega)||h(\omega, \underline{X})||^2$ is an important part of the structure of a detector forming $b(\underline{u}, \underline{X})$. (It appears in two places in Eqs. 3 - 6 and 3 - 9 for $b(\underline{u}, \underline{X})$).

Two examples are now presented to show how the measure \mathcal{H} may be applied. In the first, a test signal source is placed at an angle of 60° with the axis of the array and at a range of 2 kilometers from the center of the array. The array is 50 meters long and consists of 12 equally spaced hydrophones. The background noise is 13 sea noise plus -30 db of self noise in the hydrophones. The target signal source generates Gaussian noise of constant spectral density 10 db below the background noise at the center of the array in a band from 30 hz to 130 hz. The power outside this band is assumed to be negligible. With a uniform a priori location density function $f_1(\underline{X})$ and a 50 second observation time, the location uncertainty according to Eq. 5 - 24 is as shown in Fig. 5 - 4 (a). If an actual random waveform $v(t, \underline{X})$ were received, an exact but random location uncertainty function could be generated. The measure \mathcal{H} , which is itself not random, should be a reasonable description of the significant shape aspects of this exact, random location uncertainty function.

Fig. 5 - 4 (b) shows how a section through the measure plotted in Fig. 5 - 4 (a) changes with observation time. The measure \mathcal{H} is plotted at the test signal range of 2 kilometers over a range of angles around the test signal angle of 60 degrees. The observation times are 10, 20, 50, and 150 seconds.

Fig. 5 - 4 (c) shows how the same section through the measure varies as the low frequency cutoff is raised. Raising this lower cutoff until the original bandwidth is reduced by 60% decreases the bearing resolution

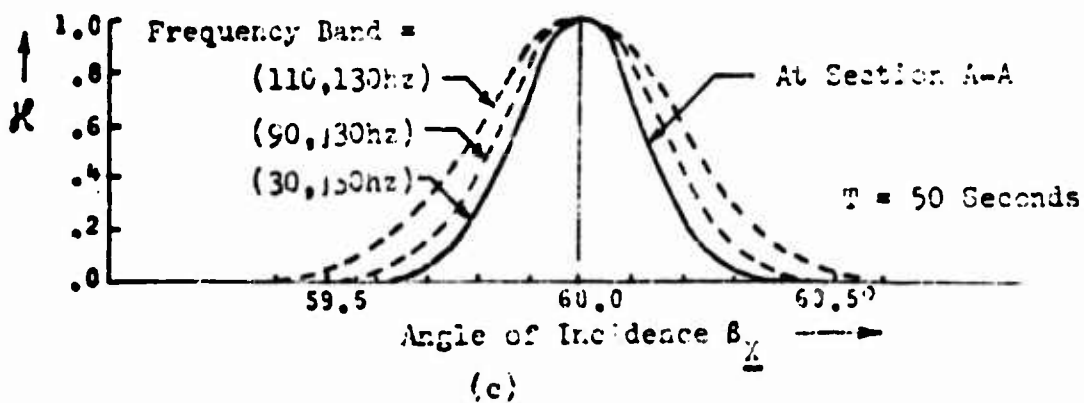
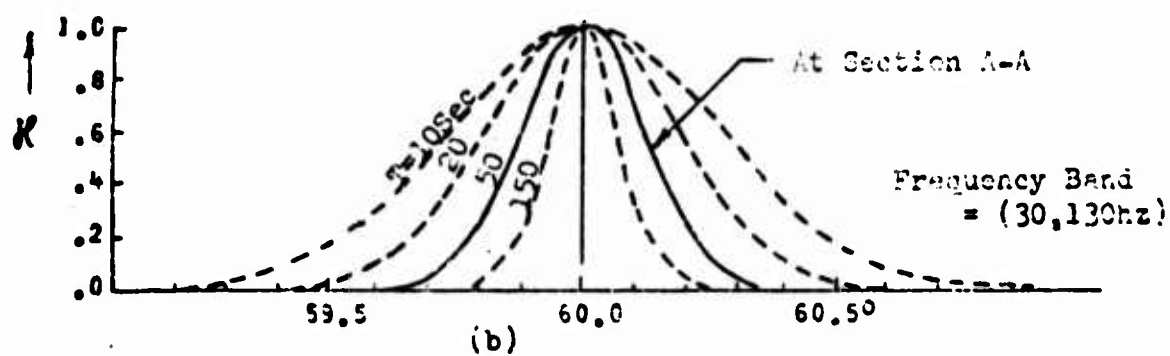
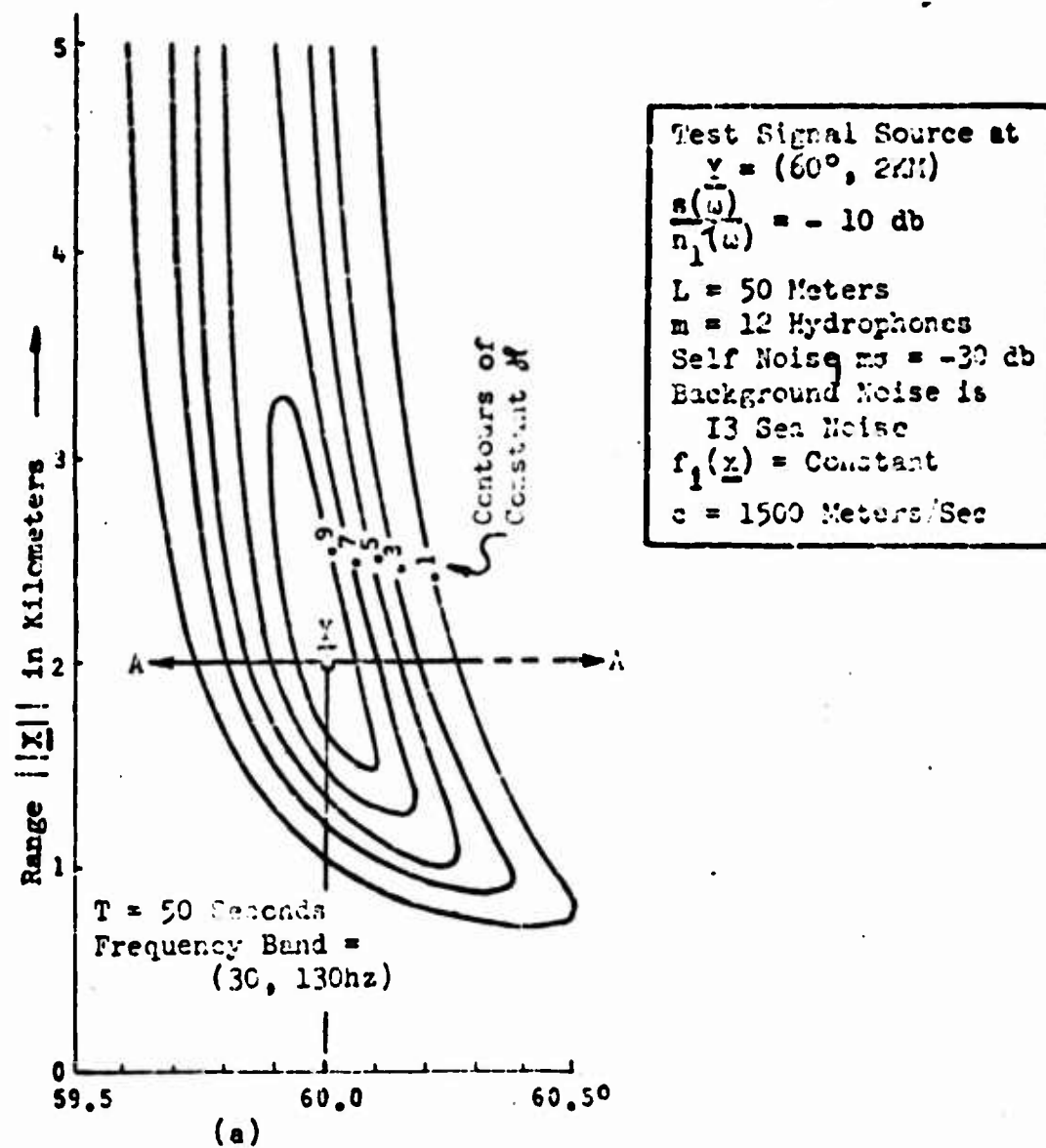


Figure 5-4 Location Uncertainty Using the B-Detector

by only 20% . In fact the detector still has over half its original bearing resolution after the lower 80% of its frequency band is removed. In this example in which there is strong correlation between the noise received at separate hydrophones, it is apparent that the highest frequencies present carry almost all of the location information.

As a second example, the angle resolution is determined for the same array in a background of both I2 sea noise and I3 sea noise. The same signal source is moved to a range of 10 kilometers from its two kilometer range in the first example. Assuming spherical spreading, this lowers the signal-to-noise ratio to -24 from -10 db in the first example. Now at this range, the source is moved in 10° increments around the array. And at each position, the constant range cross-section of the location uncertainty H is plotted in Fig. 5 - 5. (Constant bearing cross-sections are virtually flat in the region of 10 km.) With the I2 sea noise background, the bearing resolution in the endfire region is worse than with the I3 sea noise background. In the broadside region, the situation is reversed. This is to be expected from a comparison of the two dimensional spectra for the two noise fields pictured in Fig. 2 - 1 and Fig. 2 - 2. In fact Fig. 4 - 2 shows that the b-detector array gain in an I2 sea noise background is higher near broadside but lower near endfire than in an I3 sea noise background.

--- 12 Noise Background
 --- 13 Noise Background
 Steering Range $||x|| = 10$ KM
 Self Noise = $m_0 = -30$ db
 $L = 50$ Meters
 $c = 1500$ Meters/Sec
 Test Signal Source
 $\beta_y = 0^\circ, 10^\circ, \dots, 90^\circ$
 $||y|| = 10$ KM
 $\frac{s(\omega)}{n_1(\omega)} = -24$ db $T = 50$ Sec
 Frequency Band = (30, 130 hz)

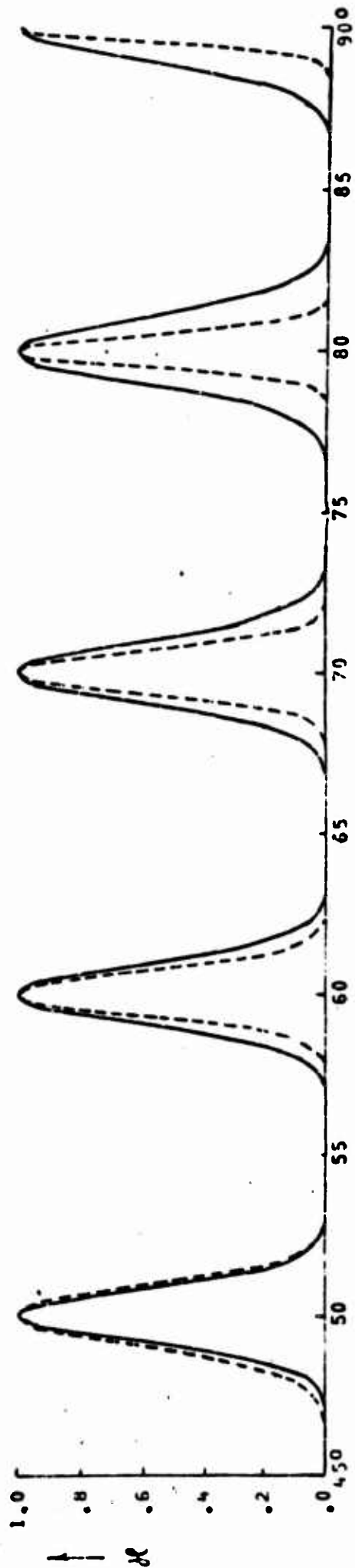
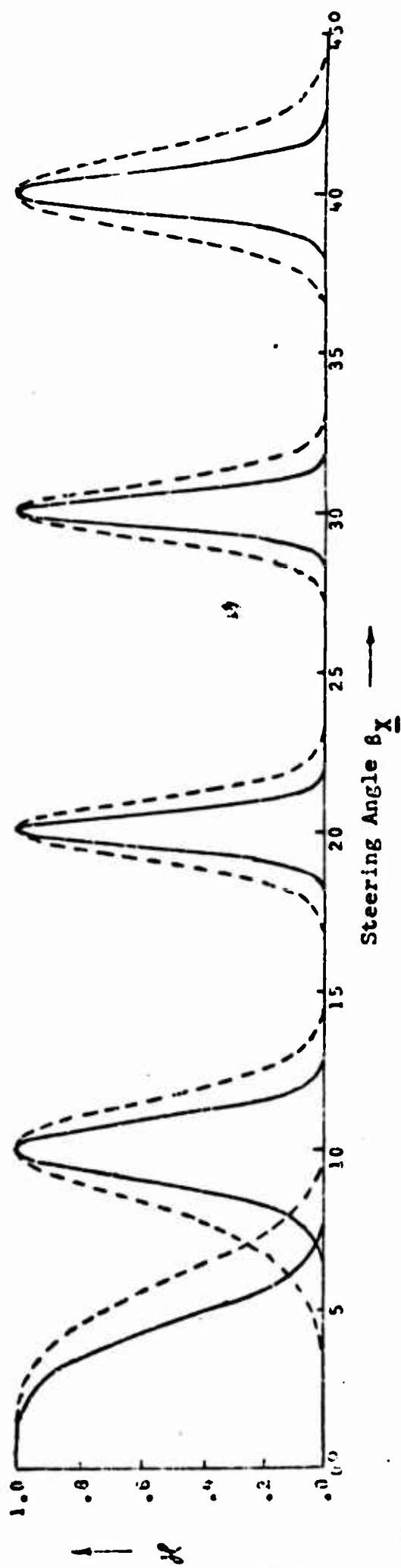


Figure 5-5 b-Detector Bearing Resolution

5.4 A Bias Measure for the c-Detector

When a target signal is present at \underline{Y} , the output of the c-detector will be a maximum when steered at some location other than \underline{Y} . A non-random indication $B^{(c)}$ of the difference between this location and \underline{Y} is a measure of the bias in the c-detector. As in Eq. 5 - 14 for the b-detector, the c-detector output may be written

$$c(\underline{u}, \underline{X}) = 2 \sum_{i \in \Omega^+} \left\{ \frac{s_1}{\lambda_1} \frac{|h_1^*(\underline{X}) u_1|^2}{1 + \frac{s_1}{\lambda_1} LM(\underline{X})} - \ln \left(1 + \frac{s_1}{\lambda_1} LM(\underline{X}) \right) \right\} + \ln f_1(\underline{X}) . \quad 5 - 25$$

The bias measure $B^{(c)}$ will be derived from this random output using the notation, assumptions and methods of Sect. 5.3.

It has been assumed thus far that the signal power s and the noise power n_1 are known. In interpreting the results of this section it will be of interest to note the significance of this assumption. To allow this, a notational distinction is made between the values of the signal and noise power that are used in implementing the detector and those that prevail in the received signal \underline{u} . The values of the signal and noise power used in the implementation will be denoted by \hat{s} and \hat{n}_1 respectively.

The quantity λ_1 called for by the implementation according to Eq. 5 - 25 is given by Eq. 3 - 26.

$$\lambda_1 \equiv \lambda_1(\underline{Z}) = \frac{1}{LM(\underline{Z})} \Lambda_1 ||h_1(\underline{Z})||^2 = \frac{L \hat{n}_1(\omega_1)}{J^{(c)}(\omega, \underline{Z} | \underline{Z})} \quad 5 - 26$$

where \underline{Z} is some representative vector in the region of scan \mathcal{R} .

(For most analyses, \underline{Z} may be set equal to the signal source location vector \underline{Y}).

Furthermore, two simplifying assumptions are made:

1. only plane wave signals are considered, i.e., $M(\underline{X}) = M(\underline{Y}) = 1$;
2. the a priori location probability density $f_1(\underline{X})$ is assumed uniform over the incidences of interest.

Under assumption 1, the bias is expressed as an angular difference between the incidence $\beta_{\underline{Y}}$ of the signal and the steering angle $\beta_{\underline{X}}$ at which the c-detector output $c(\underline{u}, \underline{X} | \underline{Y})$ is a maximum. And under both assumptions this bias is determined by the first term in the right-hand side of Eq. 5 - 25. This term is

$$t(\underline{u}, \underline{X}) = 2 \sum_{1 \in \Omega} \frac{\hat{s}(\omega_1) \mathcal{J}^{(c)}(\omega_1, \underline{Z} | \underline{Z})^2 |\underline{h}_1^{*'}(\underline{X}) \underline{u}_1|^2}{L^2 \hat{n}_1(\omega_1)^2 \left(1 + \frac{\hat{s}_1}{\hat{n}_1(\omega_1)} \mathcal{J}^{(c)}(\omega_1, \underline{Z} | \underline{Z}) \right)} . \quad 5 - 27$$

Now a non-random description of this term is obtained by the methods of Sect. 5.3. First, t is written

$$t(\underline{u}, \underline{X}) = 2 \sum_{p \in P} \frac{\mathcal{J}^{(c)}(\omega_{1(p)}, \underline{Z} | \underline{Z})^2}{L^2 \hat{n}_1(\omega_{1(p)}) \left(1 + \frac{\hat{s}(\omega_{1(p)})}{\hat{n}_1(\omega_{1(p)})} \mathcal{J}^{(c)}(\omega_{1(p)}, \underline{Z} | \underline{Z}) \right)} \\ \cdot \frac{\Delta \omega_p}{2\pi} \frac{\hat{s}(\omega_{1(p)})}{\hat{n}_1(\omega_{1(p)})} \frac{1}{H(\Delta_p)} \sum_{1 \in \Delta_p} |\underline{h}_1^{*'}(\underline{X}) \underline{u}_1|^2 . \quad 5 - 28$$

Then the sample variance

$$\frac{1}{H(\Delta_p)} \sum_{1 \in \Delta_p} |\underline{h}_1^{*'}(\underline{X}) \underline{u}_1|^2 \quad 5 - 29$$

is replaced by the actual variance

$$V(\underline{h}_{1(p)}^*(\underline{X})\underline{u}_{1(p)}) = \Lambda_{1(p)} \| \underline{h}_{1(p)}(\underline{X}) \|^2 + s(\omega_{1(p)}) | \underline{h}_{1(p)}^*(\underline{X}) \underline{h}_{1(p)}(\underline{Y}) |^2 \quad 5 - 30$$

to yield the non-random quantity

$$\hat{t}(\underline{u}, \underline{X}) =$$

$$\begin{aligned} & \frac{T}{L^2 \pi} \sum_{p \in P} \frac{\hat{s}(\omega_{1(p)}) \mathcal{D}^{(c)}(\omega_{1(p)}, \underline{Z}|\underline{Z})^2 (\Lambda_{1(p)} \| \underline{h}_{1(p)}(\underline{X}) \|^2 + s(\omega_{1(p)}) | \underline{h}_{1(p)}^*(\underline{X}) \underline{h}_{1(p)}(\underline{Y}) |^2)}{\hat{n}_1(\omega_{1(p)})^2 \left(1 + \frac{\hat{s}(\omega_{1(p)})}{\hat{n}_1(\omega_{1(p)})} \mathcal{D}^{(c)}(\omega_{1(p)}, \underline{Z}|\underline{Z}) \right)} \Delta \omega_p \\ & \approx \frac{T}{L^2 \pi} \int_0^\infty \frac{\hat{s}(\omega) \mathcal{D}^{(c)}(\omega, \underline{Z}|\underline{Z})^2 (\Lambda(\omega) \| \underline{h}(\omega, \underline{X}) \|^2 + s(\omega) | \underline{h}^*(\omega, \underline{X}) \underline{h}(\omega, \underline{Y}) |^2)}{\hat{n}_1(\omega)^2 \left(1 + \frac{\hat{s}(\omega)}{\hat{n}_1(\omega)} \mathcal{D}^{(c)}(\omega, \underline{Z}|\underline{Z}) \right)} d\omega \\ & = \frac{T}{L^2 \pi} \int_0^\infty \frac{\hat{s}(\omega) s(\omega)}{\hat{n}_1(\omega)^2} \frac{\mathcal{D}^{(c)}(\omega, \underline{Z}|\underline{Z})^2 | \underline{h}^*(\omega, \underline{X}) \underline{h}(\omega, \underline{Y}) |^2}{1 + \frac{\hat{s}(\omega)}{\hat{n}_1(\omega)} \mathcal{D}^{(c)}(\omega, \underline{Z}|\underline{Z})} \\ & \quad \cdot \left(1 + \frac{1}{\frac{s(\omega)}{\hat{n}_1(\omega)} \mathcal{D}^{(c)}(\omega, \underline{Y}|\underline{Y}) \mathcal{D}^{(c)}(\omega, \underline{X}|\underline{Y})} \right) d\omega . \end{aligned} \quad 5 - 31$$

It is noted (Eq. 5 - 28) that this description \hat{t} improves as the observation time T is increased while the product of T and the estimated signal-to-noise ratio $\frac{\hat{s}(\omega)}{\hat{n}(\omega)}$ is held constant.

The term \hat{t} provides the basis for the c-detector plane wave bias measure $B^{(c)}$ as follows. With \mathcal{R} limited to sources which would produce essentially plane wave signals at the array, the bias in receiving a signal from $\underline{Y} \in \mathcal{R}$ is given by

$$B^{(c)}(\underline{Y}) = \beta_{\underline{X}} - \beta_{\underline{Y}} \quad 5 - 32$$

in which $\tilde{X} \in \mathcal{R}$ is such that

$$\hat{t}(\tilde{X}|Y) \geq \hat{t}(X|Y)$$

5 - 33

for all $X \in \mathcal{R}$.

The expression for $\hat{t}(X|Y)$ evidences four factors that determine $B^{(c)}(Y)$. The first, $\mathcal{D}^{(c)}(\omega, X|Y)$, may be considered the source of the bias. The less the bias in the directivity $\mathcal{D}^{(c)}$ the less will be the bias indicated by $B^{(c)}$. Fig. 5 - 2 shows, for example, that with a signal incidence of 50.0° at 40 hz in I3 sea noise, the directivity measure $\mathcal{D}^{(c)}$ has a 5° bias toward endfire. Since this appears in the denominator of

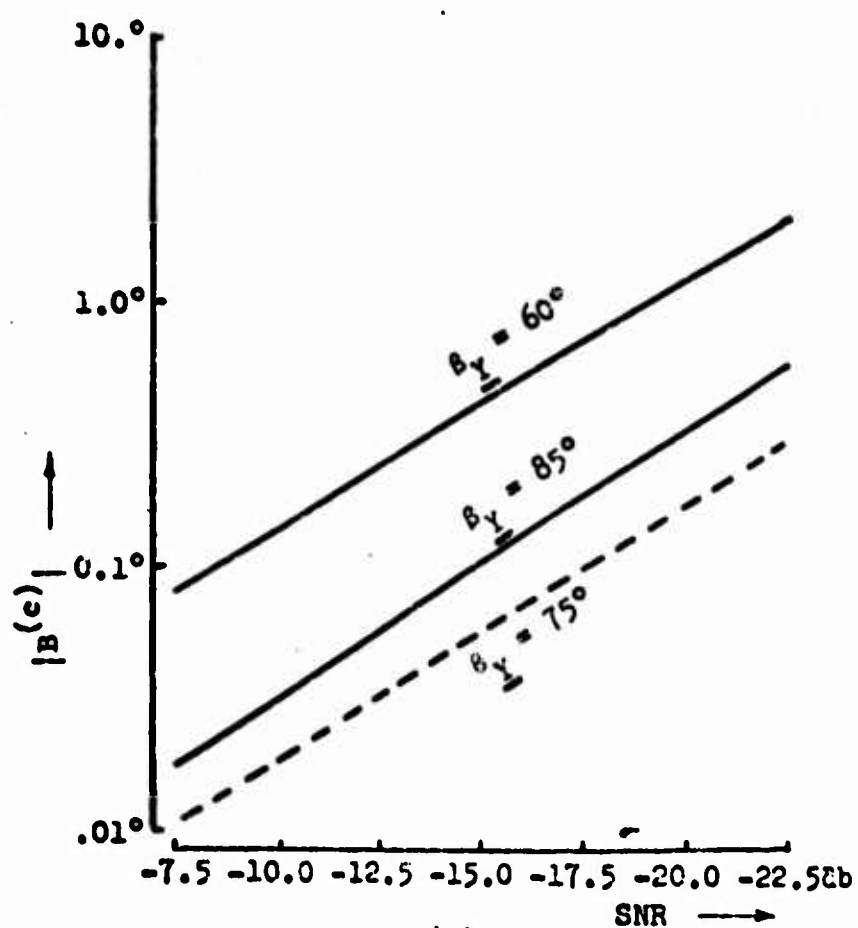
$$\frac{1}{\frac{s(\omega)}{n_1(\omega)} \mathcal{G}^{(c)}(\omega, Y|Y) \mathcal{D}^{(c)}(\omega, X|Y)},$$

5 - 34

a c-detector bias toward broadside would be indicated by $B^{(c)}$.

The second factor determining the bias is the c-detector array gain $\mathcal{G}^{(c)}(\omega, Y|Y)$ at the signal incidence Y . The smaller this is, the greater will be the bias. Though this separation into the factors $\mathcal{G}^{(c)}$ and $\mathcal{D}^{(c)}$ serves well in an analysis of the bias, it is of limited interest to the designer because these factors cannot be controlled independently. For a fixed noise field, in fact, a rise in $\mathcal{G}^{(c)}$ is always accompanied by a decrease in the bias evidenced by $\mathcal{D}^{(c)}$.

The third and perhaps most interesting factor in the bias is the received signal-to-noise ratio $\frac{s(\omega)}{n_1(\omega)}$. The weaker the signal, the greater will be the bias in the c-detector. This characteristic is apparent in Fig. 5 - 6 (a) in which $B^{(c)}$ is plotted versus signal-to-noise ratio for plane waves incident at 60° , 75° , and 85° . The



— $B(c)$ Positive
 - - - $B(c)$ Negative
 Plane Wave Signals
 Frequency Band
 = (30, 130 Hz)
 $s(\omega)$ and $n_1(\omega)$ are
 Constant over
 Frequency Band
 $\hat{s}(\omega) = s(\omega)$
 $\hat{n}_1(\omega) = n_1(\omega)$
 $SNR = s(\omega)/n_1(\omega)$
 $L = 50$ Meters
 $m = 12$ Hydrophones
 Background Noise
 is I3 Sea Noise
 $m_0 = -20$ db
 $c = 1500$ Meters/Sec
 Z in c-Detector is
 Signal Vector \underline{Y}

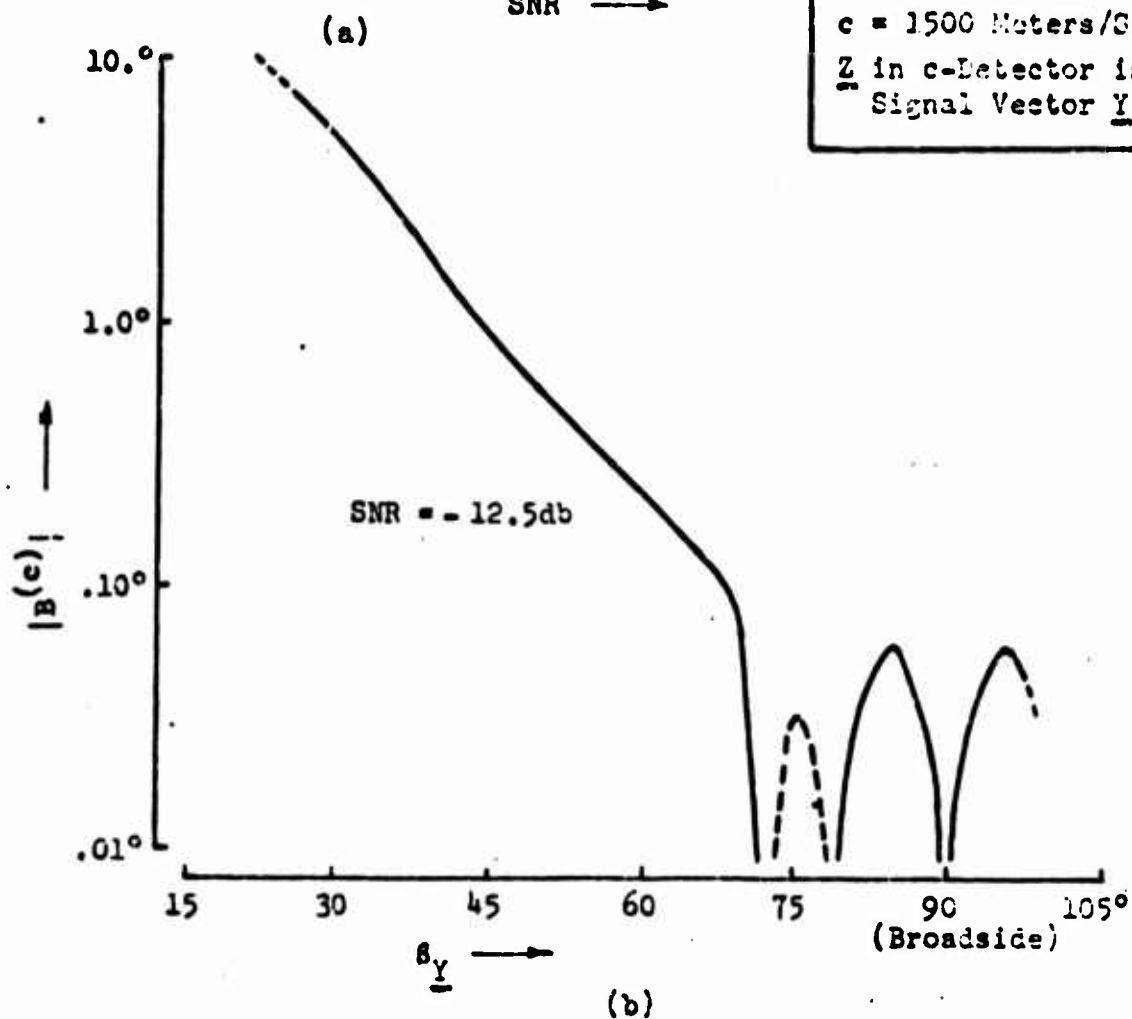


Figure 5-6 Bias in the c-Detector

frequency range is 30 to 130 hz and the background noise is 13 sea noise. The received signal power $s(\omega)$ and noise power $n_1(\omega)$ are constant over this frequency range and the implementation values \hat{s} and \hat{n}_1 are set equal to s and n_1 respectively. The term λ in Eq. 5 - 25 is determined by setting \underline{z} in Eq. 5 - 26 equal to the signal incidence vector \underline{y} . Fig. 5 - 6 (b) shows the variation in the bias with signal incidence. In this example the bias is less than a tenth of a degree in the broadside region (70° to 110°).

The fourth factor is the frequency dependent multiplier

$$\frac{\hat{s}(\omega)}{\hat{n}_1(\omega)^2} \frac{1}{1 + \frac{\hat{s}(\omega)}{\hat{n}_1(\omega)} \mathcal{A}^{(c)}(\omega, \underline{z}|\underline{z})} \quad . \quad 5 - 35$$

This factor embodies all of the dependence in $\hat{\epsilon}$ on the implementation values \hat{s} and \hat{n}_1 .

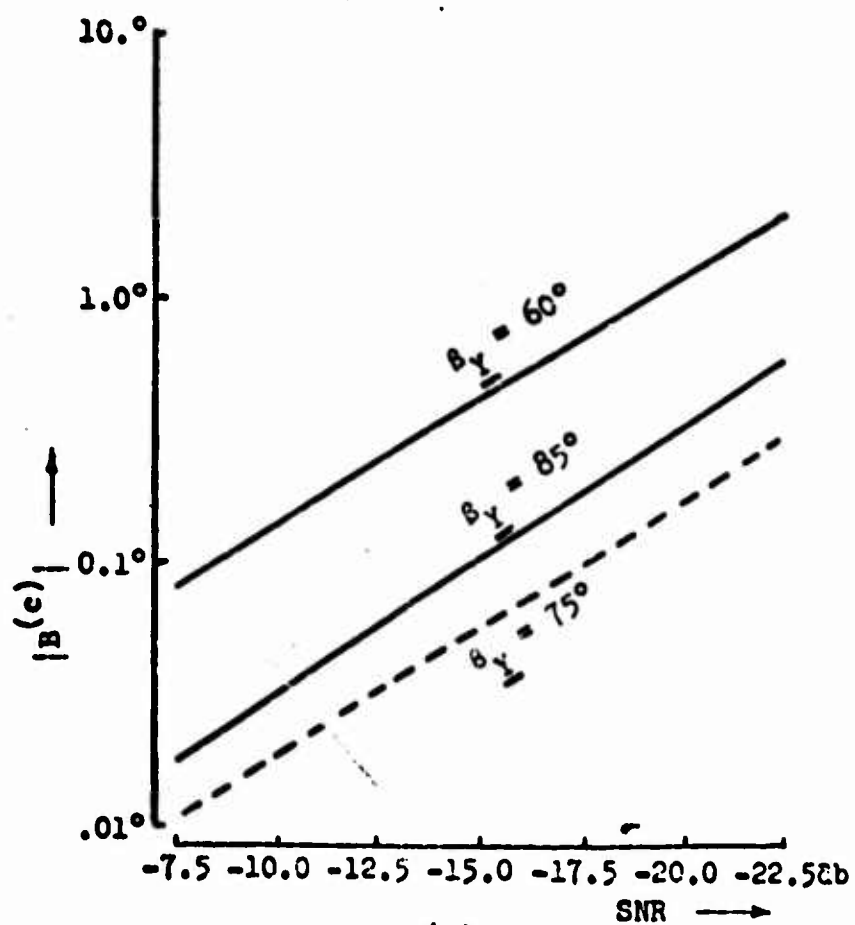
Throughout the preceding analysis and in particular in the preparation of Fig. 5 - 6 the received signal power s and noise power n_1 were assumed known. This then permitted their use in the c-detector implementation, i.e.,

$$\hat{s} = s \quad 5 - 36$$

and

$$\hat{n} = n_1 \quad 5 - 37$$

in Eq. 5 - 25. The influence of s and n_1 in determining the bias may be assessed from the factor presented above (Eq. 5 - 35). Most significantly, it is apparent (Eqs. 5 - 35, 5 - 36 and 5 - 37) that the influence is negligible whenever



— $B(c)$ Positive
 - - - $B(c)$ Negative
 Plane Wave Signals
 Frequency Band
 = (30, 130 Hz)
 $s(\omega)$ and $n_1(\omega)$ are
 Constant over
 Frequency Band
 $\hat{s}(\omega) = s(\omega)$
 $\hat{n}_1(\omega) = n_1(\omega)$
 $SNR = s(\omega)/n_1(\omega)$
 $L = 50$ Meters
 $m = 12$ Hydrophones
 Background Noise
 is I3 Sea Noise
 $m_0 = -20$ db
 $c = 1500$ Meters/Sec
 \underline{Z} in c-Detector is
 Signal Vector \underline{Y}

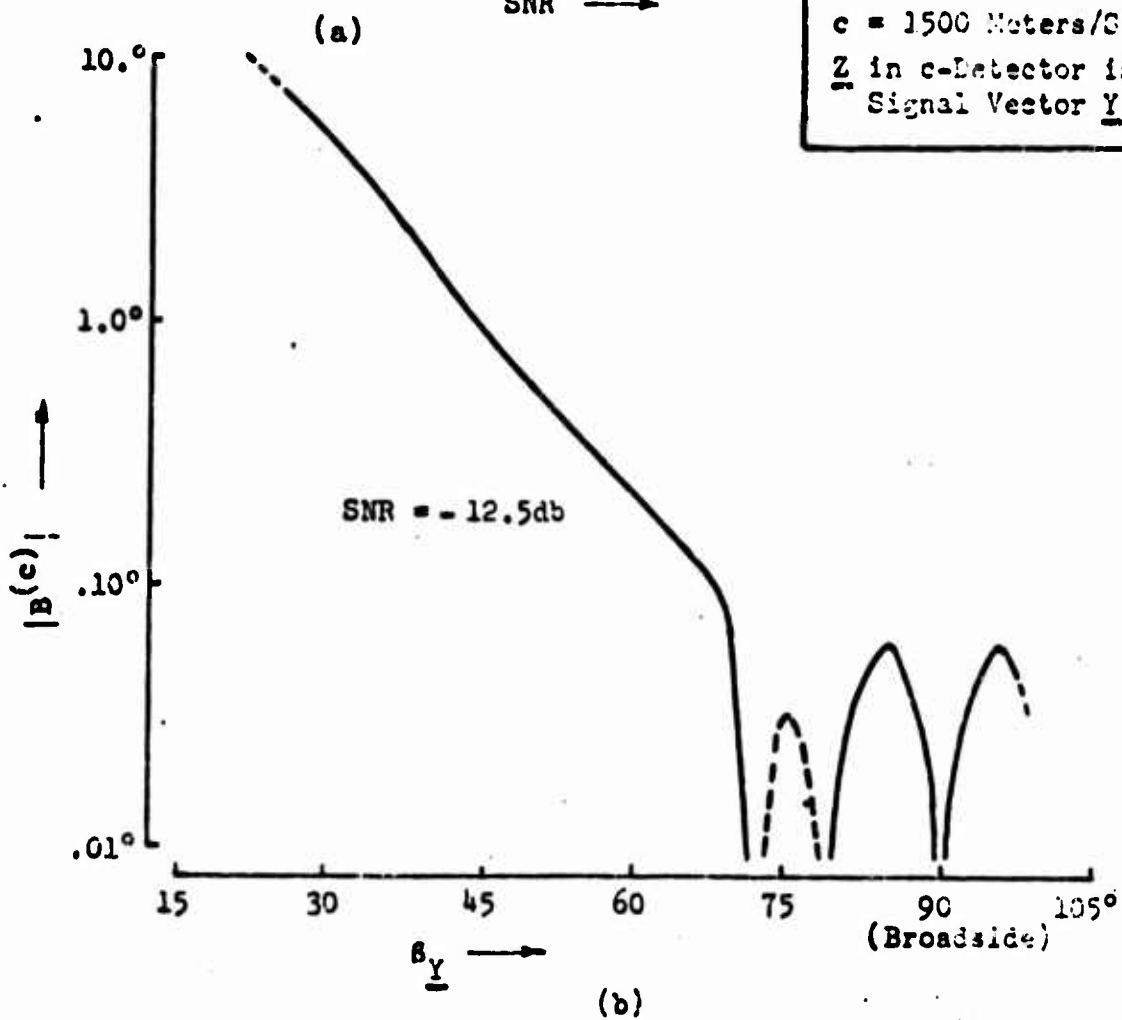


Figure 5-6 Bias in the c-Detector

frequency range is 30 to 130 hz and the background noise is I3 sea noise. The received signal power $s(\omega)$ and noise power $n_1(\omega)$ are constant over this frequency range and the implementation values \hat{s} and \hat{n}_1 are set equal to s and n_1 respectively. The term λ in Eq. 5 - 25 is determined by setting \underline{z} in Eq. 5 - 26 equal to the signal incidence vector \underline{y} . Fig. 5 - 6 (b) shows the variation in the bias with signal incidence. In this example the bias is less than a tenth of a degree in the broadside region (70° to 110°).

The fourth factor is the frequency dependent multiplier

$$\frac{\hat{s}(\omega)}{\hat{n}_1(\omega)^2} \frac{1}{1 + \frac{\hat{s}(\omega)}{\hat{n}_1(\omega)} \mathcal{J}^{(c)}(\omega, \underline{z}|\underline{z})} . \quad 5 - 35$$

This factor embodies all of the dependence in \hat{t} on the implementation values \hat{s} and \hat{n}_1 .

Throughout the preceding analysis and in particular in the preparation of Fig. 5 - 6 the received signal power s and noise power n_1 were assumed known. This then permitted their use in the c-detector implementation, i.e.,

$$\hat{s} = s \quad 5 - 36$$

and

$$\hat{n} = n_1 \quad 5 - 37$$

in Eq. 5 - 25. The influence of s and n_1 in determining the bias may be assessed from the factor presented above (Eq. 5 - 35). Most significantly, it is apparent (Eqs. 5 - 35, 5 - 36 and 5 - 37) that the influence is negligible whenever

1. the received signal power $s(\omega)$ and noise power $n_1(\omega)$ are essentially constant over the frequency band of interest, and
2. the received signal-to-noise ratio $s(\omega)/n_1(\omega)$ is so small that the quantity $\frac{s(\omega)}{n_1(\omega)} \mathcal{B}^{(c)}(\omega, \underline{Z}|\underline{Z})$ is negligible with respect to unity.

Suppose now that conditions 1 and 2 are known to be satisfied but that the exact signal and noise levels s and n_1 are unknown. The measure $\mathcal{B}^{(c)}$ will remain representative of the true bias if the implementation values \hat{s} and \hat{n}_1 reflect the known conditions, that is, if $\hat{s}(\omega)$ and $\hat{n}_1(\omega)$ are constant with frequency and

$$\frac{\hat{s}(\omega)}{\hat{n}_1(\omega)} \mathcal{B}^{(c)}(\omega, \underline{Z}|\underline{Z}) \ll 1.$$

When the input signal power s and noise power n_1 are not exactly known, two design strategies are suggested by the above discussion. One is to provide additional processing for estimating s , n_1 , and the noise covariance matrix, and then correcting for the bias using curves similar to those in Fig. 5.6. The other strategy also uses curves such as these. It is apparent in Fig. 5.6 (a) that if there is a fixed limit on the tolerable bias then there is also a minimum signal strength at each incidence that the c-detector should be allowed to detect. By limiting the observation time one could effectively limit detection to signals whose strength exceeds this minimum.

Appendix A The "Boxcar" Function

The "boxcar" function \mathbb{H} is defined by

$$\mathbb{H}(s;a,b) = \begin{cases} 1 & a < s < b \\ 1/2 & s = a \text{ or } s = b \\ 0 & s < a \text{ or } s > b \end{cases} \quad \text{A - 1}$$

(see Fig. A-1).

Its Fourier transform Ψ is

$$\begin{aligned} \Psi(\alpha;a,b) &= \frac{1}{2\pi} \int_{-\infty}^{\infty} \mathbb{H}(s;a,b) e^{j\alpha s} ds \\ &= \frac{1}{2\pi} \int_a^b e^{j\alpha s} ds = \frac{1}{2\pi} \frac{e^{j\alpha b} - e^{j\alpha a}}{j\alpha} \end{aligned} \quad \text{A - 2}$$

Inversely,¹

$$\mathbb{H}(s;a,b) = \lim_{W \rightarrow \infty} \int_{-W}^W \Psi(\alpha;a,b) e^{-j\alpha s} d\alpha \quad \text{A - 3}$$

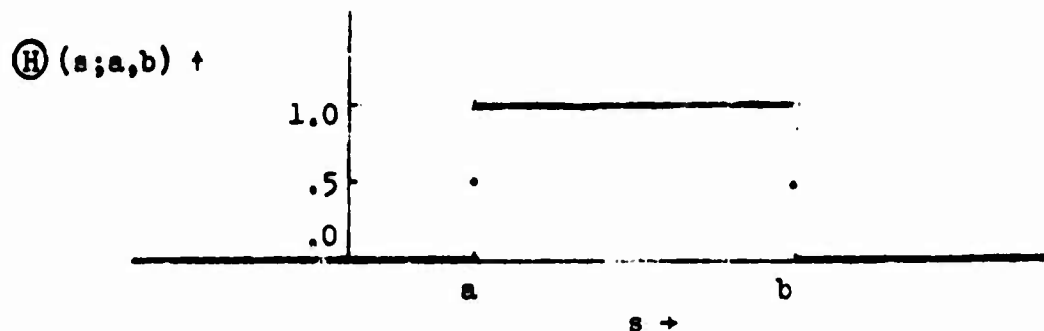


Figure A - 1 The "Boxcar" Function

¹Yaglom, p. 40.

Three properties of Ψ are

$$1. \quad \Psi(0; a, b) = \frac{b-a}{2\pi}$$

A - 4

$$2. \quad |\Psi(a; a, b)|^2 = \frac{1}{\pi^2} \frac{\sin^2 \frac{\alpha(b-a)}{2}}{a^2}$$

A - 5

$$3. \quad \Psi(a; -a, a) = \frac{1}{\pi} \frac{\sin \alpha a}{a}$$

A - 6

Appendix B Derivation of the Power Spectrum of I2 Sea Noise

An isotropic, Gaussian sea noise field in two dimensions (designated I2 sea noise) may be constructed by superimposing an infinite number of independent, infinitesimally small, single frequency plane waves, whose direction vectors are uniformly distributed within a horizontal plane. Each plane wave is a member of the set $\{u_{ij}\}$, $ij \in A$ where

$$A = \{ij\} \quad B - 1$$

such that

$$\begin{aligned} 0 < i \leq I \\ -J < j \leq J \end{aligned} \quad B - 2$$

As observed by a horizontal array in time t and in the array dimension x , each plane wave is

$$\begin{aligned} u_{ij}(t, x) &= 2\text{Re}[\xi_{ij}] \cos \omega_i(t + \frac{x}{c} \cos \beta_j) - 2\text{Im}[\xi_{ij}] \sin \omega_i(t + \frac{x}{c} \cos \beta_j) \\ &= \xi_{ij} e^{j\omega_i(t + \frac{x}{c} \cos \beta_j)} + \xi_{ij}^* e^{-j\omega_i(t + \frac{x}{c} \cos \beta_j)} \end{aligned} \quad B - 3$$

The complex amplitude ξ_{ij} is a normally distributed random variable with zero mean. The constant c is the velocity of propagation in the medium, and the angle β is the angle of incidence of the plane wave, in the coordinate system pictured in Fig. 1-1.

A member v of the sea noise process is defined by

$$v(t, x) = \lim_{W \rightarrow \infty} \sum_{ij \in A} \left[\xi_{ij} e^{j\omega_i(t + \frac{x}{c} \cos \beta_j)} + \xi_{ij}^* e^{-j\omega_i(t + \frac{x}{c} \cos \beta_j)} \right]$$

$$W \rightarrow \infty$$

$$\text{MAX } |\omega_i - \omega_{i-1}| \rightarrow 0 \quad 0 = \omega_0 < \omega_1 < \dots < \omega_I = W$$

$$\text{MAX } |\beta_j - \beta_{j-1}| \rightarrow 0 \quad -\pi = \beta_{-J} < \beta_{-J+1} < \dots < \beta_J = \pi$$

$$= \int_{-\infty}^{\infty} \int_{-\pi}^{\pi} e^{j\omega(t + \frac{x}{c} \cos \beta)} d_{\omega, \beta} Y(\omega, \beta) \quad . \quad B - 4$$

where Y is a complex random point function with zero mean and normally distributed orthogonal increments. This function is constrained by

$$Y(-\omega, \beta) = -Y^*(\omega, \beta) \quad . \quad B - 5$$

The power spectral density function f on ω and β is defined by

$$f(\omega, \beta) = (2\pi)^2 \lim_{\substack{\Delta\omega \rightarrow 0 \\ \Delta\beta \rightarrow 0}} \frac{\langle (Y(\omega, \beta) - Y(\omega - \Delta\omega, \beta - \Delta\beta)) (Y^*(\omega, \beta) - Y^*(\omega - \Delta\omega, \beta - \Delta\beta)) \rangle}{\Delta\omega \Delta\beta}$$

$$= (2\pi)^2 \frac{\langle d_{\omega, \beta} Y(\omega, \beta) d_{\omega, \beta}^* Y^*(\omega, \beta) \rangle}{d\omega d\beta} \quad . \quad B - 6$$

The constraint given by Eq. B-5 implies that

$$f(-\omega, \beta) = f(\omega, \beta) \quad . \quad B - 7$$

Since $-\pi < \beta < \pi$ includes all possible incidence angles,

$$f(\omega, \beta) = 0 \quad \begin{array}{l} \beta > \pi \\ \text{or } \beta \leq -\pi \end{array} \quad . \quad B - 8$$

This truncation is expressed by the "boxcar" function $\mathbb{H}(\beta; -\pi, \pi)$ defined by (App. A)

$$\mathbb{H}(\beta; -\pi, \pi) = \begin{cases} 1 & -\pi < \beta < \pi \\ 1/2 & \beta = \pi \text{ or } \beta = -\pi \\ 0 & \beta < -\pi \text{ or } \beta > \pi \end{cases} \quad . \quad B - 9$$

Finally since the noise is isotropic, f may be written

$$f(\omega, \beta) = f(\omega) \mathbb{H}(\beta; -\pi, \pi) \quad . \quad B - 10$$

Imperfect agreement at $\beta = -\pi$ and π is ignored.

The member v is now written in a form that leads to a spectral representation and spectral power measure on ω and v instead of ω and β . Splitting

the domain of integration in the right-hand side of Eq. B-4,

$$\begin{aligned}
 v(t,x) &= \int_{-\infty}^{\infty} \int_{-\pi}^0 e^{j\omega(t + \frac{x}{c} \cos\beta)} d_{\omega,\beta} Y(\omega,\beta) + \int_{-\infty}^{\infty} \int_0^{\pi} e^{j\omega(t + \frac{x}{c} \cos\beta)} d_{\omega,\beta} Y(\omega,\beta) \\
 &= \int_{-\infty}^{\infty} \int_0^{\pi} e^{j\omega(t + \frac{x}{c} \cos\beta)} d_{\omega,\beta} Y(\omega,-\beta) + \int_{-\infty}^{\infty} \int_0^{\pi} e^{j\omega(t + \frac{x}{c} \cos\beta)} d_{\omega,\beta} Y(\omega,\beta) \\
 &= \int_{-\infty}^{\infty} \int_0^{\pi} e^{j\omega(t + \frac{x}{c} \cos\beta)} d_{\omega,\beta} [-Y(\omega,-\beta) + Y(\omega,\beta)] \quad B - 11
 \end{aligned}$$

Changing the variable according to

$$v = \frac{\omega}{c} \cos\beta \quad B - 12$$

the above becomes

$$\begin{aligned}
 v(t,x) &= \int_{-\infty}^{\infty} \int_{-\omega/c}^{\omega/c} e^{j(\omega t + vx)} d_{\omega,v} \left[Y(\omega, -\cos^{-1} \frac{cv}{\omega}) - Y(\omega, \cos^{-1} \frac{cv}{\omega}) \right] \\
 &= \int_{-\infty}^{\infty} \int_{-\omega/c}^{\omega/c} d_{\omega,v} Z(\omega,v) \quad B - 13
 \end{aligned}$$

where

$$Z(\omega,v) \equiv Y(\omega, -\cos^{-1} \frac{cv}{\omega}) - Y(\omega, \cos^{-1} \frac{cv}{\omega}) \quad B - 14$$

Since Y is a random point function with normally distributed orthogonal increments, so is Z . The constraint on Z corresponding to the constraint on Y in Eq. B-5 is as follows.

$$\begin{aligned}
 Z(-\omega, -v) &= Y(-\omega, -\cos^{-1} \frac{cv}{\omega}) - Y(-\omega, \cos^{-1} \frac{cv}{\omega}) \\
 &= -Y^*(\omega, -\cos^{-1} \frac{cv}{\omega}) + Y^*(\omega, \cos^{-1} \frac{cv}{\omega}) = -Z^*(\omega, v) \quad B - 15
 \end{aligned}$$

The measure $n(\omega, \nu)$ of spectral power on ω and ν is

$$\begin{aligned}
 n(\omega, \nu) &= (2\pi)^2 \langle d_{\omega, \nu} Z(\omega, \nu) d_{\omega, \nu}^* Z^*(\omega, \nu) \rangle \\
 &= (2\pi)^2 \langle d_{\omega, \nu} [Y(\omega, -\cos^{-1} \frac{c\nu}{\omega}) - Y(\omega, \cos^{-1} \frac{c\nu}{\omega})] \\
 &\quad - d_{\omega, \nu}^* [Y^*(\omega, -\cos^{-1} \frac{c\nu}{\omega}) - Y^*(\omega, \cos^{-1} \frac{c\nu}{\omega})] \rangle \\
 &= (2\pi)^2 \langle d_{\omega, \nu} Y(\omega, -\cos^{-1} \frac{c\nu}{\omega}) d_{\omega, \nu}^* Y^*(\omega, -\cos^{-1} \frac{c\nu}{\omega}) \rangle \\
 &\quad + \langle d_{\omega, \nu} Y(\omega, \cos^{-1} \frac{c\nu}{\omega}) d_{\omega, \nu}^* Y^*(\omega, \cos^{-1} \frac{c\nu}{\omega}) \rangle .
 \end{aligned}
 \tag{B-16}$$

Evaluating the first term in this expression,

$$\begin{aligned}
 &(2\pi)^2 \langle d_{\omega, \nu} Y(\omega, -\cos^{-1} \frac{c\nu}{\omega}) d_{\omega, \nu}^* Y^*(\omega, -\cos^{-1} \frac{c\nu}{\omega}) \rangle \\
 &= f(\omega) \mathcal{H}(\nu; -\frac{\omega}{c}, \frac{\omega}{c}) d\omega \left| \frac{\partial -\cos^{-1} \frac{c\nu}{\omega}}{\partial \nu} \right| d\nu \\
 &= \frac{f(\omega)}{\sqrt{\frac{\omega^2}{c^2} - \nu^2}} \mathcal{H}(\nu; -\frac{\omega}{c}, \frac{\omega}{c}) d\omega d\nu .
 \end{aligned}
 \tag{B-17}$$

The second term in the right-hand side of Eq. B-16 is also equal to

$$\frac{f(\omega)}{\sqrt{\frac{\omega^2}{c^2} - \nu^2}} \mathcal{H}(\nu; -\frac{\omega}{c}, \frac{\omega}{c}) d\omega d\nu .
 \tag{B-18}$$

and therefore,

$$n(\omega, \nu) = \frac{2f(\omega)}{\sqrt{\frac{\omega^2}{c^2} - \nu^2}} \mathcal{H}(\nu; -\frac{\omega}{c}, \frac{\omega}{c}) d\omega d\nu .
 \tag{B-19}$$

A more useful form of this result is obtained by expressing $f(\omega)$ in terms of the one-dimensional power spectral density function $n_1(\omega)$ defined by Eq. 1-36. Restating Eq. 2-16,

$$n_1(\omega) = \frac{1}{2\pi} \int_{-\infty}^{\infty} n(\omega, v) dv$$

$$= \frac{1}{2\pi} \int_{-\infty}^{\infty} \frac{2f(\omega)}{\sqrt{\frac{\omega^2}{c^2} - v^2}} \mathcal{H}\left(v; -\frac{\omega}{c}, \frac{\omega}{c}\right) dv = f(\omega) , \quad B - 20$$

so that Eq. B-19 becomes

$$n(\omega, v) = \frac{2n_1(\omega)}{\sqrt{\frac{\omega^2}{c^2} - v^2}} \mathcal{H}\left(v; -\frac{\omega}{c}, \frac{\omega}{c}\right) . \quad B - 21$$

Appendix C Output Statistics for the General Detector

Some output statistics are derived here for a general detector whose output \mathcal{V} is

$$\mathcal{V} = 2 \sum_{i \in \Omega+} |\mathcal{G}_i^* \underline{u}_i|^2 + C_1 \quad C - 1$$

where

$$\underline{\mathcal{G}}_i = (\mathcal{G}_{ik}) \quad ik \in D_i \quad C - 2$$

is some linear functional and C_1 is a bias term. With the definitions

$$v_i = \mathcal{G}_i^* \underline{u}_i \quad C - 3$$

and

$$W_i = |v_i|^2, \quad C - 4$$

this output may be written

$$\mathcal{V} = 2 \sum_{i \in \Omega+} (W_i + C_1) \quad C - 5$$

Both the b and c detectors are of this type. The mean $\langle \mathcal{V} \rangle$ and the variance $V(\mathcal{V})$ are derived for use in performance measures for these detectors.

Assuming \underline{u}_i independent of $\underline{u}_{i'}$ for $i, i' \in \Omega+,$, each output component W_i will be independent of $W_{i'}$ for $i \neq i'$ and $i, i' \in \Omega$. Then

$$\langle \mathcal{V} \rangle = \left\langle 2 \sum_{i \in \Omega+} (W_i + C_1) \right\rangle = 2 \sum_{i \in \Omega+} (\langle W_i \rangle + C_1) \quad C - 6$$

and

$$V(\mathcal{V}) = V\left(2 \sum_{i \in \Omega+} (W_i + C_1)\right) = V\left(2 \sum_{i \in \Omega+} W_i\right) = 4 \sum_{i \in \Omega+} V(W_i) \quad C - 7$$

For use in the above expressions, the mean $\langle W_i \rangle$ and the variance $V(W_i)$

are determined from the moment generating function for the distribution of W_1 . By definition,

$$M_1(t) = \langle e^{W_1 t} \rangle \quad C - 8$$

so that the mean

$$\langle W_1 \rangle = \left. \frac{dM_1(t)}{dt} \right|_{t=0}, \quad C - 9$$

and the variance

$$V(W_1) = \frac{d^2 M_1(t)}{dt^2} - \langle W_1 \rangle^2. \quad C - 10$$

The moment generating function is obtained from the distribution of W_1 , which in turn follows from the distribution of w_1 .

The distribution of w_1 is now derived. Since w_1 is obtained from \underline{u}_1 by a linear operation, and \underline{u}_1 is assumed normally distributed, w_1 is also normally distributed. The mean of w_1 is

$$\langle w_1 \rangle = \langle \underline{g}_1^* \underline{u}_1 \rangle = \underline{g}_1^* \langle \underline{u}_1 \rangle = 0, \quad C - 11$$

and the variance is

$$\begin{aligned} V(w_1) &= \langle (w_1 - \langle w_1 \rangle)^2 \rangle = \langle w_1^2 \rangle \\ &= \underline{g}_1^* \langle \underline{u}_1 \underline{u}_1^* \rangle \underline{g}_1 = \langle \underline{u}_1 \underline{u}_1^* \rangle ||\underline{g}_1||^2 = A_1 ||\underline{g}_1||^2, \end{aligned} \quad C - 12$$

where the matrix A_1 is the covariance matrix of \underline{u}_1 (Eq. 1-13). The probability density function of w_1 is therefore

$$f(w_1) = \frac{1}{\pi A_1 ||\underline{g}_1||^2} e^{-\frac{|w_1|^2}{A_1 ||\underline{g}_1||^2}}. \quad C - 13$$

The distribution of W_1 is obtained from this through the change of variable $W_1 = |w_1|^2$ in $f(w_1)$. The term W_1 is real and nonnegative. The probability that W_1 lies within a dW_1 is equal to the probability that w_1 lies within an origin-centered annular ring in the complex plane. The area of this ring is

$$2\pi \sqrt{W_1} d(\sqrt{W_1}) = 2\pi \sqrt{W_1} \frac{dW_1}{2\sqrt{W_1}} = \pi dW_1 \quad C - 14$$

The probability density function of W_1 is therefore

$$f(W_1) = \frac{1}{A_1 ||g_1||^2} e^{-\frac{W_1}{A_1 ||g_1||^2}} \quad W_1 \geq 0 \quad C - 15$$

The moment generating function $M_1(t)$ is now written for the distribution of W_1 .

$$M_1(t) = \langle e^{W_1 t} \rangle = \frac{1}{A_1 ||g_1||^2} \int_0^\infty e^{W_1 t - \frac{W_1}{A_1 ||g_1||^2}} dW_1 = \frac{1}{1 - t A_1 ||g_1||^2} \quad C - 16$$

In virtue of Eqs. C-9 and C-10, then, the statistics of the component W_1 are

$$\langle W_1 \rangle = A_1 ||g_1||^2 \quad C - 17$$

and

$$V(W_1) = 2A_1 ||g_1||^4 - A_1 ||g_1||^4 = A_1 ||g_1||^4 = \langle W_1 \rangle^2 \quad C - 18$$

Substituting these results into Eqs. C-6 and C-7,

$$\langle W \rangle = 2 \sum_{i \in \Omega^+} (A_i ||g_i||^2 + C_i) \quad C - 19$$

and

$$V(W) = 4 \sum_{i \in \Omega^+} A_i ||g_i||^4 \quad C - 20$$

Appendix D ℓ -Detector Statistics

In this appendix the mean and variance of the ℓ -detector output are obtained. The usual assumption is made that u_i is independent of $u_{i'}$ for i and $i' \in \Omega+$ whenever $i \neq i'$. Referring to the ℓ -detector definition (Eq. 3-30),

$$\langle \ell(\underline{u}) \rangle = 2 \sum_{i \in \Omega+} \sum_{1k \in D_i} \left[\frac{\langle |u_{1k}|^2 \rangle}{\lambda_{1k}} + \ln \pi \lambda_{1k} \right] + \ln f_1, \quad D-1$$

and

$$\begin{aligned} V(\ell(\underline{u})) = & \quad D-2 \\ & 4 \sum_{i \in \Omega+} V \left(\sum_{1k \in D_i} \left[\frac{|u_{1k}|^2}{\lambda_{1k}} + \ln \pi \lambda_{1k} \right] + \ln f_1 \right) \\ & = 4 \sum_{i \in \Omega+} \left[\left\langle \left[\sum_{1k \in D_i} \frac{|u_{1k}|^2}{\lambda_{1k}} \right]^2 \right\rangle - \left[\sum_{1k \in D_i} \frac{\langle |u_{1k}|^2 \rangle}{\lambda_{1k}} \right]^2 \right] \\ & = 4 \sum_{i \in \Omega+} \left[\sum_{1k \in D_i} \sum_{1k' \in D_i} \frac{\langle |u_{1k}|^2 |u_{1k'}|^2 \rangle}{\lambda_{1k} \lambda_{1k'}} - \left[\sum_{1k \in D_i} \frac{\langle |u_{1k}|^2 \rangle}{\lambda_{1k}} \right]^2 \right] \\ & = 4 \sum_{i \in \Omega+} \left[\sum_{1k \in D_i} \frac{\langle |u_{1k}|^4 \rangle}{\lambda_{1k}^2} + \sum_{1k \in D_i} \sum_{1k' \in D_i} \frac{\langle |u_{1k}|^2 |u_{1k'}|^2 \rangle}{\lambda_{1k} \lambda_{1k'}} - \left[\sum_{1k \in D_i} \frac{\langle |u_{1k}|^2 \rangle}{\lambda_{1k}} \right]^2 \right] \\ & = 4 \sum_{i \in \Omega+} \left[2 \sum_{1k \in D_i} \frac{\langle |u_{1k}|^2 \rangle^2}{\lambda_{1k}^2} - \sum_{1k} \frac{\langle |u_{1k}|^2 \rangle^2}{\lambda_{1k}^2} \right] \\ & = 4 \sum_{i \in \Omega+} \sum_{1k \in D_i} \frac{\langle |u_{1k}|^2 \rangle^2}{\lambda_{1k}^2}. \end{aligned}$$

Appendix E Approximate Eigenfunctions for Use in a Practical b-Detector

Some of the performance characteristics of the b-detector are discussed in the text, but no mention is made of the realization of this detector. In fact, the exact equations used to describe the b-detector, though well suited for analysis, are not in a form that is practical for actual detection. Such a functional form can be obtained in two ways:

1. by returning to the power detector with shading shown in Fig. 3-2, or
2. by an approximation to the form used in the analysis (Fig. 3-1). The first approach was covered in [1] and the second will be considered in the following. This second form has been very successful in the analysis of the b-detector, and it seems reasonable to guess that it may also have advantages in the synthesis. Already it is apparent that delay lines are not required, and that there is a logical separation of internal functions, which makes the configuration flexible. A limitation on this application is the capacity of the processing computer in storage and speed. This may be a major obstacle when a large scale detector is planned.

The approximation to the analytical form of the b-detector that makes it practically realizable is a further approximation in defining the set of eigenfunctions of Q (Eq. 1-15). This is the subject of appendix E. Appendix F concerns the description of the "signal only" covariance matrix G that results from the use of particular approximate eigenfunction sets. The nature of G will largely determine the amount of computer processing required in the system.

a) A Practical Requirement

Specifically, the main objection to using the eigenfunctions as they are defined so far is that their duration is the whole observation time T . Consequently, no elements u_{1k} of \underline{u} can be available for further processing

until this total observation time has elapsed. In practice, processed detection information is required more or less continuously from $t=0$ until a final decision is made.

b) Breakup of the Observation Time into Subintervals

An approximate set of eigenfunctions consisting of consecutive functions of short duration is proposed here to meet the above requirement. The sinusoidal form for the time eigenfunctions (Eq. 1-25) will be retained. Now to construct the approximate set, sinusoids will be defined over a system of subintervals within $(0,T)$. The most easily analysed system is obtained by breaking up $(0,T)$ into consecutive subintervals of duration T' . In fact, the orthonormal set of time eigenfunctions $\{\phi_1^{(n)}(t)\}$ considered first will be defined by

$$\phi_1^{(n)}(t) = e^{j\omega_1 t} \textcircled{H}(t; t^{(n)}, t^{(n)} + T'), \omega_1 \equiv \frac{2\pi 1}{T'} \quad E - 1$$

where $t^{(n)}$ is the beginning of the n^{th} time interval. This set is represented by a set of horizontal lines in Fig. E-1(a). The frequency of $\phi_1^{(n)}$ is represented by the vertical intercept ω_1 , and the time duration is represented by the length of a horizontal line having this intercept. The line for $\phi_1^{(n)}$ begins at $t^{(n)}$ and ends at $t^{(n+1)}$. When $T=T'$, the set is the original one defined by Eq. 1-25 and is represented, for comparison, by the time-frequency plot in Fig. E-1(b).

The quality of the above approximation depends upon the "smoothness" of the intermediate form $q_1(\omega, x, y)$ in Eq. 1-24. Indeed, if $q_1(\omega, x, y)$ is relatively constant over all ω intervals $(\omega_1 - W, \omega_1 + W)$ such that $1 \ll W$ and W is somewhat greater than $\frac{2\pi}{T'}$ then the approximation will be good. The error introduced by using the new set of time eigenfunctions thus increases as T' decreases; the variation in the form q_1 is an important factor in determining how small to set T' . (Other factors, which will be considered in a later part

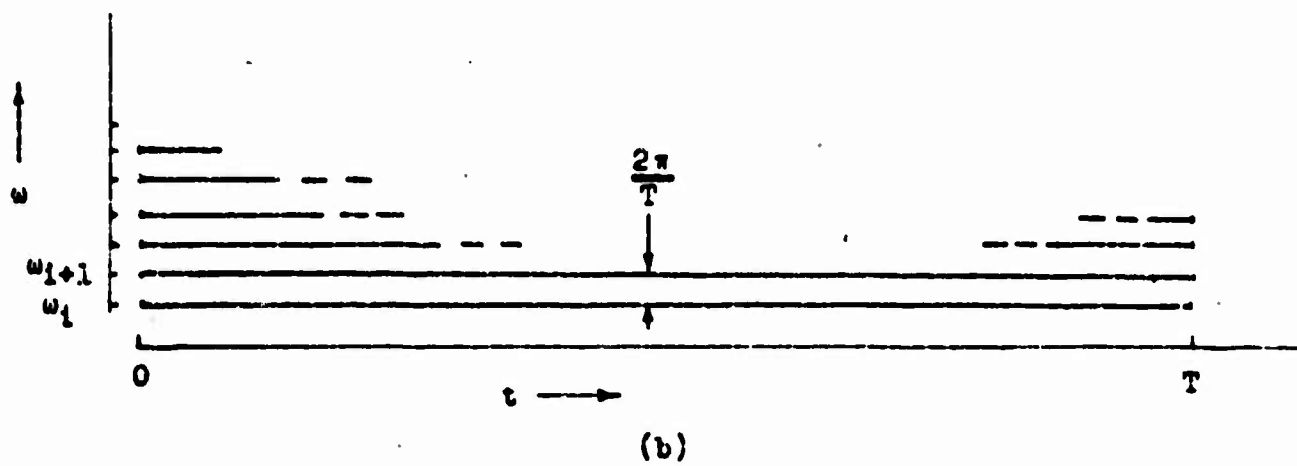
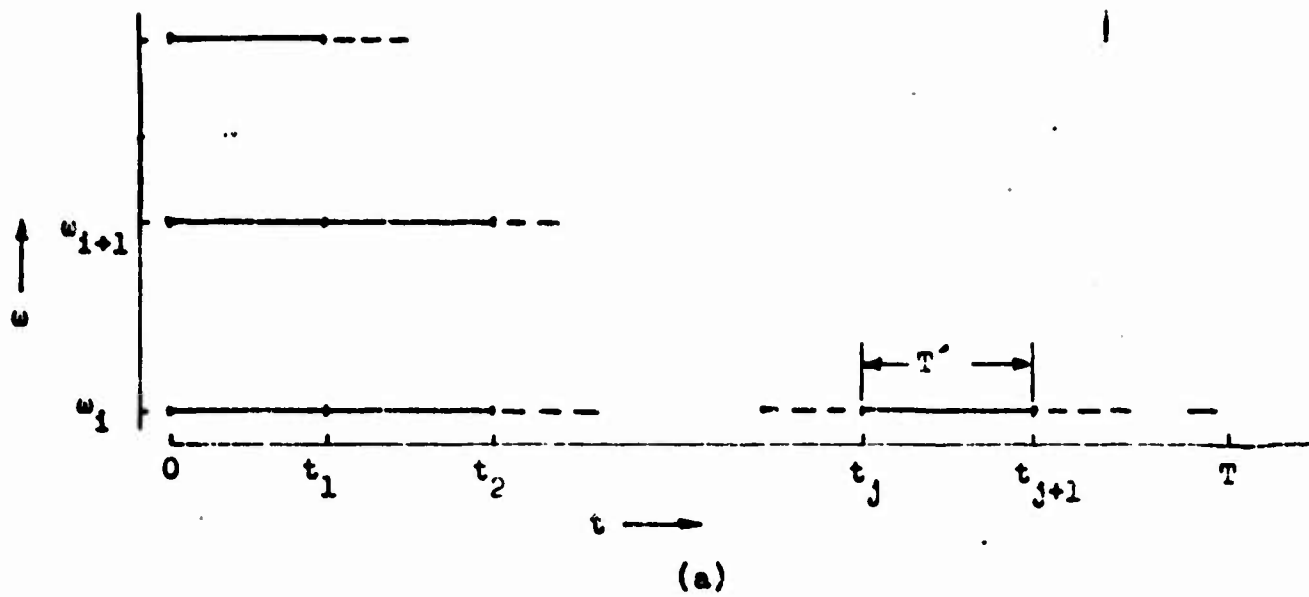


Figure E-1 Frequency-Time Plots for Sinusoidal Time Eigenfunctions

of this appendix and in Appendix F, are the processing frequencies and the nature of the resulting signal matrix G).

As developed below, the set of approximate time eigenfunctions defined in Eq. E-1 suggests another set which may be even more practical.

c) Frequency Dependent Time Intervals

In going from sinusoids of duration T to those of duration T' , the spacing between frequencies $\{\omega_i\}$ increased. If the design of the detector requires separate time filters at each frequency ω_i , it is desirable that this spacing be set as wide as possible. Another set of sinusoids is now proposed in an attempt to cover a given frequency band with sinusoidal time eigenfunctions at as few frequencies as possible. It is noted that the "smoothness" is a local condition on q_i , and this suggests determining the duration T_i of a sinusoid at frequency ω_i by the smoothness of the spectra in the neighborhood of ω_i .

With T_i varying with frequency, however, it is not generally possible to choose a spacing between frequencies such that the resulting set of sinusoids is orthogonal. To obtain approximate orthogonality, the spacing between adjacent frequencies may be determined by

$$\omega_{i+1} - \omega_i = \frac{4\pi}{T_{i+1} + T_i} \quad \text{E-2}$$

With this spacing, the approximately orthogonal set $\{\phi_i^{(n)}\}$ is defined by

$$\phi_i^{(n)}(t) = \frac{e^{j\omega_i t}}{\sqrt{T_i}} \textcircled{R}(t; t_i^{(n)}, t_i^{(n)} + T_i) \quad \text{E-3}$$

where $t_i^{(n)}$ is the beginning of the n^{th} time interval at frequency ω_i .

For example, if the smoothness of the noise process spectra is directly proportional to the frequency ω , an appropriate set of time durations T_i is N periods of the oscillation at ω_i with N a positive integer, i.e.,

$$T_1 = \frac{2\pi N}{\omega_1} \quad E-4$$

The lowest permissible T_1 is determined by two factors:

1. the smoothness of q_1 as described in the previous section, and 2. the orthogonality of the set. Error associated with each of these factors decreases as N is increased.

Eq. E-2 sets the local spacing of the frequencies at the inverse of the average local time duration. Solving this equation and Eq. E-4 simultaneously,

$$\omega_{i+1} = p\omega_i \quad E-5$$

where

$$p = \sqrt{1 + \frac{2}{N} \sqrt{1 + \frac{2}{N} \sqrt{\dots}}} \quad E-6$$

The multiplier p versus N is plotted in Fig. E-2. The resulting local spacing is most simply expressed in terms of the average local frequency

$$\omega = \frac{\omega_{i+1} + \omega_i}{2} \quad E-7$$

Using Eq. E-5,

$$\Delta\omega = \omega_{i+1} - \omega_i = \omega_i(p-1)$$

and

$$\omega = \frac{\omega_{i+1} + \omega_i}{2} = \frac{\omega_i(p+1)}{2}$$

Dividing,

$$\frac{\Delta\omega}{\omega} = \frac{2(p-1)}{p+1} \quad E-8$$

Using this result and Fig. E-2, the ratio $\frac{\Delta\omega}{\omega}$ is plotted versus N in Fig. E-3.

A typical sequence is now given for $N = 3$ and a lowest frequency of 10 Hz. Using Fig. E-2,

$$\omega_{i+1} = p\omega_i = 1.38 \omega_i$$

The sequence of frequencies is therefore

10 Hz, 13.8, 19.0, 26.2, 36.1, 49.9, 68.9, ...

According to Eq. E-4, the corresponding time durations are

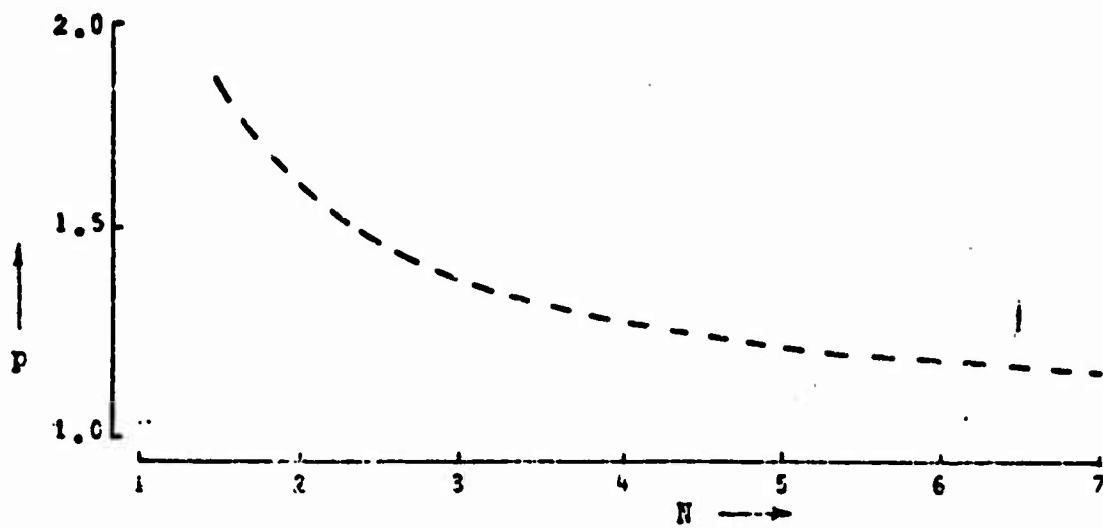


Figure E-2 The Spacing Parameters p

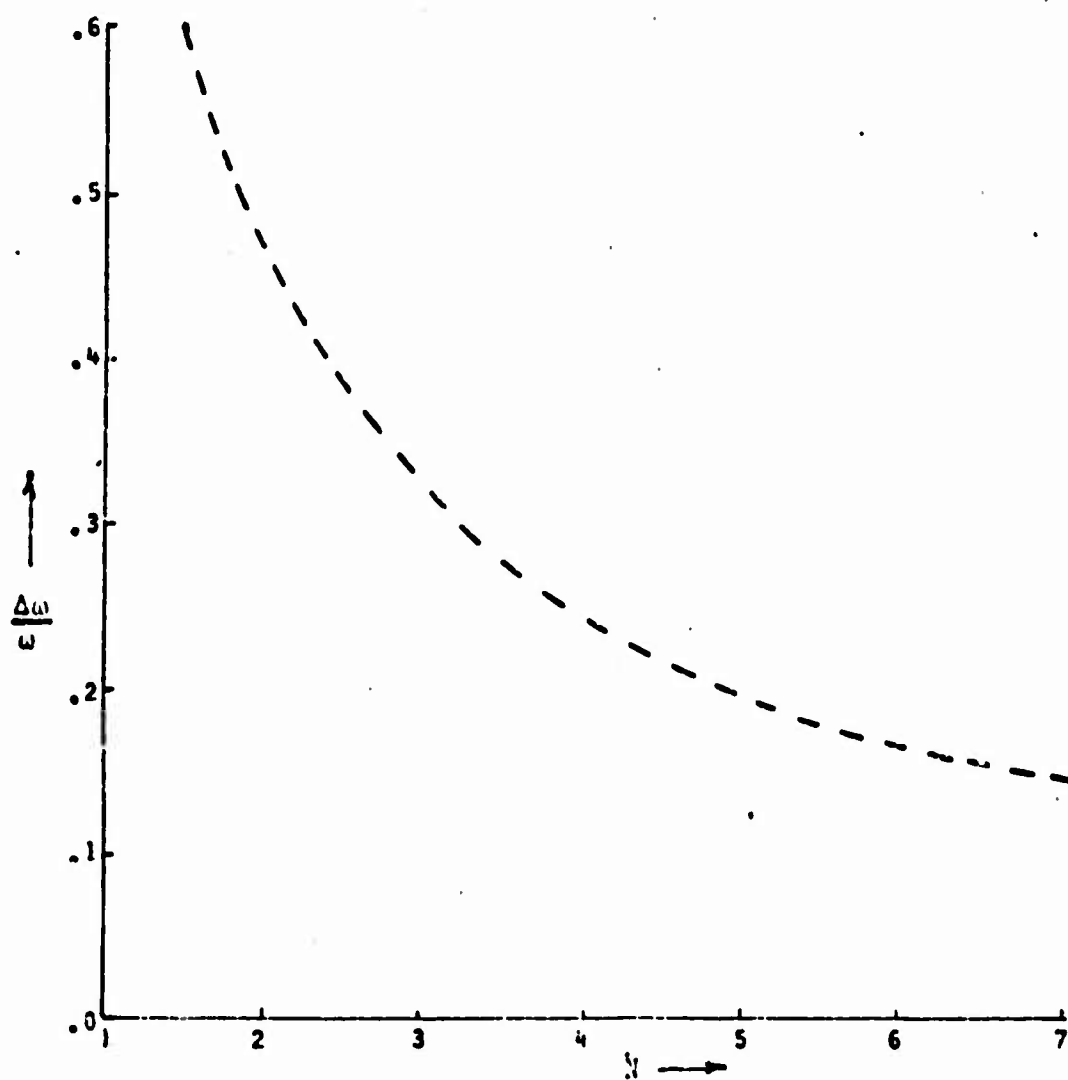


Figure E-3 The Normalized Spacing $\frac{\Delta\omega}{\omega}$

.3 sec., .22, .16, .11, .083, .0605, .044, ...

These durations are plotted in Fig. E-4 at their respective frequencies.

d) Time Intervals with Space Dependent Phase

In the example just considered, the time intervals decrease with time frequency. At sufficiently high frequency, the coherent wavefronts of signals near endfire will extend over a number of time intervals. As is shown in Fig. E-5(b) this will cause signal power received in one time subinterval to be dependent on that received in adjacent time subintervals. To eliminate this dependence, the time subintervals may be phased to match the signal wavefront. If the time delay relative to the center of the array along a signal wavefront is $-\gamma(x|Y)$ then the set of sinusoidal time eigenfunctions may be written $\{\phi_1^{(n)}\}$ where

$$\phi_1^{(n)}(t, x) = \frac{e^{j\omega_1 t}}{\sqrt{T_1}} \mathcal{H}(t; t_1^{(n)} - \gamma(x|Y), t_1^{(n)} - \gamma(x|Y) + T_1) \quad E-9$$

A disadvantage of this set is that it changes with signal incidence.

e) Breakup of the Array Dimension into Subintervals

The above discussion of sinusoidal eigenfunctions and their definition over subintervals may sometimes be applied to the space eigenfunctions as well as the time eigenfunctions. Since preliminary design calculations of G are simplified when the space eigenfunction may be approximated by sinusoids and since a breakup of the array into subintervals may simplify the processing, the relevant conditions and observations from the preceding are restated below for the space eigenfunctions.

Conditions for a sinusoidal function

$$\psi_{1k}(x) = \frac{e^{jv_k x}}{\sqrt{L'}} \mathcal{H}(x; -\frac{L'}{2}, \frac{L'}{2}) \quad v_k = \frac{2\pi k}{L'} \quad E-10$$

of duration $L' \leq L$ solving the space eigenfunction equation (Eq. 1-29) are

$$\begin{aligned}
 N &= 3 \\
 \omega &= 2\pi f \\
 T_1 &= \frac{2\pi N}{\omega_1}
 \end{aligned}$$

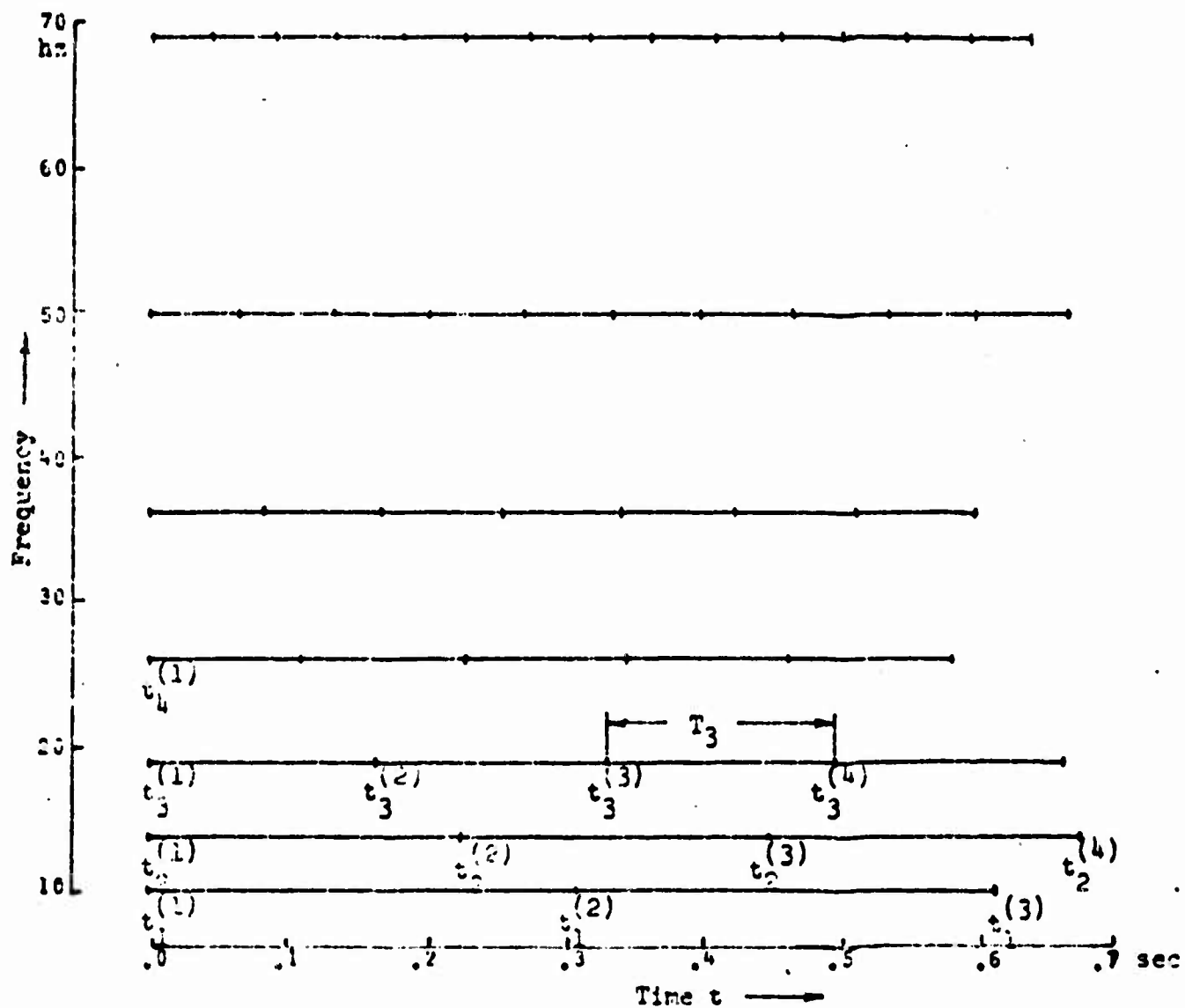


Figure E-4 Variable Duration Sinusoids
in the Frequency-Time Plane

1. that the time eigenfunction ϕ_1 is approximately sinusoidal,
2. that the noise process is homogeneous,
- and 3. that the spectrum $n(\omega_1, \nu)$ is relatively constant over the ν interval $(\nu_k - W, \nu_k + W)$ in which W is somewhat less than $\frac{2\pi}{L'}$.

In Appendix E calculations of G will be carried out using sinusoidal space eigenfunctions for which $L' = L$.

When a breakup of the time duration into subintervals is combined with a breakup along the array dimension, the result is a rectangular grid on the t, x domain. This domain and grid are pictured in Fig. E-5 for the following example: the time frequency is 1000 hz, the array length is 50 meters, and the background noise is I3 sea noise. The time subinterval T' and the space subinterval L' are twice the period of their respective oscillations. The smoothness condition 3 on the noise spectrum is satisfied for ν_k somewhat less than 1.3π . The space frequency chosen for this example is π , corresponding to a plane wave incident at 41.4° . Wavefronts at this incidence are shown in the t, x domain in Fig. E-5.

An advantage of this grid pattern is that blocks containing the same wavefront may be grouped and processed together. The processed output from distinct groups of such blocks are then almost independent. The same result is obtained using the phased time subintervals discussed in part d. However, this grid configuration has the advantage that it does not change with signal incidence.

The grid concept is also useful in the design of an array when portions of $(-\frac{L}{2}, \frac{L}{2})$ are unavailable. This occurs when it is not possible to place hydrophones within some subinterval of $(-\frac{L}{2}, \frac{L}{2})$.

L	$= 50 \text{ Meters}$
ω	$= 2\pi \times 1000 = 6283$
θ	$= 41.4^\circ$
c	$= 1500 \text{ Meters/Sec}$
T'	$= 2\pi \frac{2\pi}{\omega}$
L'	$= 2\pi \frac{2\pi}{\nu}$

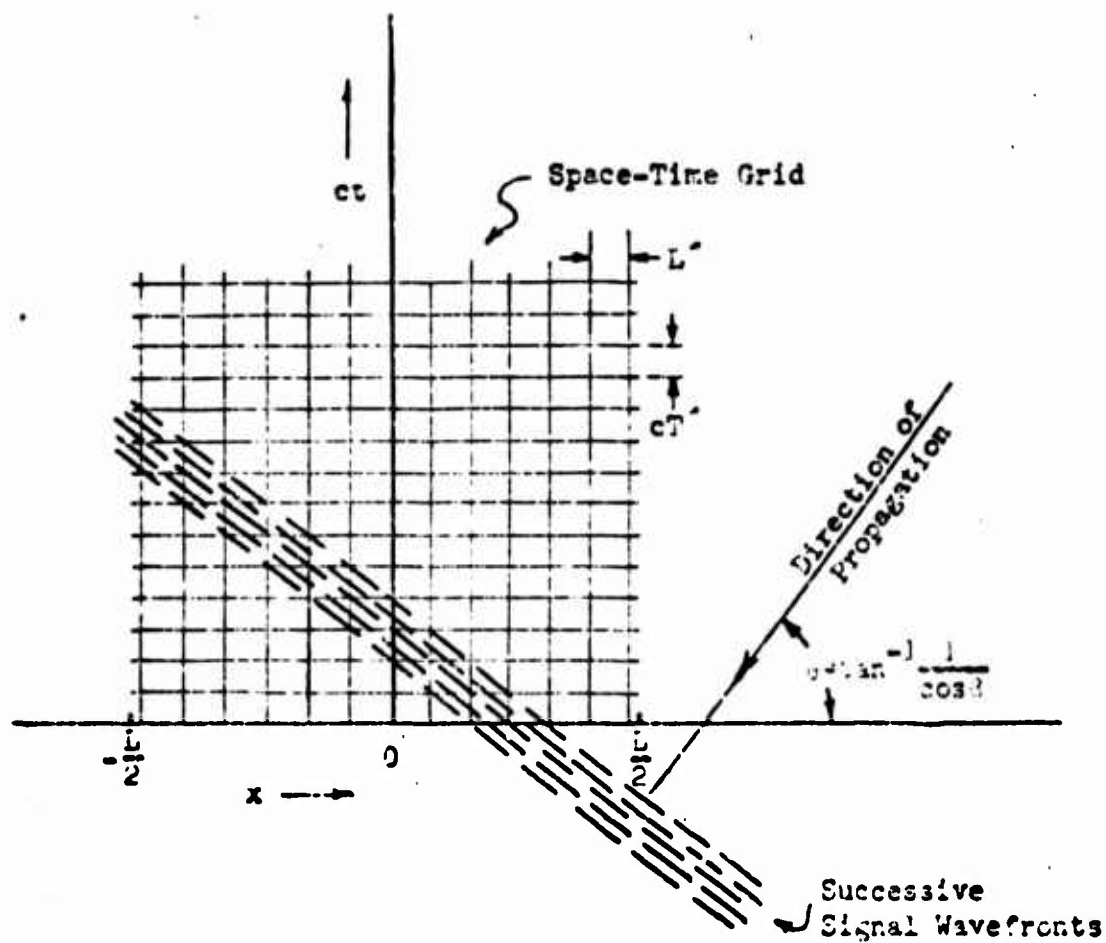


Figure E-5 Subinterval Grid in the Time-Space Domain

Appendix F The Signal Covariance Matrix G

a) The General Form of G

The consequences of the subinterval breakups discussed in appendix E are expressed in the following in terms of the resulting signal covariance matrix G. It is the nature of G that determines the ease with which the forms $(\Lambda + G)^{-1}$ and $\det(\Lambda + G)$ may be realized for use in the b-detector (Eqs. 1-54 and 1-55). At its simplest perhaps,

$$G = \dots, G_1, \dots \quad F-1$$

$$G_1 = s_1 \underline{h}_1 \underline{h}_1^*$$

in the analysis of the preceding chapters; however, the conditions (pg. 47) under which this form is valid are not satisfied for all subinterval choices. Properties of G under other conditions are presented in the following.

In the development below, the set of approximate eigenfunctions defined over the system of time subintervals of duration T' is used (part b of App. E). Use of this set most simply demonstrates the effect of time subinterval duration on G. The set of eigenfunctions defined over the system of frequency dependent subintervals could be used, but the notation is more complicated while the results are virtually the same. With subintervals, the generalization of Eqs. 2-70 and 2-71 for G is

$$G(\underline{Y}) = \left[\underline{G}_{ik \times ik}^{(n \times n')}(\underline{Y}) \right] \quad F-2$$

$$\underline{G}_{ik \times ik}^{(n \times n')}(\underline{Y}) = \int_{-L/2}^{L/2} \psi_{ik}^*(x) \rho(x|\underline{Y}) \int_{-L/2}^{L/2} \underline{F}_{i \times i}^{(n \times n')}(\tau(x, y|\underline{Y})) \psi_{i-k}(y) \rho(y|\underline{Y}) dy dx \quad F-3$$

in which

$$\underline{F}_{i \times i}^{(n \times n')}(\tau) = \int_0^T \phi_i^{(n)*}(t) \int_0^T \frac{1}{2\pi} \int_{-\infty}^{\infty} e^{j\omega(t-s-\tau)} s(\omega) d\omega \phi_i^{(n)}(s) ds dt. \quad F-4$$

But after replacing ϕ by the right-hand side of Eq. E-1, changing the order of the integration, and using Eq. A-2,

$$F_{i \times i'}^{(n \times n')}(\tau) = \frac{2\pi}{T} \int_{-\infty}^{\infty} s(\omega) e^{-j\omega\tau} \psi(\omega - \omega_1; t^{(n)}, t^{(n)} + T) \psi^*(\omega - \omega_1; t^{(n')}, t^{(n')} + T) d\omega \quad F - 5$$

The signal power spectral density function $s(\omega)$ must be specified before the above integral can be evaluated. Functions $s(\omega)$ that are relatively constant at

$$s_1 \equiv s(\omega_1) \quad F - 6$$

over an interval surrounding ω_1 and ω_1' , and that do not become extremely large in the vicinity of this interval allow a simple approximation to $F_{i \times i'}^{(n \times n')}(\tau)$. Specifically, choosing $\omega_1' > \omega_1$, when $s(\omega)$ is such that

$$\begin{aligned} & \int_{-\infty}^{\infty} s(\omega) e^{-j\omega\tau} \psi(\omega - \omega_1; t^{(n)}, t^{(n)} + T) \psi^*(\omega - \omega_1'; t^{(n')}, t^{(n')} + T) d\omega \\ & \approx s_1 \int_{\omega_1' - W}^{\omega_1 + W} e^{-j\omega\tau} \psi(\omega - \omega_1; t^{(n)}, t^{(n)} + T) \psi^*(\omega - \omega_1'; t^{(n')}, t^{(n')} + T) d\omega \end{aligned} \quad F - 7$$

for W somewhat larger than $\omega_1' - \omega_1$, then $F_{i \times i'}^{(n \times n')}(\tau)$ is approximately the complex convolution of the Fourier transform of ψ with itself. The same result is obtained if $\omega_1' < \omega_1$. This result is

$$\begin{aligned} F_{i \times i'}^{(n \times n')}(\tau) & \approx \frac{s_1}{T} \int_{-\infty}^{\infty} e^{-j\omega_1\xi} \mathbb{H}(\xi; t^{(n)}, t^{(n)} + T) e^{-j\omega_1'(\tau - \xi)} \mathbb{H}(\xi - \tau; t^{(n')}, t^{(n')} + T) d\xi \\ & = \frac{2\pi s_1}{T} e^{-j\omega_1\tau} \begin{cases} \psi(\omega_1' - \omega_1; t^{(n)}, t^{(n')} + T + \tau) & t^{(n)} - t^{(n')} - T < \tau < t^{(n)} - t^{(n')} \\ \psi(\omega_1' - \omega_1; t^{(n')} + \tau, t^{(n)} + T) & t^{(n)} - t^{(n')} < \tau < t^{(n)} - t^{(n')} + T \\ 0 & \text{elsewhere} \end{cases} \quad F - 8 \end{aligned}$$

As $|i-i'|$ increases, the interval $(\omega_i, \omega_{i'})$ lengthens until at $|i-i'|$ equal to some integer r it may no longer be stated that $s(\omega)$ is relatively constant over this interval and its vicinity. When $|i-i'| > r$, the approximation in Eq. F-7 is invalid and Eq. F-8 for $F_{i \times i'}^{(n \times n')}$ does not hold. Fortunately, however, the γ term in Eq. F-7 (see Eq. A-5) indicates that unless there is considerable variation in $n(\omega)$, r will be large enough that $F_{i \times i'}^{(n \times n')}$ will have become negligibly small before $|i-i'|$ reaches r .

The above approximate expression for $F_{i \times i'}^{(n \times n')}$ simplifies considerably when $i=i'$. According to Eq. A-4 in fact

$$F_{i \times i}^{(n \times n)}(\tau) = \frac{s_i}{T} e^{-j\omega_i \tau} \begin{cases} t^{(n)}_{-t^{(n)}+T} + \tau & t^{(n)}_{-t^{(n)}-T} < \tau < t^{(n)}_{-t^{(n)}} \\ t^{(n)}_{-t^{(n)}+T} - \tau & t^{(n)}_{-t^{(n)}} < \tau < t^{(n)}_{-t^{(n)}+T} \\ 0 & \text{elsewhere} \end{cases} \quad F - 9$$

With the definition of the triangle function

$$\mathcal{J}_{r \times r'}(x) = (1 - |x - r + r'|) \mathcal{H}(x; r - r' - 1, r - r' + 1) \quad F - 10$$

(see Fig. F-1), the above may be written

$$F_{i \times i}^{(n \times n)}(\tau) = s_i e^{-j\omega_i \tau} \mathcal{J}_{n \times n}\left(\frac{\tau}{T}\right). \quad F - 11$$

Returning to Eq. F-3, then,

$$\begin{aligned} s_{i k \times i k'}^{(n \times n')} &= \int_{-L/2}^{L/2} \psi_{i k}^*(x) \int_{-L/2}^{L/2} a(x, y | \underline{Y}) F_{i \times i}^{(n \times n')}(\tau(x, y | \underline{Y})) \psi_{i k'}(y) dy dx \\ &= s_i \int_{-L/2}^{L/2} \psi_{i k}^*(x) \int_{-L/2}^{L/2} a(x, y | \underline{Y}) e^{-j\omega_i \tau(x, y | \underline{Y})} \mathcal{J}_{n \times n}\left(\frac{\tau(x, y | \underline{Y})}{T}\right) \psi_{i k'}(y) dy dx \end{aligned} \quad F - 12$$

In interpreting this result it is recognized that the term

$$a(x, y | \underline{Y}) F_{i \times i}^{(n \times n')}(\tau(x, y | \underline{Y})) \quad F - 13$$

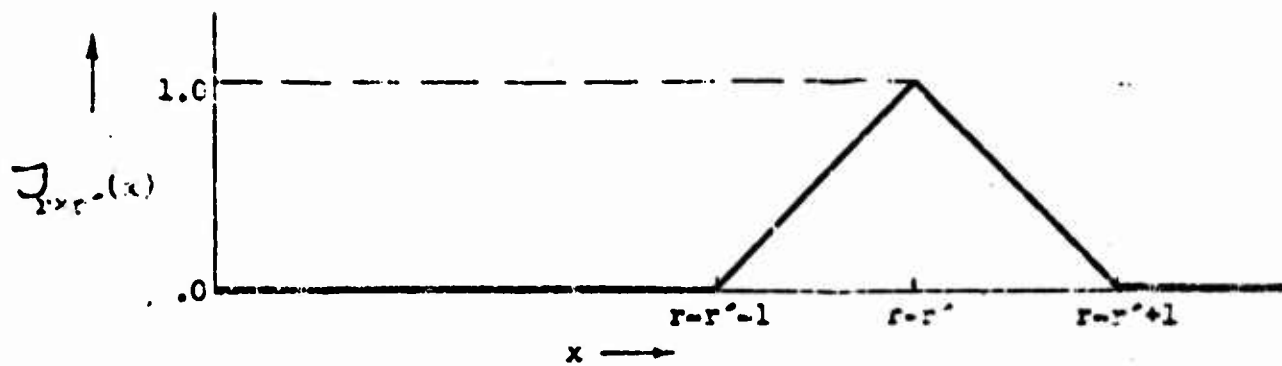


Figure F-1 The "Triangle" Function Defined by Eq. F-10

is the spatial covariance function of the signal process. Thus when $i=i'$ this signal covariance is

$$s_{ii}(x,y|\underline{Y}) = e^{-j\omega_1 \tau(x,y|\underline{Y})} \int_{n \times n} \left(\frac{\tau(x,y|\underline{Y})}{T} \right) \quad F-14$$

whose basic form depends upon J relative to the array length. If, for instance, J is approximately unity over the domain x and y within $(-\frac{L}{2}, \frac{L}{2})$, the covariance function is

$$s_{ii}(x,y|\underline{Y}) = e^{-j\omega_1 \tau(x,y|\underline{Y})} \quad F-15$$

In this case the signal process of index i is a single attenuating sinusoid. If on the other hand J decays rapidly with respect to the size of the interval $(-\frac{L}{2}, \frac{L}{2})$ in x and y , then the spatial signal process of index i is a wideband random process. Independent spatial components of the process are widely spread in the space frequency domain. These two cases are considered in greater detail in part b. In general, the first applies in most analyses of optimum detection and in the design of broadside detectors. The second applies in the design of high frequency off-broadside detectors.

The expression for g in general (Eqs. F-3 and F-8) and when $i = i'$ (Eq. F-12) are now used to determine or at least bound terms g in G . Simple results are obtained in certain special situations. An exhaustive account of the possible situations is not attempted; only a few of the more easily analysed situations are discussed.

In describing these situations, the parameter l introduced on page 47 will be extensively used. Physically

$$l = \frac{cT}{\cos \beta} \quad F-16$$

is the distance that a plane wave signal wavefront travels along the array

in time T' . For a signal with a curved wavefront and source vector \underline{y} , the number l is defined to be the same as that for a plane wave whose source vector is parallel to \underline{y} . Thus an l is associated with every signal as soon as the time subinterval duration T' is set.

Elements of G are determined in the following cases.

1. $l = l', l \gg L$.

This condition on l holds when detecting broadside signals (l is then infinite) or at any incidence angle if T' is large enough. This was the case in the analysis of Sect. 2.4.

2. Plane wave signals, sinusoidal ψ , $l = l', k = k', n = n', l \geq L$.

Though this and the following case require plane wave signals, unless the analysis or design specifically concerns the effects of curvature of the signal wavefront, the results are quite generally applicable.

3. Plane wave signals, sinusoidal ψ , $l = l', l \ll L$.

This condition on l holds off broadside at high time frequencies if T' is being kept small as it might be in a detector design. It is recalled that use of sinusoidal space eigenfunctions requires that $n(\omega_1, v)$ meet a smoothness condition in the neighborhood of the space frequency v_k . In general, higher ω favors this condition and since ω must be fairly high anyhow when $l \ll L$, the sinusoidal approximation may be expected to be valid. In case 2. above, this approximation may or may not be valid depending upon ω_1 and L .

Approximate upper bounds on elements of G are obtained in the following cases.

1. Plane wave signals, $n = n', l \geq L$.
2. Plane wave signals, $l \gg L$.
3. Plane wave signals, $l \ll L$.

Subsections below for each case contain the derivations, results and some

sample calculations. The above list provides the order and headings for the subsections.

b) Elements of G When $i=i'$

When $i=i'$, the elements g may be obtained using Eq. F-12, which is repeated here for convenience.

$$g_{ik \times ik'}^{(n \times n')} = s_1 \int_{-L/2}^{L/2} \psi_{ik}^*(x) \int_{-L/2}^{L/2} \alpha(x, y | \underline{Y}) e^{-j\omega_1 \tau(x, y | \underline{Y})} J_{n \times n'} \left(\frac{\tau(x, y | \underline{Y})}{T'} \right) \psi_{ik'}(y) dy dx. \quad F - 17$$

In this the argument $\frac{\tau(x, y | \underline{Y})}{T'}$ of J is approximately equal to $\frac{y-x}{l}$ (exactly equal for plane wave signals). It follows that

$$\begin{aligned} \text{MAX}_{\substack{x \text{ and } y \\ \in (-\frac{L}{2}, \frac{L}{2})}} \left[\frac{\tau(x, y | \underline{Y})}{T'} \right] &\approx \frac{L}{l}. \quad F - 18 \end{aligned}$$

Now according to Fig. F-1, if $\text{MAX} \left[\frac{|x|}{T'} \right] \ll 1$, then $J_{n \times n}$ is almost unity, and

$J_{n \times n'}$, $|n-n'| > 0$, is small within the domain of integration. Therefore, when $l \gg 1$, Eq. F-17 may be written

$$g_{ik \times ik'}^{(n \times n')} = \begin{cases} s_1 \int_{-L/2}^{L/2} \psi_{ik}^*(x) \int_{-L/2}^{L/2} \alpha(x, y | \underline{Y}) e^{-j\omega_1 \tau(x, y | \underline{Y})} \psi_{ik'}(y) dy dx & n = n' \\ 0 & n \neq n' \end{cases} \quad F - 19$$

But this is the same form as Eq. 2-77 and may be written (recalling Eqs. 2-65, 2-66, and 2-79)

$$g_{ik \times ik'}^{(n \times n')} = \begin{cases} s_1 \underline{h}_1^*(\underline{Y}) \underline{h}_1(\underline{Y}) & n = n' \\ 0 & n \neq n' \end{cases} \quad F - 20$$

The calculation of g using this form has already been discussed and illustrated

on pages 48 - 51.

Elements of G for Plane Wave Signals, Sinusoidal ψ , $i=i'$, $k=k'$, $n=n'$, and $l>L$.

If plane waves alone are considered,

$$\tau(x,y|\underline{Y}) = \frac{\cos \beta}{c} (y-x) = \frac{v}{\omega_1} (y-x) = \frac{T}{l} (y-x) \quad F - 21$$

and

$$\alpha(x,y|\underline{Y}) = 1 \quad F - 22$$

If, in addition, the set of space eigenfunctions may be approximated by the set $\{\psi_{ik}\}$ in which

$$\psi_{ik}(x) = \frac{e^{jv_k x}}{\sqrt{L}} \otimes \left(x; -\frac{L}{2}, \frac{L}{2}\right) \quad v_k = \frac{2\pi k}{L} \quad F - 23$$

then the expression for g in Eq. F-17 becomes

$$g_{ik \times i'k'}^{(n \times n')} = \frac{s_1}{L} \int_{-L/2}^{L/2} \int_{-L/2}^{L/2} e^{j[(v-v_k)x - (v-v_{k'})y]} \left| 1 - \frac{y-x}{l} - n+n' \right| \cdot \otimes \left| \frac{y-x}{l}; n-n'-1, n-n'+1 \right| dy dx \quad F - 24$$

The domain of integration in the right-hand side of this equation is the square shown in Fig. F-2. With $n \neq n'$, the condition $l>L$ insures that \otimes in the integrand is unity on the entire domain. Rotating and expanding this square domain with the change of variable

$$\begin{aligned} \xi &= y-x \\ \eta &= y+x \end{aligned} \quad F - 25$$

Eq. F-24 becomes

$$g_{ik \times i'k'}^{(n \times n')} = \frac{s_1}{2L} \int_{-L}^L \int_{-(L-|\xi|)}^{L-|\xi|} e^{-\frac{j}{2}[(v-v_k)(\eta-\xi) - (v-v_{k'})(\eta+\xi)]} \left| 1 - \frac{|\xi|}{l} \right| d\eta d\xi \quad F - 26$$

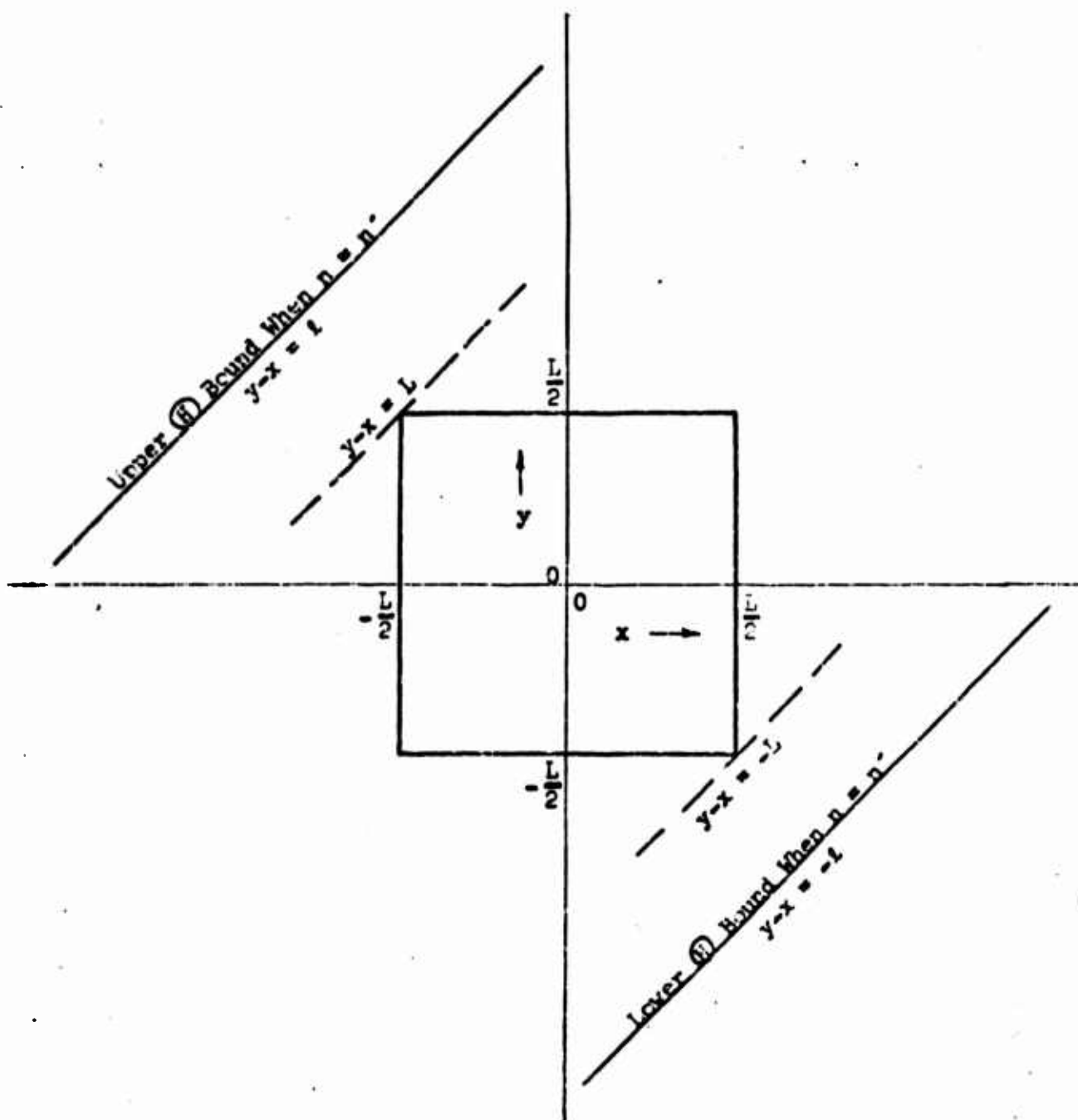


Figure F-2 The Domain of Integration in the x,y Plane When $l > L$

This integral, with k set equal to k' , is now evaluated.

$$\begin{aligned}
 g_{ik \times ik}^{(n \times n)} &= \frac{s_1}{2L} \int_{-L}^L \int_{-(L-|\xi|)}^{L-|\xi|} e^{-j(v-v_k)\xi} \left(1 - \frac{|\xi|}{L}\right) d\eta d\xi \\
 &= s_1 L \left\{ \left(1 + \frac{L}{l}\right) \text{sinc}^2 \left[\frac{L}{2}(v-v_k) \right] + \frac{4}{lL(v-v_k)^2} (\cos [L(v-v_k)] - \text{sinc} [L(v-v_k)]) \right\} \\
 &= s_1 L \left\{ \left(1 + \frac{L}{l}\right) \text{sinc}^2 \left[\frac{L}{2}(v-v_k) \right] - \frac{4L}{l} \left[\frac{2}{3!} - \frac{4}{5!} L^2(v-v_k)^2 + \frac{6}{7!} L^4(v-v_k)^4 - \dots \right] \right\}.
 \end{aligned}$$

F - 27

The above expression shows the signal selectivity of G . For instance, if the signal incidence β is such that

$$v = \frac{u}{c} \cos \beta = \frac{2\pi k}{L} = v_k \quad \text{F - 28}$$

for some k , then $g_{ik \times ik}^{(n \times n)}$ performs the greatest interception of this signal, and

$$\begin{aligned}
 g_{ik \times ik}^{(n \times n)} &= s_1 \left(1 - \frac{L}{3l}\right) \\
 v &= v_k
 \end{aligned}$$

F - 29

As the angle of incidence of the signal changes, the decrease in interception by $g_{ik \times ik}^{(n \times n)}$ is given by the above. In particular, when the change is such that $v = v_{k'}$ for some $k' \neq k$ so that

$$v - v_k = v_{k'} - v_k = \frac{2\pi}{L} (k' - k) \quad \text{F - 30}$$

then

$$\begin{aligned}
 g_{ik \times ik}^{(n \times n)} &= s_1 L \frac{4}{lL(v-v_k)^2} = s_1 L \frac{L/l}{\pi^2 (k-k')^2} \\
 v &= v_{k'} \\
 k' &\neq k
 \end{aligned}$$

F - 31

Thus the signal interception by $g_{ik \times ik}^{(n \times n)}$ is decreased by the factor

$$\frac{g_{ik \times ik}^{(n \times n)} \quad v = v_{k'}, k' \neq k}{g_{ik \times ik}^{(n \times n)} \quad v = v_k} = \frac{L/l}{\pi^2 (1 + \frac{L}{l}) (k-k')^2} \quad \text{F - 32}$$

When the processing interval T' is large or when the signal incidence is near 90° , l is large. For l sufficiently large,

$$G_{ik \times ik}^{(n \times n)} = s_1 L \quad F - 33$$

$$v = v_k$$

and

$$G_{ik \times ik}^{(n \times n)} = 0 \quad F - 34$$

$$v = v_{k'}$$

$$k' \neq k$$

An example is now considered. Let the array length L be 50 meters and the time frequency be 200 hz, and let the time interval T' be determined by Eq. E-4 with $N=3$. Using Eq. F-16, the inequality condition $l > L$ is then satisfied for $\beta > 63.2^\circ$.

Continuing, let the noise background be I3 sea noise. Since the spectrum $n(\omega_1, v)$ (Fig. 2-2) is flat for $v < \frac{\omega_1}{c}$, sinusoidal space eigenfunctions of frequency

$$v = \frac{2\pi k}{L} \quad F - 35$$

may be used as long as k is somewhat less than $\frac{L\omega_1}{2\pi c} = 6.6$.

In Fig. F-3 the term $G_{ik \times ik}^{(n \times n)}$ is plotted versus signal incidence for $63.2^\circ < \beta < 90^\circ$ and $k=0, \dots, 3$. The selectivity of the array in this example may be compared with that of the array in the first example considered on page 49 (Fig. 2-8) in which the time frequency is 40 hz and $l \gg L$.

Elements of G For Plane Wave Signals, Sinusoidal ψ , $i=i'$, and $l \ll L$.

When l is very much smaller than the length L of the array, the expression for $G_{ik \times ik}^{(n \times n)}$ in Eq. F-17 is an integral over a narrow, diagonally located strip in the x, y plane. This integral is evaluated after aligning new coordinate axes ξ and η with this strip, and neglecting a slight error at the

$\omega = 2\pi \times 200 = 1256$ Rads/Sec
 $L = 50$ Meters
 $N = 3$
 Background Noise is
 I3 Sea Noise
 $c = 1500$ Meters/Sec
 $m = 12$ Hydrophones

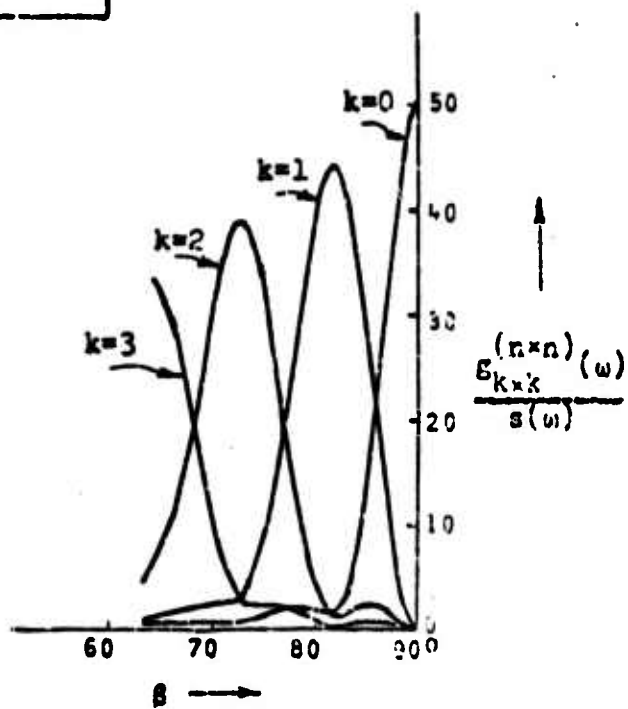


Figure F-3 Relative Spatial Spectra of the Signal

ends of the strip. Let

$$\xi = y - x - (n - n')l \quad F - 36$$

and

$$\eta = y + x \quad F - 37$$

(Fig. F-4). Then

$$\begin{aligned} \epsilon_{ik \times ik'}^{(n \times n')} &= \frac{s_1}{2L} \int_{-(L-|n-n'|)l}^{L-|n-n'|l} \int_{-l}^l e^{\frac{j}{2}[(v-v_k)(\eta-\xi-(n-n')l) - (v-v_{k'})(\eta+\xi+(n-n')l)]} \\ &\quad \cdot \left(1 - \frac{|\xi|}{l}\right) d\xi d\eta \mathcal{H}\left(n-n'; \frac{L}{l}, \frac{L}{l}\right) \\ &= s_1 l \mathcal{J}_{n \times n}\left(\frac{(n-n')l}{L}\right) e^{j(n-n')l \left(\frac{v_k + v_{k'}}{2} - v\right)} \text{sinc}\left[\mathcal{J}_{n \times n}\left|\frac{(n-n')l}{L}\right| \pi(k-k')\right] \\ &\quad \cdot \text{sinc}^2\left[\frac{l}{2} \left(\frac{v_k + v_{k'}}{2} - v\right)\right]. \end{aligned} \quad F - 38$$

The function \mathcal{J} was defined by Eq. F-10 and pictured in Fig. F-1. In particular, when $n=n'$

$$\epsilon_{ik \times ik'}^{(n \times n)} = \begin{cases} s_1 l \text{sinc}^2\left(\frac{l}{L}(v_k - v)\right) & k=k' \\ 0 & k \neq k' \end{cases} \quad F - 39$$

The spatial signal process observed after the n^{th} time subinterval is therefore composed of essentially independent components over a band of discrete space frequencies v_k .

As previously mentioned, these results apply when the time subinterval duration T' and the signal incidence angle are small enough that $l = \frac{T'c}{\cos\beta}$ is much smaller than the length L of the array. If the design described in part c of App. E is used, in which the time subinterval duration T' is a fixed

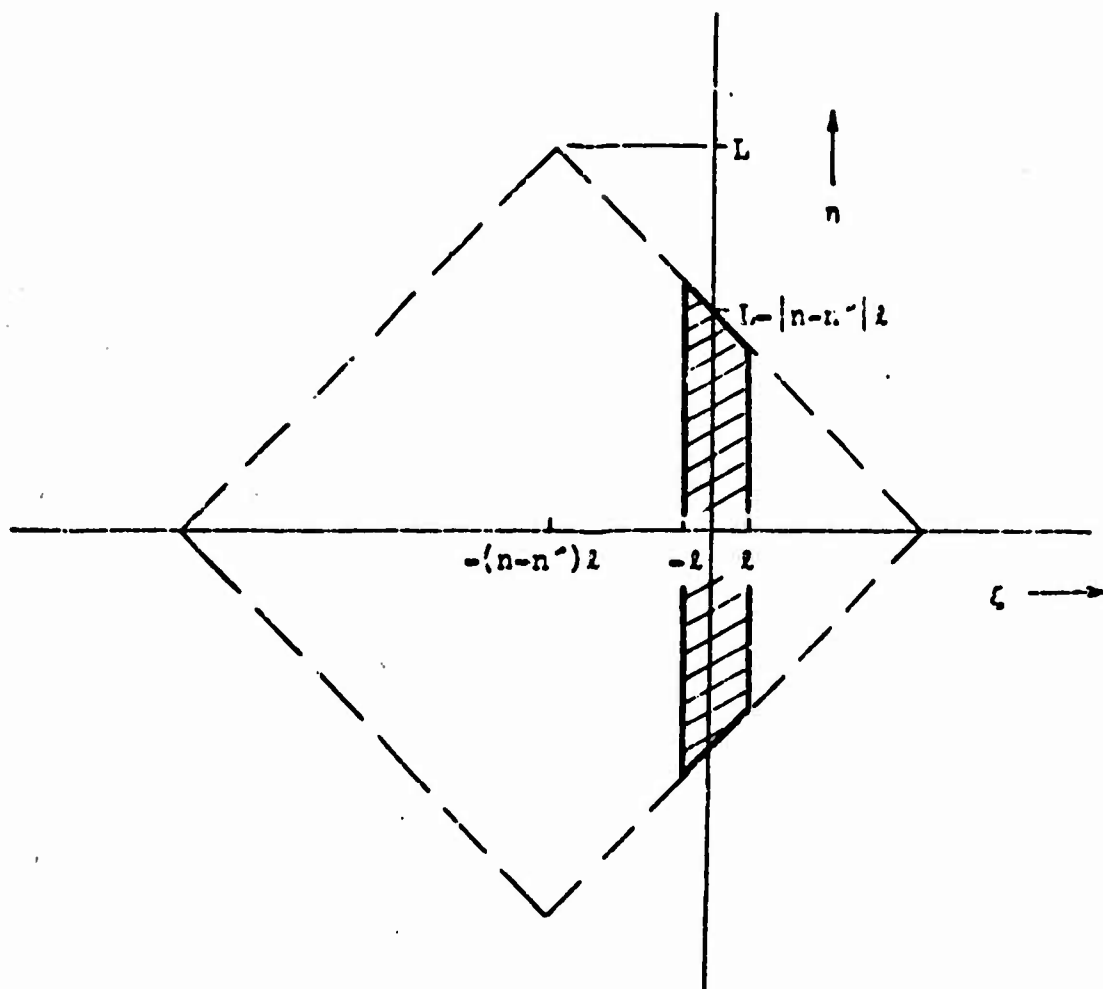


Figure F-4 The Domain of Integration in the ξ, η Plane When $l \ll L$

number N of periods of time oscillation at ω_1 (Eq. E-4), this condition that $l \ll L$ may be written

$$l = \frac{2\pi}{\omega_1} \frac{Nc}{\cos\beta} \ll L. \quad \text{F-40}$$

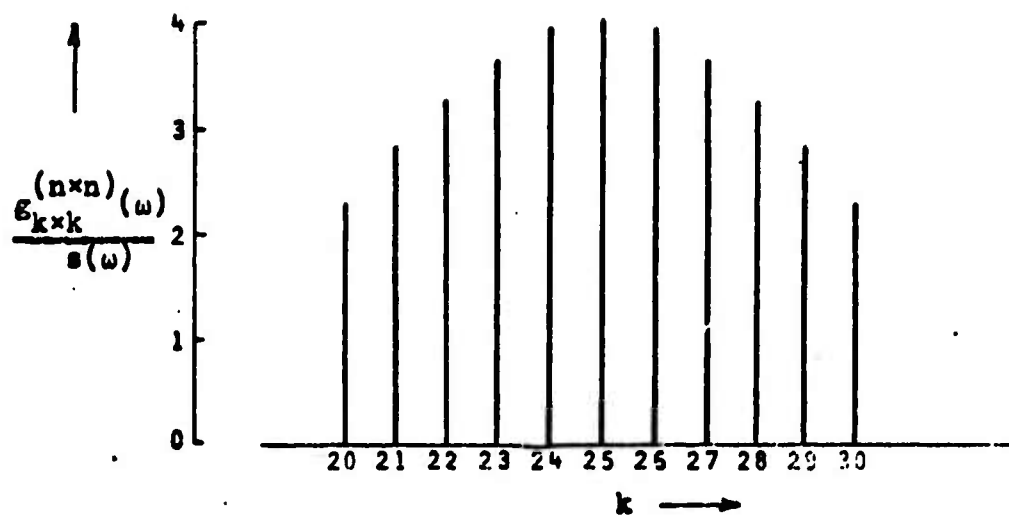
As an example, Eq. F-38 is now used to obtain G at 1000 hz for a plane wave signal in I3 noise. The array length is 50 meters and the processing subinterval T' is determined by Eq. E-4 in which $N = 2$. As shown in Fig. 2-2 the noise spectrum $n(\omega, \nu)$ is flat for $\nu < \frac{\omega}{c}$. Consequently sinusoidal space eigenfunctions of frequency $\nu_k = \frac{2\pi k}{L}$ may be used as long as ν_k is somewhat less than $\frac{\omega}{c}$. Using the above parameters, k must be somewhat less than 33. The signal incidence β is chosen such that $l \ll L$. According to Eq. F-40, $l < \frac{L}{10}$ for $\beta < 53^\circ$.

Some representative elements of G are given below for the plane wave signal that is maximally intercepted by the eigenfunction whose index k is 25. Its incidence β is 41.4° . The diagonal elements $g_{1k \times 1k}^{(n \times n)}$, $20 < k < 30$ of the diagonal submatrix $G_1^{(n)} = (g_{1k \times 1k}^{(n \times n)})$ are pictured in Fig. F-5(a). A large signal spread in space frequency is apparent. Elements $g_{1k \times 1k}^{(n \times n')}$ for $k = 25$ are pictured in Fig. F-5(b) to show the signal dependence from one time subinterval to another. Both the signal spread in the space frequency domain (Fig. F-5(a)) and the signal dependence between time subintervals (Fig. F-5(b)) are reduced by increasing l . In a design, l may be made large by increasing T' , by using phased time subintervals (part d of App. E), or by processing along separate subintervals of the array (part e of App. E).

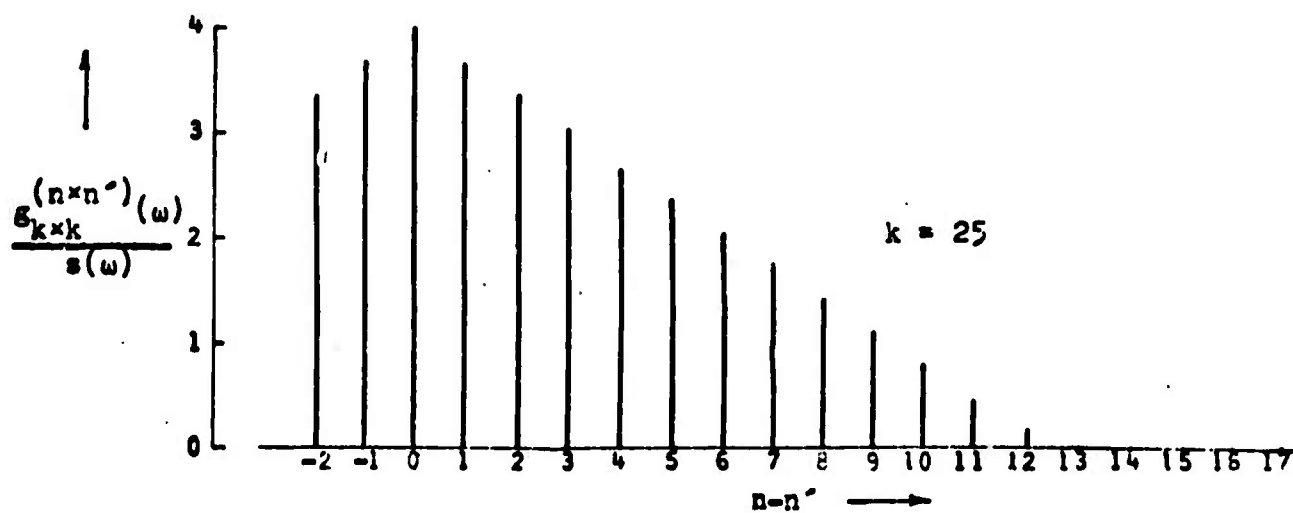
c) Upper Bounds on Elements of G When $i \neq i'$

In the preceding subsections some of the elements of G were derived under the condition that $i = i'$. Upper bounds on elements of G are obtained below without this condition.

$N = 2$
 $\theta = 41.4^\circ$
 $L = 50 \text{ Meters}$
 $\omega = 2\pi \times 1000 = 6283 \text{ RPS}$
 $m = 12 \text{ Hydrophones}$
 $c = 1500 \text{ Meters/Sec}$



(a)



(b)

Figure P-5 Elements of G When $l \ll L$

Applying the Schwarz inequality to Eq. F-3

$$\begin{aligned}
 |F_{i \times i'}^{(n \times n')}|^2 &\leq \int_{-L/2}^{L/2} |\psi_{ik}(x)|^2 dx \int_{-L/2}^{L/2} |\psi_{i'k'}(y)|^2 dy \int_{-L/2}^{L/2} \int_{-L/2}^{L/2} \left| \alpha(x,y|\underline{Y}) \frac{\tau(x,y|\underline{Y})}{T'} \right|^2 dy dx \\
 &= \int_{-L/2}^{L/2} \int_{-L/2}^{L/2} \alpha(x,y|\underline{Y}) \left| F_{i \times i'}^{(n \times n')} \left(\frac{\tau(x,y|\underline{Y})}{T'} \right) \right|^2 dy dx . \quad F - 41
 \end{aligned}$$

The magnitude of F is determined from Eq. F-8 using the magnitude of ψ given in Eq. A-5

$$\begin{aligned}
 |F_{i \times i'}^{(n \times n')}(\tau)|^2 &= \frac{4\pi^2 s_1^2}{T'^2} \begin{cases} |\psi(\omega_1, -\omega_1; t^{(n)}, t^{(n')} + T' + \tau)|^2 & t^{(n)} - t^{(n')} - T' < \tau < t^{(n)} - t^{(n')} \\ |\psi(\omega_1, -\omega_1; t^{(n')} + \tau, t^{(n)} + T')|^2 & t^{(n)} - t^{(n')} < \tau < t^{(n)} - t^{(n')} + T' \\ 0 & \text{elsewhere} \end{cases} \\
 &= \frac{4s_1^2}{T'^2} \frac{\sin^2 \left[\frac{1}{2} (\omega_1 - \omega_1') (T' - |\tau - (t^{(n)} - t^{(n')})|) \right]}{(\omega_1 - \omega_1')^2} \textcircled{H} (\tau; t^{(n)} - t^{(n')} - T', t^{(n)} - t^{(n')} + T'). \quad F - 42
 \end{aligned}$$

Since $(\omega_1 - \omega_1') T' = 2\pi(1 - 1')$ and $\frac{t - t'}{T'} = n - n'$, the above may be written

$$\begin{aligned}
 |F_{i \times i'}^{(n \times n')}(\tau)|^2 &= \frac{s_1^2 \sin^2 [\pi(1 - 1')(1 - |\frac{\tau}{T'} - n|)]}{\pi^2(1 - 1')^2} \textcircled{H} \left(\frac{\tau}{T'}; n - n' - 1, n - n' + 1 \right) \\
 &= \frac{s_1^2 \sin^2 [\pi(1 - 1') \mathcal{J}_{n \times n'}(\frac{\tau}{T'})]}{\pi^2(1 - 1')^2} , \quad F - 43
 \end{aligned}$$

where \mathcal{J} is defined by Eq. F-10. When $i \neq i'$, this simplifies to

$$|F_{i \times i'}^{(n \times n')}(\tau)|^2 \underset{i \neq i'}{=} s_1^2 \frac{\sin^2 \left[\frac{\pi \tau}{T'} (1 - 1') \right]}{\pi^2(1 - 1')^2} \textcircled{H} \left(\frac{\tau}{T'}; n - n' - 1, n - n' + 1 \right) . \quad F - 44$$

As a result, Eq. F-41 becomes

$$|g_{ik \times i'k'}^{(n \times n')}|^2 \leq \frac{s_1}{\pi^2 (1-i')^2} \int_{-L/2}^{L/2} \int_{-L/2}^{L/2} a(x, y|Y)^2 \sin^2 \left[\frac{\pi \tau(x, y|Y)(1-i')}{T'} \right] \\ \textcircled{10} \left| \frac{\tau(x, y|Y)}{T'} \right| ; n-n'-1, n-n'+1 \Big| dydx$$

F - 45

where the symbol \leq means "less than or approximately equal to". Bounds calculated using this expression may be compared with those terms $g_{ik \times i'k'}^{(n \times n')}$ calculated using Eq. F-17 in the preceding subsection.

When $T' \gg |\tau(x, y|Y)|$ then

$$\text{MAX}_{\substack{x \text{ and } y \\ \in (-\frac{L}{2}, \frac{L}{2})}} \left[\frac{|\tau(x, y|Y)|}{T'} \right] \approx 0$$

F - 46

Consequently the integrand in the bound on $g_{ik \times i'k'}^{(n \times n')}$, $i \neq i'$, (Eq. F-44) and hence the bound itself are approximately zero. Terms $g_{ik \times ik}^{(n \times n)}$ under the same condition are determined by Eq. F-27.

Now with plane wave signals,

$$\tau(x, y|Y) = \frac{\cos \theta}{c} (y-x) = \frac{T'}{l} (y-x)$$

F - 47

and

$$a(x, y|Y) = 1$$

F - 48

so that Eq. F-45 becomes

$$|g_{ik \times i'k'}^{(n \times n')}|^2 \leq \frac{s_1^2}{\pi^2 (1-i')^2} \int_{-L/2}^{L/2} \int_{-L/2}^{L/2} \sin^2 \left[\frac{\pi (1-i')(y-x)}{l} \right] \\ \cdot \textcircled{H}(y-x; l(n-n'-1), l(n-n'+1)) dydx$$

F - 49

This integral is easily evaluated in the three cases listed on page 153 .

A Bound on Elements of G for Plane Wave Signals with $n=n'$ and $l \gg L$.

This bound is determined from Eq. F-49 using the domain of integration

pictured in Fig. F-2. With $n=n'$, the condition that $l \geq L$ insures that (H) in the integrand is unity on the entire domain. Rotating and expanding this square domain with the change of variable

$$\xi = y-x$$

$$\eta = y+x$$

F - 50

Eq. F-49 becomes

$$\begin{aligned} |g_{ik \times i'k'}^{(n \times n)}|^2 &\leq \frac{s_1}{2\pi^2(i-i')^2} \int_{-L}^L \int_{-L+|\xi|}^{L-|\xi|} \sin^2\left[\frac{\pi\xi}{l}(i-i')\right] d\eta d\xi \\ &= \frac{s_1}{2\pi^2(i-i')^2} \left(1 - \text{sinc}^2\left[\frac{\pi L}{l}(i-i')\right]\right) \end{aligned}$$

F - 51

When l is very much larger than L , this upper bound is close to zero.

Consider again the example given on page 158. In this example, the time frequency is 200 hz, the array length L is 50 meters, the processing interval T' is determined by Eq. E-4 in which $N=3$, and the noise background is I3 sea noise. Bounds on the elements $g_{ik \times i'k'}^{(n \times n)}$, $i \neq i'$ of G are plotted in Fig. F-6 for plane wave signals with incidence such that $63.2^\circ < \beta < 90^\circ$. In Fig. F-3, the most prominent terms in G are on the order of $50 s_1$. Since the bounds calculated here are 20% of this when $|i-i'|=1$, exact calculation of $g_{ik \times i'k'}^{(n \times n)}$, $|i-i'|=1$, may be necessary in the specification of an optimum detector. At the 10% level, it is unnecessary to calculate such terms when $|i-i'| \geq 2$.

A Bound on Elements of G for Plane Wave Signals and $l \gg L$.

According to Eq. F-47

$$\begin{aligned} \text{MAX}_{\substack{x \text{ and } y \\ \epsilon(-\frac{L}{2}, \frac{L}{2})}} \left[\frac{\tau(x, y | \underline{y})}{T'} \right] &= \text{MAX}_{\substack{x \text{ and } y \\ \epsilon(-\frac{L}{2}, \frac{L}{2})}} \left[\frac{y-x}{l} \right] \end{aligned}$$

F - 52

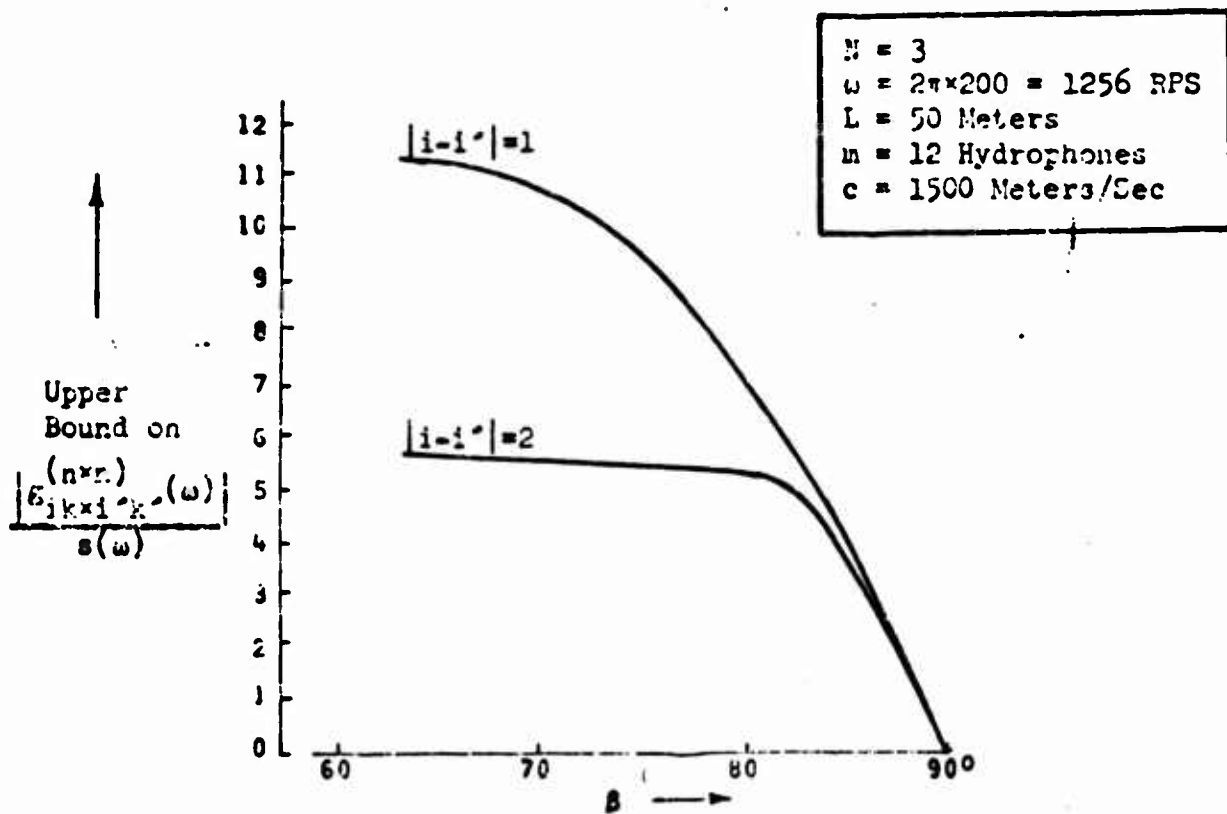


Figure F-6 A Bound on Elements of G When $l \geq L$

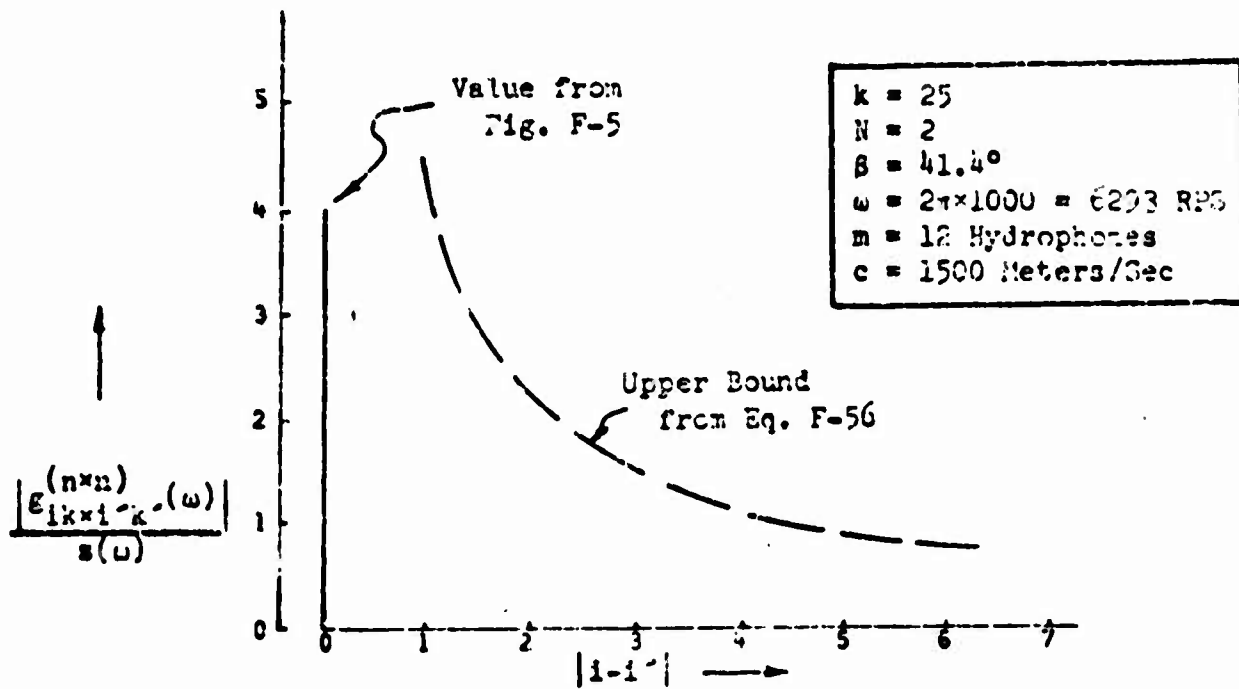


Figure F-7 A Bound on Elements of G When $l \ll L$

so that when $l \gg L$, the integrand in Eq. F-45 is approximately zero.

Therefore the upper bound on $|g_{ik \times i'k'}^{(n \times n)}|$ is practically zero.

A Bound on Elements of G for Plane Wave Signals and $l \ll L$.

A bound in this instance is determined by the right-hand side of Eq. F-49 in which the domain of integration is the diagonally located strip shown in Fig. F-4. Changing the variables of integration to

$$\xi = y - x - (n - n')l \quad \text{F - 53}$$

and

$$\eta = y + x \quad , \quad \text{F - 54}$$

and neglecting a small error at the ends of the strip, Eq. F-49 becomes

$$|g_{ik \times i'k'}^{(n \times n)}|^2 \leq \frac{s_1}{2\pi^2(i-i')^2} \int_{-(L-|n-n'|l)}^{L-|n-n'|l} \int_{-l}^l \sin^2 \left[\frac{\pi(i-i')}{l} \xi \right] d\xi d\eta \mathcal{H} \left(n-n'; -\frac{L}{l}, \frac{L}{l} \right) \quad \text{F - 55}$$

Carrying out the integration,

$$|g_{ik \times i'k'}^{(n \times n)}|^2 \leq \frac{s_1 L l}{\pi^2(i-i')^2} \mathcal{J}_{n \times n} \left(\frac{(n-n')l}{L} \right) \quad \text{F - 56}$$

The function \mathcal{J} was defined by Eq. F-10.

This bound is plotted in Fig. F-7 for the example on page 162 in which the time frequency is 1000 Hz, the array length is 50 meters, the processing interval T' is determined by Eq. E-4 with $N=2$, and the noise background is I3 sea noise.

REFERENCES

- (1) Bryn, F., "Optimum Signal Processing of Three Dimensional Arrays Operating on Gaussian Signals and Noise," J.A.S.A. 34, pp. 289-297, 1962.
- (2) Edelblute, D.J., J.M. Fisk, and Gerald L. Kinnison, "Criteria for Optimum Signal Detection Theory for Arrays," J.A.S.A. 41, pp. 199-205, 1967.
- (3) Vanderkulk, W., "Optimum Processing for Acoustic Arrays," J. Brit. I.R.E. 26, pp. 285-292, 1963.
- (4) Shapiro, A., "Criterion under Which the Standard Detector is Optimal," J.A.S.A. 41, pp. 445-447, 1967.
- (5) Middleton, D., and H.L. Groginsky, "Detection of Random Acoustic Signals by Receivers with Distributed Elements: Optimum Receiver Structures for Normal Signal and Noise Fields," J.A.S.A. 36, pp. 727-737, 1963.
- (6) Courant, R., and D. Hilbert, Methods of Mathematical Physics 1, Ch. 2, Interscience Publishers, Inc., New York, 1953.
- (7) Halmos, P.R., Introduction to Hilbert Space, Chelsea Publishing Co., New York, 1951.
- (8) Arens, R., "Complex Processes for Envelopes of Normal Noise," I.R.E. Trans. on Information Theory IT-3, pp. 204-207, 1957.
- (9) Yaglom, A.M., Stationary Random Functions, Prentice-Hall, Englewood Cliffs, 1962.
- (10) Helstrom, C.W., Statistical Theory of Signal Detection, Pergamon Press, New York, 1960, pp. 2, 35.
- (11) Slepian, D., H.O. Pollak, and H.J. Landau, "Prolate Spheroidal Wave Functions, Fourier Analysis and Uncertainty," B.S.T.J. 40, pp. 43-84, 1961.
- (12) Gilbert, E.N., and S.P. Morgan, "Optimum Design of Directive Antenna Arrays Subject to Random Variations," E.S.T.J. 34, pp. 637-661, 1955.
- (13) Middleton, D., Introduction to Statistical Communication Theory, Ch. 17, McGraw-Hill Book Company, Inc., New York, 1960.
- (14) Lawson, J.L., and G.E. Uhlenbeck, eds., Threshold Signals, Ch. 7, McGraw-Hill Book Company, Inc., New York, 1950.
- (15) Eckart, C., S10 Ref. 52-11, University of California, Marine Physical Laboratory, Scripps Institute of Oceanography, 1952.



ADAPTIVE SONAR SIGNAL DESIGN

By

Francis S. Hill, Jr.

Progress Report No. 36

General Dynamics/Electric Boat Research

(8050-31-55001)

June, 1968

DEPARTMENT OF ENGINEERING
AND APPLIED SCIENCE

YALE UNIVERSITY

ABSTRACT

The problem of designing sonar signal waveforms, or 'pings', to locate a submarine target is considered. It is assumed that a single target is present, and that the observer has measured its angular bearing and bearing rate by means of passive sonar equipment. The active sonar is used to measure the target's range and range rate. The target is assumed to be moving on a fixed course with constant speed.

In Chapter 2 the optimal single ping estimation of target parameters in colored gaussian noise is considered using a maximum inverse probability philosophy. The ambiguity problem is analyzed, and for the case of large signal-to-noise ratio, the optimal estimator is evaluated in terms of the signal and noise spectra. The pronounced effect of target range rate on the estimation accuracies in the colored noise case is discussed.

In Chapter 3 the results are extended to multiple ping situations, and the effect of interping times is evaluated. It is assumed that the observer must wait a fixed amount of time following the final ping before using the estimates obtained, and the performance measure adopted is the range estimate variance at the end of the wait time. The important case of two pings is considered in detail. The severe degradation due to a long wait time is analyzed, and shown to be ameliorated by using a long interping time. Optimum signals are designed for the white noise case, and a design philosophy is developed for the colored noise case. It is shown that, when a long interping time is used, the roles of the two pings become separated. Then the first ping should measure target range rate, and the second ping should estimate range.

In Chapter 4 signal design is examined for the specific problem of a strong reverberation (clutter) environment. The reverberation spectrum is derived, and the implications of its dependence on the transmitted signal are examined. It is shown that the first ping should be made very narrowband to obtain an accurate range rate estimate, and that this range rate knowledge can then be used to redesign the second ping. Greatly increased range estimate accuracy is achievable by this procedure for, over a wide range of target speeds and reverberation parameters, proper signal design can completely eliminate the effect of reverberation once the target range rate has been measured.

Chapter 5 summarizes the main results of the research and recommends further areas for study.

TABLE OF CONTENTS

	<u>Page</u>
Table of Contents	B-ii
List of Figures	B-iv
CHAPTER 1. STATEMENT OF THE PROBLEM	
1-1 Introduction	B-1
1-2 Statement of the Problem and Assumptions	B-4
1-3 Previous Work	B-7
CHAPTER 2. THE ESTIMATION OF RANGE AND RANGE RATE FROM A SINGLE PING	
2-1 The Estimation Problem	B-11
2-2 The Inverse Probability Approach	B-13
2-3 Maximum Inverse Probability Vs. Maximum Likelihood	B-16
2-4 Derivation of the Estimator	B-17
2-5 The Performance of the Estimator	B-24
2-5.1 Approximate Analysis of the Ambiguity Problem	B-29
2-5.2 Analysis of Estimate Variance for "Small" Errors	B-33
2-6 The Ellipse of Estimate Variances	B-36
2-7 The Form of the Estimate Variances	B-38
CHAPTER 3. MULTIPLE-PING RECEPTION: EFFECT OF ELAPSED TIME	
3-1 Effect of Elapsed Time on Estimates	B-54
3-2 Multiple Ping Processing	B-62
3-3 The Final Range Estimate Variance	B-69
3-4 Behavior of REV as a Function of the Design Parameters	B-71
3-5 Design of ρ_1 and ρ_2 for Optimum Performance in White Noise	B-81
3-6 A Design Perspective for the Reverberation Noise Case	B-89
CHAPTER 4. SIGNAL DESIGN OF TWO PINGS IN THE STRONG REVERBERATION ENVIRONMENT	
4-1 The Reverberation Noise Spectrum	B-95
4-2 Basic Signal Design Implications of the Reverberation Spectrum	B-99
4-3 Design of the First Ping	B-101
4-4 Design of the Second Ping	B-105
4-5 Some Bounds on A_g and Simple Cases	B-112
4-6 Some Commonly Used Signals	B-114
4-7 Multi-lobe Spectra	B-120

TABLE OF CONTENTS (Cont'd)

	<u>Page</u>
CHAPTER 5. CONCLUSIONS AND PROPOSALS FOR FURTHER RESEARCH	B-138
Recommendations for Future Research	B-144
APPENDIX A. DISCUSSION OF TARGET MOTION GEOMETRY	B-147
APPENDIX B. APPROXIMATE PROBABILITY OF GROSS ERRORS	B-149
APPENDIX C. DERIVATION OF THE ELLIPSE PARAMETERS	B-158
APPENDIX D. EQUIVALENT SIGNAL FOR MATCHED FILTERING	B-170
APPENDIX E. DERIVATION OF UNIFIED FORMS OF A, B, C	B-171
APPENDIX F. LIFMOP AND RAFMOP SIGNAL EXAMPLES	B-174
I Calculation of the Ellipse Parameters	B-174
II Proof that the LIFMOP Signal Attains Largest B for Fixed A	B-177
III The RAFMOP Spectrum	B-178
APPENDIX G.	B-181
1 Proof that A and C are Maximum for White Noise Alone	B-181
2 The Uncertainty Principle for Δ in White Noise	B-181
APPENDIX H. APPROXIMATE CALCULATION OF C FOR A MOTIONLESS TARGET	B-183
APPENDIX I. FORM OF J	B-185
APPENDIX J. DEMONSTRATION THAT A, C ARE ATTAINABLE IN WHITE NOISE CASE	B-187
APPENDIX K. DETERMINE ρ_2 FOR MINIMUM J IN SINGLE PING CASE	B-189
APPENDIX L. CLUTTER ELIMINATION UNDER DISPERSION BANDWIDTH CONSTRAINT	B-190
APPENDIX M. OPTIMUM $g(x)$ FOR NO TARGET OR SCATTERER MOTION	B-193
REFERENCES	B-197

LIST OF FIGURES

<u>Figure</u>		<u>Page</u>
1-1	Sequence of Events	B-5
2-1	An Inverse Probability Function	B-15
2-2	Different Classes of Ambiguity Functions	B-28
2-3	Approximate Probability of a Gross Error	B-32
2-4	Ellipse of Estimate Variances	B-37
2-5	Sample Signal and Noise Spectra	B-44
2-6	A Signal Envelope and Two Examples of Frequency Modulation	B-46
2-7	Error Ellipses for RAFMOP & LIFMOP Signals	B-53
3-1	Evolution of Points on the θ -plane	B-56
3-2	Evolution of Error Ellipse	B-60
3-3	Combination of Ellipses to Form Joint Ellipse	B-66
3-4	Geometrical Interpretation of γ and $\rho \gamma$	B-75
3-5	Basic Shape of J versus t_i	B-76
3-6	Effect of Long Interping Time	B-78
3-7	J vs τ_i for $\tau_w=1$	B-83
3-8	J vs τ_i for $\tau_w=10$	B-84
3-9	J vs τ_i for $\tau_w=50$	B-85
3-10	Optimum ρ_1 and ρ_2 vs τ_i	B-86
3-11	J vs t_i/t_w for General Case with $B_1=B_2=0$	B-93
4-1	Sample Signal and Noise Spectra, and Resultant $P(\omega)$	B-102
4-2	Two-Lobe Spectrum and Autocorrelation Function	B-111
4-3	A_g vs R in Some Extreme Cases	B-115
4-4	A_g vs Target Speed	B-117
4-5	Sinc ² Spectrum Example	B-119
4-6	Sample n-lobe Signal Spectrum	B-121
4-7	Sample Spectrum, and Resulting Reverberation Spectrum	B-124
4-8	Necessary α and Lobe Spacing for Reverberation Elimination	B-124
4-9	$C(\mu)$ for n Equally Spaced Spectral Lobes	B-127
4-10	Spectrum for RAFMOP Signal	B-130
4-11	AMB(μ) for Spectrum of Example 4-3	B-133
4-12	A_g vs. α for Multi-Lobe Spectra	B-135
A-1	Target Motion Geometry	B-148
L-1	Spectrum for Reverberation Elimination	B-191
M-1	Lagrange Multiplier and Dynamic Programming Results	B-195

CHAPTER I

Statement of the Problem

1.1 Introduction

The research described in this report deals with the estimation of a target's position relative to an observer, and with the design of efficient systems and sonar waveforms for this use. The problem of first detecting the target's presence is not considered in detail, for it is assumed that the observer has been monitoring his passive sonar equipment for some time, has picked up the emissions of the target and consequently knows that it is present. It is also assumed that the observer has a reliable estimate of the target's bearing and bearing rate (it is well known that passive sonar systems have direction-measuring capability).^[1] The observer has the advantage of time in these measurements, for he can monitor the passive signals for a long period before making a decision. Thus these

estimates can be quite accurate. When the observer has decided that a target is present, and has estimated the bearing and bearing rate, he uses the active sonar equipment to measure the target's range and range rate.

The measurement requirements are thus divided between the active and passive sonar systems. This report will consider only the role of the active sonar measurements, so that the problem reduces to the estimation of range and range rate of a target with known bearing and bearing rate. Such an assumption also allows the observer to send the active bursts (or "pings") in a single direction, rather than requiring a scanning procedure.

The problem is extended in two directions over this simple formulation. First, it is assumed that the observer may send two separate pings (each ping may be a complicated waveform), and may redesign the second ping according to information received from the first. The pings may be separated by a substantial time interval, at the discretion of the observer. This permits a certain amount of adaptability. Secondly, it is assumed that the observer is interested in a precise estimate of the target's position at a

certain time after the second ping is sent. This time may be as much as a few minutes, and could be the time required for preparing and sending some type of interceptor. Thus the sonar system is being used for tracking the target over a period of time. The observer will estimate the target's present range and range rate on each ping, and use this information to calculate the target's range at the later time. This range estimate, along with the bearing estimates (which may be updated passively between pings) will serve to locate the target.

The accuracy of these estimates is diminished by the presence of interfering noise. One common source is circuit noise generated in the receiving apparatus, commonly called "white noise" for its broadband nature. Another source is ambient noise generated by surface wave motion, as well as fish or crustacean sounds.^[2] These sources are uncontrollable by the observer, although he can attempt to reduce their effect by signal processing. A third type is reverberation, (called "clutter" in the radar case) due to sonar echoes from scattering objects in the ocean, such as fish, flora, and the ocean boundaries.

This type of interference depends on the transmitted signal waveshape, and thus requires special attention when one is designing sonar signals, in order to reduce its effect.

There are two main types of reverberation: boundary reverberation, caused by reflections from the ocean surface and bottom; and volume reverberation, caused by scatterers located throughout the bulk of the environment.

This report will consider in detail only white noise and volume reverberation, although many of the derivations are applicable to other kinds of noise.

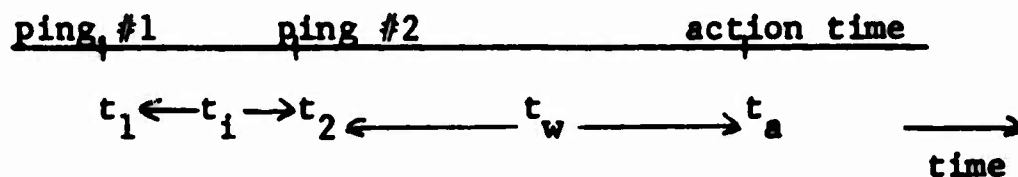
1.2 Statement of the Problem and Assumptions

1. It is assumed that a single target is present in the surveillance region, and is maintaining a constant course and speed.
2. The observer is stationary, has acquired the target, and has estimated its bearing and bearing rate.
3. The observer can send two pings, but after these are sent there is a fixed and known wait time required before the "action" time.

The observer may choose the "interping" time, although

it will have a minimum value due to signal processing time limitations.

4. The observer's goal is to estimate the range of the target at the action time. The criterion of accuracy is the statistical variance of the range estimate. The sequence is illustrated in Figure 1-1.



t_i = interping time; t_w = wait time

Figure 1-1 Sequence of events

5. The target range as a function of time is described by

$$r(t) = r_0 + v_0(t-t_1) \quad (1-1)$$

so that r_0 is the true range at the time of ping #1, and v_0 is the true (receding) radial speed for all time. In Appendix A this relationship is examined and shown to apply to remote targets proceeding in any direction.

6. Propagation in the ocean medium is assumed to be rectangular, and all scatterers including the target are point reflectors, so that the signal received from each is a version of the transmitted signal, delayed and Doppler shifted.
7. The reverberation model (considered in detail in Chapter 4) assumes that the scatterers have random locations and motions, that all scatterers have identical statistical properties, and that they are mutually independent in all respects.
8. The interfering noise is a stationary gaussian process with spectral density $N(\omega)$. In Chapter 4 for purposes of signal design this spectrum is specialized to that of volume reverberation plus white noise.
9. The waveforms allowed are narrowband in the sense that only Doppler shifts in the carrier frequency need be considered in the reflected signal. The sonar system is assumed to have a bandwidth limitation of $2W$ radians per second, and signal durations are limited to d seconds. The equipment is also assumed to impose a peak power limitation on the waveforms, such that the signal envelope is limited to m_0 volts.

10. The sonar system operates through an array of hydrophones, but due to the narrowband nature of the signals, this array is considered as a point source with directional properties.

1.3 Previous Work

The problem stated is one in the theory of estimation of signal parameters, and certain aspects of it have been studied extensively before. Most of the work has been done for the case of gaussian white noise interference only. The most notable case in point is the fundamental work of Woodward and Davies,^[3] which in 1950 applied the concepts of inverse probability to the radar problem. They derived the form of the optimum estimator for determination of target range only, and demonstrated that the accuracy of the range estimate was proportional to the signal bandwidth. Thus all signals having the same bandwidth were equally good. Woodward^[4] collected these results in an elegant book in 1953, and further introduced the concept of ambiguity, which has become a cornerstone in radar theory. The idea of ambiguity is as follows: due to certain characteristics of the signal, the optimum

processor will indicate that certain distinct values, or a range of values, of the range parameter all have high probability of being the correct one. In the noise-free case the correct one will always be indicated as the most probable, but when noise enters the system it can alter the indicated probabilities, and make a false value appear most probable. Proper signal design can reduce this possibility, however, and consequently researchers have sought ways of designing signals to fit prescribed ambiguity requirements. Cook and Bernfeld^[5] have collected many of these results in a recent book.

In 1957 Kelly, Reed & Root^[6] (hereafter KR&R) reported a rigorous analysis of the maximum likelihood estimation problem for several parameters in general stationary noise. They obtained the statistics for the accuracy of the estimates in the case of large signal to noise ratio. Their results are unfortunately rather difficult to apply to the signal design problem, as they require the solution of an integral equation. However, they did obtain simple results for the white noise case, which showed that the target range rate estimate accuracy

improved as the signal duration increased. Correlation between the range and range rate estimates degraded all of the estimates, and the degradation was severe if the correlation was significant. No readily usable results were given for the "colored" noise case. Hence one of the goals of Chapter 2 here will be to adapt their answers for signal design in the more general noise case.

Helstrom^[7] collected previous work into a useful volume in 1960, in which he outlined and compared the many estimation philosophies which one might apply to the sonar situation. He also considered in more detail the KR&R white noise example, relating it to some important waveforms.

On the subject of the effect of elapsed time between data taking and data usage, Cahlander^[8] considered the sonar signals of bats, and noted that bat signals were designed to yield the best position information at the time of interception with the prey. Cook and Bernfeld^[5] and Rihaczek^[15] have also mentioned the evolution of the ambiguity function with time, but an extensive analysis of the situation has not been made.

The combination of data obtained from a sequence of pings was touched upon by Woodward^[4] in a brief expository way, but not developed in any detail. The problem of signal redesign based on previous signal information has not been examined previously to the knowledge of the writer.

CHAPTER 2

THE ESTIMATION OF RANGE AND RANGE RATE FROM A SINGLE PING

The method of KR&R is presented in this chapter in summary form, adapted to the more interpretable Fourier coefficients. The inverse probability philosophy is first discussed, then applied to the particular problem following the lines of KR&R, and the form of the optimum estimator is derived. The performance of the estimator is then evaluated, and the results given in terms of Fourier transforms of the signal, instead of the KR&R Karhunen-Loève coefficients.

2.1 The Estimation Problem

A signal is transmitted into the medium, and the target echo plus noise is received. It is desired to obtain a measurement of the target's range and range rate. The range manifests itself in the signal delay, while the range rate causes a Doppler compression in the time structure of the signal. For narrowband signals this Doppler compression may be approximated by a Doppler shift in the carrier frequency.

Consider transmitted signal $s_t(t)$:

$$s_t(t) = m(t) \cos(Qt + \varphi(t)) = \text{Re } s(t) e^{jQt} \quad (2-1)+$$

with complex envelope $s(t)$ ⁽⁷⁾

$$s(t) = m(t) e^{j\varphi(t)} \quad (2-2)$$

$m(t)$ is the amplitude modulation, $\varphi(t)$ the phase modulation, and Q is the carrier frequency. (The approximation in using the complex exponential form instead of the precise but awkward "analytic" form is discussed in Cook & Bernfeld⁽⁵⁾, p. 61. The representation is perfect if the spectrum of $s(t) e^{jQt}$ vanishes for negative frequencies. For time-limited signals this is impossible, but if the signal is sufficiently narrowband, the approximation is a good one.)

The signal received from the target is

$$\begin{aligned} s_{\text{rec}}(t) &= \sigma_0 m(t - \tau_0) \cos \left[(Q - \omega_0)(t - \tau_0) + \varphi(t - \tau_0) \right] \\ &= \text{Re } \underline{\sigma}_0 s(t, \theta_0) e^{jQt} \end{aligned} \quad (2-3)$$

where

$$s(t, \theta_0) = s(t - \tau_0) e^{j\omega_0(t - \tau_0)}$$

⁺Re = real part

In these relations τ_0 is the true target delay and w_0 is the target Doppler shift.* The target "state" is conveniently denoted by $\theta_0 = (\tau_0, w_0)$. σ_0 is the target reflection coefficient (including propagation loss, etc.) and is conveniently extended to the complex version $\underline{\sigma}_0$ above which includes the rapidly fluctuating phase term: $\underline{\sigma}_0 = \sigma_0 e^{-jQ\tau_0}$

The total complex envelope of the received signal may be written,

$$y(t) = \underline{\sigma}_0 s(t, \theta_0) + n(t) \quad (2-4)$$

where $n(t)$ is the complex envelope of the noise received.

The estimation problem then takes the form: Given $y(t)$, estimate θ_0 .

2.2 The Inverse Probability Approach

The tenet that supports all of the work to follow is this: If a quantity x is converted in some random way into a quantity y , then the most one can ever know about the value of x from observing the value of y is the function $\text{Pr}(x=X/y=Y)$. This function is read "the probability that $x=X$ when one knows that $y=Y$." It is taken as a function of

* $\tau_0 = 2r_0/c$, $w_0 = -2Qv_0/c$, for propagation speed c , true target range r_0 , and true target range rate v_0 (receding).

X for a fixed (observed) value Y. If the observer calculates $\Pr(x=X/y=Y)$ for all possible values of X, then it represents his total "state of mind" regarding the value of x. (Woodward⁽⁴⁾, p. 62).

By Bayes law, one can rewrite this function (ibid p. 63),

$$\Pr(x=X/y=Y) = \Pr(x=X)\Pr(y=Y/x=X)/\Pr(y=Y) \quad (2-5)$$

where $\Pr(x=X)$ is the a priori probability function for x, representing the totality of the observer's knowledge concerning x before y was observed. $\Pr(y=Y)$ is just a constant after y has been observed, and thus can be ignored. $\Pr(y=Y/x=X)$ is called the likelihood function. It is taken as a function of X, and may be thought of as the likelihood of observing the value Y when $x=X$.

In the present sonar context the quantity x corresponds to the parameter set $\theta=(\tau,w)$ while the observable y is the received waveform $y(t)$. The inverse probability philosophy then directs the observer to form $p(\theta/y(t))$ for each possible θ , and to display this function in some fashion. A possible result is shown in Figure 2-1.

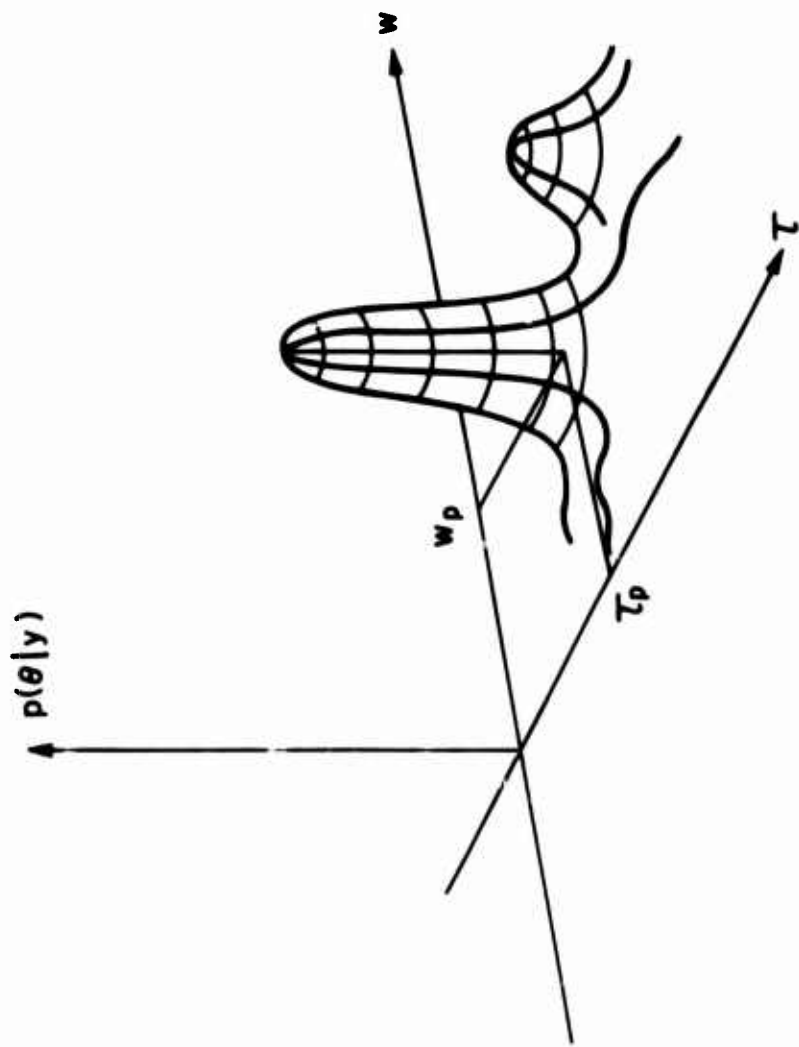


FIGURE 2-1 AN INVERSE PROBABILITY FUNCTION

Hopefully this function will reach its maximum at a value θ near the true value θ_0 . The observer, who must eventually make a decision as to the value of θ , will clearly choose the $\theta = \theta_p$ at which the function peaks, since this is the most probable value of θ given all available information. Making decisions destroys some information (Woodward⁽⁴⁾, p. 60), but this is unavoidable if action is required.

2.3 Maximum Inverse Probability vs. Maximum Likelihood

Many writers prefer to use a similar decision method called the maximum likelihood estimator (hereafter MLE). This process differs from the inverse probability function (hereafter InvPF) method in only one way: the elimination of the a priori probability function. Referring to (2-5) one sees that $\Pr(x=X)$ is one of the factors in the InvPF. Many investigators criticize the concept of a priori distributions, saying that the observer rarely would know them, if indeed they existed at all. Woodward⁽⁴⁾ (p. 74) and Seibert⁽⁹⁾ (p. 206) answered these criticisms by saying the MLE scheme just begs the issue. If the observer ever makes a decision by choosing the θ having maximum likelihood, then he has effectively chosen a priori probabilities anyway,

in this case saying all θ are equally probable a priori. They say that instead the observer should use all the information at his disposal and make an educated guess at the a priori distribution. In many cases the observer will have so little to go on he will use a uniform distribution also.

In this work it will be assumed that the observer has insufficient information to guess at any a priori distribution -- here denoted $p_0(\theta)$ -- other than a uniform one within the surveillance region. The surveillance region requires some guess work on his part, and it is assumed he has decided to look in a delay interval T seconds long (beginning at some t_b and going to t_b+T), and in a Doppler interval $(-w_{\max}, w_{\max})$, determined in this narrow-band case mainly by the possible target speeds anticipated. Because of this uniform $p_0(\theta)$, (at least for the first ping), the InvPF and MLE techniques become essentially identical. Hence, the likelihood function of (2-5), given now by $p(y(t)/\theta)$, will be the function of prime interest.

2.4 Derivation of the Estimator (following KR&R)

The signal processing operations which the InvPF estimator must perform on the received signal are now

derived. The main difference between the analysis here and that in KR&R is the use of Fourier coefficients instead of Karhunen-Loève coefficients.

Since the a priori probabilities have been chosen uniform, the estimator form must be embodied in the likelihood function $p(y(t)/\theta)$. This function is derived by hypothesizing a particular value of θ as well as a value of the unknown reflection coefficient g , (2-4), and thus hypothesizing that the received waveform is

$$y(t) = gs(t-\theta) + n(t) \quad (2-6)$$

In order to form the probability function for the entire waveform, $y(t)$ is represented by an orthogonal expansion. The most convenient schemes are those yielding uncorrelated coefficients. The Karhunen-Loève coefficients used by KR&R are always uncorrelated, but require the solution of an integral equation. The Fourier coefficients have much more intuitive appeal and have been shown to grow less correlated as the expansion interval (which is here the observation interval) grows larger. (If the observation time is much larger than the correlation time of the process, the error

in assuming the coefficients uncorrelated goes down as $1/T^2$. (7,10) We assume here that the observation time is indeed sufficiently long.

The Fourier coefficients for any complex waveform, say $y(t)$, are given by

$$y_k = \frac{1}{T} \int_T y(t) e^{-j\omega_k t} dt \quad (2-7)$$

where i. $\omega_k = 2\pi k/T$

ii. the integration limits are indicated by T , meaning the interval T : $(|t| \leq T/2)$, centered at the origin for symmetry.

For the noise waveform $n(t)$ we define coefficients n_k , and for the received signal waveform $s(t, \theta)$ we define the set $s_k(\theta)$. Thus from (2-4) we have

$$y_k = \underline{g} s_k(\theta) + n_k \quad (2-8)$$

The n_k , being the result of linear processing of the gaussian process $n(t)$, are themselves jointly gaussian. (Helstrom⁽⁷⁾ p. 50). Lack of correlation therefore implies independence. In addition the real and imaginary parts of

each coefficient are independent, and each part has variance $\frac{1}{2}N(\omega_k)/T$ (Davenport & Root⁽¹⁰⁾ p. 94). $N(\omega)$ is the spectral density of the process $n(t)$.*

KR&R⁽⁶⁾ (Eq. 17, p. 323) use this information to form $p(y/\theta)$:

$$p(y/\theta) = K_1 \exp \left[-T \sum_k \frac{|y_k - \underline{g} s_k(\theta)|^2}{N(\omega_k)} \right] \quad (2-9)$$

where \underline{g} , θ are hypothesized values and K_1 is a normalization constant. The maximum value of $p(y/\theta)$ occurs when the exponent is a minimum. We expand the exponent, and name the significant parts:

$$\begin{aligned} -T \sum_k \frac{|y_k - \underline{g} s_k(\theta)|^2}{N(\omega_k)} &= -T \sum_k \frac{|y_k|^2}{N(\omega_k)} + 2T \operatorname{Re} \underline{g}^* \sum_k \frac{y_k s_k^*(\theta)}{N(\omega_k)} \\ &\quad - T \sigma^2 \sum_k \frac{|s_k(\theta)|^2}{N(\omega_k)} \\ &= -T \sum_k \frac{|y_k|^2}{N(\omega_k)} + 2 \operatorname{Re} \underline{g}^* D(\theta) K(\theta) - \sigma^2 D^2(\theta) \quad (2-10)** \end{aligned}$$

*The real noise process of which $n(t)$ is the complex envelope has spectral density $N_r(\omega)$, equal to $N(\omega-Q) + N(-\omega-Q)$ (Helstrom⁽⁷⁾, p. 50).

**notation: Re=real part, Im=imaginary part, *=conjugate

where we have called

$$K(\theta) = \frac{1}{D(\theta)} T \sum_k \frac{y_k s_k^*(\theta)}{N(\omega_k)}$$

$$D^2(\theta) = T \sum_k \frac{|s_k(\theta)|^2}{N(\omega_k)} \quad (2-11)$$

The first term of (2-10) depends in no way on the hypothesized θ , and is simply a constant once the waveform has been received. It is incorporated into K_1 . $K(\theta)$ is the actual signal processing term, as it alone depends on the waveform $y(t)$. The other term, coupled with the reflection coefficient \underline{g} , is a post-processing signal-to-noise ratio (hereafter SNR).

We call the latter two terms of (2-10) $L(\underline{g}, \theta)$, and complete the square:

$$L(\underline{g}, \theta) = -|\underline{g}D(\theta) - K(\theta)|^2 + |K(\theta)|^2 \quad (2-12)$$

The observer desires to eliminate the unknown reflection coefficient \underline{g} rather than display all possible values, and he does this by making a MLE estimate on \underline{g} , and substituting the estimate back into (2-12) (Helstrom⁽⁷⁾ p. 205). As this is equivalent to maximizing $L(\underline{g}, \theta)$ with respect to \underline{g} , the observer of course chooses $\hat{\underline{g}}$:

$$\hat{\underline{g}} = K(\theta)/D(\theta) \quad (2-13)$$

which eliminates the first part of (2-12), leaving only $|K(\theta)|^2$.

The observer must display the inverse probability function:

$$p(\theta/y) = k p_0(\theta) \exp(|K(\theta)|^2) \quad (2-14)$$

Thus $K(\theta)$ is clearly the important term to the observer, and it merits discussion. We pass to the integral form of the sum (2-11). This will yield Fourier transforms instead of Fourier coefficients:

$$Y(\omega) = \int y(t) e^{-j\omega t} dt \quad (2-15)*$$

But for waveforms that are zero outside of the interval T , the infinite limits may be reduced to $T/2$ and $-T/2$. Then the only difference between the transform and expansion coefficients is the scaling factor T . From (2-7)

$$Y(\omega_k) = T y_k \quad (2-16)$$

We similarly define $S(\omega_k, \theta) = T s_k(\theta)$. To determine the form $S(\omega, \theta)$ in terms of the transform of the transmitted signal $S(\omega)$, we note

$$\begin{aligned} S(\omega_k, \theta) &= T s_k(\theta) = \int_T s(t-\tau) e^{-j\omega_k t} e^{j\omega(t-\tau)} dt \\ &= e^{-j\omega_k \tau} \int_T s(u) e^{-j(\omega_k - \omega)u} du \\ &= S(\omega_k - \omega) e^{-j\omega_k \tau} \end{aligned} \quad (2-17)$$

*When the integration limits are omitted, the integration interval is taken to be $(-\infty, \infty)$.

Thus the effect of the target is to cause a frequency translation by amount w , and a phase shift by amount $\omega_k \tau$.

We pass to the integral forms for $K(\theta)$ and $D^2(\theta)$ directly by noting that the frequency interval between successive Fourier coefficients is $2\pi/T$, and approximating the sum by the integral.

$$K(\theta) = \frac{1}{D(\theta)} \sum_k \frac{Y(\omega_k) S^*(\omega_k - w) e^{j\omega_k \tau}}{N(\omega_k)} \frac{1}{T}$$

$$= \frac{1}{D(\theta)} \int \frac{Y(\omega) S^*(\omega - w) e^{j\omega \tau}}{N(\omega)} \frac{d\omega}{2\pi} \quad (2-18)$$

Similarly

$$D^2(\theta) = \int \frac{|S(\omega - w)|^2}{N(\omega)} \frac{d\omega}{2\pi} \quad (2-19)$$

It is noted that $D^2(\theta)$ depends on w but not on τ . Thus the SNR will depend on the target speed, which is not so in the white noise case.

The form of $K(\theta)$ is recognized as a matched filter (Helstrom⁽⁷⁾ p. 214 ; Wainstein & Zubakov⁽¹¹⁾ p. 266), which

passes the received waveform with spectrum $Y(\omega)$ through a filter with transfer function:

$$\frac{1}{D(\theta)} \frac{S^*(\omega-w)}{N(\omega)} \quad (2-20)$$

then passes the filter output through a magnitude squaring device (Cook & Bernfeld⁽⁵⁾ p. 285), and examines the output at time τ . The filter divides by the noise spectrum level at each frequency, in order to "prewhiten" the noise portion of $y(t)$. A different filter would be needed for each hypothesized Doppler shift w , since both $D^2(\theta)$ and $S^*(\omega-w)$ depend on w .

The main results of this section are (2-14), (2-18), and (2-19), showing the inverse probability function which the observer must form, and the dependence of the component functions on the signal and noise spectra. The observer displays $p(\theta/y)$, and chooses as his estimates the θ_p at which it peaks. Due to the presence of noise in $y(t)$, however, this maximum will not necessarily occur at the true value θ_0 . It is consequently important to examine the accuracy of the estimator statistically.

2.5 The Performance of the Estimator

The actual received waveform contains the true parameter values:

$$y(t) = g_o s(t, \theta_o) + n(t) \quad (2-21)$$

Thus from (2-14) the observer will have formed the essential quantity

$$|K(\theta)|^2 = \frac{1}{D^2(\theta)} \left| g_o \int \frac{S(\omega - \omega_o) S^*(\omega - \omega_o) e^{j\omega(\tau - \tau_o)}}{N(\omega)} \frac{d\omega}{2\pi} + \int \frac{n(\omega) S^*(\omega - \omega_o) e^{j\omega\tau}}{N(\omega)} \frac{d\omega}{2\pi} \right|^2 \quad (2-22)$$

This consists of a "signal function" and a "noise function" $N'(\theta)$, (to use terminology corresponding to Woodward's case⁽⁴⁾ p. 86) and it is convenient to rename the former through the equation

$$G(\theta, \theta_o) = \frac{1}{D(\theta)D(\theta_o)} \int \frac{S(\omega - \omega_o) S^*(\omega - \omega_o) e^{j\omega(\tau - \tau_o)}}{N(\omega)} \frac{d\omega}{2\pi} \quad (2-23)$$

so that

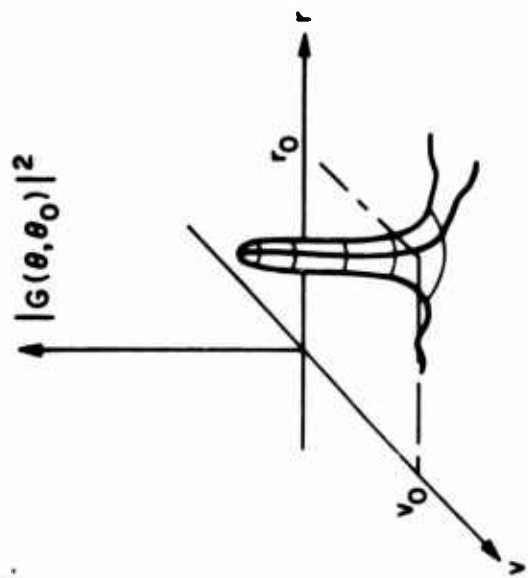
$$|K(\theta)|^2 = |g_o D(\theta_o) G(\theta, \theta_o) + N'(\theta)|^2 \quad (2-24)$$

The function $|G(\theta, \theta_0)|^2$ is a generalized ambiguity function, extended from Woodward's form to the general noise spectrum⁽⁴⁾ (p. 120). It reaches a peak of unity height at $\theta = \theta_0$ (see KR&R⁽⁶⁾ p. 484). Thus if the noise function happened to be zero in a particular received waveform $|K(\theta)|^2$ would peak at the true value and the observer would obtain a perfect measurement. However, the normal non-zero functional form of the noise function perturbs the behavior of $|K(\theta)|^2$ and can cause the peak to occur at some other $\theta = \theta_p$. The degree to which $|K(\theta)|^2$ is perturbed depends on the SNR and the specific shape of $|G|^2$. (Arguments of G are suppressed for convenience).

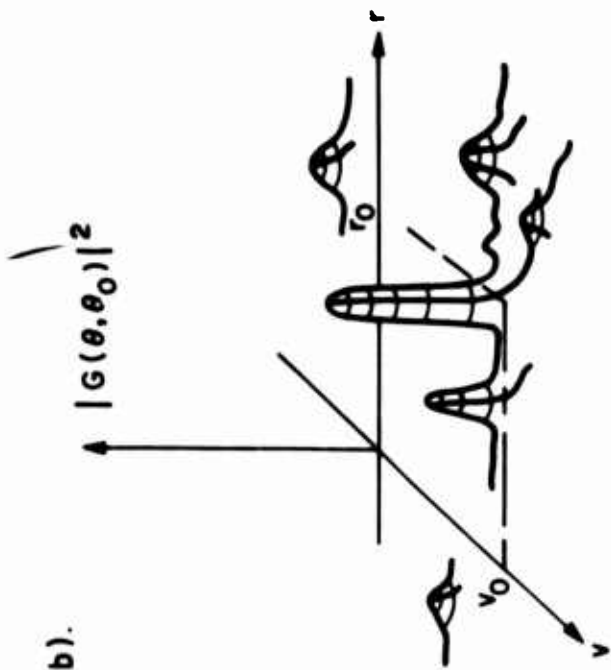
If $|G|^2$ has a single major lobe near θ_0 and is small elsewhere, and if the SNR is large, the noise function will with high probability merely cause the peak of $|K(\theta)|^2$ to shift from θ_0 to a nearby value still on the major lobe. This is the situation examined by KR&R, and explored further below. This type of error will here be called a "small error." However, if $|G|^2$ has other lobes of non-negligible height (compared to that of the main lobe), then the noise function can actually cause the peak of $|K(\theta)|^2$ to occur on

one of these sidelobes, which may be located quite far from the main lobe. This type will be called a "gross" error. It is the possibility of this kind of error that gives rise to the term "ambiguity", since large sidelobes of $|G|^2$ can permit several regions of high inverse probability. The various possible situations are sketched on Fig. 2-2, showing $|G(\theta, \theta_0)|^2$ as a function of θ . Fig. 2-2a shows the case of negligible ambiguity, since only a simple lobe is present, and $|K(\theta)|^2$ will with very high probability peak somewhere on this lobe. Fig. 2-2b shows the appearance of some significant sidelobes scattered over the θ -plane. For such cases one must examine the probability of a gross error occurrence. For Fig. 2-2c the sidelobes are so high there is a very good chance that $|K(\theta)|^2$ will peak on a sidelobe, resulting in a gross error. The signal giving rise to such a $|G(\theta, \theta_0)|^2$ would thus be unacceptable. There is still another situation, illustrated in Fig. 2-2d, where the sidelobes are rather high, but occur very near the main lobe. In certain circumstances the observer may be willing to accept this $|G(\theta, \theta_0)|^2$ since even if a gross error does occur the resulting estimate will not be disastrously different

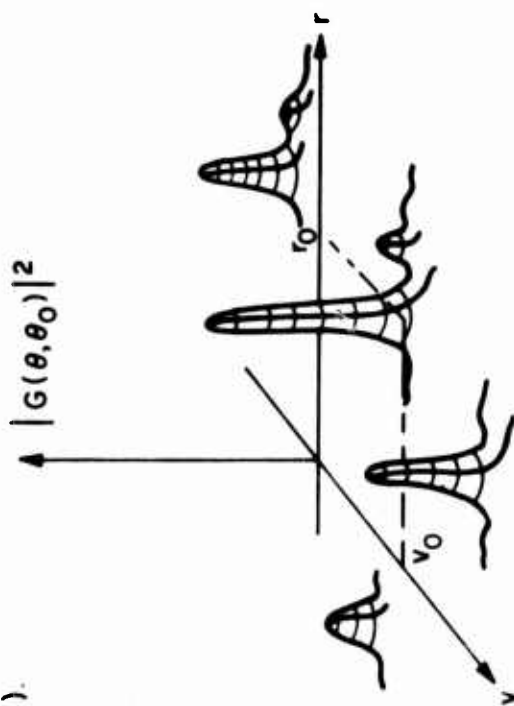
a).



b).



c).



d).

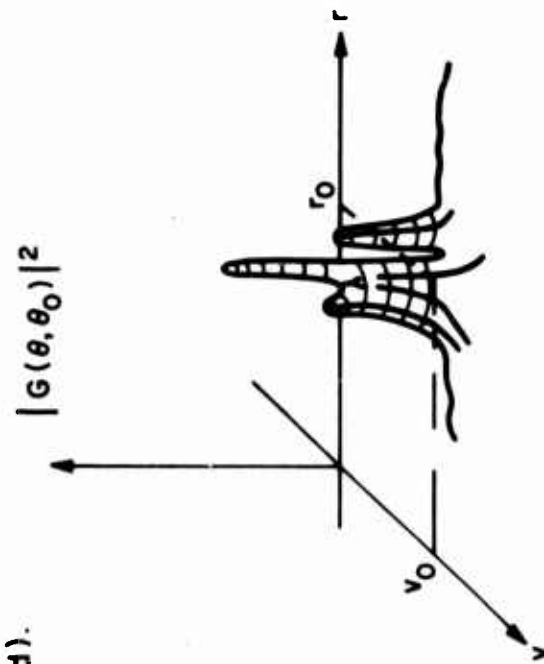


FIGURE 2-2 DIFFERENT CLASSES OF AMBIGUITY FUNCTIONS

from θ_0 . This last case will not be considered further here, and it will be assumed that all gross errors are unacceptable.

If a gross error can occur with high probability, then the method of KR&R for measuring estimator performance simply does not apply. It is important, therefore, to study the inter-relation between i.) sidelobe heights of $|G|^2$, ii.) the probability that a gross error will occur, and iii.) the SNR required to keep this probability small. This is done in an approximate fashion below.

2.5.1 Approximate Analysis of the Ambiguity Problem

It would be very difficult to determine the probability of a gross error precisely, for this would require calculating the probability that $|K(\theta)|^2$ will be larger at one or more points θ not on the main lobe than it is at any of the points on the main lobe. An observation of many different $|G|^2$ functions reveals, on the other hand, that there are normally only one or two sidelobes of any significant height, the others being quite small. Thus we assume that gross errors will be caused by these one or two sidelobes, the other lobes contributing nothing to the probability of a gross error. We further assume that

the behavior of $|K(\theta)|^2$ on a lobe is predominantly determined by the local maximum level of $|G|^2$, since a gross error will with highest probability occur at the peak of the lobe. These two assumptions allow us to obtain a simple but only approximate expression for the probability of a gross error.

The computation is approached by finding the joint probability density function of the two random variables $|K(\theta_0)|^2 \equiv K_0^2$ and $|K(\theta_1)|^2 \equiv K_1^2$, where θ_1 is any point on the θ plane. It is shown in Appendix B that in the large SNR case these variables are approximately jointly gaussian, with moments:

$$\begin{aligned} EK_0^2 &= \text{SNR}, & EK_1^2 &= \text{SNR}|G(\theta_0, \theta_1)|^2 \\ \text{var } K_0^2 &= 2\text{SNR} & \text{var } K_1^2 &= 2\text{SNR}|G(\theta_0, \theta_1)|^2 \\ \text{covar } K_1^2, K_0^2 &= 2\text{SNR}|G(\theta_0, \theta_1)|^2 \end{aligned} \quad (2-25)$$

where $\text{SNR} = \sigma_0^2 D^2(\theta_0) \cdot *$

Thus the statistics depend only on the SNR and the height of the ambiguity function at θ_1 . Given these statistics,

$*|g_0|^2 \equiv \sigma_0^2$, E is the expectation operator.

it is a simple, although tedious process to determine the probability that $K_1^2 > K_0^2$, which is approximately the probability of occurrence of a gross error when only one strong sidelobe exists. This is carried out in Appendix B with the result,

$$P_e = \text{Prob}(K_1^2 > K_0^2) = \textcircled{H} \left[-\sqrt{\frac{1}{2} \text{SNR}(1 - |G(\theta_0, \theta_1)|^2)} \right] \quad (2-26)$$

where

$$\textcircled{H}(x) = \int_{-\infty}^x \frac{1}{\sqrt{2\pi}} e^{-1/2 x^2} dx \quad (2-27)$$

is the normal probability integral (Handbook⁽¹²⁾, p. 966).

P_e is plotted in Figure 2-3 versus the sidelobe height $|G(\theta_0, \theta_1)|^2$. It can be seen that for SNR of the order 15 dB, sidelobes as high as .5 will only cause error probabilities of the order of 10^{-3} , which can be acceptable in many situations. As the SNR decreases the allowed sidelobe level rapidly drops for a fixed P_e , until the prescribed P_e cannot be met at all. If there are two significant sidelobes of approximately equal height, P_e will be larger, but no more than twice as large as the value shown in Fig. 2-3 (Appendix B).

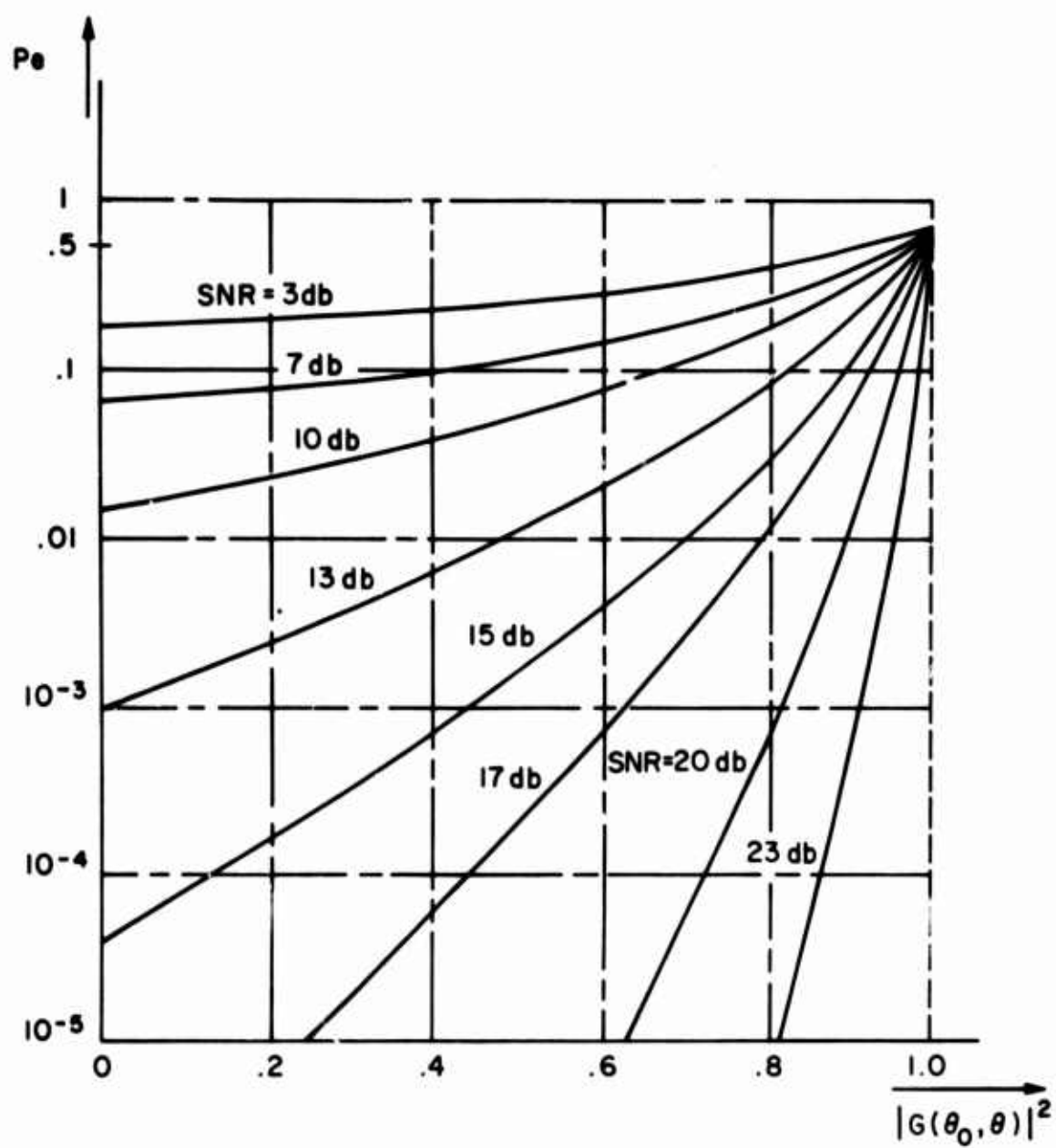


FIGURE 2-3 APPROXIMATE PROBABILITY OF A GROSS ERROR

These approximate results can be used as guidelines when designing signals. In the signal design portion of Chapter 4, an allowable sidelobe height will be fixed, and only signals satisfying this constraint will be considered. A more precise method would be to fix an admissible P_e , and then determine the allowable sidelobe height for each value of SNR. However, the observer will not know the value of SNR until after the signal has been received and processed, and so an exact determination of the maximum permissible sidelobe level could not be made beforehand. We choose to follow the simpler scheme of selecting the maximum sidelobe height rather than the P_e . This scheme thus assumes that the SNR is sufficiently large.

2.5.2 Analysis of Estimate Variance for "Small" Errors

If gross errors occur with very small probability, then the KR&R estimate variance method applies, for one is almost certain that $|K(\theta)|^2$ will peak in the immediate vicinity of θ_0 . Following KR&R for the large SNR case, $|K(\theta)|^2$ is first approximated by deleting the squared magnitude of the noise function $N'(\theta)$ of (2.24):

$$|K(\theta)|^2 = \text{SNR} |G(\theta, \theta_0)|^2 + 2 \text{Re} \int_0^D G(\theta, \theta_0) N'^*(\theta) d\theta \quad (2-28)$$

where $D_o = D(\theta_o)$ and $SNR = \sigma_o^2 D_o^2$ (see (2.25)). Now this function is expanded in a Taylor series about θ_o , with only a few terms retained:

$$|K(\theta)|^2 = K_o + K_r(r-r_o) + K_v(v-v_o) - \frac{1}{2} \left[A(r-r_o)^2 + 2B(r-r_o)(v-v_o) + C(v-v_o)^2 \right] + \dots$$

where $K_o = SNR |G(\theta_o, \theta_o)|^2 + 2\text{Re} \sigma_o D_o G(\theta_o, \theta_o) N'^*(\theta_o)$

$$K_r = -SNR \frac{\partial}{\partial r} |G(\theta, \theta_o)|^2 + 2\text{Re} \sigma_o D_o \frac{\partial}{\partial r} G(\theta, \theta_o) N'^*(\theta) \Big|_{\theta_o}$$

$$K_v = -SNR \frac{\partial}{\partial v} |G(\theta, \theta_o)|^2 + 2\text{Re} \sigma_o D_o \frac{\partial}{\partial v} G(\theta, \theta_o) N'^*(\theta) \Big|_{\theta_o}$$

$$A = -SNR \frac{\partial^2}{\partial r^2} |G(\theta, \theta_o)|^2 \Big|_{\theta_o} \quad (2-29)$$

$$B = -SNR \frac{\partial^2}{\partial r \partial v} |G(\theta, \theta_o)|^2 \Big|_{\theta_o}$$

$$C = -SNR \frac{\partial^2}{\partial v^2} |G(\theta, \theta_o)|^2 \Big|_{\theta_o}$$

That is, the first partial derivatives of the noise function are retained in K_r and K_v , but only the deterministic portions of A, B, and C are retained (KR&R show that after making the approximation in (2-28) one may retain just these deterministic parts with no further loss in accuracy.)

KR&R then calculate the value $\theta_p = (r_p, v_p)^+$, (where r_p, v_p are random variables) at which the expansion of $|K(\theta)|^2$ peaks and determine the moments of the errors $e_r = r_p - r_o$, $e_v = v_p - v_o$. They show that $\bar{e}_r = \bar{e}_v = 0$, (so that the estimator is unbiased), and that

$$\overline{e_r^2} = C/\Delta$$

$$\overline{e_r e_v} = -B/\Delta$$

(2-30)⁺⁺

$$\overline{e_v^2} = A/\Delta$$

where $\Delta = AC - B^2$

If $B=0$, then $\overline{e_r^2} = 1/A$ and $\overline{e_v^2} = 1/C$.

In the work of KR&R these results were applied to a simple white noise example, but no detailed answers were

⁺For notational convenience we redefine $\theta = (r, v)$ where before we had $\theta = (\tau, w)$. The two forms differ only by scaling constants.

⁺⁺The overbar is equivalent notationally to the expectation operator E.

developed. The remainder of this chapter will give a geometric analysis of the estimate error variances, and relate A, B and C to unified forms involving the signal and noise spectra.

2.6 The Ellipse of Estimate Variances

A simple pictorial representation of the estimation variances may be obtained by considering contours of equal probability of $p(\theta/y)$ in (2-14). It is shown in Appendix B that $p(\theta/y)$ may be written as:

$$p(\theta/y) = k p_0(\theta) e^{-1/2(\theta-\theta_p)' \begin{bmatrix} A & B \\ B & C \end{bmatrix} (\theta-\theta_p)} \quad (2-31)$$

where θ_p is the observed location of the peak in $p(\theta/y)$. (It is noise dependent). A convenient choice for the probability level is that which gives the exponent the value 1/2, since this is the usual definition for the standard deviation of a gaussian density function. The resulting contour is an ellipse, centered at θ_p , and given by

$$A(r-r_p)^2 + 2B(r-r_p)(v-v_p) + C(v-v_p)^2 = 1 \quad (2-32)$$

A typical illustration is given in Figure 2-4 (Helstrom⁽⁷⁾ p. 21 gives an analogous figure).

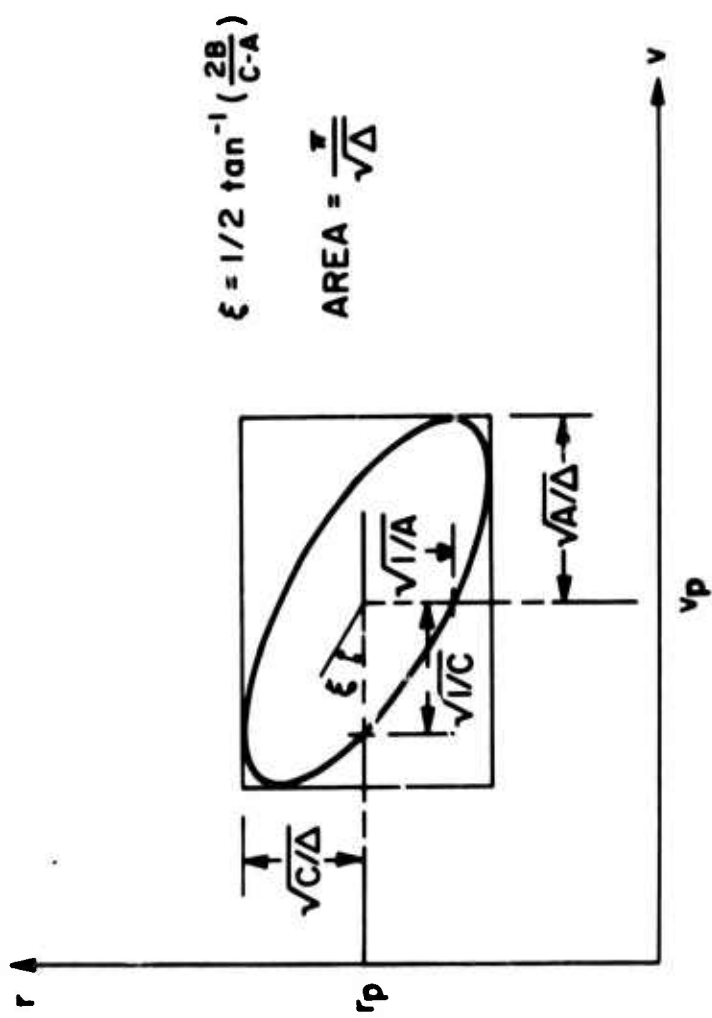


FIGURE 2-4 ELLIPSE OF ESTIMATE VARIANCES

A rectangle may be circumscribed about the ellipse, whereupon each dimension of the rectangle is just twice the standard deviation of the corresponding estimate (see (2-30)). The covariance between the estimates causes a rotation of the ellipse. Thus the ellipse dimensions embody the average properties of the estimate errors. The quantities A, B and C will hereafter be called the "ellipse parameters." They will prove very useful in the study of multiple ping and elapsed time effects.

2.7 The Form of the Estimate Variances

The ellipse parameters of (2-29) are here related to the signal and noise spectra. By evaluating the second derivatives in (2-29), we obtain

$$A = kSNR \left[\int \frac{\omega^2 |S(\omega)|^2}{D_0^2 N(\omega + \omega_0)} \frac{d\omega}{2\pi} - \left[\int \frac{\omega |S(\omega)|^2}{D_0^2 N(\omega + \omega_0)} \frac{d\omega}{2\pi} \right]^2 \right]$$

$$B = KQ SNR \left[\operatorname{Im} \int \frac{\omega S(\omega) \dot{S}^*(\omega)}{D_0^2 N(\omega + \omega_0)} \frac{d\omega}{2\pi} - \int \frac{\omega |S(\omega)|^2}{D_0^2 N(\omega + \omega_0)} \frac{d\omega}{2\pi} \right] \quad (2-33)$$

$$\operatorname{Im} \int \frac{S(\omega) \dot{S}^*(\omega)}{D_0^2 N(\omega + \omega_0)} \frac{d\omega}{2\pi}$$

$$C = KQ^2 \text{ SNR} \left[\int \frac{|\dot{S}(\omega)|^2}{D_0^2 N(\omega + \omega_0)} \frac{d\omega}{2\pi} - \left| \int \frac{S(\omega) \dot{S}^*(\omega)}{D_0^2 N(\omega + \omega_0)} \frac{d\omega}{2\pi} \right|^2 \right]$$

where $k = 8/c^2$, c being the propagation speed of sound, and the dot indicates derivatives with respect to ω . The details are given in Appendix C.

In the white-noise only case, several simplifications are possible. As shown in Appendix C, the signal-to-noise ratio (denoted WSNR for the white noise case) is $\text{WSNR} = 2E\sigma_0^2/N_0$ for transmitted energy E and noise spectrum level N_0 . Furthermore, B and C may be given as integrals in the time domain, and as such suggest useful definitions: Helstrom⁽⁷⁾ p. 18):

$$A = k \text{ WSNR} \left[\frac{1}{2E} \int \omega^2 |S(\omega)|^2 \frac{d\omega}{2\pi} - \left[\frac{1}{2E} \int \omega |S(\omega)|^2 \frac{d\omega}{2\pi} \right]^2 \right] \\ = k \text{ WSNR} [\text{dispersion bandwidth}]^2 \quad (2-34)$$

$$B = kQ \text{ WSNR} \left[\frac{1}{2E} \int t m^2(t) \dot{\phi}(t) dt - \frac{1}{2E} \int \omega |S(\omega)|^2 \frac{d\omega}{2\pi} \right. \\ \left. \frac{1}{2E} \int t m^2(t) dt \right] \\ = kQ \text{ WSNR} [\text{coupling-(center frequency) (epoch)}] \quad (2-35)$$

$$C = kQ^2 \text{ WSNR} \left[\frac{1}{2E} \int t^2 m^2(t) dt - \left[\frac{1}{2E} \int t m^2(t) dt \right]^2 \right]$$

$$= kQ^2 \text{ WSNR} [\text{dispersion duration}]^2 \quad (2-36)$$

The terms "dispersion bandwidth" and "dispersion duration" are used to distinguish these definitions, which involve second moments, or moments of inertia of the signal functions, from other definitions of bandwidth and duration which might be used. These forms are frequently used for their tractability, but they are not always appropriate from a physical point of view, as will be seen in Chapter 4. The "center frequency"* and the "epoch" as defined above are frequently made zero by proper choice of the time and frequency origins. This choice deletes the second terms in each of the expressions above. The coupling term disappears if there is no frequency modulation, and the duration does not depend on the frequency modulation in any way.

In the white noise case one can apply the "uncertainty principle" (Helstrom⁽⁷⁾, p. 20) to demonstrate

*This applies to the center frequency of the envelope $s(t)$; the center frequency of the actual signal lies Q radians per second higher.

that for any signal, the resulting Δ satisfies $\Delta \geq \frac{1}{4}(k \text{ SNR } Q)^2$, with equality holding only for "gaussian signals", of the form $s(t) = \exp(-1/2(a+jb)t^2)$. The derivation of this fact is outlined in Appendix G. A similar result does not seem to prevail in the colored noise case, although $\Delta > 0$ in all cases.

A unified form for the ellipse parameters in the colored noise case may be given in terms of an integral operator. The operator has a kernel $P(\omega)$ which is a density function,* given by

$$P(\omega) = \frac{1}{D_0^2} \frac{|S(\omega)|^2}{N(\omega + \omega_0)} \quad (2-37)$$

The overbar operator notation indicates the operation:

$$\overline{g(\omega)} = \int P(\omega) g(\omega) \frac{d\omega}{2\pi} \quad (2-38)$$

We further define the phase spectrum $\psi(\omega)$ for the transmitted signal such that:

$$S(\omega) = |S(\omega)| e^{j\psi(\omega)} \quad (2-39)$$

*A density function is any positive, unit-area function.

and in addition a normalized derivative of the amplitude spectrum:

$$a(\omega) = \frac{1}{|S(\omega)|} \frac{d}{d\omega} |S(\omega)| \quad (2-40)$$

When these definitions are applied to (2-33), and simplifications are made, there results (see Appendix E)

$$\begin{aligned} A &= k \text{ SNR } \overline{(\omega - \bar{\omega})^2} \\ B &= -kQ \text{ SNR } \overline{(\omega - \bar{\omega}) (\dot{\psi} - \bar{\dot{\psi}})} \\ C &= kQ^2 \text{ SNR } \overline{(\omega - \bar{\omega})^2 + (\dot{\psi} - \bar{\dot{\psi}})^2} \end{aligned} \quad (2-41)$$

$$\text{SNR} = \sigma_o^2 D_o^2 = \sigma_o^2 \int \frac{|S(\omega)|^2}{N(\omega + \omega_o)} \frac{d\omega}{2\pi}$$

where $\dot{\psi}(\omega) = d/d\omega \psi(\omega)$.

These unified forms show that the ellipse parameters are analogous to central moments in statistics. The expressions are particularly convenient conceptually because the noise properties and target speed dependence appear only in $P(\omega)$. For the white noise case $P(\omega)$ simplifies to $|S(\omega)|^2/2E$. The unified forms also permit a very simple proof that $\Delta = AC - B^2$ is always positive (see Appendix E).

The terminology "dispersion bandwidth", "center frequency" etc. used in (2-34) to (2-36) for the white noise case may be employed here in the general case as well. Now, however, the definitions refer not to $s(t)$ but to a signal $s'(t)$ having transform $S(\omega)/\sqrt{N(\omega+\omega_0)}$, as discussed in Appendix D.

Example 2-1: Pictorial Demonstration of the Effect of Target Speed on $P(\omega)$ and D_0^2

Sample shapes for $|f(\omega)|^2$ and $N(\omega)$ are shown in Figure 2-5 followed by four examples of the ratio $|S(\omega)|^2/N(\omega+\omega_0)$. The area under $|S(\omega)|^2/N(\omega+\omega_0)$ is D_0^2 see (2-41), whereas if each curve were adjusted for unit area, it would show $P(\omega)$.

Several features of this example are listed below:

- 1) $N(\omega)$ consists of white noise level added to which is a narrow-band noise portion, such as that due to reverberation.
- 2) $|S(\omega)|^2$ and $N(\omega)$ need not be symmetrical about $\omega=0$ (Papoulis⁽¹³⁾ p. 131) since they are generated by complex processes. Nor need the spectra fall-off so rapidly in practice.

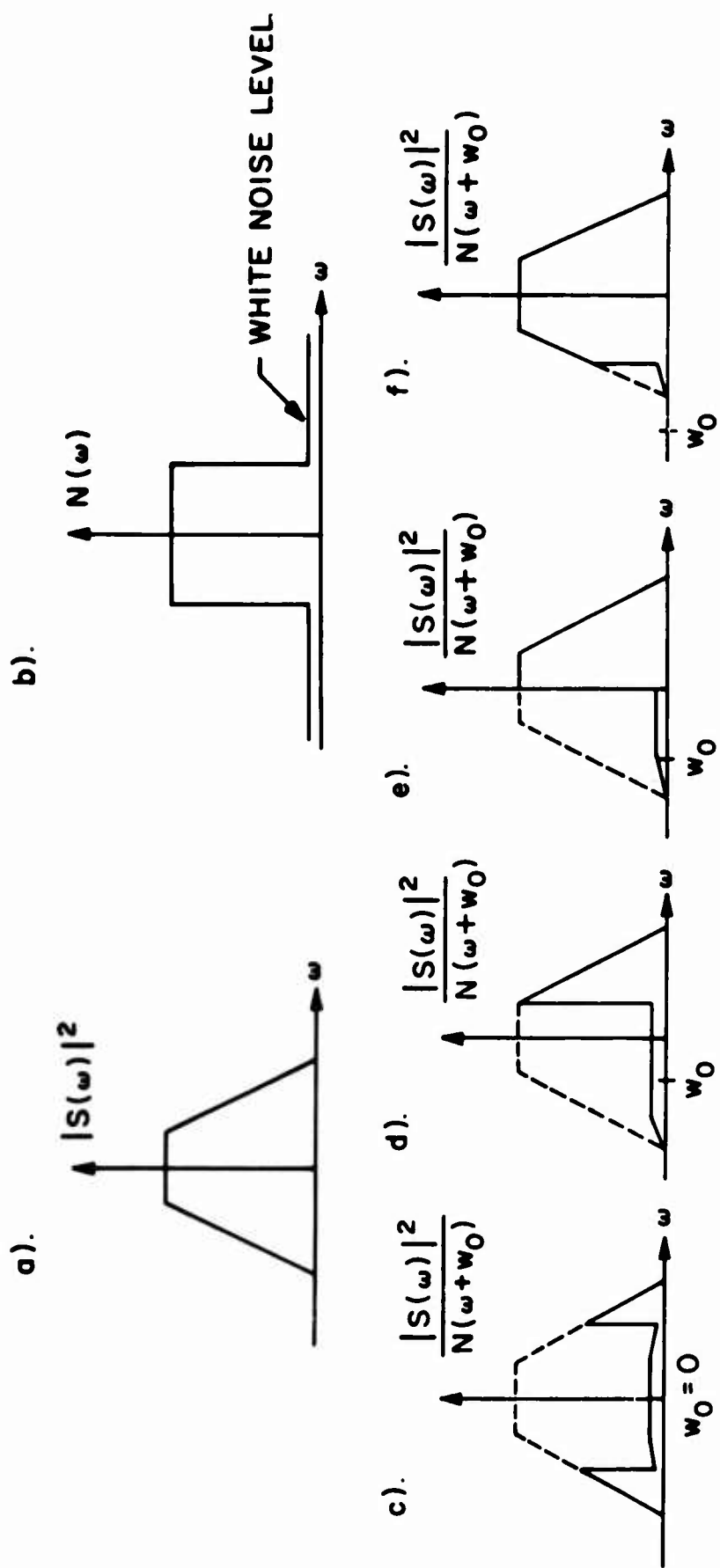


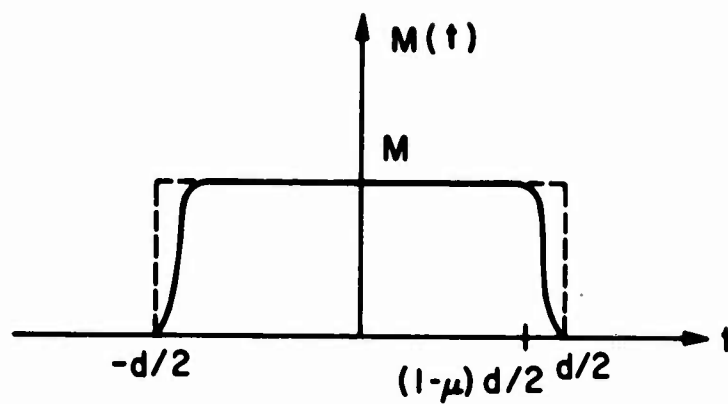
FIGURE 2-5 SAMPLE SIGNAL AND NOISE SPECTRA, AND THE
RESULTING $P(\omega)$, D_0^2 FOR DIFFERENT ω_0

- 3) If the spectra are not symmetrical, then $P(\omega)$ and D_0^2 will be sensitive to the sign of ω_0 . Thus receding targets could be easier to locate than approaching ones, or vice versa.
- 4) For large ω_0 the noise spectrum is completely shifted away from the signal spectrum, and the estimator is effectively white noise limited. Hence fast moving targets could be relatively easy to locate.
- 5) $P(\omega)$ is entirely independent of the levels of $|S(\omega)|^2$ and $N(\omega)$ because of its normalization, but depends strongly on the relative level changes in the spectra. Thus an important parameter is the narrowband noise-to-white-noise level ratio, shown in Fig. 2-5 as 10:1.
- 6) The SNR is severely degraded by the narrow-band noise portion of $N(\omega)$, especially for low target speeds. For large ω_0 there is no such degradation.

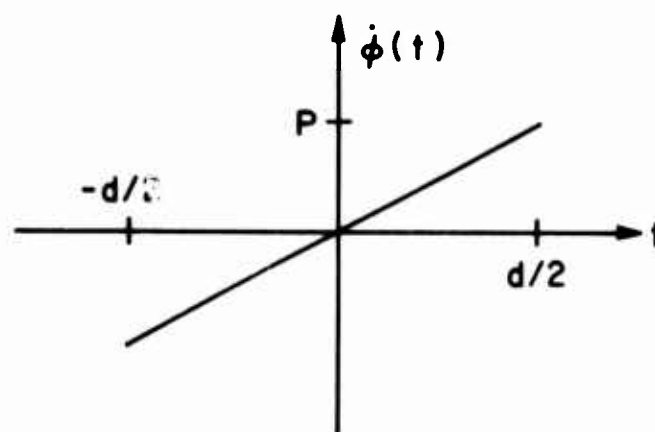
Example 2-2: Typical Values of A, B and C for Specific Signals in White Noise

Two signal classes will be used in this example. The first is the popular LIFMOP (Linear Frequency Modulated Pulse) signal, which has several desirable properties.

a) ENVELOPE



b) LIFMOP
FREQUENCY MODULATION



c) RAFMOP
FREQUENCY MODULATION

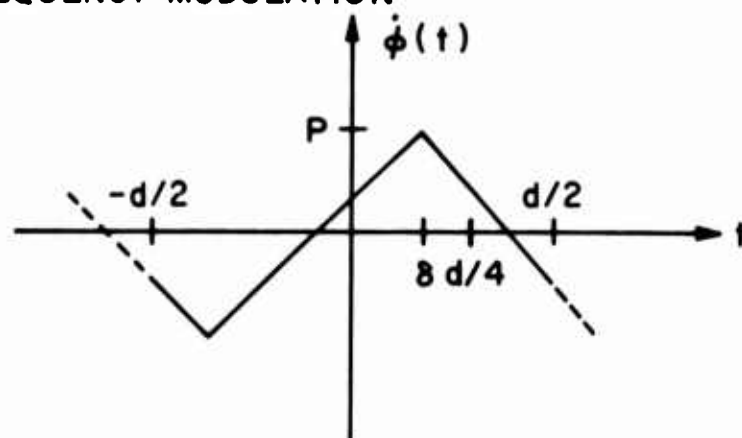


FIGURE 2-6 A SIGNAL ENVELOPE AND TWO
EXAMPLES OF FREQUENCY MODULATION

(Ramp and Wingrove⁽¹⁴⁾). The signal $s(t) = m(t)e^{j\varphi(t)}$ is described by a nearly rectangular envelope lasting d seconds, and a phase derivative that is linear. A so-called "up-chirp" is shown in Fig. 2-6.

In Appendix F the ellipse parameters are evaluated for the case where the roll-off portion of the envelope $m(t)$ is small:

$$A \triangleq k \text{ WSNR} \left(\left(\frac{\pi}{2} \right)^2 \frac{2}{\mu d^2} + P^2/3 \right)$$

$$B \triangleq kQ \text{ WSNR} Pd/6$$

$$C \triangleq kQ^2 \text{ WSNR} d^2/12$$

$$\Delta \triangleq (kQ \text{ WSNR})^2 \left(\frac{\pi}{2} \right)^2 \frac{1}{6\mu} \quad (2-42)$$

The first term in A is due to the roll-off of the envelope. It is assumed small here, but is retained as otherwise $\Delta=0$ for this signal. It is shown in Appendix F that this form for $\phi(t)$ yields the maximum B^2 for a given A . This property will be very important.

The second class of signals adds a degree of design freedom by making B adjustable. Signals of this class will

be called RAFMOP (Rotationally Aadjustable Frequency Modu-
lated Pulses) since they introduce an effective periodicity in
the frequency modulation. The frequency modulation is
thought of as periodic, and may be translated with respect
to the time origin. The envelope picks out the portion
in $t \in (-d/2, d/2)$. The set of translations of interest
are $\delta \in (-d/4, d/4)$, for if P can take on positive and
negative values this exhausts the possible waveforms.
(Cook & Bernfeld,⁽⁵⁾ p. 97, have considered the single
case $\delta=0$, and we extend the class to other δ). Ignoring
the small effects due to envelope roll-off, the results
become: (App. F)

$$A \doteq k \text{ WSNR } P^2/3$$

$$B \doteq kQ \text{ WSNR } Pd/8 (4\delta/d)(2-4|\delta|/d)$$

$$C \doteq kQ^2 \text{ WSNR } d^2/12$$

$$\Delta = (KQ \text{ WSNR})^2 (Pd/6)^2 \left[1 - (3\delta/d)^2 (2-4|\delta|/d)^2 \right] \quad (2-43)$$

It is seen that B can be adjusted from 0 to $\pm kQ \text{ WSNR } Pd/8$,
only .75 as large as B for the LIFMOP signal with the same
bandwidth. The appeal of this signal is its adjustability.

The only effect of the translation of $\dot{\phi}(t)$ is in the value of B, allowing independent variation of this parameter for constant bandwidth and duration.

We now consider the estimation performance achieved by these two types of signals in the white noise, single-ping, and no-wait-time situation. Eq. (2-30) applies directly to give the estimate error variances. We do the RAFMOP case first, using (2-43).

RAFMOP:

$$\begin{aligned}\overline{e_r^2} &= \frac{1}{k \text{ WSNR}} \frac{3}{p^2} \left[1 - \frac{9}{16} \left(\frac{4\delta}{d} \right)^2 \left(2 - 4 \frac{|\delta|}{d} \right)^2 \right]^{-1} \\ \overline{e_v^2} &= \frac{1}{k \text{ WSNR}} \frac{12}{(dQ)^2} \left[1 - \frac{9}{16} \left(\frac{4\delta}{d} \right)^2 \left(2 - 4 \frac{|\delta|}{d} \right)^2 \right]^{-1} \quad (2-44) \\ \overline{e_r e_v} &= \frac{-1}{k \text{ WSNR}} \frac{9}{2} \frac{1}{PdQ} \left(\frac{4\delta}{d} \right) \left(2 - 4 \frac{|\delta|}{d} \right) \left[1 - \frac{9}{16} \left(\frac{4\delta}{d} \right)^2 \right. \\ &\quad \left. \left(2 - 4 \frac{|\delta|}{d} \right)^2 \right]^{-1}\end{aligned}$$

and when $\delta=0$

$$\overline{e_r^2} = \frac{1}{k \text{ WSNR}} \frac{3}{p^2}$$

$$\overline{e_v^2} = \frac{1}{k \text{ WSNR}} \frac{12}{(dQ)^2} \quad (2-45)$$

$$\overline{e_r e_v} = 0$$

The range estimate accuracy improves with the signal bandwidth, while the range rate estimate accuracy improves with the signal duration, the type behavior frequently noted for matched filter estimators (6, 7, 11). By inspection the highest accuracy is achieved for the choice $\delta=0$, which eliminates correlation between the estimates.

If one wishes to consider the performance of this signal under a peak or average power constraint, it is a simple matter to decompose the WSNR term into its constituents $\text{WSNR} = m_0^2 d \sigma_0^2 / N_0$ and then consider the envelope level m_0 as fixed.

For the LIFMOP signal we can apply (2-42) to (2-30), and obtain:

LIFMOP:

$$\begin{aligned} \overline{e_r^2} &= \frac{\mu d^2}{2k \text{ WSNR}} \left(\frac{2}{\pi} \right)^2 \\ \overline{e_v^2} &= \frac{2\mu}{k \text{ WSNR}} \left(\frac{P}{Q} \right)^2 \left(\frac{2}{\pi} \right)^2 \end{aligned} \quad (2-46)$$

$$\overline{e_r e_v} = - \frac{2\mu}{k \text{ WSNR}} \frac{P}{Q} d \left(\frac{2}{\pi} \right)^2$$

Here a rather different behavior is observed with respect to the parameters involved. The range estimate variance now increases with signal duration, and is independent of the frequency modulation, while the range rate estimate variance increases with signal bandwidth. This dependence arises because of the very high range and range rate estimate correlation, which causes the area of the estimate variance ellipse to be independent of signal bandwidth and duration. Referring to Figure 2-4, we note that as duration and bandwidth grow, both $1/\sqrt{A}$ and $1/\sqrt{C}$ decrease (by (2-42)), and the property of constant area thus forces the ellipse to stretch out rapidly. The ellipse quickly becomes long and narrow, yielding poorer estimate accuracies (See Fig. 2-7).

Because the range estimate accuracy does not increase with the amount of frequency modulation P , the observer must attempt to reduce $\overline{e_r^2}$ by decreasing d or μ , effectively shortening and sharpening the pulse envelope. These considerations indicate that the LIFMOP signal is not a good choice of signal in the single-ping, no-wait-time situation. On the

other hand, it will prove to be a very desirable signal waveform when a wait time is involved. This case is developed in Chapter 3.

The estimate variances of (2-44) are evaluated using the set of sample parameter values given below:

$$c = 5000 \text{ feet per second}$$

$$Q = (2\pi) 3000 \text{ radians per second} \quad (2-47)$$

$$\text{WSNR} = 10$$

$$d = 1/2 \text{ second}$$

$$P = (2\pi) 50 \text{ rps}$$

$$\mu = .1$$

This yields the following table:

	$\sqrt{e_r^2} \text{ feet}$	$\sqrt{e_v^2} \text{ ft/sec}$	$\frac{1}{\sqrt{C}} \text{ ft/sec.}$	$\frac{1}{\sqrt{A}} \text{ ft.}$	$\overline{e_r e_v} \text{ sec}^{-1}$	
LIFMOP	56.3	3.76	.206	3.08	-157.9	$\Delta=1.09$
$\delta=d/4$	4.65	.311	.206	3.08	-1.09	$A=.046$
RAFMOP $\delta=0$	3.08	.206	.206	3.08	0.	$B=1.188$ $C=10.34$

TABLE 2-1: ESTIMATE STANDARD DEVIATIONS

The error ellipses for these examples are drawn in Figure 2-7, and show the large size difference that makes the LIFMOP signal less suitable here.

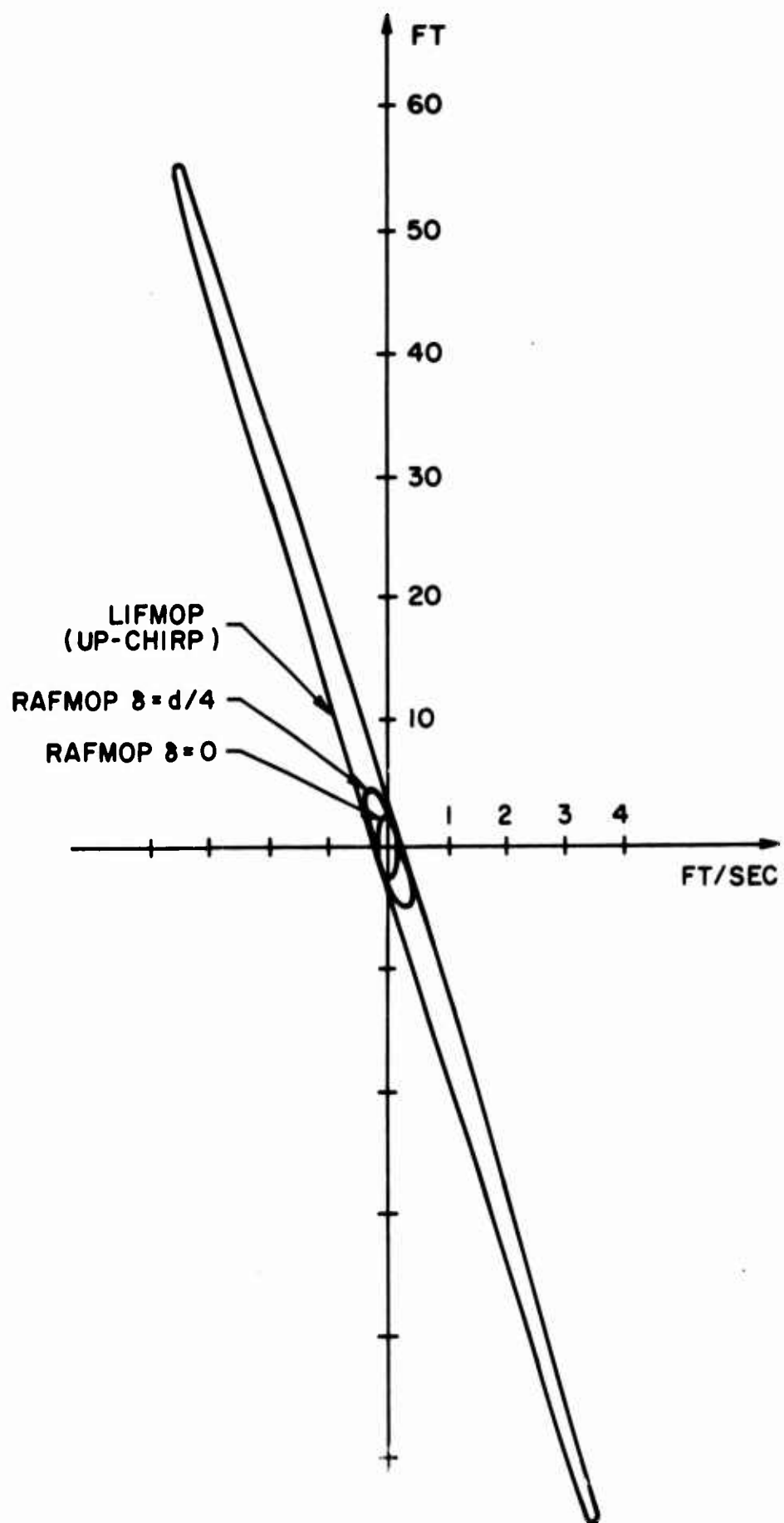


FIGURE 2-7 ERROR ELLIPSES FOR RAFMOP & LIFMOP SIGNALS

CHAPTER 3

MULTIPLE PING RECEPTION; EFFECT OF ELAPSED TIME

In the present chapter the optimum estimator for two or more pings will be found and evaluated, and the effects of inter-ping time and wait time will be determined.

3.1 Effect of Elapsed Time on Estimates

If the observer must wait for some reason after he has taken data before he can use it, he must update the measurements so that they apply at the time they are used. In the present context, the observer has imperfect estimates of range and range rate at $t=0$ (origin chosen at ping time for convenience), and he wants to extrapolate them to time t in an optimum fashion.

To do this extrapolation he must rely on one basic assumption: the target will not alter its course or speed after the ping is sent. (More generally, it may alter its course and speed in some way known to the observer.) The assumption here is that the target maintains the trajectory described by:

$$r(t) = r_0 + v_0 t \quad (3-1)$$

Considering the true state vector $\theta_0(t) = (r_0 + v_0 t, v_0)$ as a function of time, $\theta_0(t)$ may be obtained from $\theta_0(0)$ by the linear transformation Z_t :

$$\theta_0(t) = Z_t \theta_0(0), \text{ where } Z_t = \begin{bmatrix} 1 & t \\ 0 & 1 \end{bmatrix} \quad (3-2)$$

The evolution of $\theta_0(t)$ is sketched in Figure 3-1 for a few cases.

Since the observer knows that the target has constant course and speed, his hypothesis will also take the form $\theta(t) = Z_t \theta(0)$. The Inv PF for the evolved target state then follows immediately in terms of $p(\theta(0)/y)$ of (2-31). We simply substitute $Z_t^{-1} \theta(t)$ for $\theta(0)$ and $Z_t^{-1} \theta_p(t)$ for $\theta_p(0)$ to obtain

$$\begin{aligned} p(\theta(t)/y) &= k p_0(\theta) e^{-\frac{1}{2}(\theta(t) - \theta_p(t))' Z_t^{-1} \begin{bmatrix} A & B \\ B & C \end{bmatrix} Z_t^{-1} (\theta(t) - \theta_p(t))} \\ &= k p_0(\theta) e^{-\frac{1}{2}(\theta(t) - \theta_p(t))' \begin{bmatrix} A & B - At \\ B - At & At^2 - 2Bt + C \end{bmatrix} (\theta(t) - \theta_p(t))} \end{aligned} \quad (3-3)$$

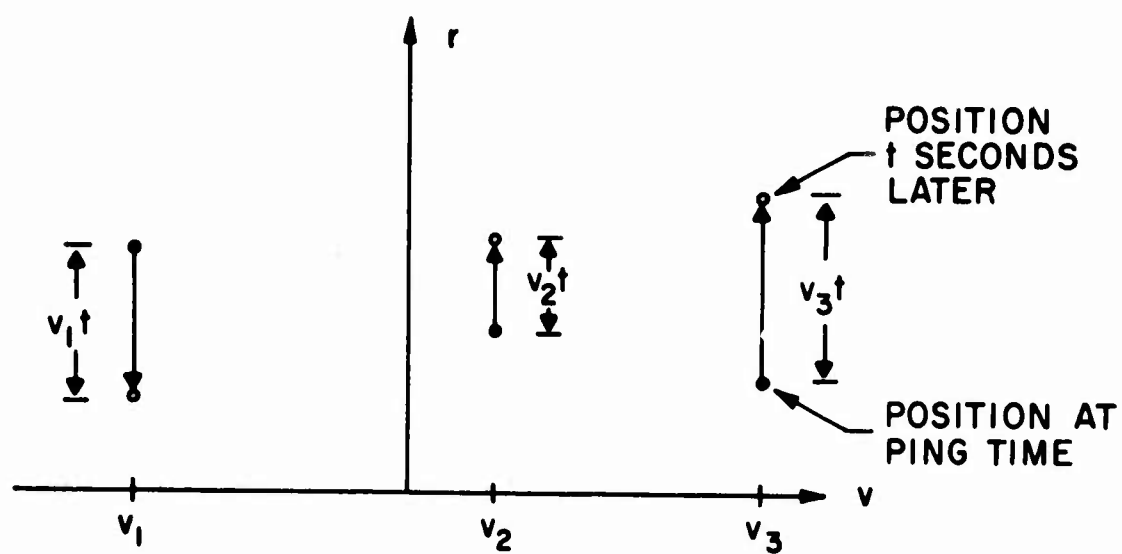


FIGURE 3-1 EVOLUTION OF POINTS ON THE θ -PLANE

which makes use of:

$$Z_t^{-1} = \begin{bmatrix} 1 & -t \\ 0 & 1 \end{bmatrix} \quad (3-4)$$

Thus the evolved ellipse has center $(r_p', v_p') = (r_p + v_p t, v_p t)$ and ellipse parameters

$$\begin{aligned} A_t &= A \\ B_t &= B - At \\ C_t &= C - 2Bt + At^2 \end{aligned} \quad (3-5)$$

The following points are noted:

- 1) the new ellipse has the same area for all t , since Z_t has unit Jacobean. $\Delta_t = \Delta$.
- 2) B_t evolves linearly with time, causing a rotation of the ellipse. C_t always remains positive since the roots of $At^2 - 2Bt + C = 0$ are complex (note: $\Delta > 0$).

We now consider the evolution of the shape of the ellipse with time, introducing a method which permits a simple understanding of the process. Instead of describing ellipse orientation by the slope of the major axis (see Figure 2-4) we consider instead a "regression line."

If we solve the ellipse quadratic equation
 $A_t y^2 + 2B_t xy + C_t x^2 = 1$ (using $y=r-r'_p, x=v-v'_p$), we obtain

$$y = (-B_t/A_t)x \pm \frac{1}{A_t} \sqrt{A_t - \Delta x^2} \quad (3-6)$$

for $\Delta = AC - B^2$. Then in terms of the original parameters:

$$y = (t-B/A)x \pm \frac{1}{A} \sqrt{A - \Delta x^2} \quad (3-7)$$

Only the first term depends on time. The second is constant, and determines the basic properties of the ellipse for all time. For this reason we define the "generic ellipse" by

$$y = \pm \frac{1}{A} \sqrt{A - \Delta x^2} \quad (3-8)$$

or $Ay^2 + \frac{\Delta}{A} x^2 = 1$

The time dependent term contributes a straight line with slope $(t-B/A)$. It is called a "regression line" by analogy with the mean square regression line for bivariate

distributions (Cramer,^[17] p. 272). The slope of this line is called the "regression line slope" (hereafter RLS).

$$\text{RLS} = t-B/A \quad (3-9)$$

These ideas are illustrated in Figure 3-2, for three instants of time, and for a receding target. The middle instant yields a generic ellipse. The regression line intersects the points of maximum horizontal extension in the ellipse. It coincides with the major or minor axis only in the generic case. If the RLS is initially negative, the generic case will sooner or later occur. (Note: the ellipses shown in Figure 3-2 are drawn to scale for the RAFMOP signal of Example 2-2 using the typical values listed there. The scales used are given in the figure.)

One immediate consequence of these considerations is that the range error is smallest for the generic case. This is easily shown by considering:

$$\overline{e_r^2} = C_t/\Delta = \frac{A_t C_t - B_t^2 + B_t^2}{A_t \Delta} = (1 + \frac{B_t^2}{\Delta})/A_t \quad (3-10)$$

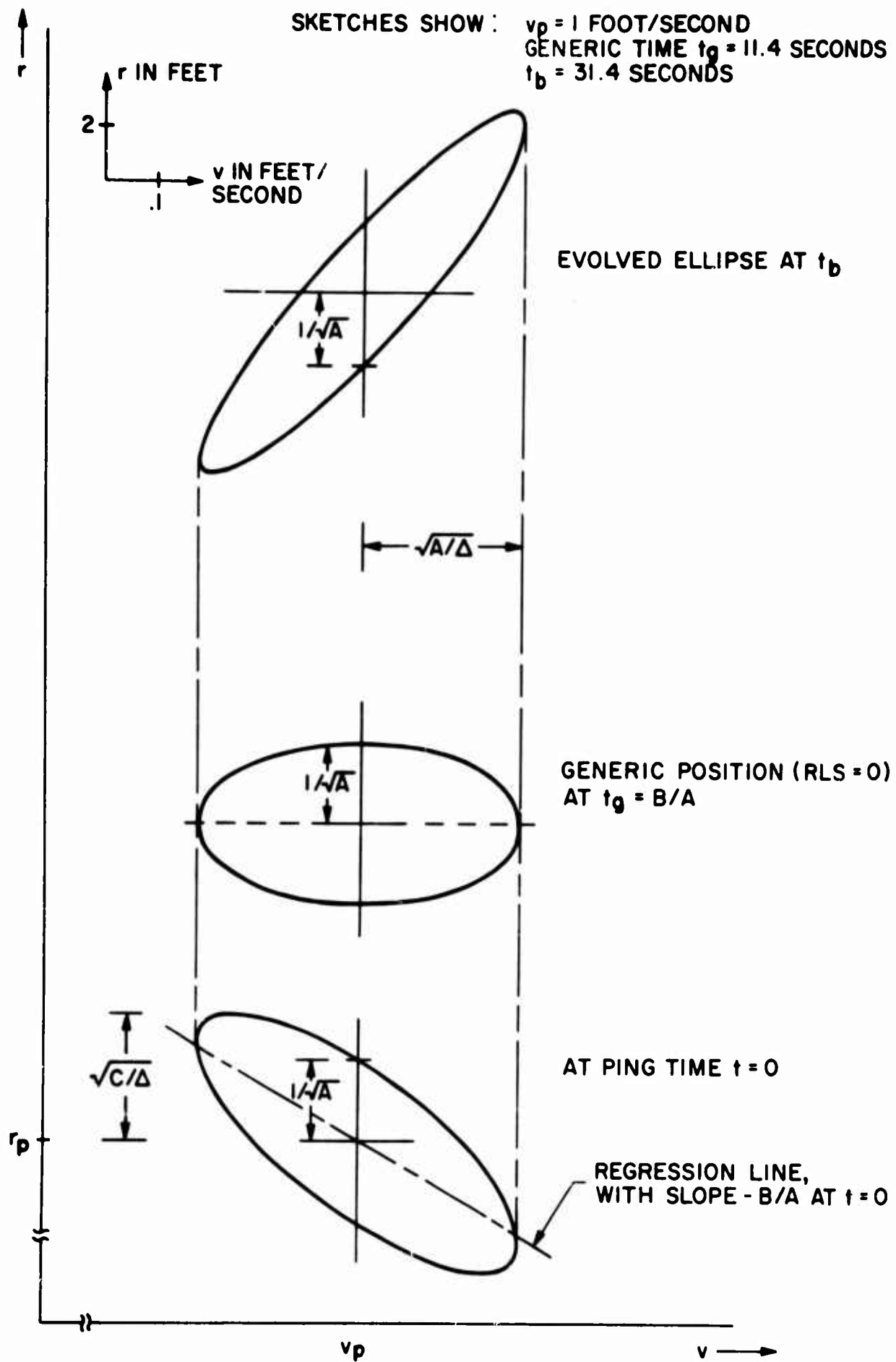


FIGURE 3-2 EVOLUTION OF ERROR ELLIPSE

Thus the standard deviation is $\hat{e}_r \equiv \sqrt{e_r^2}$:

$$\hat{e}_r = \frac{1}{\sqrt{A}} \cdot \sqrt{1 + \frac{1}{\Delta}(B-At)^2} \quad (3-11)$$

which clearly is minimized when $B=At$. Thus the observer, who is assumed to know the wait time t , should design the ping so that $B/A=t$. He thus "pre-rotates" the ellipse by choice of B/A so that it evolves into the generic position at the correct time. This may not be possible, as will be shown in Sect. 3-4.

It may seem strange that the observer should be able to obtain more accurate estimates just by waiting, since he is obtaining no additional information after the ping. The answer is that information is being transformed into a more useful form for the observer's purpose. Because errors in the v estimate affect later errors in the r estimate, the observer wishes to bias the measurements so that on the average the v estimate errors do not enter at the action time. He does this by designing B/A .

Thus elapsed time between data acquisition and data usage alters the simple estimation problem by introducing another degree of freedom, which the observer attempts to control by signal design.

3.2 Multiple Ping Processing

The question here is: how should the observer combine data taken from two pings separated in time? The answer was basically given by Woodward^[4] (p. 64), and follows from the Inv PF philosophy: After the first ping has been processed, the Inv PF of ping #1 becomes the a priori probability function for ping #2, because it represents the observer's total "state of mind" concerning θ . Thus for the second ping (using subscripts to index the corresponding ping):

$$p(\theta/y_2) = k p(\theta/y_1)p(y_2/\theta) = kp_0(\theta)p(y_1/\theta)p(y_2/\theta) \quad (3-12)$$

which can be generalized to n pings:

$$p(\theta/y_n) = k p_0(\theta)p(y_1/\theta)p(y_2/\theta)\dots p(y_n/\theta) \quad (3-13)$$

where the a priori function for the n^{th} ping has been broken down into its constituents. The noise must be independent ping to ping so that the probabilities may be multiplied.

As Woodward points out, the quantities being estimated may not change between data samples in order for this scheme to work. In the present context the target is indeed moving, but the information desired about the target (r_o, v_o) does not change. The transformation Z permits one to extrapolate from any target position back to (r_o, v_o) . Thus we can use the result in (3-13).

Eq (3-13) causes a fundamental change from the single ping case procedure, as it instructs the observer to retain the entire Inv PF from each ping, rather than just the estimates. Each ping's Inv PF is transformed the appropriate amount, and they are all combined finally at the action time.

Specializing to the two ping case, the joint Inv PF for two pings is found using (2-14), the basic Inv PF form. Referring to Fig. 1-1, the first ping has a total wait time of $t_t = t_1 + t_w$ seconds, while the second ping has a wait of t_w seconds. Since $K(\theta)$ in each case appears as an exponent, the properly transformed exponents must be added to comply with (3-12). There the matrices

$$z_{t_t}^{-1} \begin{bmatrix} A_1 B_1 \\ B_1 C_1 \end{bmatrix} z_{t_t}^{-1} \text{ and } z_{t_w}^{-1} \begin{bmatrix} A_2 B_2 \\ B_2 C_2 \end{bmatrix} z_{t_w}^{-1}$$

simply add (see (3-3)), and the ellipse parameters for the joint estimation ellipse are

$$A' = A_1 + A_2$$

$$B' = (B_1 - A_1 t_t) + (B_2 - A_2 t_w) \quad (3-14)$$

$$C' = (C_1 + A_1 t_t^2 - 2B_1 t_t) + (C_2 + A_2 t_w^2 - 2B_2 t_w)$$

Thus the joint ellipse parameters are simply the sums of the properly evolved individual parameters. (Subscripts indicate the corresponding ping.) The estimate variances for the two-ping case then follow immediately from (2-30) and 3-14):

$$\overline{e_r^2} = C'/\Delta'$$

$$\overline{e_r e_v} = -B'/\Delta' \quad (3-15)$$

$$\overline{e_v^2} = A'/\Delta'$$

with $\Delta' = A'C'^2 - B^2$

(It is shown in Appendix I that $\Delta' > 0$)

A geometrical interpretation is given in Figure 3-3, where the ellipses are shown at three instants of time: 1) time of ping #1 where ping #1 ellipse is shown, 2) time of ping #2 where the evolved ping #1 ellipse is shown along with the new #2 ellipse and the joint ellipse resulting, and 3) the evolved joint ellipse at the action time. The following features are noted:

- 1) The centers of the individual ellipses need not coincide. The centers have random (noise-dependent) locations, and thus can be displaced from the true centers. However, if noise were absent on both pings, both ping centers would coincide on the true target range and speed for all times thereafter.
- 2) The ellipses may differ in size, due either to signal design, or to varying target strength (the weaker the target return, the larger the area of the ellipse is). For the ellipses shown, the #2 return had a SNR one half as large as that of #1 (see example below).

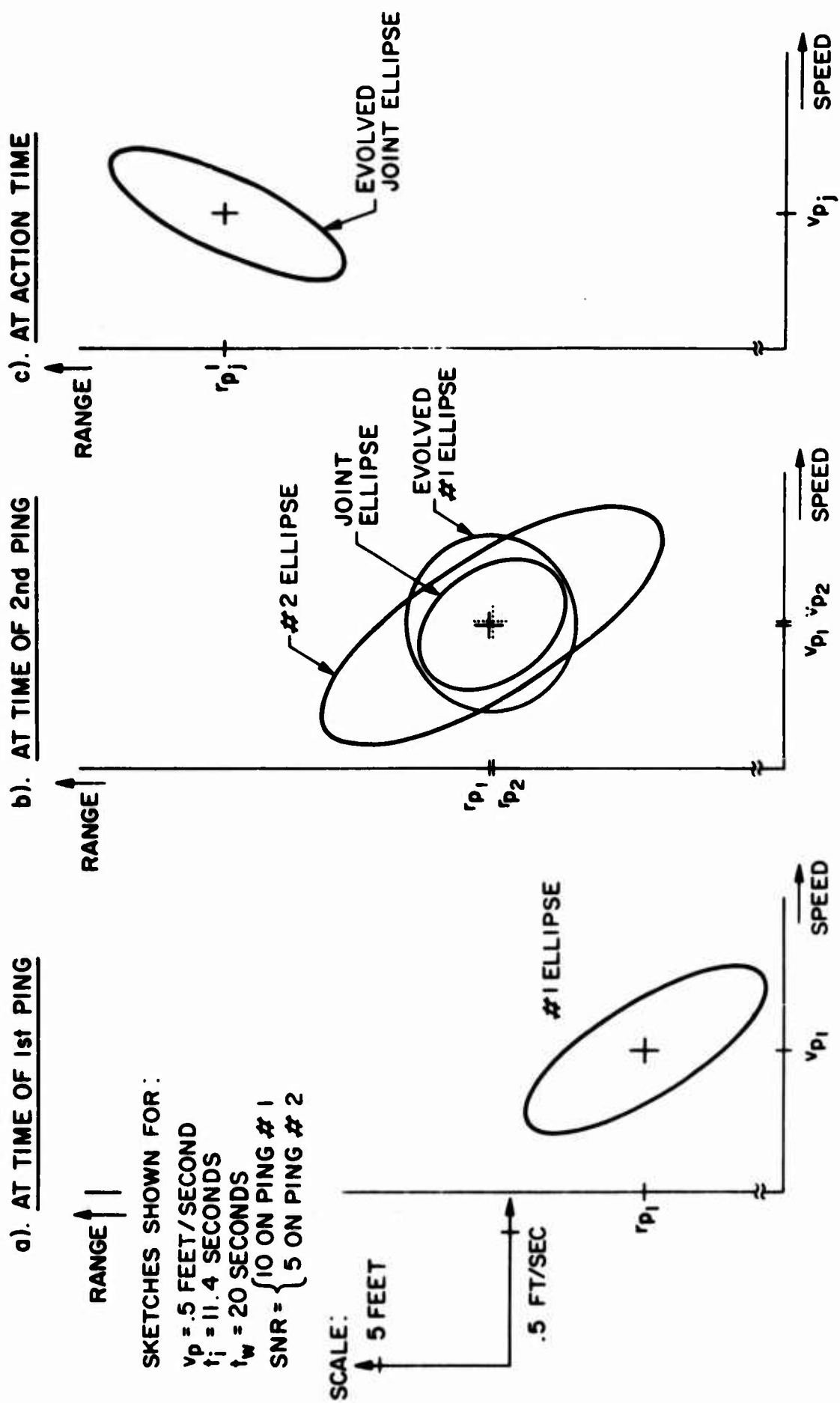


FIGURE 3-3 COMBINATION OF ELLIPSES TO FORM JOINT ELLIPSE

3) In the figure the interping time was so chosen that the #1 ping was generic at the time of #2 ping. This case was chosen for illustration only, and will later be shown to be far from the optimum choice. The wait time shown here was sufficiently large that the joint ellipse evolved through its generic position. The observer would like the joint ellipse to be generic at the action time, but as seen below this is not always possible.

Example 3-1. RAFMOP signals used on Both Pings

The ellipses shown in Figure 3-3 were based on the use of RAFMOP signals for both pings, each with $\delta=d/4$. (see ex. 2-2) The white noise case was assumed, with WSNR=10 for #1 and WSNR=5 for #2. It is informative to see how much improvement two pings as opposed to one ping affords in this example. We assume the observer waits t_w seconds after the final ping in both cases. In the first case this is the only ping sent, whereas in the second case there was a previous ping sent t_i seconds before the final ping. In the table below the estimate standard deviations are given for three choices of t_w . (Figure 3-3 shows $t_w=20$ seconds). $t_i=11$ seconds in each case.

$\sqrt{e_r^2}$	$t_w=0$	$t_w=10$	$t_w=20$	$\sqrt{e_v^2}$	all t_w
#2 alone	6.57	4.4	5.8		.44
both pings	2.65	2.9	4.4		.23

ft ft/sec.

TABLE 3-1: Effect of First Ping, and of Wait Time

There is a significant amount of improvement achieved in the two-ping case for small t_w , but this degree of improvement diminishes for larger t_w . We note that $\sqrt{e_r^2}$ for the #2 ping-alone case decreases for $t_w=10$. This is because its ellipse is generic about 11 seconds after ping time. When both pings are used, the joint ellipse is generic only 3.8 seconds after the #2 ping time, and so the joint ellipse has evolved well beyond its generic position at the action time.

It will be shown below that the rewards obtained by using two pings over just a single ping can be very great if the interping time and signal shapes are chosen more carefully. The results in this example are less dramatic since no attempt was made at an optimal selection of either t_1 or δ .

3.3 The Final Range Estimate Variance

The stated goal of the observer is to minimize the range estimate variance (hereafter REV) t_w seconds after the second ping. From (3-15) this is $REV = \overline{e_r^2} = C'/\Delta'$ which may be simplified (see (3-10)):

$$REV = \frac{1}{A'} \left(1 + \frac{B'^2}{\Delta'^2} \right) \quad (3-16)$$

Therefore the minimum value of REV is $1/(A_1 + A_2)$, which is attainable if the observer can make $B'^2 = 0$. As the structure of B'^2/Δ'^2 is rather complicated, we first examine the behavior of REV with respect to A_1 , A_2 , C_1 , and C_2 in a general way. Taking partial derivatives, it is easy to see that

$$\partial REV / \partial A_1 = -(C' + B' t_t)^2 / \Delta'^2 < 0$$

$$\partial REV / \partial A_2 = -(C' + B' t_w)^2 / \Delta'^2 < 0 \quad (3-17)$$

$$\partial REV / \partial C_1 = \partial REV / \partial C_2 = -B'^2 / \Delta'^2 \leq 0$$

Since the partial derivatives are negative, REV is a decreasing function of each variable for all values of the others. Consequently, if the parameters A and C can be designed independently for each ping, then the observer must always maximize A and C on each ping, regardless of wait or interping times. The dependence on C_1 , C_2 vanishes if $B'=0$. Once the A's and C's are maximized, the only remaining problem is to adjust the B's and t_i in order to minimize REV.

The question of designing A and C independently in the white noise case is considered in Appendix J, where it is shown that the maximum allowable values of A and C can always be obtained independently. (The duration and bandwidth constraints considered use the dispersion duration and bandwidth definitions of (2-34) and (2-36)). However, in the general colored noise case no such results have been obtained. It is possible that an attempt to maximize, say, C, would restrict the attainable values of A, B such that REV would be higher than for a reduced value of C. It is felt, however, that a good design procedure is to attempt to maximize A and C in any case.

3.4 Behavior of REV as a Function of Design Parameters

As seen in (3-16), B'^2/Δ' represents the fractional increase in REV over its absolute minimum of $1/A'$. B' can be made zero by making each ping ellipse generic at the action time:

$$B_1/A_1 = t_t \quad ; \quad B_2/A_2 = t_w \quad (\text{desired}) \quad (3-18)$$

One need not know the target strength to achieve this condition, since only ratios such as B_1/A_1 appear. If this condition could be attained for all t_w the problem would be solved. The observer would select a convenient t_t , and design each B/A so that the corresponding ellipse would be generic at the action time. The error would always be $1/A'$.

However, there are two problems with this plan.

- 1) The observer cannot always predict B_1/A_1 with certainty except in the white noise case, because this ratio will in general depend on target speed. (He may be able to predict B_2/A_2 if the first ping gives acceptable range rate accuracy.)

2. t_w may be too large. Since all sets A, B, and C satisfy $AC - B^2 > 0$, B/A is always smaller than $\sqrt{C/A}$. Consequently if t_w exceeds the attainable $\sqrt{C/A}$ then condition (3-18) may not be used.

In view of these difficulties it is more appropriate to determine the general behavior of REV in terms of the B's and interping time, in order to form guidelines for the observer. These guidelines will dictate which ranges of the parameters are to be used, and which avoided, in order to make REV reasonably small.

It is convenient to consider a normalized version of REV. This allows us to compare the two-ping and single-ping situations. The normalization is with respect to A_2 , since the error would be $1/A_2$ for a single ping and no wait time:

$$REV = \frac{1}{A_2} J$$

where

$$J = R_2(1 + B'^2/\Delta') \quad (3-19)$$

and

$$R_2 = \frac{A_2}{A_1 + A_2} \quad (3-19b)$$

For convenience we also define $R_1 = 1 - R_2 = A_1 / (A_1 + A_2)$.

J may be put into a more meaningful form by defining further the quantities

$$\rho_1 = \frac{B_1}{\sqrt{A_1 C_1}} \quad , \quad \gamma_1 = \sqrt{C_1 / A_1} \quad (3-20)$$

and similarly for ρ_2 and γ_2 . γ_1 has dimensions of time, while ρ_1 is dimensionless and satisfies $|\rho_1| < 1$.^{*} ρ is called a correlation coefficient, since in the single ping case (see (2-30))

$$\rho = \frac{\overline{-e_r e_v}}{\sqrt{\overline{e_r^2} \overline{e_v^2}}} \quad (3-21)$$

ρ may be made to approach ± 1 for signals with large time bandwidth products (see Appendix G). Each ρ and γ is independent of target strength and SNR (all this information is now in R_1 , R_2 , and A_2), and γ terms may be compared

^{*} Similar statements apply to γ_2 , ρ_2 .

directly with t_i and t_w . γ and $\rho\gamma$ are identified with the slopes of the lines in Figure 3-4. It is noted that $\rho\gamma$ is the time required for an ellipse to evolve into the generic position.

It is shown in Appendix I that J now takes the form:

$$J = R_2 \left[1 + \frac{[(t_w - \rho_2 \gamma_2) + R_1(t_i - \rho_1 \gamma_1 + \rho_2 \gamma_2)]^2}{R_1 \gamma_1^2 (1 - \rho_1^2) + R_2 \gamma_2^2 (1 - \rho_2^2) + R_1 R_2 (t_i + \rho_2 \gamma_2 - \rho_1 \gamma_1)^2} \right] \quad (3-22)$$

and has the shape sketched in Figure 3-5. The quantities noted in Figure 3-5 are given by

$$t_n = (\rho_1 \gamma_1 - t_w) + \frac{R_2}{R_1} (\rho_2 \gamma_2 - t_w)$$

$$\Delta_s = R_1 \gamma_1^2 (1 - \rho_1^2) + R_2 \gamma_2^2 (1 - \rho_2^2) \quad (3-23)$$

$(t_w - \rho_2 \gamma_2)$ is the RLS of the ellipse #2 at the action time, t_n is the interping time for which the joint ellipse is generic (i.e. $B'=0$).

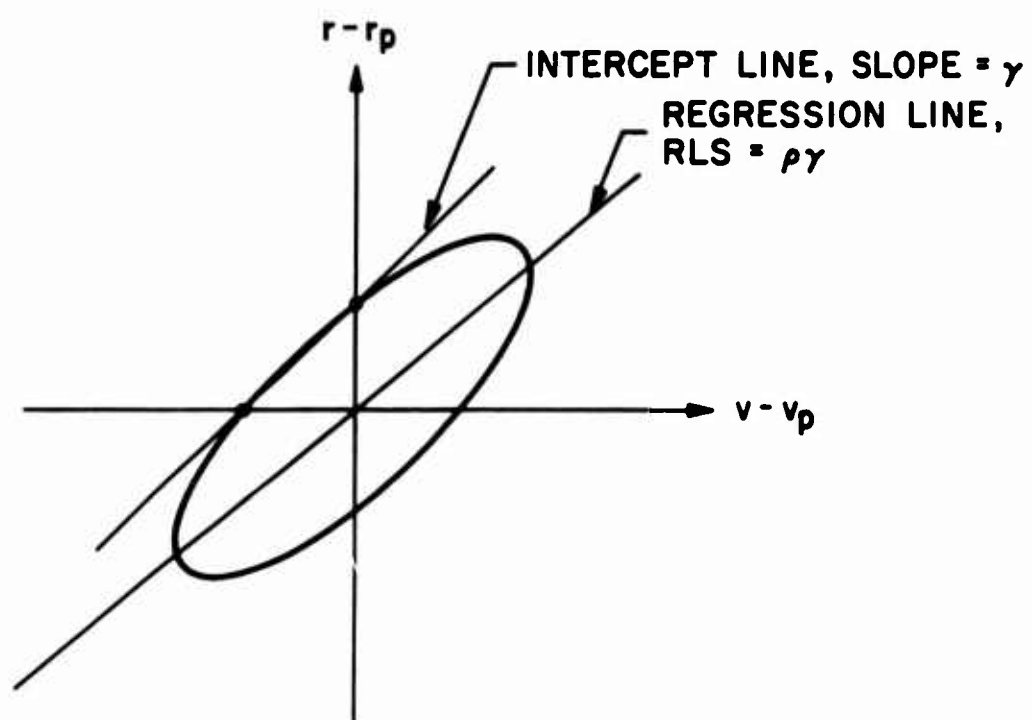


FIGURE 3-4 GEOMETRICAL INTERPRETATION OF γ AND $\rho\gamma$

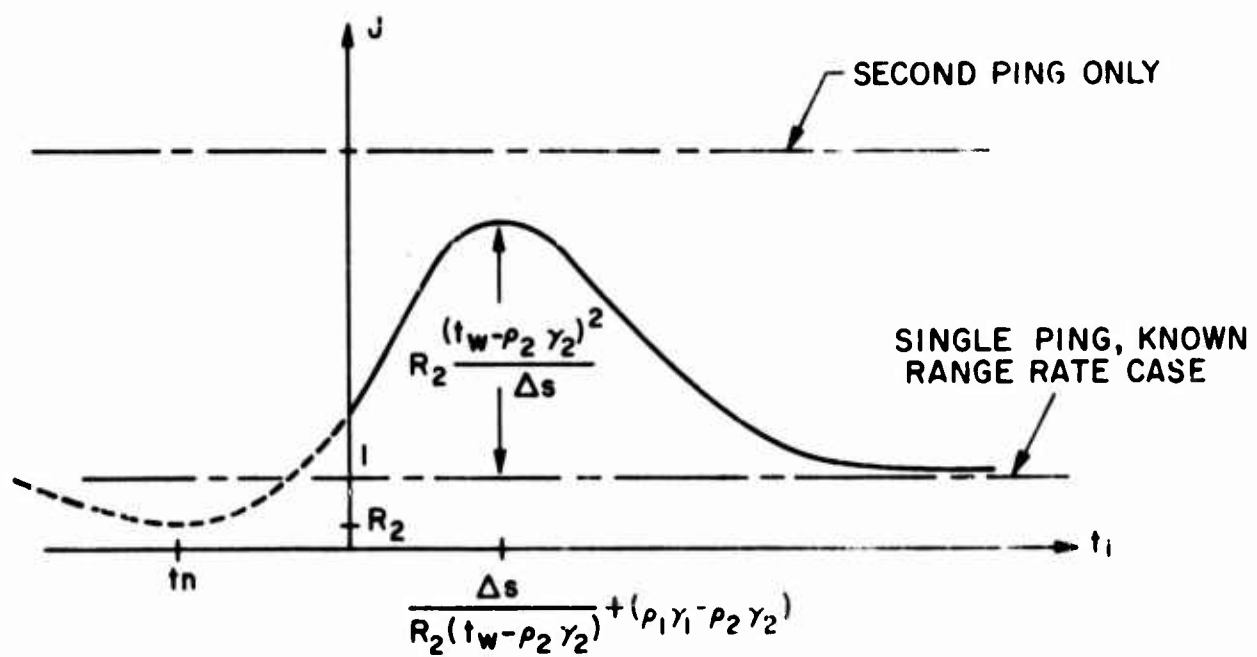


FIGURE 3-5 BASIC SHAPE OF J VERSUS t_1

Several features are apparent from (3-22) and the shape of Figure 3-5:

- 1) A desirable minimum for J exists at $t_1 = t_n$, for which $J = R_2$, or $REV = 1/A'$, its absolute minimum. Unfortunately the values of t_w to be expected in practice are much larger than the $\rho_2 \gamma_2$ values attainable so that this minimum cannot always be achieved.
- 2) For sufficiently small t_1 , the relative rotation between the #1 and #2 ping ellipses is not significant and the joint ellipse parameters at the second ping time are simply: $A_1 + A_2$, $B_1 + B_2$, and $C_1 + C_2$ respectively. Thus the performance is equivalent to a single ping situation with these new parameters.
- 3) In the limit of large t_1 an asymptote is observed at which $J = 1$. For such large t_1 the first ping ellipse will evolve into an almost vertical line as shown in Figure 3-6. When the second ping ellipse is added, the joint ellipse will also be thin and nearly vertical, with vertical extent determined mainly by A_2 . The wait time will consequently have little effect on the range variance. The resulting performance will be

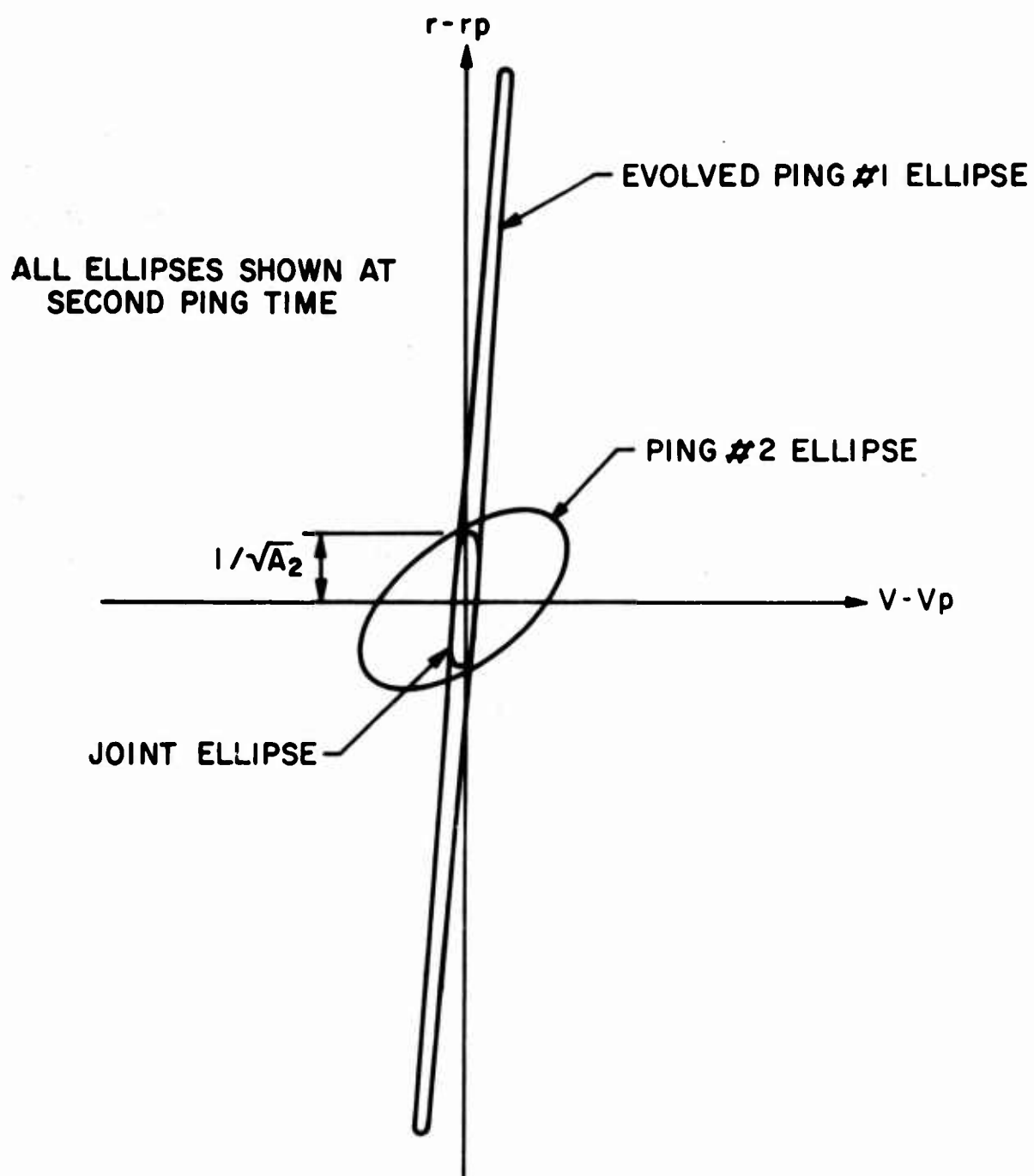


FIGURE 3-6 EFFECT OF LONG INTERPING TIME

called the "single-ping, known range rate" performance, since in effect the long interpinging time leaves only a narrow region of the range-rate plane with significant inverse probability, and thus eliminates most of the range rate ambiguity. Then the second ping can be used to obtain range information only, and the REV will be approximately $1/A_2$. The use of very large interpinging times thus separates the roles of the two pings, using the first for range rate estimates, and the second for range estimates.

- 4) For the single ping case (effectively $R_1=0$), the optimal signal design (choice of ρ_2) is determined using simple minimization techniques in Appendix K, yielding

i. if $t_w < \gamma_2$, $J_{\text{single}}=1$ for $\rho_2 \gamma_2 = t_w$

ii. if $t_w > \gamma_2$, $J_{\text{single}} = (t_w / \gamma_2)^2$ for $\rho_2 = \gamma_2 / t_w$ (3-24)

Therefore for a single ping, t_w causes the REV to increase as t_w^2 (when $t_w > \gamma_2$). For large wait times this can result in a severe degradation of performance.

The use of two pings can work to overcome this deficiency.

- 5) The single ping case always results in a larger J than the two-ping case (where $R_1 \neq 0$). The single ping case yields (use $R_1=0$, $R_2=1$ in (3-22)):

$$J = 1 + \frac{(t_w - \rho_2 \gamma_2)^2}{\gamma_2^2 (1 - \rho_2^2)} \quad (3-25)$$

Comparing this with the peak value of J observed in Figure 3-5, it is easy to see that the distance between the levels is

$$J_{\text{single ping}} - J_{\text{both pings}}$$

$$= \frac{(t_w - \rho_2 \gamma_2)^2}{\gamma_2^2 (1 - \rho_2^2)} \cdot \frac{R_1 \gamma_1^2 (1 - \rho_1^2)}{R_1 \gamma_1^2 (1 - \rho_1^2) + R_2 \gamma_2^2 (1 - \rho_2^2)} \quad (3-26)$$

which is large if t_w is large and R_1 is reasonably far

from zero. Thus the use of two pings can yield a sizable improvement even for the worst choice of t_1 .

3.5 Design of ρ_1 and ρ_2 for Optimum Performance in

White Noise

In order to understand more clearly the effects of t_w , t_1 and R_1 , we now consider the absolute minimum value that J may have for given values of these variables. These minima will occur in the white-noise-only case, since A and C are maximized in this case (see Appendix G), and performance improves monotonically with A and C .

For the white noise case, the values of γ_1 and γ_2 are determined by the allowable bandwidth and duration constraints. Since these constraints will be the same on each ping, and the observer will use the largest allowable values in order to maximize his performance, the two values will be equal: $\gamma_1 = \gamma_2 = \gamma$.

The observer will know only t_w before he sends the first ping, and he must choose ρ_1 before sending this ping, and t_1 as well as ρ_2 before sending the second. He will not know R_1 until both pings have been sent. To determine an upper bound on performance, however, we choose values

of t_w , t_i and R_1 , and pretending they are known beforehand, minimize J by proper choice of ρ_1 and ρ_2 .

With γ common to both pings, it is convenient to normalize the times t_i and t_w as well in (3-22):

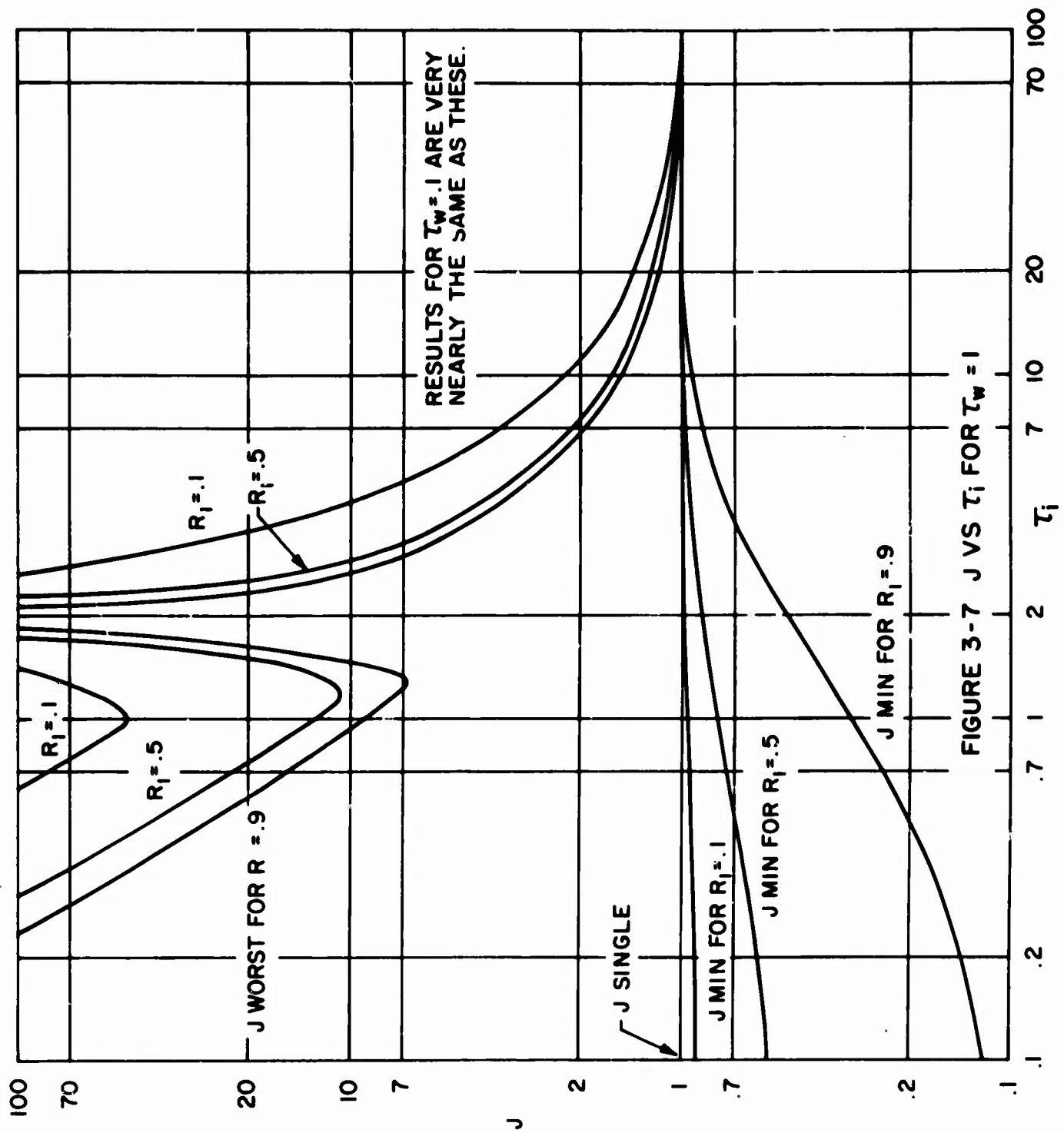
$$\tau_w = t_w/\gamma \quad ; \quad \tau_i = t_i/\gamma \quad (3-27)^*$$

Then J simplifies to

$$J = A_2 \text{ REV} \\ = R_2 \left[1 + \frac{\left[(\tau_w - \rho_2) + R_1 (\tau_i - \rho_1 + \rho_2) \right]^2}{1 - R_1 \rho_1^2 - R_2 \rho_2^2 + R_1 R_2 (\tau_i - \rho_1 + \rho_2)^2} \right] \quad (3-28)$$

A numerical search procedure was employed to find the ρ_1 and ρ_2 which minimize J for fixed values of τ_w , τ_i and R_1 . The results are shown in Figures 3-7 through 3-10. In figures 3-7 through 3-9 J_{\min} is plotted versus τ_i for different values of R_1 and τ_w . J_{\max} (the performance resulting from the worst choice possible of ρ_1 , ρ_2) is also shown to demonstrate the variability of J with signal design.

* For reference purposes recall that $\gamma=15$ seconds for the LIFMOP and RAFMOP signals of example 2-2.



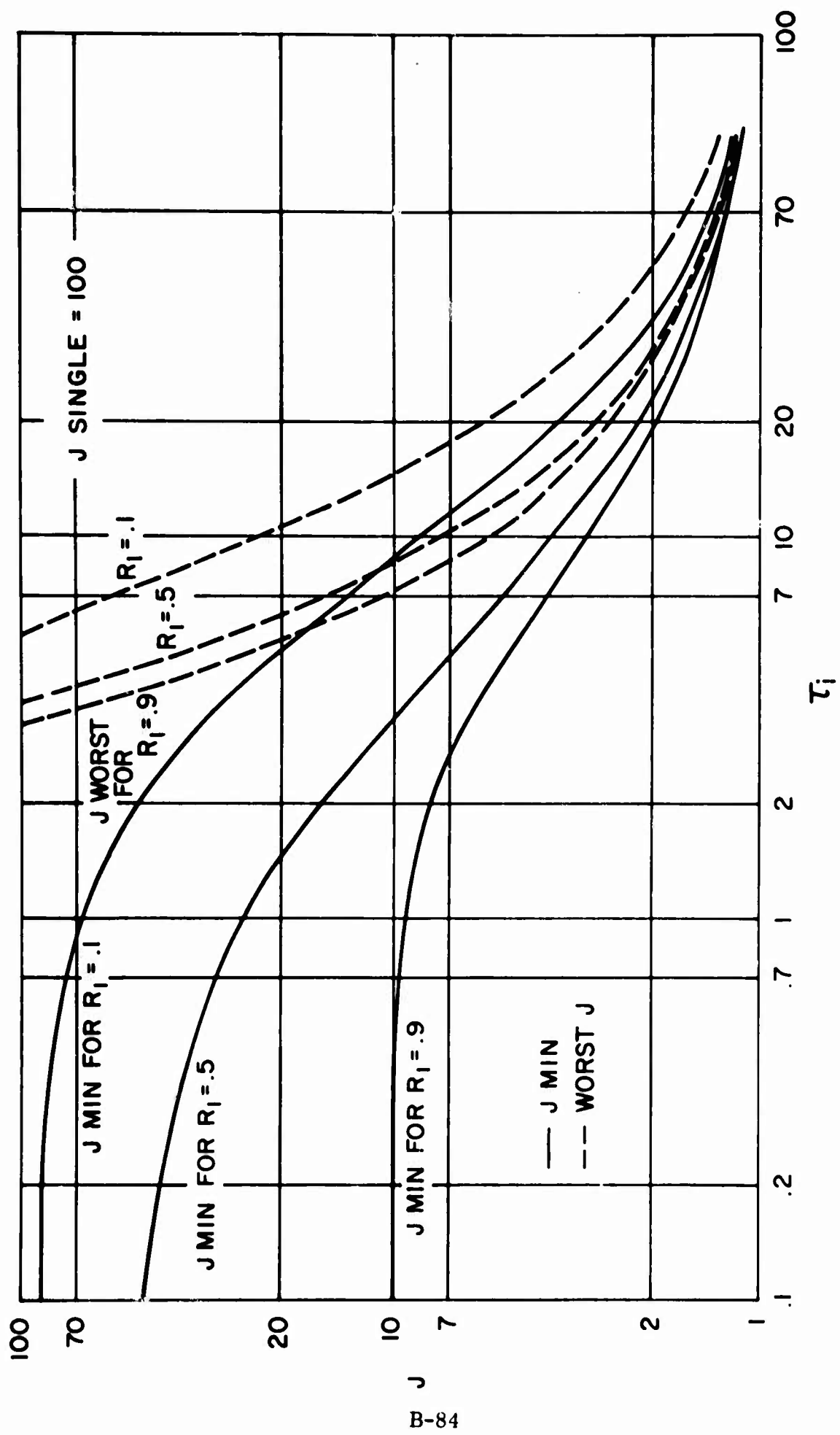


FIGURE 3-8 J VS τ_i FOR $\tau_w = 10$

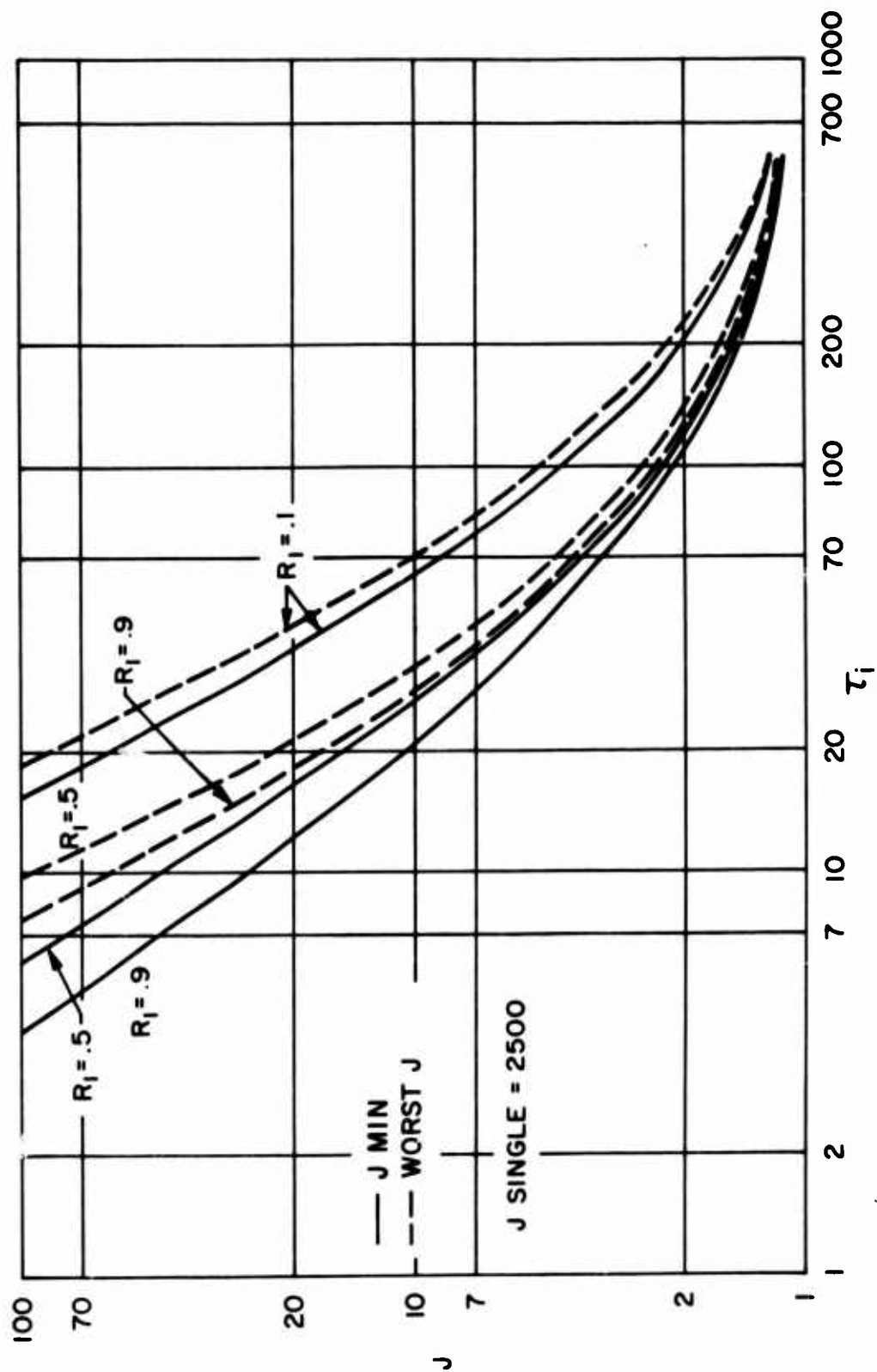


FIGURE 3-9 J VS τ_i FOR $\tau_w = 50$

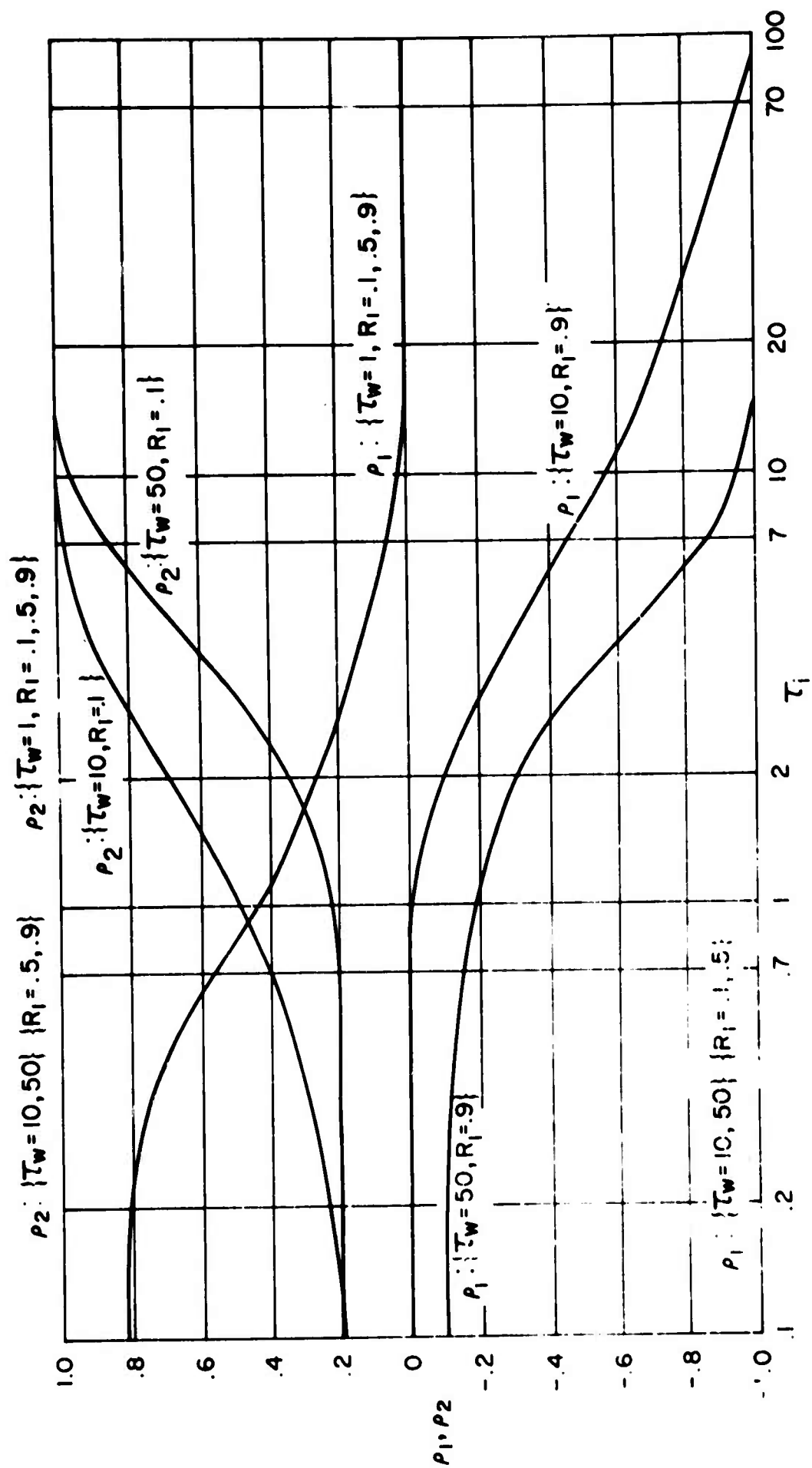


FIGURE 3-10 OPTIMUM ρ_1 AND ρ_2 VS τ_i

J_{single} given by (3-24) is also included. Finally in Figures 3-10 the optimum values of ρ_1 and ρ_2 are shown for the parameter values considered.

The three major issues of interest here are:

- 1) A comparison of the single ping and two-ping performances.
- 2) The importance of signal design on the value of J .
- 3) The effect of the interpinging time on the performance.
-
- 1) For large values of τ_w the two-ping performance is far superior to that for a single ping, especially if the first ping return is strong (large R_1). (As R_1 approaches zero, the two cases perform equally well, of course.) This superiority requires that reasonable choices for ρ_1 and ρ_2 be made. On the other hand, when τ_w is small only slight improvement is possible for the two-ping case, and this requires careful choice of ρ_1 and ρ_2 .
- 2) Proper signal design is seen to be very important for small values of τ_w and τ_i , as very different performance levels are exhibited for the best and worst

choices of ρ_1 and ρ_2 . As τ_i becomes large all signals yield the same value of J , ($J \pm 1$). This is the "single-ping, known range rate" situation discussed previously. Also as τ_w becomes large, the performance is poor regardless of signal design due to the extreme ellipse evolution.

From Figure 3-10 the best choices for ρ_1 and ρ_2 are seen to form two rather distinct groups, such that ρ_1 should generally be negative (ellipse #1 already beyond its generic position at ping time) except when τ_w is very small, and ρ_2 should be positive in all cases (ellipse #2 prerotated so that it will move toward its generic position as time elapses). In many cases the best choices for ρ_1 and ρ_2 do not depend heavily on R_1 , so that the actual lack of knowledge of R_1 will not be too significant. The worst choices were found to be:

$$\begin{aligned} \rho_2 &= -1 \quad \text{always} \\ \rho_1 &= \begin{cases} -1 & \text{for } \tau_i \leq 1 \\ +1 & \text{for } \tau_i > 1 \end{cases} \end{aligned} \quad (3-29)$$

The worst choice for ρ_1 always tends to align the two ellipse RLS's.

- 3) The general conclusion that may be drawn with regard to τ_1 is that it should be as large as possible if τ_w is large, in order to approach the "single-ping known range rate" condition. Only for τ_w of the order unity can any gains be made by reducing τ_1 . When τ_w is large, the value of τ_1 required to achieve the asymptotic condition is about four times larger, and may be too large to use in practice. These results indicate that large waiting times can markedly degrade the estimator performance.

3-6 A Design Perspective for the Reverberation Noise Case

The last section discussed the effects of signal design for the white noise only case, for which the observer will always use the largest A and C parameters permitted by the bandwidth and duration constraints. The design procedure there was quite simple because the observer does not make use of first ping information in designing the second ping. However, in the general noise case discussed in Chapter 2 the performance depends strongly on the true target range rate, and so if the observer can accurately

measure this quantity on the first ping, he may be able to redesign the second ping to achieve a greatly improved final range estimate. When the noise is signal dependent as in the next chapter this will be particularly true.

We now show that the observer's best design procedure is to consider only range rate measurement on the first ping, and range measurement on the second ping. This vastly simplifies his task since he need only strive to maximize C_1 and A_2 , the other ellipse parameters having little effect. We have shown that for large values of t_1 , $REV \approx 1/A_2$ (see Figure 3-5), and that this corresponds to the performance level for the known range rate situation. The absolute minimum for REV is $REV = 1/(A_1 + A_2)$, (see (3-19)) but this value will not be significantly smaller than $1/A_2$ since in practice $A_2 \gg A_1$ (the observer has more information with which to design the second ping, and so can do a better job). Thus if a sufficiently large t_1 is used the final performance depends mainly on A_2 , and this is clearly the quantity to maximize. The range rate needn't actually be measured on the first ping to arrive at this conclusion: the only requirement is that t_1 be very large. However,

there are two important reasons for making an accurate range rate estimate on the first ping: 1). The required value of t_1 needn't be impractically large, and 2). knowledge of target range rate permits much greater values of A_2 to be achieved. The second point will become apparent in the signal design study of the next chapter, but the first point deserves more comment here. We must again examine the behavior of J to determine the size of t_1 required.

Because the signals used to combat reverberation in Chapter 4 will have extremely small B_1 and B_2 , we rewrite J of (3-22) with $\rho_1 = \rho_2 = 0$.

$$\begin{aligned}
 J &= R_2 \left[1 + \frac{(t_w + R_1 t_1)^2}{R_1^2 \gamma_1^2 + R_2^2 \gamma_2^2 + R_1 R_2 t_1^2} \right] \\
 &= R_2 \left[1 + \frac{(1 + R_1 T_1)^2}{\Gamma + R_1 R_2 T_1^2} \right]
 \end{aligned} \tag{3-30}$$

where $T_1 = t_1/t_w$ and

$$\Gamma = \frac{C_1 + C_2}{A_1 + A_2} \frac{1}{t_w^2} \quad (3-31)$$

J is plotted as a function of T_1 in Figure 3-11 for different values of R_1 and Γ . If Γ is of the order one then any value of T_1 will be acceptable (where "acceptable" could be considered as the region of $J \leq 2$, for instance). For smaller values of Γ , T_1 must be about 10 when $R_1 = .01$, and must be about 30 when $R_1 = .001$. The case $R_1 = .5$, which corresponds to the situation $A_1 = A_2$ as in the white noise cases in Figures 3-8 and 3-9, requires that T_1 be about 3. Thus two things are clear:

- 1) The value of t_1 required to keep $J < 2$ does indeed increase as R_1 becomes very small (due to disregarding a careful design of A_1 for the first ping), but the increase is not prohibitively large.
- 2) Γ should be made large (of the order one) if possible. This may be accomplished by using a large value of C_1 , provided t_w is not excessively great. Then any value of T_1 is satisfactory. However, if Γ cannot be made more than about .1, then at the sizes of T_1 required J is insensitive to Γ .

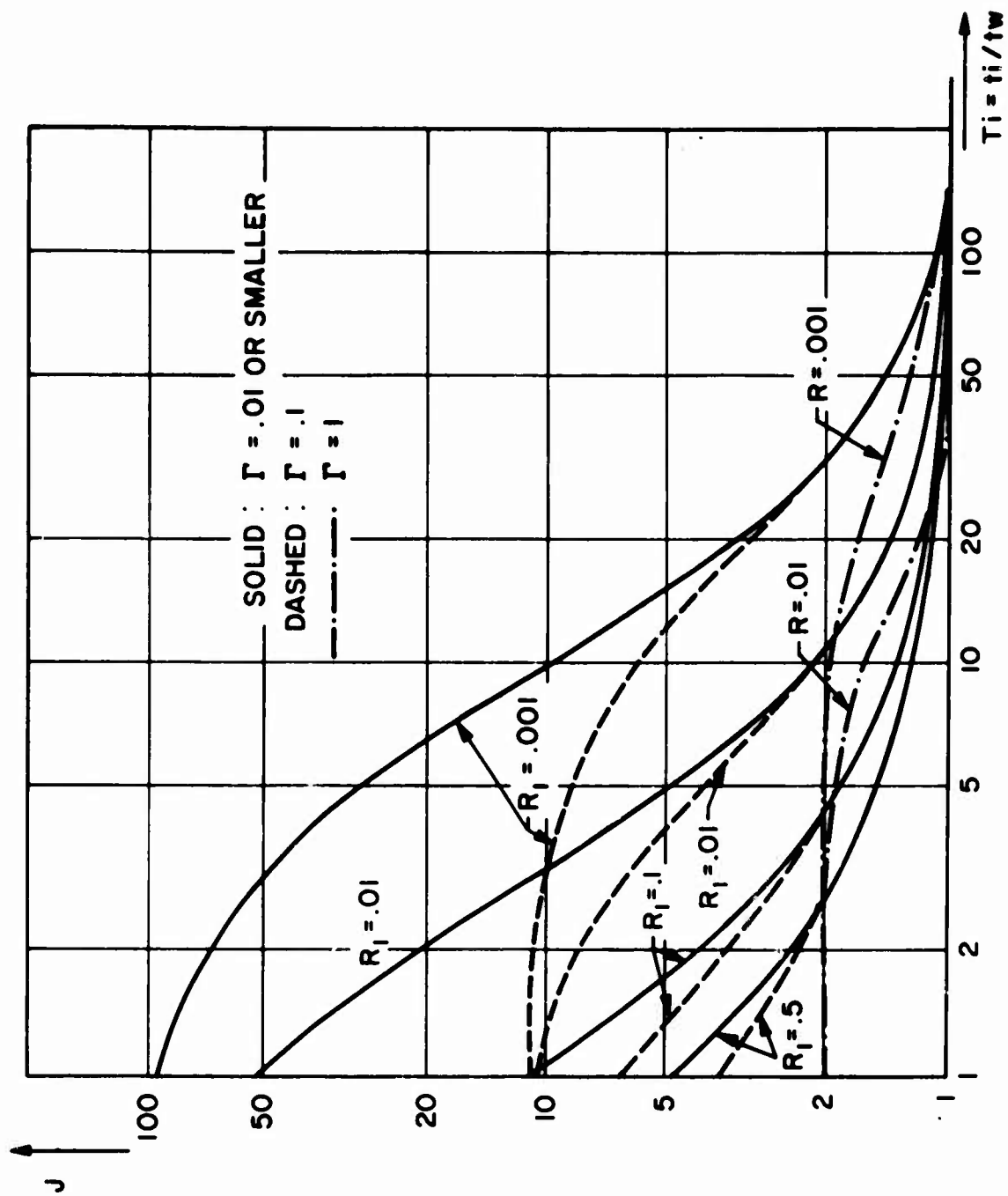


FIGURE 3-11 J VS t_i/t_w FOR GENERAL CASE WITH $B_1 = B_2 = 0$.

The above arguments have shown that the observer need only strive to maximize C_1 on the first ping, and A_2 on the second. The principal reason for obtaining a large C_1 is that an accurate range rate measurement will permit careful second ping design to achieve much larger values of A_2 than otherwise possible. The details of this last point are considered in the next chapter.

CHAPTER 4

Signal Design of Two Pings in the Strong Reverberation Environment

4.1 The Reverberation Noise Spectrum

The noise model used here was recently treated by Van Trees^[16]. It assumes a distribution of scatterers through a volume of the ocean medium, each scatterer acting as a point reflector of sonar energy. The scatterers are assumed to have random positions, velocities and scattering strengths, and all of the quantities are statistically independent one from the other. This model, therefore, would rather poorly describe the case of surface reverberation or of small clouds of interacting scatterers, but it is a useful model for volume reverberation.

The reverberation model makes the following specific assumptions: The complex envelope $n(t)$ of the noise waveform is given by

$$n(t) = \sum_i Z_i s(t-\tau_i) e^{j\omega_i t} \quad (4-1)$$

where for the i^{th} scatterer

τ_i = time delay of reflected waveform

w_i = doppler shift of waveform

Z_i = complex reflection coefficient

$s(t)$ is the complex envelope of the transmitted waveform
(see (2-2)).

The summation is performed over all scatterers that yield noise energy in the observation interval T given by $T = t: \{t \in (t_b, t_b + T)\}$ (see p. 2-6). Van Trees uses two assumptions that will be retained here. The reflection coefficient of the i^{th} scatterer is independent of the scatterer's exact position, and the average number of scatterers per unit increment in range (or delay) is constant. These assumptions are reasonable approximations if $T/t_b \ll 1$, as will now be indicated. Inverse square law spreading loss causes the received power from a scatterer to decrease as the fourth power of the distance. Hence the ratio of the powers received from scatterers at delays $t_b + T$ and t_b is

$$\frac{\text{power from scatterer at } t_b + T}{\text{power from scatterer at } t_b} = \frac{t_b^4}{(t_b + T)^4}$$
$$\approx 1 - 4T/t_b \quad (4-2)$$

if $T \ll t_b$. Similarly, a sonar beam intercepts an area which increases linearly with range, so that if the average density of scatterers in any volume is the same then

$$\frac{\text{avg. number intercepted at } t_b + T}{\text{avg. number intercepted at } t_b} = 1 + T/t_b \quad (4-3)$$

which again will be nearly unity if $T \ll t_b$. Thus the approximations involved in Van Trees assumptions are quite reasonable as long as the target distance is large compared with the distance covered by sound in T sec.

The statistics assumed for the random variables are

- 1) $EZ_i = 0$, $E|Z_i|^2 = \overline{|Z|^2}$ for all i
 - 2) $p_{\tau_i}(\tau_i) = \begin{cases} 1/T & \tau_i \in T \\ 0 & \text{otherwise} \end{cases}$
 - 3) avg. number of scatterers in summation = $\gamma_s T$
 - 4) prob. density function of w_i is $p_w(w)$ for all i .
- (4-4)

Statement 3 contains the additional assumption that the number of scatterers present is large. We can then say that the actual number of scatterers illuminated (a random

variable) will with high probability be close to the stated mean value $\gamma_s T$.

Van Trees uses these assumptions to calculate the complex autocorrelation function $R(\tau)$ for the noise process consisting of the reverberation noise and an added white noise component representing receiver noise. His result is exact in the limit of large observation interval T , but is a good approximation as long as the observation interval is much larger than the correlation time of the process, (but still short compared with t_b above).

$$R(\tau) = \Lambda R_s(\tau) \int p_w(w) e^{jw\tau} dw + N_o \delta(\tau) \quad (4-5)$$

where

$$R_s(\tau) = \int s(t) s^*(t+\tau) dt$$

N_o = spectrum level of white noise component

$$\Lambda = \frac{1}{2} \gamma_s \overline{|Z|^2}$$

The noise autocorrelation function is thus the product of the scatterer Doppler characteristic function and the signal "correlation function." The noise spectral density

$N(\omega)$ is the Fourier transform of $R(\tau)$, and is then the convolution of $p_w(w)$ with the transform of $R_s(\tau)$. Since the transform of $R_s(\tau)$ is simply $|S(\omega)|^2$, (Papoulis⁽¹³⁾, Eq. 2-71), we have

$$N(\omega) = \Lambda \int p_w(w) |S(\omega-w)|^2 dw + N_o \quad (4-6)$$

The reverberation spectrum is essentially the transmitted signal spectrum, "smeared" out by the convolution with $p_w(w)$. If the scatterers do not move, $p_w(w) = \delta(w)$, and

$$N(\omega) = \Lambda |S(\omega)|^2 + N_o \quad (4-7)$$

The dependence of the noise spectrum on the transmitted signal spectrum adds significantly to the complexity of the signal design problem.

4.2 Basic Signal Design Implications of the Reverberation Spectrum

In Section 3-3, it was shown that the ellipse parameters A and C should be maximized in order to minimize REV, the final range estimate variance. With the white noise

level N_0 fixed, A and C are always maximized when the effect of the reverberation component of $N(\omega)$ can be eliminated (see App. G).

To see how this might be accomplished, we note that in (2-41) the ellipse parameters, as well as SNR, are functionals involving $P(\omega)$ of (2-37):

$$P(\omega) = \frac{1}{D_0^2} \frac{|S(\omega)|^2}{N(\omega + \omega_0)} \quad (4-8)$$

For the noise spectrum given in (4-6), this becomes

$$P(\omega) = \frac{1}{D_0^2} \frac{|S(\omega)|^2}{\Lambda |S(\omega + \omega_0)|_p^2 + N_0} \quad (4-9)$$

where for convenience we have set

$$|S(\omega)|_p^2 = \int p_w(\omega) |S(\omega - \omega)|^2 d\omega \quad (4-10)$$

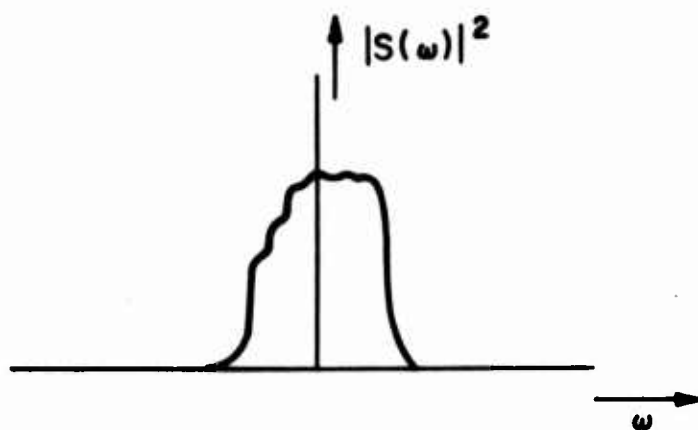
Roughly speaking, in order to maximize A and C, the observer will try to choose $|S(\omega)|^2$ so that in the frequency ranges where $|S(\omega)|^2$ is large $|S(\omega + \omega_0)|_p^2$ will be small relative to the white noise level N_0 . To do this he must take advantage

of the shift w_0 due to the target range rate. If he is successful, then the reverberation interference will have been essentially eliminated. Figure 4-1 shows a sample situation: a) a possible $|S(\omega)|^2$, b) the "smeared" version shifted by amount w_0 and added to the white noise level, and c) the resultant $P(\omega)$, scaled to unit area. In the case shown, the shift w_0 was not quite sufficient to completely eliminate the reverberation.

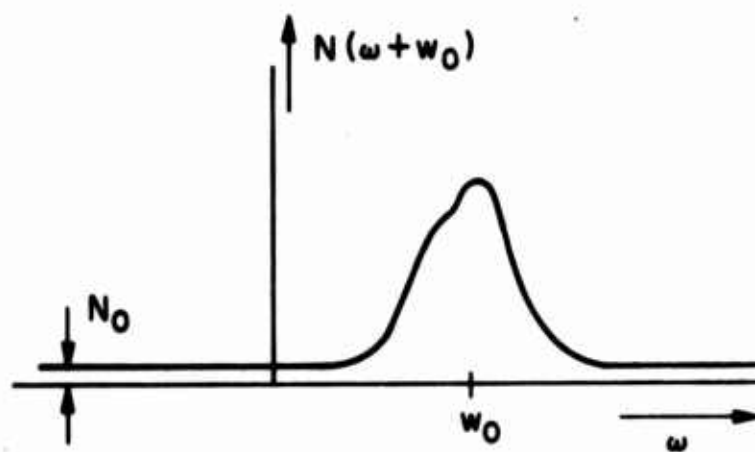
4.3 Design of the First Ping

In order to design $|S(\omega)|^2$ using these principles, the observer must know w_0 . On the first ping, however, he does not have the benefit of this knowledge, and so he must use a signal which will perform well over a large range of target range rates. Since the observer must concentrate on maximizing C_1 on the first ping, a natural signal to use is a very narrowband ping with long duration. For a narrowband $|S(\omega)|^2$ even rather small target range rates will be sufficient to shift the signal spectrum off of the reverberation spectrum, leaving only white noise interference. In the white noise case (2-36) applies, and so C_1 is proportional to the signal duration squared.

a).



b).



c).

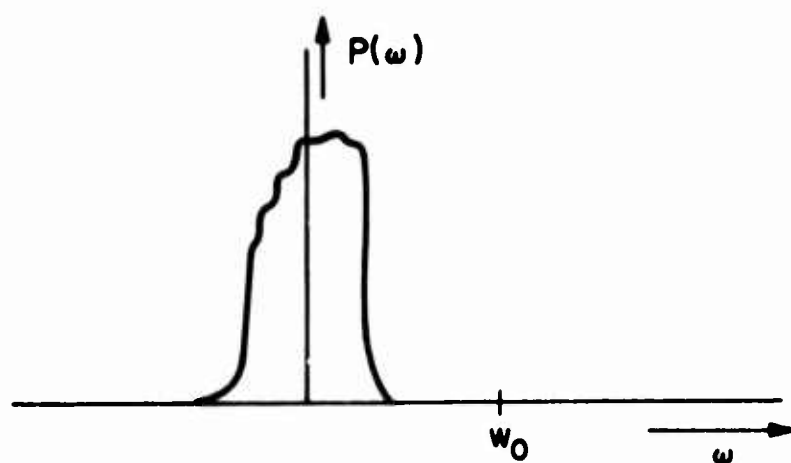


FIGURE 4-1 SAMPLE SIGNAL AND NOISE SPECTRA

The observer is thus led to use a long pulse with no frequency modulation, such as a pure tone lasting d seconds. (This is a special case of the LIFMOP signal of example 2-2, with $P=0$.) If w_0 is sufficient to shift the resulting narrow lobe of $|S(\omega)|^2$ off of the reverberation lobe, then the results of (2-42) apply. We see that $B=0$, the SNR is maximized (for constraints of fixed d and peak signal amplitude m_0), and so the signal is optimum in terms of maximizing C_1 . $S(\omega)$ for the constant frequency tone has significant amplitude only in the band $|\omega| \leq 2\pi/d$, so that $w_0 \approx 4\pi/d$ is sufficient to eliminate the reverberation if the scatterers are not moving.* A larger w_0 is required if the scatterers do move. For insufficiently large w_0 partial elimination will be achieved.

When only partial elimination is obtained due to small w_0 , this is still a good signal to use, since:

1) a narrowband signal has a very concentrated spectrum lobe with high power density. Since scatterer motion smears out this lobe to form $|S(\omega+w_0)|_P^2$, a significant amount of reverberation power can be shifted out of the target echo band. Thus $P(\omega)$ of (4-9) can still be large over much of its range even for small w_0 .

* Using typical values of (2-47), $w_0 = 4\pi/d$ corresponds to a target range rate of 3.3 ft/sec.

2) As a special case of the last comment, where the target is not moving at all, it can be shown that C_1 will increase as the signal becomes more narrowband under ordinary circumstances. A calculation of C_1 is performed in Appendix H for the gaussian-shaped signal:

$$s(t) = m_o \frac{1}{\sqrt{2\pi} d} e^{-\frac{1}{2}(t/d)^2} \quad (4-11)$$

and for scatterer Doppler probability density function

$$p_w(w) = \frac{1}{\sqrt{2\pi} B} e^{-\frac{1}{2}(w/B)^2} \quad (4-12)$$

The signal here has a narrow spectral lobe similar to that of the constant frequency tone above, and this signal form leads to tractable mathematics. It is shown in Appendix H that for the strong reverberation interference case

$$C_1 \approx \frac{1}{B} \left[\frac{1+2B^2d^2}{2Bd} \right]^2 \quad (4-13)$$

Hence if $B \gg 1/d$ (i.e., if the rms scatterer doppler shift is much larger than the signal bandwidth) then C_1 is

proportional to βd^2 , and d should be made large, or equivalently the bandwidth should be made very narrow.*

4.4 Design of the Second Ping

The observer's primary goal with the second ping is to measure range, and so he will strive to maximize A_2 given in (2-33). Only the spectrum $|S(\omega)|^2$ is involved in the range measuring capability of a signal; the phase function $\psi(\omega)$ of (2-39) has no effect.

We assume that the estimate of target range rate made with the first ping was sufficiently accurate that w_0 can be considered known. The designer will make use of this knowledge in an attempt to put signal power in frequency bands disjoint from those of the reverberation. However, the previous device of using very narrowband signals is unsatisfactory here since A_2 is essentially a variance of $P(\omega)$ as seen in (2-41), so that $|S(\omega)|^2$ must be dispersed over a wideband.

The problem is then to maximize (see (2-41) and (4-9))

* For rms scatterer velocity of 2 ft/sec., and the typical values of (2-47), $2\beta^2 d^2 \approx 114$.

$$A = k\sigma_o^2 \int_{-\infty}^{\infty} \frac{\omega^2 |S(\omega)|^2}{\Lambda |S(\omega+\omega_o)|_p^2 + N_o} \frac{d\omega}{2\pi} -$$

$$\frac{k\sigma_o^2}{D_o^2} \left[\int_{-\infty}^{\infty} \frac{\omega |S(\omega)|^2}{\Lambda |S(\omega+\omega_o)|_p^2 + N_o} \frac{d\omega}{2\pi} \right]^2 \quad (4-14)$$

The constraints imposed on the signal are:

- i. time-limiting: the signal is wholly contained in $|t| \leq d/2$.
- ii. band-limiting: the signal has bandwidth $2W$.

It is not meaningful in the present context to use the "dispersion bandwidth" of (2-34) as the bandwidth definition, because if only the dispersion bandwidth is restricted in size, the designer is led to use totally unrealistic signal spectra in order to eliminate reverberation. It is shown in Appendix L that reverberation may always be eliminated by spreading the signal power over a sufficiently wide band. The band required would normally be exorbitantly large. Consequently a more realistic constraint is used; an allowed processing band $(-W, W)^*$ is fixed, and is beyond

* This bandwidth might be the fundamental passband of the hydrophone array. Note: W is not to be confused with w , which is a doppler shift.

the control of the observer. All energy at frequencies outside of this band is rejected. This constraint on usable bandwidth is frequently used in practical systems and is convenient analytically: its use simply requires that the integration limits in (4-14) be altered.

The finite limits of integration in (4-14) permit a very useful normalization, which will throw into perspective the quantities under consideration. We define the normalized frequency variable $x = \omega/W$ so that the processing band becomes $|x| \leq 1$. Then we may define normalized signal and reverberation spectra:

$$g(x) = \frac{W}{2\pi 2E} |S(Wx)|^2$$

$$g_p(x) = \frac{W}{2\pi 2E} |S(Wx)|_p^2 \quad (4-15)$$

These functions have unit area (since $|S(\omega)|^2$ has area $2E2\pi$, as in (C-19)):

$$\int_{-1}^1 g(x) dx = \int_{-\infty}^{\infty} g_p(x) dx = 1 \quad (4-16)*$$

* The infinite limits in (4-16) must be used since some of the reverberation power may be spread outside of the processing band $|x| \leq 1$.

If we further define the normalized probability density function of scatterer range rate $p'(x) = W p_w(W_x)$, then from (4-10)

$$g_p(x) = \int_{-1}^1 p'(x-y)g(y) dy \quad (4-17)$$

Hence signal design in the x-domain amounts to choosing appropriate positive unit-area shapes for $g(x)$ in the interval $|x| \leq 1$. Now using the definition of A in (4-14), we obtain

$$A_g = \frac{A}{k \text{ WSNR } W^2} = \int_{-1}^1 \frac{x^2 g(x)}{R g_p(x+\alpha)+1} dx = \frac{1}{\text{SNRF}} \left[\int_{-1}^1 \frac{x g(x)}{R g_p(x+\alpha)+1} dx \right]^2 \quad (4-18)$$

where we define

$$R = 2\pi \frac{2E\lambda}{N_o W} \quad (4-19)$$

$\alpha = w_o/W$: normalized target range rate

$$\text{SNRF} = \text{SNR}/\text{WSNR} = \int_{-1}^1 \frac{g(x)}{R g_p(x+\alpha)+1} dx$$

$$\text{WSNR} = \frac{2E\sigma_o^2}{N_o} \quad : \quad (\text{see page 2-25})$$

A is normalized to A_g by isolating terms which the observer cannot control, and A_g is dimensionless. R is a reverberation power to white-noise-power ratio, since E is proportional to the total reverberation power received, and $N_o W$ is proportional to the white noise power in the processing band. SNRF is the ratio of the signal-to-noise ratio achieved by a particular set $(g(x), \alpha, R, p'(x))$ to that always obtained in the white noise only case. It is a measure of the degradation in signal-to-noise ratio due to reverberation, and equals one if the reverberation is eliminated.

Efficient signal design must also consider the ambiguity problem discussed in Section 2-5, since the performance measure A applies only if gross errors occur with very small probability. In the known range rate case considered here, the ambiguity function $|G(\theta, \theta_o)|^2$ of (2-23) becomes

$$|G(\theta, \theta_o)|^2 \Big|_{\omega=\omega_o} = \left| \frac{1}{D_o^2} \int_{-W}^W \frac{|S(\omega-\omega_o)|^2 e^{j\omega(\tau-\tau_o)}}{N(\omega)} \frac{d\omega}{2\pi} \right|^2 \quad (4-20)$$

Thus the ambiguity function is the squared magnitude of the Fourier transform of $P(\omega)$ of (2-37). Normalizing as before, with $u = W(\tau - \tau_0)$, the ambiguity function becomes:

$$AMB(u) = \left| \frac{1}{SNRF} \int_{-1}^1 \frac{g(x) e^{jux}}{R g_p(x+\alpha)+1} dx \right|^2 \quad (4-21)$$

ex 4-1: $AMB(u)$ for a sample $g(x)$ in White Noise

To show the basic characteristics of $AMB(u)$, we choose a $g(x)$ having two gaussian-shaped lobes separated in frequency as shown in Figure 4-2a. The placement of the lobes makes the value of A_g large. Now since $SNRF=1$ in the white noise only case, we have

$$\begin{aligned} AMB(u) &= \left| \frac{1}{2\sqrt{2\pi}} \int_{-1}^1 e^{jux} \left[e^{-\frac{1}{2}(x-m_1)^2/\beta^2} + e^{-\frac{1}{2}(x-m_2)^2/\beta^2} \right] dx \right|^2 \\ &= \frac{1}{2} e^{-\beta^2 u^2} (1 + \cos(m_1 - m_2)u) \end{aligned} \quad (4-22)$$

As seen in Figure 4-2b, $AMB(u)$ has many large sidelobes which would make the signal unacceptable. A_g , which is proportional to the curvature of $AMB(u)$ at $u=0$ (see the definition of A , (2-26)) is large, but the high sidelobes would make gross errors quite probable so that A_g is a poor measure

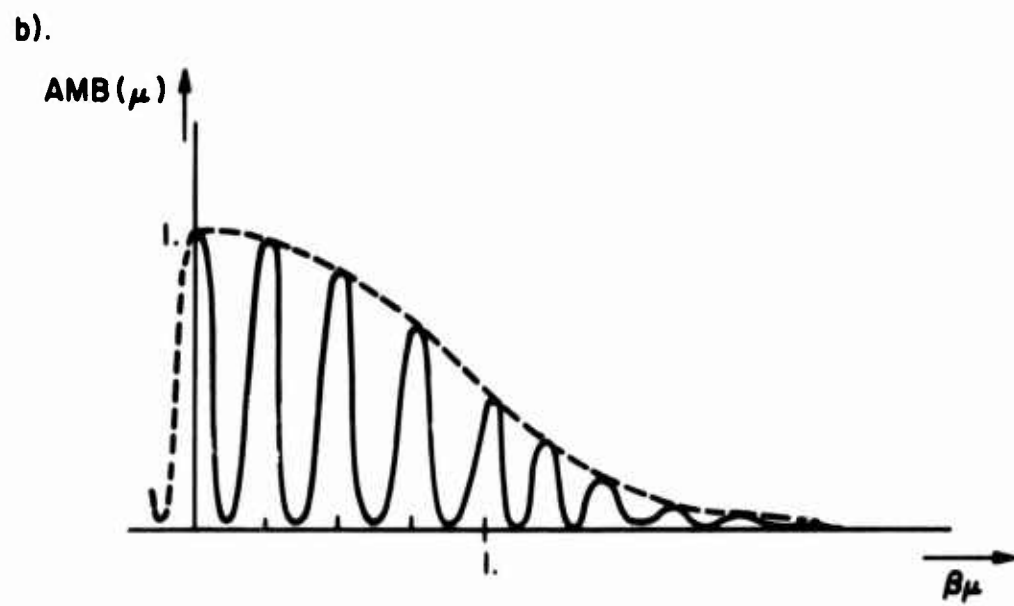
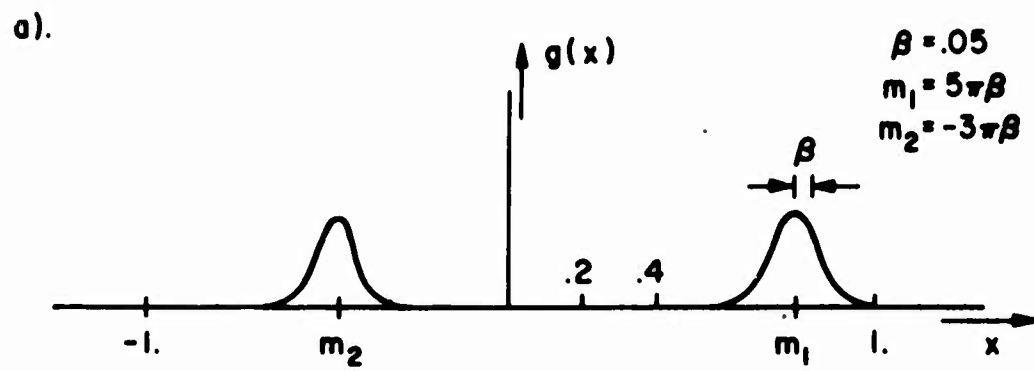


FIGURE 4-2. 2-LOBE SPECTRUM AND AUTOCORRELATION FUNCTION

of performance. The dotted line in Figure 4-2b is the ambiguity function for a $g(x)$ consisting of only a single lobe centered at $x=0$. The curvature of $AMB(u)$ at $u=0$ is much smaller for this signal, but there are no longer any sidelobes. This simple example thus shows the tradeoff that must be made between "small error" estimate variance and ambiguity sidelobes.

4.5 Some Bounds on A_g and Simple Cases

A_g is maximized when only white noise is present, as discussed in Section 4.2. Choosing $g(x)$ symmetrical for convenience, we have from (4-18)

$$A_g = \int_{-1}^1 x^2 g(x) dx \quad (4-23)$$

This is clearly maximized with respect to $g(x)$ by setting $g(x) = \frac{1}{2}(\delta(x-1) + \delta(x+1))$, which yields $A_g=1$. Thus an absolute upper bound for A_g is unity. However, this form for $g(x)$ implies a signal consisting of two sinusoids at $\omega=\pm W$. Such a signal (i), is not duration limited, and (ii) has a totally unacceptable $AMB(u)$. As may be seen by setting $\beta=0$, $m_1-m_2=2$ in (4-22), $AMB(u)$ is periodic in u .

Another choice for $g(x)$ would be a flat shaped

$$g(x) = \begin{cases} \frac{1}{2} & \text{for } |x| \leq 1 \\ 0 & \text{otherwise} \end{cases} \quad (4-24)$$

which yields

$$A_g = \frac{1}{2} \int_{-1}^1 x^2 dx = 1/3, \quad \text{AMB}(u) = \left[\frac{\sin u}{u} \right]^2 \quad (4-25)$$

A_g is 5 dB below the absolute maximum, but $\text{AMB}(u)$ is now

acceptable with maximum sidelobe heights equal to .045.

This form for $g(x)$ will be called the "flat spectrum" case, and will be used as a reference case below.

In contrast to these rather high levels of performance, the strong reverberation case will give an indication of the degradation of A_g to be expected. If both the target and scatterers are not moving, so that their sonar returns look as much alike as possible, we have (see 4-18)

$$A_g = \int_{-1}^1 \frac{x^2 g(x)}{R g(x)+1} dx - \frac{1}{\text{SNRF}} \left[\int_{-1}^1 \frac{x g(x)}{R g(x)+1} dx \right]^2 \quad (4-26)$$

with

$$\text{SNRF} = \int_{-1}^1 \frac{g(x)}{R g(x) + 1} dx$$

Now if $R g(x) \gg 1$ for all x in the band, then

$$A_g \doteq \int_{-1}^1 \frac{x^2}{R} dx = 2/3R \quad (4-27)$$

Consequently, all signal spectra having energy distributed over the whole band yield equally accurate range estimates when target and scatterers are stationary. For smaller values of R where the approximation of (4-27) no longer applies, the optimum $g(x)$ was found using dynamic programming techniques, as discussed in Appendix M. The resulting A_g is shown in Figure 4-3 as a function of R , along with the other examples discussed above. The asymptote $A_g = 2/3R$ is rapidly approached as R increases.

4.6 Some Commonly Used Signals

Certain types of signals have been used frequently in sonar and radar systems⁽⁵⁾, and it is well to examine their ability to combat reverberation interference in the present context.

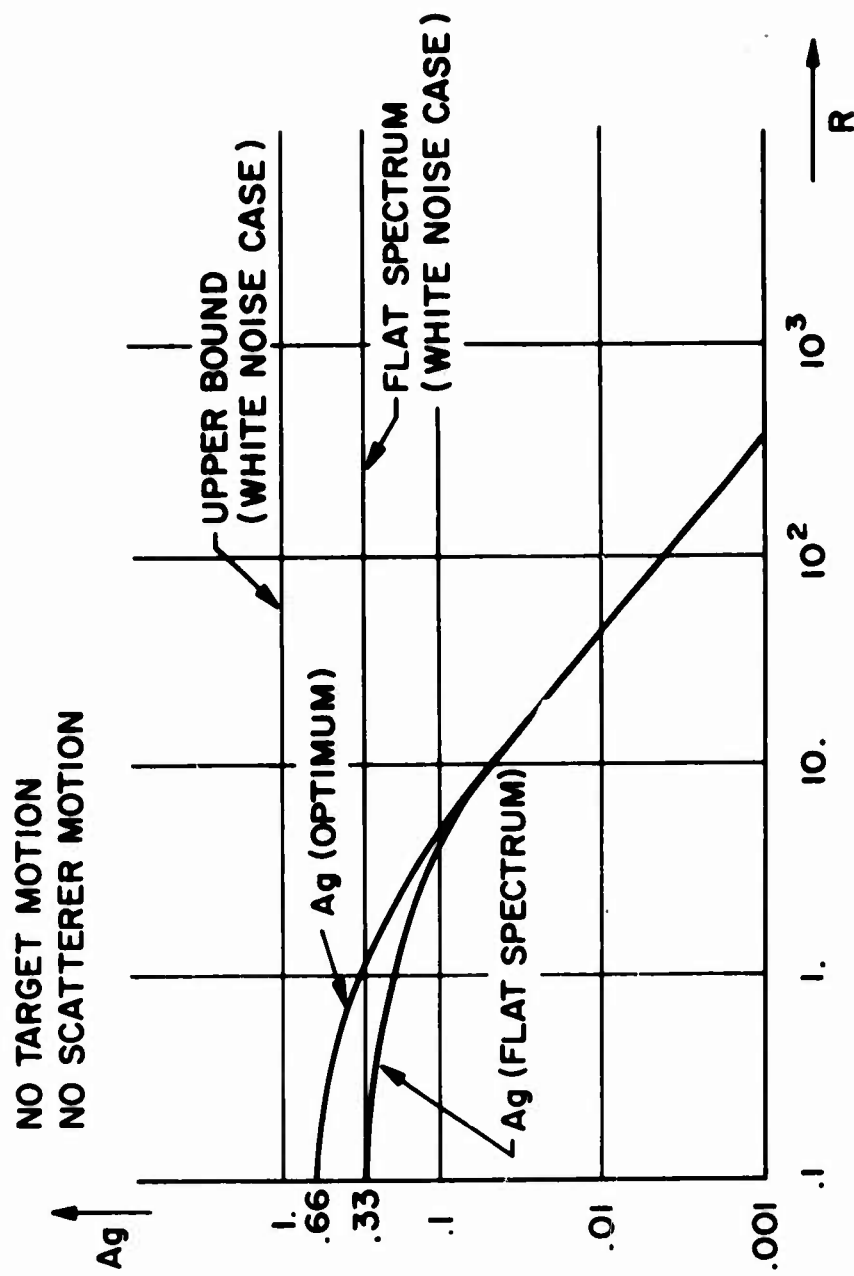


FIGURE 4-3 Ag VS R IN SOME EXTREME CASES

1) LIFMOP SIGNAL

For signals of this type with large duration-bandwidth products, the corresponding spectra are approximately flat over a wide band, and then fall off rapidly outside of this band (ref. 5, p. 208). Thus we can use as an approximation of the LIFMOP spectrum the "flat spectrum" case discussed above. A_g was calculated for such a flat spectrum as a function of target speed, and the results appear as part of Figure 4-4 for the case $R=100$ and no scatterer motion.

(Since this spectrum covers the entire processing band, and typical bandwidths would be much larger than scatterer doppler shifts, the effect of scatterer motion on the shape of $g_p(x)$ would be very small in this example). A rather slow rise in A_g versus α is noted over this range of target, since α is such a small percentage of the total signal band.*

2) Signals with Sinc x-type Spectra

The spectrum of general shape

$$g(x) \propto \text{sinc}^2 vx = \left[\frac{\sin \pi vx}{\pi vx} \right]^2 \quad (4-28)$$

* Using typical values of (2-47) and $W=2\pi(50)$, α and target speed v are related by $v=40\alpha$.

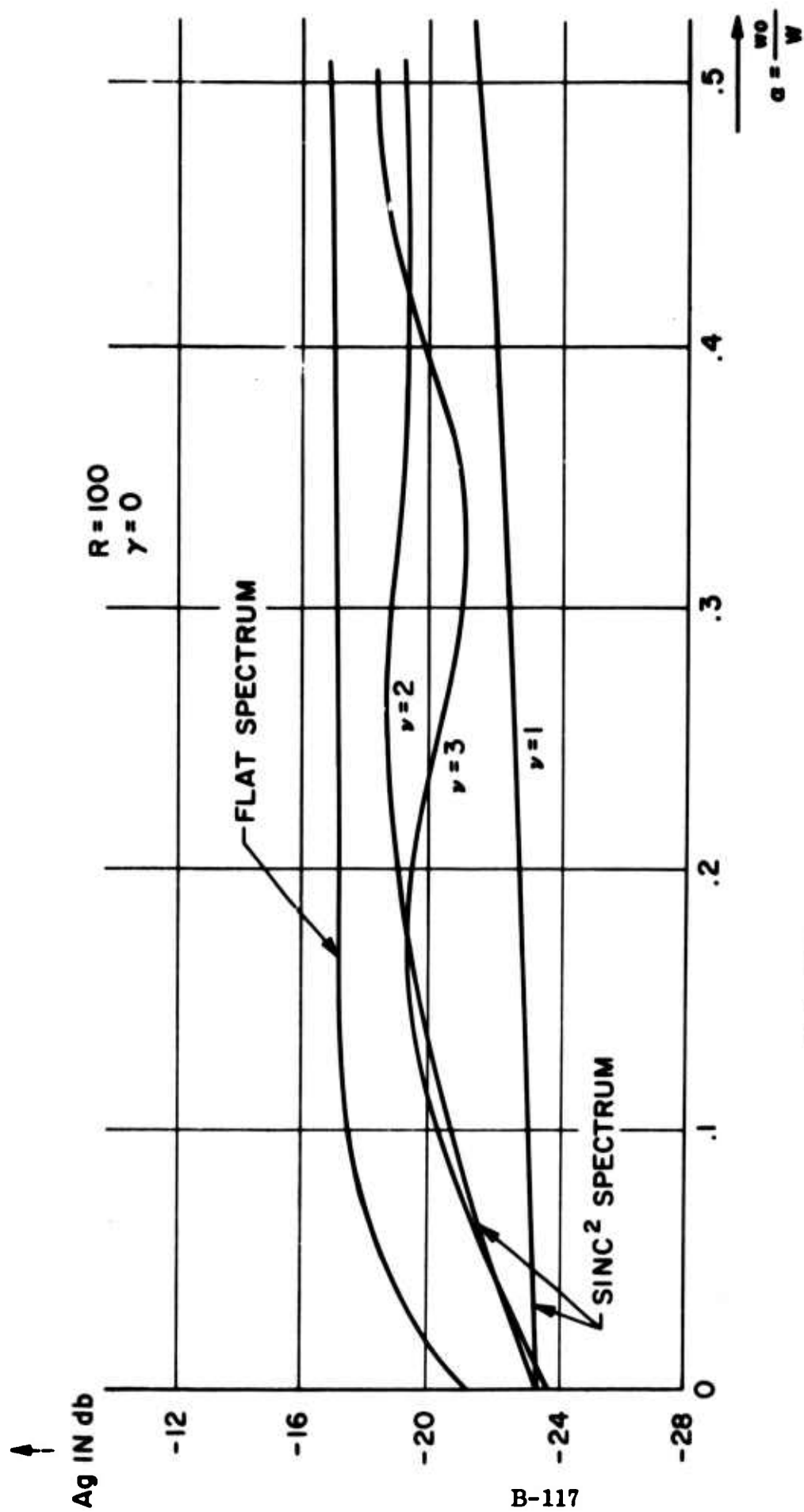


FIGURE 4-4 A_g VS TARGET SPEED

arises repeatedly in radar signal theories^[5]. Simple pulses with rectangular envelopes have spectra of this shape as do some important pulse trains. One such is the "stagger pulse train" class, (Cook & Bernfeld^[5], p. 232) consisting of a burst of, say, 8 short pulses positioned at irregular instants inside the over-all ping duration. The position staggering yields good over-all ambiguity properties. Another signal class with roughly this spectral shape is a pulse train with phase modulated according to one of the Barker codes (ref. 5, p. 245).

Thus we consider the performance A_g associated with the spectrum shape shown in Fig. 4-5. The spectrum is, of course, bandlimited to $|x| \leq 1$, so that different values of v will retain different amounts of the basic sinc^2 shape within the band. For example with $v=1$ only the major lobe of the spectrum lies in the band. For larger v the major lobe is narrower, and one would expect more variation of A_g with target speed in this case. The results are shown in Figure 4-4 for various values of v . A_g is consistently lower than that achieved for the wideband flat spectrum, and furthermore there is not a great deal of variation in

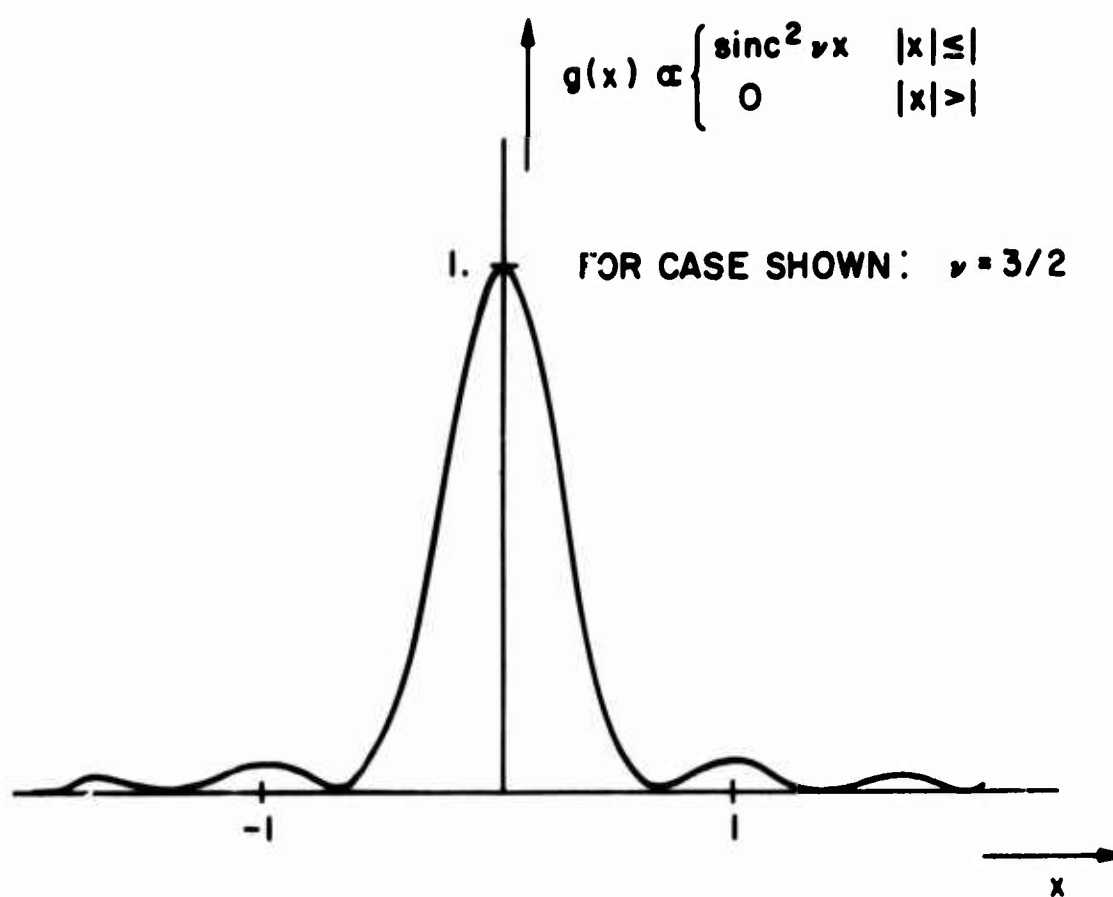


FIGURE 4-5 SINC^2 SPECTRUM EXAMPLE

A_g due to changes in γ . One concludes, therefore, that the LIFMOP signal would perform slightly better than the sinc^2 spectra signals, but that neither seems to take real advantage of the target motion in order to substantially eliminate reverberation. This drawback will be attacked in the following sections, and the RAFMOP signal will also be discussed.

4.7 Multi-lobe Spectra

We introduce the class of spectra consisting of n identical lobes distributed over the band. Each lobe has the basic shape $g_0(x)$, and the lobes are centered at the n frequencies $\underline{m} = (m_1, m_2, \dots, m_n)$. A sample case is pictured in Figure 4-6. The advantage of this spectrum class in the known target range rate case is obvious: the observer will attempt to construct the lobes sufficiently narrow and far apart so that the reverberation lobes will not coincide at all with the signal lobes, yielding complete reverberation elimination. The ambiguity problem will be important here as it limits the observer's ability to choose freely the lobe shapes and positions.

If the chosen spectrum is successful in eliminating the reverberation then we can calculate the ambiguity function $\text{AMB}(u)$ using (4-21).

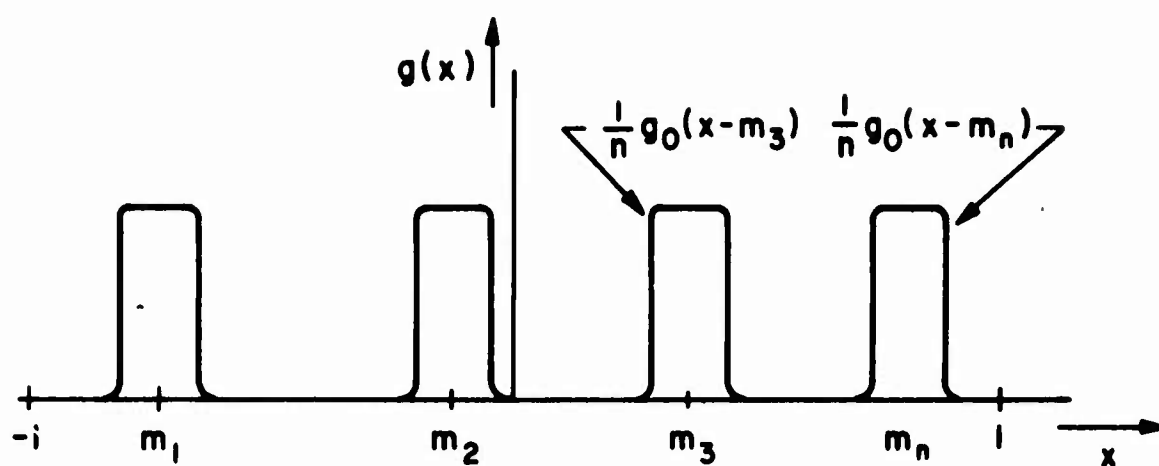


FIGURE 4-6 SAMPLE n -LOBE SIGNAL SPECTRUM

Then

$$\begin{aligned}
 \text{AMB}(\mu) &= \left| \frac{1}{n} \sum_{i=1}^n \int_{-1}^1 g_0(x-m_i) e^{j\mu x} dx \right|^2 \\
 &= \left| \frac{1}{n} \sum_{i=1}^n e^{jm_i\mu} \int_{-1}^1 g_0(y) e^{j\mu y} dy \right|^2 \\
 &= \left| G_0(\mu) \right|^2 C(\mu)
 \end{aligned} \tag{4-29}$$

where $G_0(\mu)$ is the Fourier transform of $g_0(x)$, and

$$C(\mu) = \left| \frac{1}{n} \sum_{i=1}^n e^{j\mu m_i} \right|^2 = \frac{1}{n^2} \left[n + 2 \sum_{i=1}^{n-1} \sum_{j=i+1}^n \cos(m_i - m_j)\mu \right] \tag{4-30}$$

is an oscillatory function consisting of all the intermodulation products, or "beat frequencies" arising from the n frequencies \underline{m} . $C(\mu)$ satisfies $0 \leq C(\mu) \leq C(0) = 1$.

The goal of the observer is to choose the function $g_0(x)$ and the set \underline{m} , under the constraints imposed by the known target range rate and scatterer Doppler spread, so that $R(\mu)$ will have no sidelobe levels above a permissible

height. He must choose \underline{m} carefully so that the white-noise-only case is approximately maintained, and so that $C(\mu)$ remains small for all μ up to some value where the "envelope" $|G_0(\mu)|^2$ has dropped to the allowable sidelobe level. This may or may not be possible depending on the constraints imposed on \underline{m} .

We consider the easily visualized case of a rectangular $g_0(x)$, which drops to zero outside of a set band, $|x| \leq \lambda$, so that $|G_0(\mu)| = \text{sinc}^2\left(\frac{\lambda\mu}{\pi}\right)$. Also, the probability density function of the scatterer motion is chosen rectangular for convenience. (Actually, the only property of $p'(x)$ used is that it drops to zero outside of a given band.) Using $g_0(x)$ and $p'(x)$ as shown in Figure 4-7a) and b), the convolved version $g_p(x)$ is easily obtained and is shown for two cases in Figure 4-7c) and d). From these forms it is a simple matter to determine the target speed α required to shift each signal lobe off its corresponding reverberation lobe. Also one can infer how close the signal lobes may be spaced. The signal and reverberation spectra are superposed in Figure 4-8 for the case where the reverberation interference will just be eliminated,

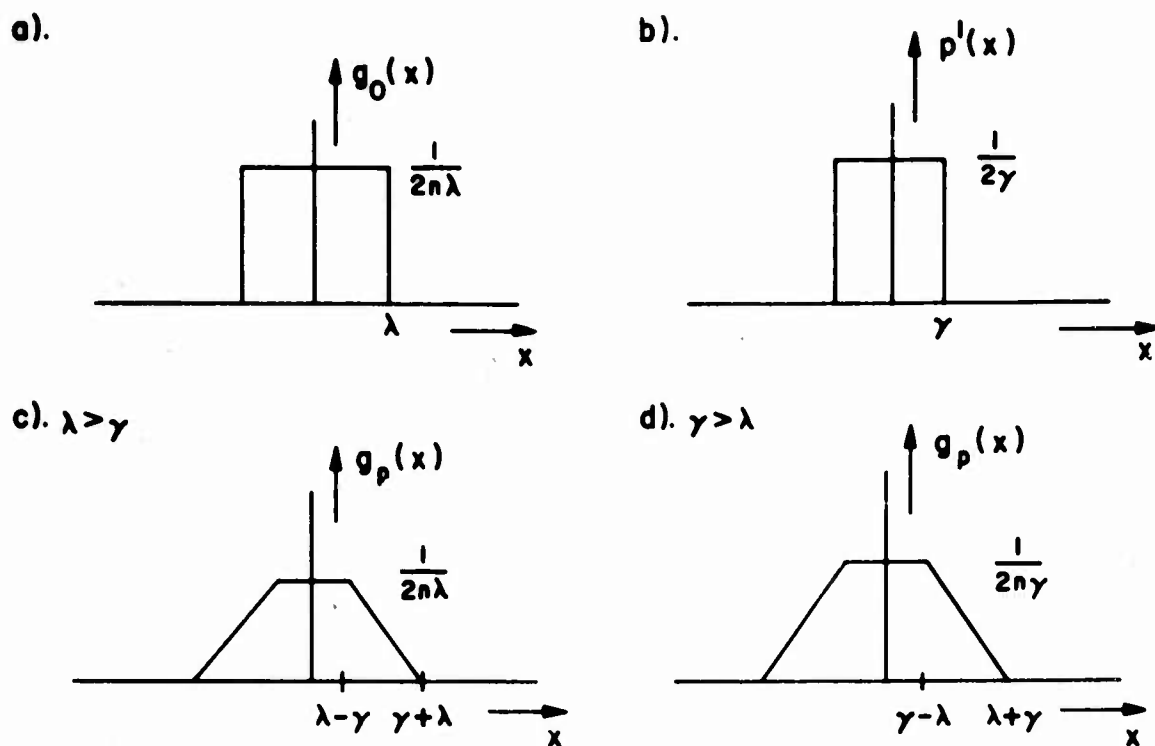


FIGURE 4-7 SAMPLE SPECTRUM, AND RESULTING REVERBERATION SPECTRUM

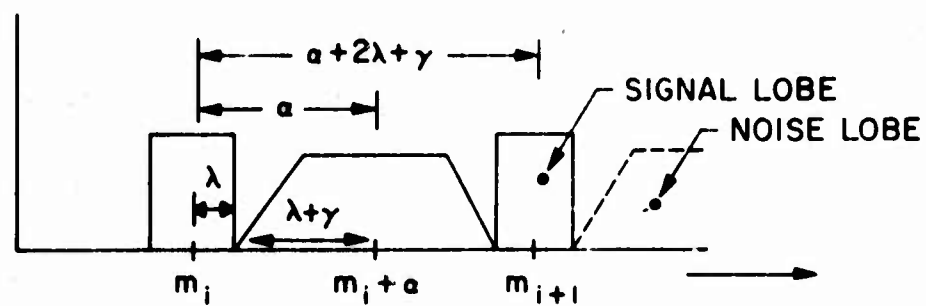


FIGURE 4-8 NECESSARY α AND LOBE SPACING FOR REVERBERATION ELIMINATION

such that any increase in the lobe width would cause some overlap. This then illuminates the constraints that exist. For any given α and γ , we must choose λ and each lobe spacing $\Delta m = m_i - m_{i-1}$, $i = 2, 3, \dots, n$ so that

$$2\lambda + \gamma \leq \alpha$$

$$\Delta m_i \geq \alpha + (2\lambda + \gamma)$$

$$|m_i| \leq 1 - \lambda, \quad \text{all } i \quad (4-31)$$

The last constraint on the size of each m_i forces the lobes to lie wholly within the processing band $|x| \leq 1$. The first constraint shows that if $\gamma > \alpha$ (target range rate smaller than maximum scatterer range rate) the reverberation cannot be completely eliminated.

ex 4-2 Equally spaced lobes

If the observer places the lobes at equal intervals so that $m_i = i \cdot \Delta m$, $i = 0, \pm 1, \pm 2, \dots, \pm(n-1)/2$, then $C(\mu)$ may be written

$$C(\mu) = \left| \frac{1}{n} \sum_{i=-\frac{1}{2}(n-1)}^{\frac{1}{2}(n-1)} e^{j i \Delta m \mu} \right|^2 = \left[\frac{1}{n} \frac{\sin(n \Delta m \mu / 2)}{\sin(\Delta m \mu / 2)} \right]^2 \quad (4-32)$$

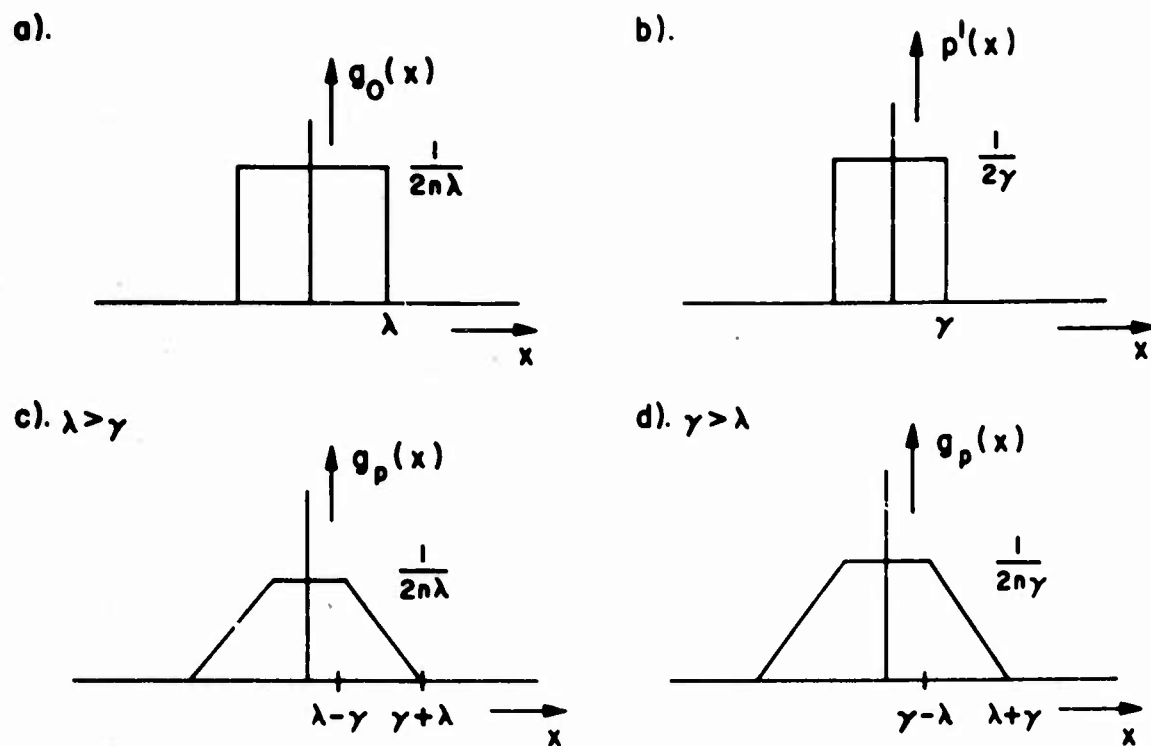


FIGURE 4-7 SAMPLE SPECTRUM, AND RESULTING REVERBERATION SPECTRUM

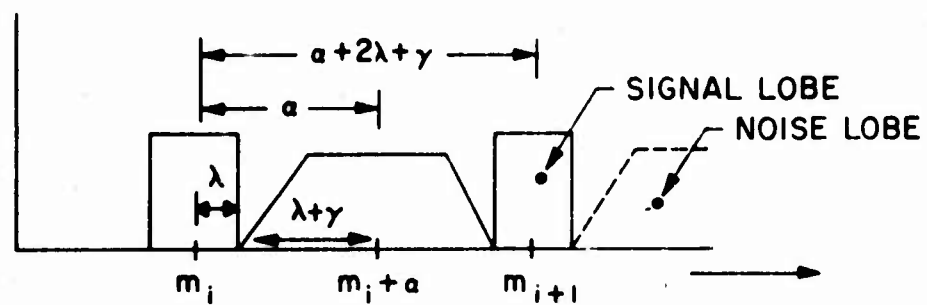


FIGURE 4-8 NECESSARY α AND LOBE SPACING FOR REVERBERATION ELIMINATION

such that any increase in the lobe width would cause some overlap. This then illuminates the constraints that exist. For any given α and γ , we must choose λ and each lobe spacing $\Delta m = m_i - m_{i-1}$, $i = 2, 3, \dots, n$ so that

$$2\lambda + \gamma \leq \alpha$$

$$\Delta m_i \geq \alpha + (2\lambda + \gamma)$$

$$|m_i| \leq 1 - \lambda, \quad \text{all } i \quad (4-31)$$

The last constraint on the size of each m_i forces the lobes to lie wholly within the processing band $|x| \leq 1$. The first constraint shows that if $\gamma > \alpha$ (target range rate smaller than maximum scatterer range rate) the reverberation cannot be completely eliminated.

ex 4-2 Equally spaced lobes

If the observer places the lobes at equal intervals so that $m_i = i \cdot \Delta m$, $i = 0, \pm 1, \pm 2, \dots, \pm(n-1)/2$, then $C(\mu)$ may be written

$$C(\mu) = \left| \frac{1}{n} \sum_{i=-\frac{1}{2}(n-1)}^{\frac{1}{2}(n-1)} e^{ji\Delta m\mu} \right|^2 = \left[\frac{1}{n} \frac{\sin(n\Delta m\mu/2)}{\sin(\Delta m\mu/2)} \right]^2 \quad (4-32)$$

sometimes called the Fourier Series kernel (Guillemin^[21], p. 485, Papoulis^[13], p. 44). This function is sketched in Fig. 4-9, and is seen to be periodic $2\pi/\Delta m$. For an even number of lobes, omitting the lobe at $x=0$, we would have

$$C(\mu) = \frac{1}{n^2} \left[\frac{\sin[(n+1)\Delta m\mu/2]}{\sin[\Delta m\mu/2]} - 1 \right]^2$$

which has the same periodicity, with slightly narrower large lobes. In both cases the sidelobes are of height inversely proportional to n and acceptably small, so that only the periodic peaks need concern us. We must insure that the function $|G_o(\mu)|^2$ is acceptably small for $\mu = 2\pi/\Delta m$ in order that this class of spectra be allowed. If the permitted sidelobe height is made equal to .5, then since $\text{sinc}^2(\lambda\mu/\pi) = .5$ for $\lambda\mu = 1.39$, we have the requirement on λ and Δm : $\lambda (2\pi/\Delta m) \geq 1.39$. If we push the constraints of (4-31) to their limit and use $\lambda = \frac{1}{2}(\alpha-\gamma)$, $\Delta m=2\alpha$, then the condition becomes

$$\frac{1}{2}(\alpha-\gamma)2\pi/2\alpha = \frac{\pi}{2}(1-\gamma/\alpha) > 1.39 \quad (4-33)$$

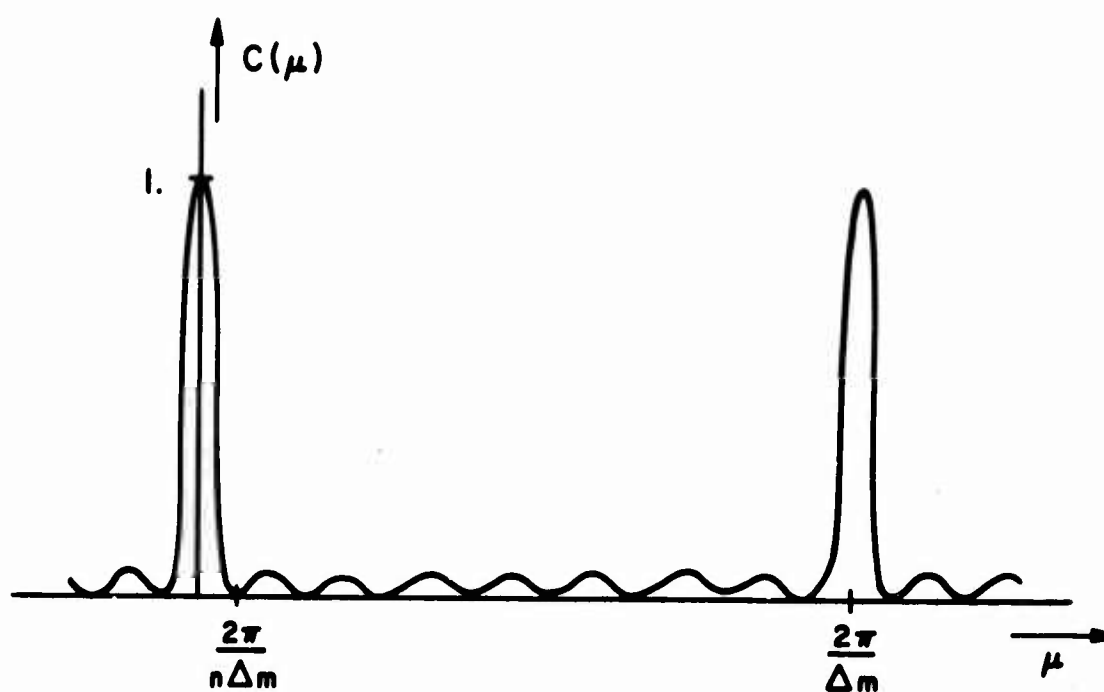


FIGURE 4-9 $C(\mu)$ FOR n EQUALLY SPACED SPECTRAL LOBES

or

$$\gamma/\alpha < .12$$

Thus if the clutter can move at speeds no more than 12% of the known target speed then one may use equally spaced lobes. Of course (4-31) also requires $2\lambda \leq \alpha$, and the signal duration constraint places a lower limit on the size of λ (note: a spectrum width of 2λ implies a signal duration of order $1/2\lambda$), so these results only pertain to the case where α is sufficiently large. One must also keep in mind that the above case yields a marginal situation. If the acceptable sidelobe level were reduced to .4, for example, the constraint on λ and Δm would be $\lambda(2\pi/\Delta m) \geq 1.6$, leading to $\frac{\pi}{2}(1 - \gamma/\alpha) \geq 1.6$, which is obviously impossible. Thus one sees that the equally spaced lobe signal has marginal utility except in special cases, and care must be exercised in judging its performance.

.

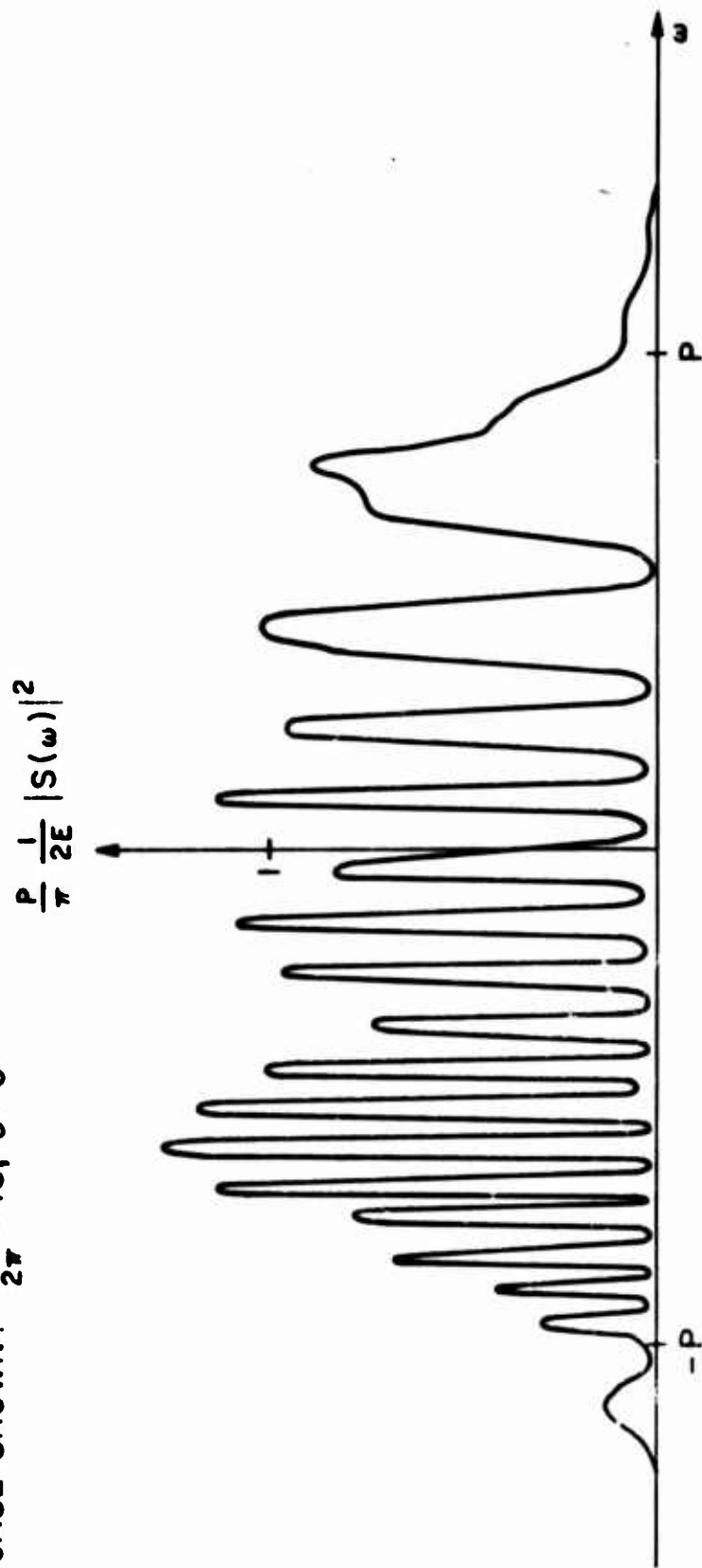
ex 4-3 The RAFMOP Class of Signals

Signals of the RAFMOP class have very complicated spectra, because the frequency modulation $\dot{\phi}(t)$ (see Figure 2-6) sweeps through its range of values more than once and

in opposite directions. This causes phase interference in the frequency domain, producing spectra with many closely spaced lobes. The general form for $|S(\omega)|^2$ is derived in Appendix F for the case $\delta=0$, and a sample spectrum is shown in Figure 4-10. A computer routine was used to generate RAFMOP spectra, and showed that changing P or δ can markedly alter both the number and spacing of the lobes. For large values of P (desirable in order to achieve a large bandwidth) the lobes are very close together and spaced in a complicated manner (see Appendix F). Despite the many narrow lobes this signal still has an acceptable ambiguity function (at least in the white noise case) as discussed by Cook & Bernfeld^[5, p. 97].

Because of the complicated spectral forms for this signal class, it would be extremely difficult to use RAFMOP signals in an attempt to combat reverberation, since there are only two degrees of design freedom (P and δ). The nature of the lobe spacing could make the RAFMOP signal useful only for very small target and scatterer speeds, and even then there is no control over any ambiguity problems that might arise in the absence of complete reverberation elimination. The observer should therefore avoid

CASE SHOWN: $\frac{P_d}{2\pi} = 16, \delta = 0$



B-130

FIGURE 4-10 SPECTRUM OF RAFMOP SIGNAL

using RAFMOP signals, since they concentrate large amounts of energy in small bands. For unfavorable target speeds at least some of the signal and reverberation lobes will tend to overlap due to the irregular spacing, causing worse interference than if a flat spectrum had been used.

Returning to the multi-lobe spectrum class of Figure 4-6, for non-equally spaced lobes the periodic structure of $C(\mu)$ can be destroyed, in hopes that these large sidelobes will be reduced to acceptable levels. From (4-30) the goal will be to prevent too many of the "beat frequency" cosines from adding constructively at any value of μ away from $\mu=0$. This requires that the beat frequencies be in some way incommensurate. Considering the multiplicity of constraints on the m_i , no straight forward algorithm for choosing \underline{m} seems possible. Instead a trial and error method was used for each pair δ, γ , selecting λ and a permissible \underline{m} (for reverberation elimination) and determining the sidelobe heights, until the desired conditions were met.

ex 4-3 Sample Result

Let $\alpha = .1$, $\gamma = .05$, and the acceptable minor lobe height be $.5$. Then the constraints are $\lambda \leq .025$, $\Delta m \geq .2$. If $\lambda = .025$ is actually used, then at most 10 lobes can be

fitted into the band. The following vector \underline{m} was found to be satisfactory, with performance A_g also noted. (SNRF=1 since reverberation was eliminated.) $AMB(\mu)$ is sketched in Figure 4-11.

$$\underline{m} = [.9, .7, .45, .2, 0., -.25, -.48, -.82]$$

$$A_g = .305 = -5.15 \text{ dB} \quad (4-34)$$

One can see by examining the differences $m_i - m_j$ above that there are several occurrences of $\Delta m = .2$ and $.25$. These make up the major contributions to the main sidelobes (at $\mu = 2\pi/\Delta m$, which here were $\mu = 8\pi$ and 10π). Only eight lobes were used here, in order to allow more freedom in placing them. The performance level $A_g = .305$ is very near the level of $.333$ achieved for the flat spectrum signal in white noise (see (4-25)). Thus the placement of several narrow lobes across the band both eliminates reverberation and achieves the same level of performance as the simple broadband signal in white noise.

Other choices of \underline{m} were made, and for slight shifts of the lobes the function $AMB(\mu)$ changed markedly. Therefore

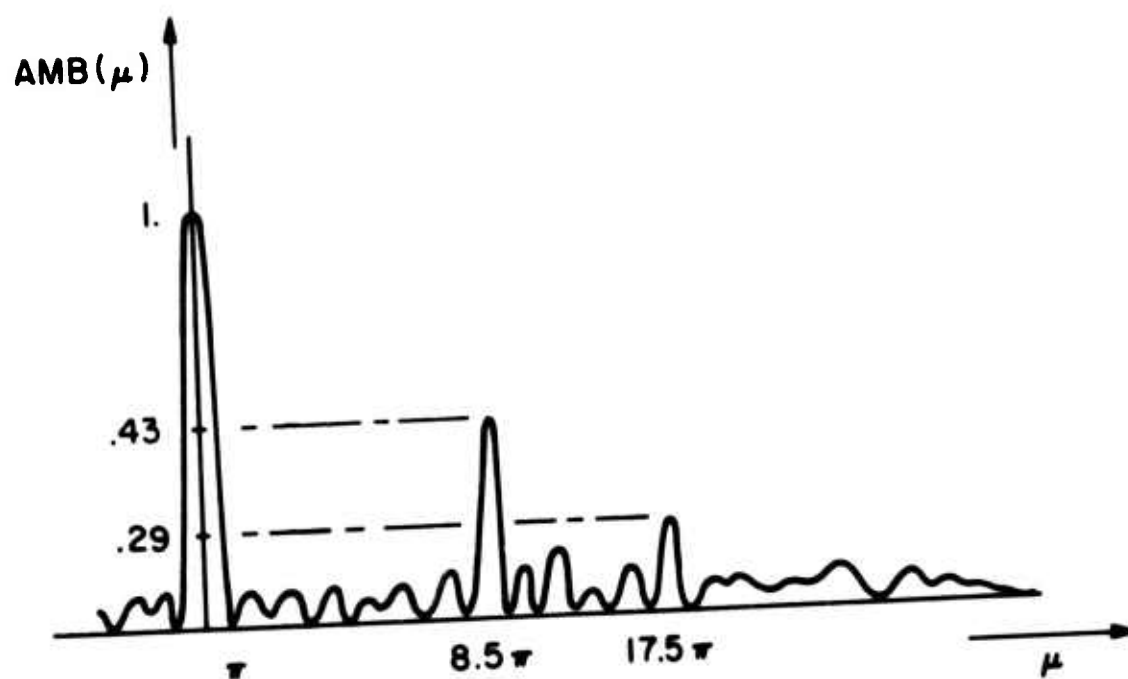


FIGURE 4-11 $AMB(\mu)$ FOR SPECTRUM OF EXAMPLE 4-3

this scheme does not offer an easily implemented design procedure, although with care the observer could indeed construct such a signal by sending tones at the frequencies \underline{m} , either in rapid succession or simultaneously. (The phase interference problem associated with the RAFMOP signals would be absent since only different tones are sent during the ping duration.) The important conclusion here is that there exists a signal which eliminates reverberation while yielding an acceptable ambiguity function.

.

The trial and error procedure mentioned above yielded the results plotted in Figure 4-12, showing A_g versus α . The sidelobe height permitted was set to .5 when SNRF=1 (reverberation elimination case). It can be seen that for a certain range of values of α and γ , A_g is equal to or slightly above the flat spectrum in white noise case (from (4-25) we had $A_g = 1/3 = -4.8$ dB), so that the effect of reverberation interference has been completely eliminated.* The regions in which this level is

* Actual levels of A_g vs α range $\pm .4$ dB about the straight line shown. The single line is shown for clarity.

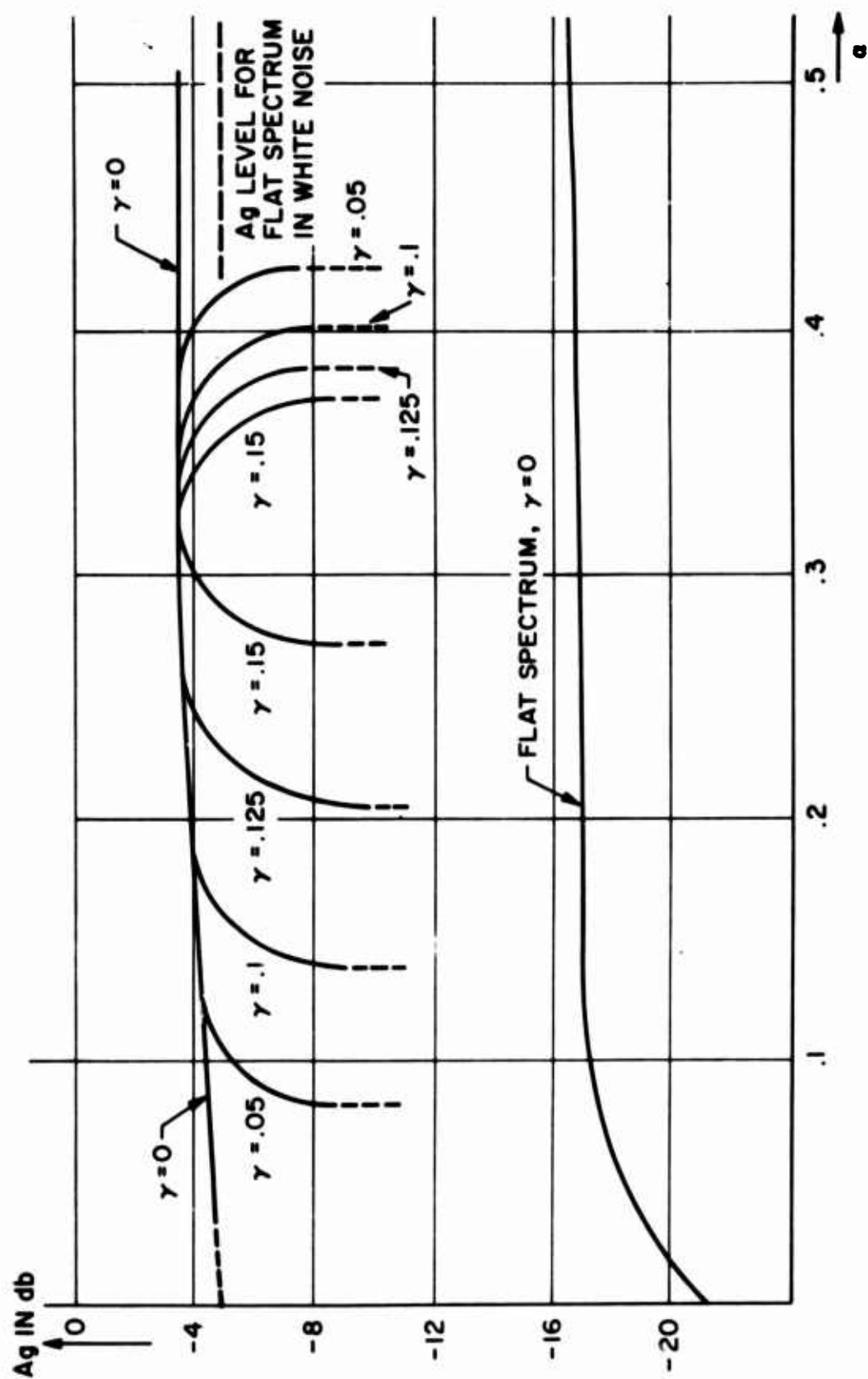


FIGURE 4-12 A_g VS α FOR MULTI-LOBE SPECTRA

attained have both upper and lower cutoffs, and outside these regions the multi-lobe spectra class cannot be used, due to excessive ambiguity.

1) $\gamma=0$.

The lower cut-off is not actually shown in the figure, as it is determined only by the minimum width of each lobe, which depends on the signal duration constraint (see discussion on page 4-26), and in practice would be very small. Since the ratio γ/α is here equal to zero, we can always use equally spaced lobes (see example 4-2).

2) $\gamma \neq 0$.

The lower cut-off now occurs when α approaches γ in value, for then λ must be made small in order to keep the signal and reverberation lobes separate (see first constraint in (4-31)) and a small λ gives rise to excessive ambiguity. The upper cut-offs occur when only a few lobes will fit in the band with the proper spacing (see second and third constraints in (4-31)). When only a few lobes may be used, there is little chance of choosing m so that the beat frequencies will interact sufficiently to keep $C(u)$ small. It is indeed possible to find 3 suitable lobes for some α and γ , but as α increases this ability finally disappears.

Beyond these cut-offs one must turn to different kinds of signals. Since the reverberation can no longer be completely eliminated, the SNRF will be reduced. With a smaller signal-to-noise ratio the allowable ambiguity sidelobe level will have to be reduced, since gross errors will become more probable (see Figure 2-3). Consequently only signals which inherently have low ambiguity levels will be usable. The most promising of these is the flat spectrum signal discussed above, and its performance displayed in Figure 4-4 is reproduced in Figure 4-12 with $R=100$ as before. (Note: the multi-lobe spectra performance in Figure 4-12 applies for all levels of R since the reverberation has been successfully avoided.) The value of A_g is about 13 dB lower for the flat spectrum signal than for the multi-lobe spectrum with the reverberation eliminated. This is a significant change in the performance level, and shows that proper signal design with the knowledge of the target range rate can yield greatly improved range estimate accuracy.

CHAPTER 5

Conclusions and Proposals for Further Research

The basic motivation for this research was a desire to see what could be done to improve the target locating abilities of active sonar in a reverberation-limited environment. The examination was enlarged to include improvements attainable if the observer could send a sequence of signal bursts, and alter successive sonar waveforms to take advantage of information already gained. Thus the problem was naturally divided into two categories: a) estimation accuracy in the presence of colored noise, and b) effect of several pings and of the interping elapsed times. An additional effect was examined: the degradation of the estimator when the observer must wait after receiving the data before making use of it; i.e., it was asked: what is the accuracy of the observer's estimate of the target's present location given data taken t_w seconds in the past?

The approach taken was based on the inverse probability principle, which was used to derive the estimator

for a single ping received in the presence of colored gaussian noise. The estimator was shown in this case to be a prewhitening filter followed by a filter matched to delayed and Doppler shifted versions of the transmitted signal. The inverse probability approach instructs the observer to examine the filter output for each possible pair of values (delay and Doppler shift), and to choose as his estimate that pair having the largest output.

The estimate accuracy was evaluated for the large signal-to-noise ratio case in the manner used by Kelly, Reed & Root⁽⁶⁾, which relates the estimate error variance to the curvature of the inverse probability function at the true value of delay and Doppler. The applicability of this method was examined, and a probability of "gross error" was defined, being the probability that the inverse probability function would not peak on the main ambiguity lobe. If a gross error occurred the estimate error variance measure did not apply. This probability of gross error was approximated and shown to depend on the signal-to-noise ratio and the relative heights of the ambiguity function sidelobes. That is, for a preset value of this probability,

and a known signal-to-noise ratio, a certain ambiguity function sidelobe level was permissible. The highest sidelobes could occur anywhere in the delay-Doppler plane.

Assuming that a gross error did not occur, the error variance measure was adopted, and was extended from the Kelly, Reed & Root formulation to a form much more easily dealt with. It was shown that the various estimate moments that arise may be expressed in the form of central moments with respect to a density function $P(\omega)$, see (2-37). This function described the effect of the noise properties as well as those of the signal spectrum, and its shape depended strongly on the true target speed. The effect of the target speed was to shift the signal and noise spectra with respect to one another along the frequency axis, an effect which has great significance in combatting reverberation.

The analysis was then extended to the multiple ping, elapsed time case, and the important case of two pings was considered in detail. The general expression for the range estimate variance at time t_w seconds after the second ping was found as a function of the individual ping

performances, the elapsed time between pings, and the wait time t_w . It was shown that the wait time, if sufficiently large, could cause severe degradation of the range estimate. The degradation resulted from the imperfect range rate knowledge, since as time progressed an error in the range rate estimate would adversely affect the observer's extrapolation to the target's range at a later time. This degradation could be ameliorated, however, by using a long inter-ping time. This long time between pings effectively separated the roles of the two pings, making the first an estimator of target range rate, and the second an estimator of target range. In this way the first ping effectively reduced the region of the ambiguity plane to be considered, so that the wait time following the second ping had only a small effect on the range estimate accuracy. For the case of white noise the optimum individual ping design parameters were found, and the optimum amount of correlation between the estimates of range and range rate was calculated. In many cases this correlation should be as large as possible (a conclusion very different from that when no elapsed time considerations are made), and thus signals such as the

linear frequency modulated chirp would be very useful. In other cases little correlation is desired, and a signal was introduced that permitted an adjustable amount of correlation. The use of two pings as opposed to a single ping was considered, and it was shown that two pings could significantly improve the final range estimate accuracy, especially if long wait times were required. In the white noise case adaptive signal design did not apply under the assumptions used, for the knowledge of target range or range rate obtained approximately from the first ping was of no use in redesigning the second ping. The optimum second ping was indeed different from the first ping, but the observer knew which second ping to send before the first ping was sent.

The problem of combatting reverberation (clutter) interference was then considered explicitly. The spectrum for a process consisting of white noise plus clutter was derived in terms of the transmitted signal spectrum, using a scatterer model of Van Trees, and the estimator performance was evaluated in terms of this spectrum. It was shown that when a long interpinging time was used (so that the first ping should be used for range rate measurement), the first

ping should be very narrowband, so that even small target range rates would be sufficient to shift the signal spectrum away from the reverberation spectrum. The degradation due to reverberation was then eliminated, and only white noise interference remained. The very accurate range rate estimate that resulted had two important effects: 1) the interping time required to cause the separation of roles of the first and second pings was reduced, and 2) the knowledge of target range rate could be put to excellent use in the design of the second ping. It is in this sense that the signal design is adaptive, for the observer must wait until the first ping echo has been processed and an estimate of range rate has been made before he can select the best second ping. Over a wide range of target and scatterer speeds it was shown that a signal consisting of several tones could eliminate the effects of reverberation. Such signals have multi-lobe spectra, the lobes of high power density being separated by frequency bands of very low power density. The target speed caused the signal and reverberation spectrum lobes to be disjoint and interleaved, so that the reverberation had no effect. The tones had to be chosen carefully so that

the signal had an acceptable ambiguity function. When the target and scatterers were moving with nearly the same range rate, or when their range rates were very large, no acceptable multi-lobe spectrum was found due to excessive ambiguity problems, and a more conventional signal had to be used. Hence the effect of reverberation could no longer be eliminated, and performance was severely degraded. It was shown that the estimate variances of signals commonly used in radar and sonar systems could be increased by about 100 times due to strong reverberation. Thus the multi-lobe signal, when applicable, could significantly improve the estimate accuracies.

Recommendations for Future Research

Probably the greatest single fault of the analysis presented here is the simplicity of the models for the target and transmission medium. The assumption of a point target and a single-path transmission is not supported by actual measurements, and the true ocean situation can lead to severe degradation of performance due to multi-path arrivals of the target echo. The estimate accuracies calculated here turned out very high, and it is believed that the simple model used was the cause of this. The model was

chosen for its mathematical tractability, since the multi-path situation is extremely difficult to analyze. Future work should consider extensions of the analysis here to two or more transmission paths, as well as two or more target reflection points, or "highlights." This could alter the conclusions concerning the signal design problem for clutter rejection, although it is not believed that the conclusions concerning elapsed time and interpulse time would be significantly changed.

Only the case of a target moving with constant course and speed was investigated, while the interesting situation where the target can change course after the first ping was not examined. This could well lead to rather different conclusions about the effects of two pings over one, and the effects of waiting time.

The reverberation model could be extended in several useful directions. It would be interesting to know what effect correlations between scatterer motions would have, to see if schools of fish would generate radically different clutter rejection problems than clusters of randomly moving scatterers. The difficulty in distinguishing a

coherently moving school of fish from a true target (with multiple reflecting highlights) could then be investigated.

APPENDIX A: Discussion of Target Motion Geometry

We consider the configuration shown in Figure A-1, where the target is assumed to be located at range r_0 at $t=0$, and is proceeding at speed v_t at an angle α with respect to line L.

The range to the target is simply described by

$$r(t) = \sqrt{(r_0 - tv_t \cos \alpha)^2 + (v_t t \sin \alpha)^2}$$
$$\approx |r_0 + v_0 t| \quad (A-1)$$

where $v_0 = -v_t \cos \alpha$

so chosen to make v_0 positive for receding targets.

The approximation used in (A-1) is clearly valid as long as the target is sufficiently remote so that the distance travelled perpendicular to L is always small compared to the distance remaining along L.

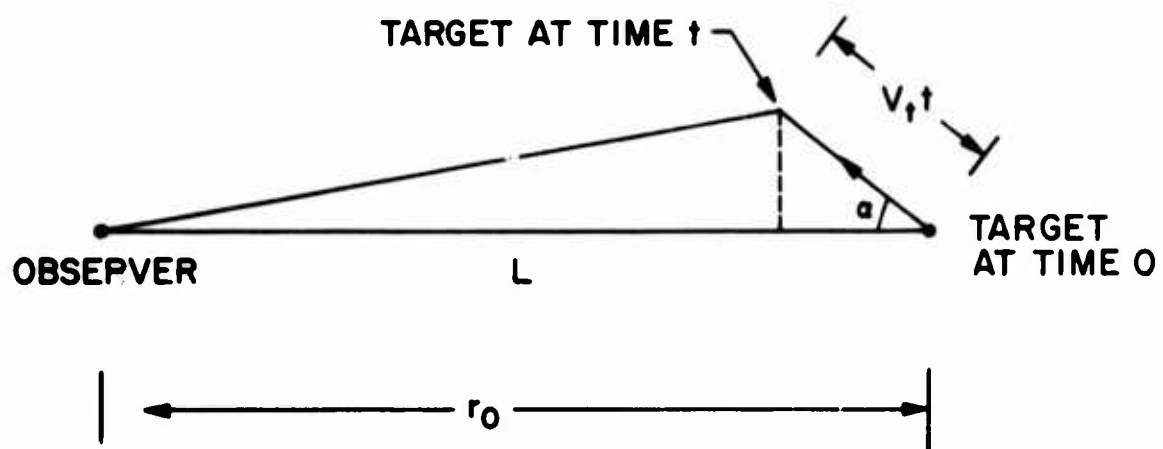


FIGURE A-1 TARGET MOTION GEOMETRY

APPENDIX B: Approximate Probability of Gross Errors

1. The Statistics of $|K(\theta)|^2$

From (2-24) we can write $|K(\theta_1)|^2$ as

$$|K(\theta_1)|^2 = \text{SNR}|G_{10}|^2 + 2\text{Re} \underline{\sigma}_0 D_0 G_{10} N'^*(\theta_1) + |N'(\theta_1)|^2 \quad (\text{B-1})^*$$

where $D_0 = D(\theta_0)$

$$\text{SNR} = \sigma_0^2 D_0^2$$

$$G_{10} = G(\theta_1, \theta_0)$$

$$N'(\theta_1) = \frac{1}{D(\theta_1)} \int \frac{n(\omega) S^*(\omega - \omega_0) e^{j\omega\tau}}{N(\omega)} \frac{d\omega}{2\pi} = \frac{1}{D(\theta_1)} \sum_k \frac{n_k s_k^*(\theta_1)}{N(\omega_k)}$$

and the n_k are independent gaussian random variables, with independent real and imaginary parts, each with variance $N(\omega_k)/2T$. For the large signal to noise ratio case, we can neglect the $|N'(\theta_1)|^2$ term. Then $|K(\theta_1)|^2$ is the sum of a deterministic part $\text{SNR}|G_{10}|^2$ and a zero mean gaussian part. Hence

$$E|K(\theta_1)|^2 = \text{SNR}|G_{10}|^2 \quad (\text{B-2})^{**}$$

$$^* |\underline{\sigma}_0|^2 \equiv \sigma_0^2,$$

** E is the expectation operator

The covariance C_{12} of two distinct random variables $|K(\theta_1)|^2$ and $|K(\theta_2)|^2$ may be calculated as follows:

$$\begin{aligned}
 C_{12} &= E \left[\left[|K(\theta_1)|^2 - \text{SNR} |G_{10}|^2 \right] \left[|K(\theta_2)|^2 - \text{SNR} |G_{20}|^2 \right] \right] \\
 &= 4E \text{Re} \left[\sigma_o D_o G_{10} N'^*(\theta_1) \right] \text{Re} \left[\sigma_o D_o G_{20} N'^*(\theta_2) \right] \\
 &= E \sigma_o^2 D_o^2 G_{10} G_{20} N'^*(\theta_1) N'^*(\theta_2) + E \left[|\sigma_o|^2 D_o^2 G_{10} G_{20}^* \right. \\
 &\quad \left. N'^*(\theta_1) N'(\theta_2) \right] \quad (B-3) \\
 &\quad + E |\sigma_o|^2 D_o^2 G_{10}^* G_{20} N'(\theta_1) N'^*(\theta_2) \\
 &\quad + E \sigma_o^{*2} D_o^2 G_{10}^* G_{20}^* N'(\theta_1) N'(\theta_2)
 \end{aligned}$$

which makes use of the identity $\text{Re}A = \frac{1}{2} (A + A^*)$. Now

$$E N'(\theta_1) N'(\theta_2) = \frac{1}{D(\theta_1) D(\theta_2)} \sum_i \sum_j \frac{\overline{n_i n_j} s_i^*(\theta_1) s_j^*(\theta_2)}{N(\omega_i) N(\omega_j)} = 0 \quad (B-4)$$

since $\overline{n_i n_j} = 0$. Similarly for $E N'^*(\theta_1) N'^*(\theta_2)$. On the other hand

$$\begin{aligned}
EN'(\theta_1)N'^*(\theta_2) &= \sum_i \sum_j \frac{\overline{n_i n_j^*} s_i^*(\theta_1) s_j(\theta_2)}{D(\theta_1) D(\theta_2) N(\omega_1) N(\omega_j)} \\
&= \frac{1}{2T} \sum_i \frac{s_i^*(\theta_1) s_i(\theta_2)}{D(\theta_1) D(\theta_2) N(\omega_1)} = G(\theta_1, \theta_2)
\end{aligned}
\tag{B-5}$$

Combining the results,

$$\begin{aligned}
C_{12} &= \sigma_o^2 D_o^2 (G_{10} G_{20}^* G_{12}^* + G_{10}^* G_{20} G_{12}) \\
&= 2 \text{ SNR } \text{Re}(G_{10} G_{12}^* G_{20}^*)
\end{aligned}
\tag{B-6}$$

Thus $|K(\theta_1)|^2$ has variance (use $\theta_2 = \theta_1$ in (B-6), and $G_{11} = 1$)

$$\text{var } |K(\theta_1)|^2 = 2 \text{ SNR } |G_{10}|^2 \tag{B-7}$$

If we consider the correlation between $|K(\theta_1)|^2$ and the value $|K(\theta_o)|^2$ at the true peak, we have (use $\theta_2 = \theta_o$)

$$C_{10} = 2 \text{ SNR } |G_{10}|^2 \tag{B-8}$$

The correlation coefficient is then

$$\rho = \frac{C_{12}}{\sqrt{\text{Var } |K(\theta_o)|^2 \text{Var } |K(\theta_1)|^2}} = |G_{10}| \tag{B-9}$$

Thus the random variables $x=|K(\theta_0)|^2$ and $y=|K(\theta_1)|^2$ are jointly gaussian with moments

$$\begin{aligned} E_x &= \text{SNR}, & E_y &= \text{SNR } \rho^2 \\ \text{var } x &= 2 \text{ SNR}, & \text{var } y &= 2 \text{ SNR } \rho^2 \end{aligned} \quad (\text{B-10})$$

so that their joint distribution is

$$\begin{aligned} p_{x,y}(x,y) &= \left[2\pi 2\text{SNR}\rho \sqrt{1-\rho^2} \right]^{-1} \exp \left[-\frac{1}{2} \frac{1}{2\text{SNR}} \frac{1}{1-\rho^2} \left[(x-\text{SNR})^2 \right. \right. \\ &\quad \left. \left. -2(x-\text{SNR})(y-\rho^2\text{SNR}) \right. \right. \\ &\quad \left. \left. + \frac{1}{\rho^2} (y-\rho^2\text{SNR})^2 \right] \right] \end{aligned} \quad (\text{B-11})$$

2. Calculation of the Probability that $|K(\theta_1)|^2$ Exceeds

$$\underline{|K(\theta_0)|^2}$$

The probability that y exceeds x is the total weight of $p_{x,y}(x,y)$ in region II given by $\{(x,y): y \geq x\}$. We have the line $y=x$ and the function $p_{x,y}(x,y)$ of Equation (B-11). To simplify these we use the following transformations:

I. Translation and Normalization:

$$\begin{aligned} x' &= (x-\text{SNR})/\sqrt{2 \text{ SNR}} \\ y' &= (y-\rho^2\text{SNR})/\rho \sqrt{2 \text{ SNR}} \end{aligned} \quad (\text{B-12})$$

II. Rotation of Coordinates in order to make the random variables uncorrelated:

$$\begin{pmatrix} x'' \\ y'' \end{pmatrix} = \frac{1}{\sqrt{2}} \begin{bmatrix} 1 & 1 \\ -1 & 1 \end{bmatrix} \begin{pmatrix} x' \\ y' \end{pmatrix} \quad (\text{B-13})$$

III. Renormalization:

$$\begin{pmatrix} \xi \\ \eta \end{pmatrix} = \begin{bmatrix} \frac{1}{\sqrt{1+\rho}} & 0 \\ 0 & \frac{1}{\sqrt{1-\rho}} \end{bmatrix} \begin{pmatrix} x'' \\ y'' \end{pmatrix} \quad (\text{B-14})$$

These transformations result in the new probability density function

$$p_{\xi, \eta}(\xi, \eta) = \frac{1}{2\pi} e^{-1/2(\xi^2 + \eta^2)} \quad (\text{B-15})$$

and in the new line describing the border of Region II,

$$\sqrt{1+\rho} \eta = \sqrt{1-\rho} \xi + \sqrt{\text{SNR}} \sqrt{1-\rho^2} \quad (\text{B-16})$$

This line has distance δ from the origin.

The distance δ is found by simple trigonometry to be

$$\delta = \sqrt{\frac{\text{SNR}}{2}} \sqrt{1 - \rho^2} \quad (\text{B-17})$$

Due to the symmetry, the probability that (ξ, η) lies in Region II is easily found:

$$\begin{aligned} \Pr(|K(\theta_1)|^2 > |K(\theta_0)|^2) &= \Pr((\xi, \eta) \in \text{Region II}) = \\ &= \textcircled{\text{H}}(-\delta) \end{aligned} \quad (\text{B-18})$$

$$\text{where } \textcircled{\text{H}}(x) = \frac{1}{\sqrt{2\pi}} \int_{-\infty}^x e^{-1/2\sigma^2} d\sigma \quad (\text{B-19})$$

is the normal probability integral, with tabulated values^[12].

3. The Case Where Several Sidelobes are Significant

If there are 2 large sidelobes instead of only one, we wish to examine the effect this has on the probability of a gross error. We call the random variables

$$x_0 = |K(\theta_0)|^2, \quad x_1 = |K(\theta_1)|^2, \quad x_2 = |K(\theta_2)|^2 \quad (\text{B-20})$$

and denote the events

$$\begin{aligned} A &= \text{event that } x_1 > x_0 \\ B &= \text{event that } x_2 > x_0 \end{aligned} \quad (\text{B-21})$$

Then using standard set theory notations,^[18] we have for the probability P_e that a gross error occurs,

$$\begin{aligned} P_e &= \Pr(A \cup B) = 1 - \Pr(\sim A / \sim B) \\ &= 1 - \Pr(\sim A) \Pr(\sim B / \sim A) \end{aligned} \quad (B-22)$$

Now due to the specific nature of the events A and B, it is clear by inspection that

$$\Pr(\sim B / \sim A) \geq \Pr(\sim B) \quad (B-23)$$

so that

$$\begin{aligned} P_e &= 1 - \Pr(\sim A) \Pr(\sim B / \sim A) \\ &\leq 1 - \Pr(\sim A) \Pr(\sim B) \end{aligned} \quad (B-24)$$

$$= \Pr(A) + \Pr(B) \quad (B-25)$$

the last form being a valid approximation when the probabilities are small. Thus P_e is bounded above by $\Pr(A) + \Pr(B)$ for any degree of correlation between the x 's. The bound would be reached if the x 's were independent. It is obviously bounded below by the larger of $\Pr(A)$ and $\Pr(B)$, since it is more likely that either A or B will occur, than that only one will occur.

This analysis may be extended to n sidelobes in a straight-forward fashion, yielding

$$P_e \leq 1 - \prod_{i=1}^n (1 - \Pr(A_i)) = \sum_{i=1}^n \Pr(A_i) \quad (B-26)$$

for events $A_i: x_i > x_0$, each $x_i = |K(\theta_i)|^2$, where the last equality is true for $\Pr(A_i) < 1$, $i=1, 2, \dots, n$

.

2. Derivation of the Form for $p(\theta/y)$ of Eq (2-31)

From (2-29) we have the expansion

$$\begin{aligned} |K(\theta)|^2 = & K_0 + K_r(r-r_0) + K_v(v-v_0) - \frac{1}{2} A(r-r_0)^2 \\ & - B(r-r_0)(v-v_0) - \frac{1}{2} C(v-v_0)^2 + \dots \end{aligned} \quad (B-27)$$

By setting $\frac{\partial}{\partial r} |K(\theta)|^2$ and $\frac{\partial}{\partial v} |K(\theta)|^2$ to zero we can see that $|K(\theta)|^2$ is a maximum at $\theta_p = (r_p, v_p)$ given by

$$\begin{aligned} r_p &= r_0 + \frac{1}{\Delta} (K_r C - K_v B) \\ v_p &= v_0 + \frac{1}{\Delta} (K_v A - K_r B) \end{aligned} \quad (B-28)$$

(Note: it is shown in Appendix E that A and Δ are always positive. Thus we are assured that the above point is

indeed a maximum.) By straightforward algebra, substituting for r_o, v_o in (B-27), we can rewrite (B-27) in the form

$$|K(\theta)|^2 = k'_o - \frac{1}{2} \left[A(r-r_p)^2 + 2B(r-r_p)(v-v_p) + C(v-v_p)^2 \right] \quad (B-29)$$

where

$$k'_o = k_o + \frac{1}{2\Delta} \left[A K_v^2 - 2BK_r K_v + C K_r^2 \right] \quad (B-30)$$

Since we are going to use (2-14) to form $p(\theta/y)$ which is a probability density, the constant term k'_o will not affect the shape of $p(\theta/y)$ as a function of r or v , and so may be incorporated in the normalization constant k of (2-14). The remaining terms may be conveniently written using matrix notation:

$$A(r-r_p)^2 + 2B(r-r_p)(v-v_p) + C(v-v_p)^2 = (\theta - \theta_p)' \begin{bmatrix} A & B \\ B & C \end{bmatrix} (\theta - \theta_p) \quad (B-31)$$

which is the desired form for (2-31), with

$$\theta - \theta_p = \begin{Bmatrix} r - r_p \\ v - v_p \end{Bmatrix} \quad (B-32)$$

APPENDIX C: Derivation of the Ellipse Parameters

We wish to determine the forms of the second derivative terms A, B, and C given by (2-29). We first find these forms for derivatives with respect to τ and w , and then convert finally to those with respect to r , v . Naming the forms for convenience:

$$\begin{aligned} a &= \frac{\partial^2}{\partial \tau^2} |G(\theta, \theta_0)|^2 \big|_{\theta=\theta_0} \\ b &= \frac{\partial^2}{\partial \tau \partial w} |G(\theta, \theta_0)|^2 \big|_{\theta=\theta_0} \\ c &= \frac{\partial^2}{\partial w^2} |G(\theta, \theta_0)|^2 \big|_{\theta=\theta_0} \end{aligned} \tag{C-1}$$

with $G(\theta, \theta_0)$ given by (2-23)

$$G(\theta, \theta_0) = \frac{1}{D(\theta)D(\theta_0)} \int \frac{S(\omega - \omega_0) S^*(\omega - \omega_0) e^{j\omega(\tau - \tau_0)}}{N(\omega)} \frac{d\omega}{2\pi} \tag{C-2}$$

This is conveniently written in the form of an inner product, which will greatly simplify the ensuing derivation:

$$G(\theta, \theta_0) = (H_0, H_\theta)$$

with $H_0(\omega) = H_{\theta_0}(\omega)$, and

$$H_{\theta}(\omega) \equiv \frac{S(\omega - \omega_0)e^{-j\omega\tau}}{D(\theta)\sqrt{N(\omega)}} \quad (C-3)$$

The inner product form is given by

$$(H_0, H_{\theta}) = \int H_0(\omega) H_{\theta}^*(\omega) \frac{d\omega}{2\pi} = (H_{\theta}, H_0)^* \quad (C-4)$$

We note in passing that $G(\theta_0, \theta_0) = 1$, and that by the definition of $D^2(\theta)$ of (2-19), $\|H_{\theta}\|^2 \equiv (H_{\theta}, H_{\theta}) = 1$, for all θ .

Consider the result of taking derivatives with respect to τ :

$$\frac{\partial}{\partial \tau} |(H_0, H_{\theta})|^2 = 2 \operatorname{Re} (H_0, H_{\theta})(H_0, \dot{H}_{\theta})^*$$

$$\frac{\partial^2}{\partial \tau^2} |(H_0, H_{\theta})|^2 = 2 \operatorname{Re} \left[|(\dot{H}_0, \dot{H}_{\theta})|^2 + (H_0, H_{\theta})(H_0, \ddot{H}_{\theta})^* \right]$$

with $\dot{H}_{\theta}(\omega) = \frac{\partial}{\partial \tau} H_{\theta}(\omega)$. Then at $\theta = \theta_0$ we have

$$a = 2 \left[|(H_0, H_{\tau})|^2 + \operatorname{Re} (H_0, H_{\tau\tau}) \right] \quad (C-5)$$

where $H_\tau(\omega) = \frac{\partial}{\partial \tau} H_\theta(\omega) \Big|_{\theta=\theta_0}$. The following argument is used to show the relation

$$\operatorname{Re}(H_0, H_{\tau\tau}) = - \|H_\tau\|^2 \quad (\text{C-6})$$

Derivation:

1. $(H_\theta, H_\theta) = 1$ for all θ .
2. Thus any derivative of this term will vanish:

$$\frac{\partial}{\partial \tau} (H_\theta, H_\theta) = 2 \operatorname{Re} (H_\theta, \dot{H}_\theta) = 0$$

3. Likewise for the second derivative:

$$2 \operatorname{Re} \left[(\dot{H}_\theta, \dot{H}_\theta) + (H_\theta, \ddot{H}_\theta) \right] = 0$$

4. So that at $\theta=\theta_0$ we have the result (C-6). qed

Similarly one can show the following identities:

$$\text{i. } \operatorname{Re} (H_0, H_{\omega\omega}) = - \|H_\omega\|^2 \quad (\text{C-7})$$

$$\text{ii. } \operatorname{Re} (H_0, H_{\tau\omega}) = - \operatorname{Re} (H_\tau, H_\omega)$$

These identities allow one to write only first derivatives of the $H_\theta(\omega)$ terms in the expressions for a, b, and c. Thus for a:

$$a = -2 \left[\|H_\tau\|^2 - |(H_o, H_\tau)|^2 \right] \quad (C-8)$$

Similarly, for the remaining two parameters, one can show:

$$\begin{aligned} b &= -2 \left[\operatorname{Re} (H_\tau, H_w) - \operatorname{Re} (H_o, H_w)(H_o, H_\tau)^* \right] \\ c &= -2 \left[\|H_w\|^2 - |(H_o, H_w)|^2 \right] \end{aligned} \quad (C-9)$$

To discover what these forms mean in terms of the signal and noise frequency functions, it is necessary to calculate the expressions for $H_\tau(\omega)$ and $H_w(\omega)$. It is convenient to separate the component $D(\theta)$ from the rest of $H_\theta(\omega)$ since $D(\theta)$ depends only on w , and derivatives with respect to w must be taken. We define

$$H_\theta(\omega) = g_\theta(\omega) D(\theta) \quad (C-10)$$

so that $g_{\theta}(\omega) = \frac{S(\omega-w)e^{-j\omega\tau}}{\sqrt{N(\omega)}}$

Thus by inspection,

$$H_{\tau}(\omega) = \frac{1}{D_0} (-j\omega g_0(\omega)) \quad (C-11)$$

where we call $D(\theta_0) = D_0$, and $g_{\theta_0}(\omega) = g_0(\omega)$.

$$\frac{\partial}{\partial \omega} D(\theta) = \frac{\partial}{\partial \omega} \sqrt{D^2(\theta)} = \frac{1}{2} \frac{1}{D(\theta)} \int \frac{-2 \operatorname{Re} S(\omega-w) S^*(\omega-w)}{N(\omega)} \frac{d\omega}{2\pi}$$

so that at θ_0 it becomes

$$\left. \frac{\partial}{\partial \omega} D(\theta) \right|_{\theta_0} = -\frac{1}{D_0} \operatorname{Re}(g_0, \dot{g}_0) \quad (C-12)$$

Hence we have for $H_w(\omega)$:

$$\begin{aligned} H_w(\omega) &= \frac{1}{D_0} \dot{g}_0(\omega) - g_0(\omega) \frac{1}{D_0} \frac{\partial}{\partial \omega} D(\theta) \Big|_{\theta_0} \\ &= \frac{1}{D_0} \left[\dot{g}_0(\omega) - \frac{1}{2} g_0(\omega) \operatorname{Re}(g_0, \dot{g}_0) \right] \quad (C-13) \end{aligned}$$

Now combining the expressions to form a, b, and c:

$$a = -2 \left[\frac{1}{D_o^2} \|\omega g_o\|^2 - \left| \frac{1}{D_o^2} (g_o, \omega g_o) \right|^2 \right] \quad (C-14)$$

$$\begin{aligned} b = & -2 \operatorname{Re} \left[\frac{1}{D_o^2} (-j\omega g_o, \dot{g}_o + \frac{1}{D_o^2} g_o \operatorname{Re}(g_o, \dot{g}_o)) \right. \\ & \left. - \frac{1}{D_o^4} (g_o, \dot{g}_o + \frac{1}{D_o^2} g_o \operatorname{Re}(g_o, \dot{g}_o)) (-j\omega g_o, g_o) \right] \\ = & -2 \operatorname{Re} \left[\frac{1}{D_o^2} (-j\omega g_o, \dot{g}_o) + \frac{1}{D_o^4} (-j\omega g_o, g_o) \operatorname{Re}(g_o, \dot{g}_o) \right. \\ & \left. - \frac{1}{D_o^4} (g_o, \dot{g}_o) (-j\omega g_o, g_o) \right. \\ & \left. - \frac{1}{D_o^6} (g_o, g_o) \operatorname{Re}(g_o, \dot{g}_o) (-j\omega g_o, g_o) \right] \\ = & -2 \left[\frac{1}{D_o^2} \operatorname{Im}(\omega g_o, \dot{g}_o) - \frac{1}{D_o^4} \operatorname{Im}(g_o, \dot{g}_o) (\omega g_o, g_o) \right] \quad (C-15) \end{aligned}$$

where the last form is obtained by noticing that in the middle form the second and fourth terms cancel since $(g_o, g_o) = D_o^2$. Also, we use $\text{Re}(-j\omega g_o, g_o) = \text{Im}(\omega g_o, g_o)$. Finally,

$$\begin{aligned}
 c &= -2 \left[\frac{1}{D_o^2} \|\dot{g}_o\|^2 + \frac{1}{D_o^2} g_o \text{Re}(g_o, \dot{g}_o) \right] \\
 &\quad \left| \frac{1}{D_o^2} (g_o, \dot{g}_o + \frac{1}{2} g_o \text{Re}(g_o, \dot{g}_o)) \right|^2 \\
 &= -2 \left[\frac{1}{D_o^2} \|\dot{g}_o\|^2 - \frac{3}{D_o^4} \text{Re}^2(g_o, \dot{g}_o) - \frac{1}{D_o^2} (g_o, \dot{g}_o) \right. \\
 &\quad \left. + \frac{1}{D_o^2} \text{Re}(g_o, \dot{g}_o) \right]^2 \\
 &= -2 \left[\frac{1}{D_o^2} \|\dot{g}_o\|^2 - \frac{1}{D_o^4} \text{Re}^2(g_o, \dot{g}_o) - \frac{1}{D_o^2} \text{Im}^2(g_o, \dot{g}_o) \right] \\
 &= -2 \left[\frac{1}{D_o^2} \|\dot{g}_o\|^2 - \left| \frac{1}{D_o^2} (g_o, \dot{g}_o) \right|^2 \right] \quad (C-16)
 \end{aligned}$$

Now these simplified forms may be written in terms of $S(\omega)$ and $N(\omega)$ by using the definitions in (C-10):

$$\begin{aligned}
 a &= -2 \left[\int \frac{\omega^2 |S(\omega - \omega_0)|^2}{D_0^2 N(\omega)} \frac{d\omega}{2\pi} - \left| \int \frac{\omega |S(\omega - \omega_0)|^2}{D_0^2 N(\omega)} \frac{d\omega}{2\pi} \right|^2 \right] \\
 b &= -2 \left[\text{Im} \int \frac{\omega S(\omega - \omega_0) \dot{S}^*(\omega - \omega_0)}{D_0^2 N(\omega)} \frac{d\omega}{2\pi} - \text{Im} \int \frac{S(\omega - \omega_0) \dot{S}^*(\omega - \omega_0)}{D_0^2 N(\omega)} \frac{d\omega}{2\pi} \right. \\
 &\quad \left. + \int \frac{\omega |S(\omega - \omega_0)|^2}{D_0^2 N(\omega)} \frac{d\omega}{2\pi} \right] \\
 c &= -2 \left[\int \frac{|\dot{S}(\omega - \omega_0)|^2}{D_0^2 N(\omega)} \frac{d\omega}{2\pi} - \left| \int \frac{S(\omega - \omega_0) \dot{S}^*(\omega - \omega_0)}{D_0^2 N(\omega)} \frac{d\omega}{2\pi} \right|^2 \right]
 \end{aligned}
 \tag{C-17}$$

The remaining steps are simple:

1. Make a change of variable by translating ω by amount ω_0 . Then expand the integrands (the terms such as $(\omega + \omega_0)^2$) and note the cancellations between integrals. These steps make $N(\omega + \omega_0)$ appear in each denominator.

2. Use the chain rule for derivatives to convert from derivatives in τ and w to those in r and v . That is, (see page 2-3)

$$\partial/\partial r = \frac{\partial}{\partial \tau} \frac{\partial \tau}{\partial r} = \frac{2}{c} \partial/\partial \tau$$

$$\partial/\partial v = \frac{\partial}{\partial w} \frac{\partial w}{\partial v} = -\frac{2Q}{c} \partial/\partial w \quad (C-18)$$

3. Use (2-29) to add the appropriate constants, thus forming the A, B, and C expressions given in (2-33).

Simplification for the White Noise Case

When $N(\omega) = N_0$ for all ω , D_0^2 becomes equal to $2E/N_0$, with transmitted signal energy defined by

$$2E = \int_{-T}^T m^2(t) dt = \int_{-\infty}^{\infty} |S(\omega)|^2 \frac{d\omega}{2\pi} \quad (C-19)$$

This follows directly from Parseval's theorem (Papoulis,^[13] p. 27). The terms remaining in B and C of (2-33) may be

simplified by suitable Fourier transform substitutions, as follows: (Helstrom^[7] p. 18)

$$1) \int \omega^2 |S(\omega)|^2 \frac{d\omega}{2\pi} = \int |\dot{s}(t)|^2 dt$$

$$2) \int \omega |S(\omega)|^2 \frac{d\omega}{2\pi} = \text{Im} \int s^*(t) \dot{s}(t) dt$$

$$3) \int |\dot{S}(\omega)|^2 \frac{d\omega}{2\pi} = \int t^2 m^2(t) dt$$

$$4) \text{Im} \int S(\omega) \dot{S}^*(\omega) \frac{d\omega}{2\pi} = \int t m^2(t) dt$$

$$5) \text{Im} \int \omega S(\omega) \dot{S}^*(\omega) \frac{d\omega}{2\pi} = \text{Im} \int t s^*(t) \dot{s}(t) dt \quad (\text{C-20})$$

The derivative definition follows from the transform definition:

$$\dot{S}^*(\omega) = j \int_T t s^*(t) e^{j\omega t} dt \quad (\text{C-21})$$

Using this in #4, for instance:

$$\begin{aligned}
\int s(\omega) s^*(\omega) \frac{d\omega}{\omega\pi} &= j \int \frac{d\omega}{2\pi} \int dt \, t \, s(t) e^{-j\omega t} \int d\mu s^*(\mu) \mu e^{j\omega\mu} \\
&= j \int dt s(t) \int d\mu \, \mu s^*(\mu) \int \frac{d\omega}{\omega\pi} e^{-j\omega(t-\mu)} \\
&= j \int dt |s(t)|^2 dt
\end{aligned} \tag{C-22}$$

which is valid if the integration order can be reversed, (requiring mild continuity properties of $s(t)$), and which makes use of the "equality"

$$\int_{-\infty}^{\infty} e^{j\omega t} \frac{d\omega}{2\pi} = \delta(t) \tag{C-23}$$

for the Dirac delta function. Although this equality is open to question on grounds of rigor, its use in an integral as in (C-22) rests firmly in the theory of distribution. (Papoulis,^[13] p. 269). The derivations for the other equivalences in (C-20) follow in the same way. However, for #5 some more discussion is merited:

$$\int \omega S(\omega) \dot{S}^*(\omega) \frac{d\omega}{2\pi} = \int \frac{d\omega}{2\pi} \omega S(\omega) \int j t s^*(t) e^{j\omega t} dt$$

$$= \int dt t s^*(t) \int \frac{d\omega}{2\pi} j \omega S(\omega) e^{j\omega t} \quad (C-24)$$

and the inner integral is recognized as $\dot{s}(t)$. The imaginary parts are then taken to yield #5. Helstrom^[7] arrives at the same result (p. 18)(with a misprint of a minus sign in his Eq. (5.7)), but this form is considered much simpler.*

The forms above are finally simplified by using $s(t) = m(t)e^{j\phi(t)}$, taking derivatives, and sorting out real or imaginary parts. For the mean square frequency deviation in #1 this gives

$$\int \omega^2 |S(\omega)|^2 \frac{d\omega}{2\pi} = \int_T \dot{m}^2(t) dt + \int_T m^2(t) \dot{\phi}^2(t) dt \quad (C-25)$$

showing that it consists of portions due to envelope derivatives and phase derivatives.

* Note: β used here has the same sign as Helstrom's b , p. 21, since his ellipse is $a\tau^2 - 2b\tau w + cw^2 = 1$ and w is proportional to $-v$.

APPENDIX D: Equivalent Signal for Matched Filtering

From (2-18) $K(\theta)$ is a filtering operation on the received signal with spectrum $Y(\omega)$, where the filter has transfer function as in (2-20). But as far as the value of $K(\theta)$ is concerned, the input could be the signal with spectrum $Y(\omega)/\sqrt{N(\omega)}$, passing through filter with characteristic

$$\frac{1}{D(\theta)} \frac{S^*(\omega - \omega_0)}{\sqrt{N(\omega)}} \quad (D-1)$$

Then the definitions of duration and bandwidth suggested for (2-34) to (2-36) apply directly to the signal part of this new normalized received signal. This makes the colored noise case identical to the white noise case with a new transmitted signal.

APPENDIX E: Derivation of Unified Forms of A, B, C

Here it is indicated how (2-41) follows from (2-33). The forms for A follow directly from the substitution of the operator form in the (2-33) version. The others arise as shown now.

Use $S(\omega) = |S(\omega)| e^{j\psi(\omega)}$ and thus $\dot{S}(\omega) = |S(\omega)|_{\omega} e^{j\psi(\omega)} + j |S(\omega)| \dot{\psi}(\omega) e^{j\psi(\omega)}$ to expand B and C in (2-33), where $\frac{d}{d\omega} |S(\omega)| \equiv |S(\omega)|_{\omega}$:

$$\begin{aligned}
 B &= kQ \text{ SNR} \left[\int \frac{|S(\omega)|^2 \omega \dot{\psi}(\omega)}{D_o^2 N(\omega + \omega_o)} \frac{d\omega}{2\pi} + \int \frac{\omega |S(\omega)|^2}{D_o^2 N(\omega + \omega_o)} \frac{d\omega}{2\pi} \right. \\
 &\quad \left. + \int \frac{|S(\omega)|^2 \dot{\psi}^2(\omega)}{D_o^2 N(\omega + \omega_o)} \frac{d\omega}{2\pi} \right] \\
 C &= kQ^2 \text{ SNR} \left[\int \frac{|S(\omega)|^2_{\omega} + |S(\omega)|^2 \dot{\psi}^2(\omega)}{D_o^2 N(\omega + \omega_o)} \frac{d\omega}{2\pi} \right. \\
 &\quad \left. - \left| \int \frac{|S(\omega)| |S(\omega)|_{\omega} - j |S(\omega)|^2 \dot{\psi}(\omega)}{D_o^2 N(\omega + \omega_o)} \frac{d\omega}{2\pi} \right|^2 \right] \quad (E-1)
 \end{aligned}$$

Now using the definition $a(\omega) = |S(\omega)|_w / |S(\omega)|$ and substituting $P(\omega)$ for its (2-37) equivalent:

$$B = -kQ \text{ SNR} \left[\int \omega \dot{\psi}(\omega) P(\omega) \frac{d\omega}{2\pi} - \int P(\omega) \omega \frac{d\omega}{2\pi} \int P(\omega) \dot{\psi}(\omega) \frac{d\omega}{2\pi} \right]$$

$$C = kQ^2 \text{ SNR} \left[\int P(\omega) \left[a^2(\omega) + \dot{\psi}^2(\omega) \right] \frac{d\omega}{2\pi} \right.$$

$$\left. - \left| \int P(\omega) \left[a(\omega) - j\dot{\psi}(\omega) \right] \frac{d\omega}{2\pi} \right|^2 \right]$$

Expanding the squared magnitude term, and resorting terms yields (2-41) exactly.

To show that $AC-B^2$ is positive one need simply write it as

$$AC-B^2 = k^2 Q^2 (\text{SNR})^2 \left[\frac{\overline{(\omega-\bar{\omega})^2} \overline{(\dot{\psi}-\bar{\dot{\psi}})^2}}{\overline{(\omega-\bar{\omega})(\dot{\psi}-\bar{\dot{\psi}})}} + \frac{\overline{(\omega-\bar{\omega})^2} \overline{(a-\bar{a})^2}}{\overline{(\omega-\bar{\omega})(\dot{\psi}-\bar{\dot{\psi}})}} \right]$$

(E-3)

The first term is non-negative by the following argument.
 (See Cramer^[17] p. 263). For any values t, u , the following function is non-negative:

$$0 \leq \overline{[t(\omega - \bar{\omega}) + u(\dot{\psi} - \bar{\dot{\psi}})]^2} = t^2 \overline{(\omega - \bar{\omega})^2} + 2tu \overline{(\omega - \bar{\omega})(\dot{\psi} - \bar{\dot{\psi}})} + u^2 \overline{(\dot{\psi} - \bar{\dot{\psi}})^2} \quad (\text{E-4})$$

and so this is a non-negative quadratic form in t, u . Hence the matrix:

$$\begin{bmatrix} \overline{(\omega - \bar{\omega})^2} & \overline{(\omega - \bar{\omega})(\dot{\psi} - \bar{\dot{\psi}})} \\ \overline{(\omega - \bar{\omega})(\dot{\psi} - \bar{\dot{\psi}})} & \overline{(\dot{\psi} - \bar{\dot{\psi}})^2} \end{bmatrix} \quad (\text{E-5})$$

has a non-negative determinant, q.e.d. The second term in (E-3) is a product of two terms which are positive by inspection, since $\overline{(\omega - \bar{\omega})^2}$ and $\overline{(\dot{\psi} - \bar{\dot{\psi}})^2}$ are positive functions of frequency.

Appendix F: LIFMOP_and_RAFMOP_signal_examples

I. CALCULATION OF THE ELLIPSE PARAMETERS

For the white noise case, the ellipse parameters are found using (2-34)-(2-36) and the time domain equivalent forms given in (C-20). By the definitions of these signal forms, both epoch and center frequency are zero.

$$A = k \text{ WSNR } \frac{1}{2E} \int_T \left[\dot{m}^2(t) + m^2(t) \dot{\phi}^2(t) \right] dt \quad (\text{F-1})$$

$$B = kQ \text{ WSNR } \frac{1}{2E} \int_T t m^2(t) \dot{\phi}(t) dt$$

$$C = kQ^2 \text{ WSNR } \frac{1}{2E} \int_T t^2 m^2(t) dt$$

For both classes of signals, the envelope roll-off is given by

$$\begin{aligned} m(t) &= \frac{1}{2} m_0 (1 - \cos \frac{2\pi}{\mu d} (t - d/2)) \quad |t| \in (d/2(1-\mu), d/2) \\ &= m_0 \sin^2 \frac{\pi}{\mu d} (t - d/2) \end{aligned} \quad (\text{F-2})$$

so that the envelope derivative contribution to the bandwidth is given by

$$\int \dot{m}^2(t) dt = 2 \left(\frac{m_o \pi}{\mu d} \right)^2 \int_{\frac{d}{2}(1-\mu)}^{d/2} \sin^2 \frac{\pi}{\mu d} (t-d/2) dt$$

$$= \left(\frac{m_o \pi}{\mu d} \right)^2 \frac{\mu d}{2} \quad (F-3)$$

The signal energy is simply given as

$$2E = \int m^2(t) dt = m_o^2 d(1-5\mu/8) \quad (F-4)$$

For the LIFMOP signal the calculation of A, B, and C is awkward but straightforward, and yields,

$$A = k \text{ WSNR } \frac{1}{2E} \left[\frac{\pi^2 m_o^2}{2\mu d} + \frac{m_o^2 P^2 d}{3} (1-\mu)^3 + \left(\frac{2P}{d} \right)^2 I \right]$$

$$B = k Q \text{ WSNR } \frac{1}{2E} \left[\frac{m_o^2}{6} P d^2 (1-\mu)^3 + \frac{2P}{d} I \right] \quad (F-5)$$

$$C = k Q^2 \text{ WSNR } \frac{1}{2E} \left[\frac{2}{3} m_o^2 \left(\frac{d}{2} \right)^3 (1-\mu)^3 + I \right]$$

$$\Delta = AC - B^2 = (k Q \text{ WSNR} / 2E)^2 \left(\frac{\pi^2 m_o^2}{2\mu d} \right) \left(\frac{2}{3} m_o^2 \left(\frac{d}{2} \right)^3 (1-\mu)^3 + I \right)$$

where

$$I = 2 \int_{\frac{d}{2}(1-\mu)}^{\frac{d}{2}} t^2 m^2(t) dt = \frac{3}{32} \mu m_0^2 d^3 + O(\mu^2) \quad (F-6)$$

We have evaluated I only to terms of order μ since the envelope roll-off lasts a small fraction of the signal duration. Now simplifying the above expressions, and keeping terms to this same order, we obtain,

$$\begin{aligned} A &= k \text{ WSNR} \left[\frac{\pi^2}{2\mu d^2} (1+5\mu/8) + P^2/3 (1-5\mu/2) \right] + O(\mu^2) \\ B &= K Q \text{ WSNR} [Pd/6] (1-5\mu/4) + O(\mu^2) \\ C &= k Q^2 \text{ WSNR} [d^2/12] (1-5\mu/4) + O(\mu^2) \\ \Delta &= (k Q \text{ WSNR})^2 \left[\frac{\pi^2}{24\mu} \right] \left(1 + \frac{35\mu}{32} \right) + O(\mu) \end{aligned} \quad (F-7)$$

Thus, for $\mu \ll 1$ we have the forms given in (2-42). Δ is independent of the frequency modulation P, depending instead on the envelope shape. The terms involving P have cancelled out because they were of equal size in AC and B^2 , a property peculiar to the LIFMOP signal, as shown below.

For the RAFMOP signal B^2 is much smaller, and there is no difficulty with Δ . Thus we may ignore the envelope roll-off in all calculations except that of the first part of A in (F-1). Ignoring the roll-off makes A independent of δ . For the B term we must compute the integral over each segment of $\dot{\phi}(t)$ separately. These calculations finally give for the $\mu \ll 1$ case: (note: $|\frac{4\delta}{d}| \leq 1$)

$$A \doteq k \text{ WSNR} \left[\frac{\pi^2}{2\mu d^2} + \frac{P^2}{3} \right]$$

$$B \doteq k Q \text{ WSNR} \left[\frac{Pd}{8} \frac{4\delta}{d} \right] (2-4|\delta|/d) \quad (\text{F-8})$$

$$C \doteq k Q^2 \text{ WSNR} d^2/12$$

$$\Delta \doteq (k Q \text{ WSNR})^2 \left[\frac{\pi^2}{24\mu} + \frac{P^2 d^2}{36} \left[1 - \frac{9}{16} \left(\frac{4\delta}{d} \right)^2 (2-4|\delta|/d)^2 \right] \right]$$

The calculation of B is done for $\delta > 0$, and then the $\delta < 0$ case follows by inspection. Δ has a term in P^2 which is positive for all permissible δ .

II. PROOF THAT THE LIFMOP SIGNAL ATTAINS LARGEST B FOR FIXED A

Neglecting the envelope roll-off and considering class of $\dot{\phi}(t)$ such that the center frequency is zero:

$$\int \dot{\phi}(t) dt = 0 \quad (F-9)$$

then,

$$A = K_1 \int \dot{\phi}^2(t) dt, \quad B = K_2 \int t \dot{\phi}(t) dt \quad (F-10)$$

and we can use the Lagrange parameter method⁽¹⁹⁾ page 151.

$$1) \text{ define } J = B + \lambda A = \int \left[K_2 t \dot{\phi}(t) + \lambda K_1 \dot{\phi}^2(t) \right] dt$$

2) Differentiate with respect to $\dot{\phi}$ and set to zero:

$$K_2 t + 2\lambda K_1 \dot{\phi}(t) = 0$$

so that

$$\dot{\phi}(t) = -(K_2/2\lambda K_1)t$$

Thus $\dot{\phi}(t)$ must be linear in t , which is indeed the LIFMOP form.

III. THE RAFMOP SPECTRUM

We consider the case of $\delta=0$ and neglect the envelope roll-off. Then the RAFMOP signal has the Fourier transform:

$$S(\omega) = m_0 \int_{-d/2}^{d/2} e^{j\phi(t)} e^{-j\omega t} dt \quad (F-12)$$

$$\text{where } \phi(t) = \begin{cases} Pt(1+2t/d) & t < 0 \\ Pt(1-2t/d) & t > 0 \end{cases} \quad (F-13)$$

Since $(\varphi(t) - \omega t)$ is odd, $S(\omega)$ is purely real:

$$S(\omega) = 2m_0 \int_0^{d/2} \cos \left[\frac{2P}{d} t^2 + (\omega - P)t \right] dt \quad (F-14)$$

This integral may be evaluated in terms of Fresnel integrals (ref. 12, p. 304, eq. 7.4.38)

$$F_C(X) = \int_0^X \cos \left(\frac{\pi}{2} t^2 \right) dt \quad (F-15)$$

$$F_S(X) = \int_0^X \sin \left(\frac{\pi}{2} t^2 \right) dt$$

The integral is given by

$$S(\omega) = \sqrt{\frac{2E\pi}{P}} \left[\cos \left(\frac{\pi}{2} \gamma^2 (x-1)^2 \right) \left[F_C(\gamma(x+1)) - F_C(\gamma(x-1)) \right] \right. \\ \left. + \sin \left(\frac{\pi}{2} \gamma^2 (x-1)^2 \right) \left[F_S(\gamma(x+1)) - F_S(\gamma(x-1)) \right] \right] \quad (F-16)$$

where $\gamma = \sqrt{Pd/4\pi}$ and $X = \omega/P$. Finally, the spectrum is $|S(\omega)|^2 = S^2(\omega)$. It is easy to show that the Fresnel term differences $F_C(\gamma(x+1)) - F_C(\gamma(x-1))$ and $F_S(\gamma(x+1)) - F_S(\gamma(x-1))$ are nearly constant over the signal band $|x| \leq 1$, and then

drop rapidly to zero. Thus the RAFMOP signal is significant only for $|\omega| \leq P$. The sine and cosine terms oscillate rapidly over this band, and when $\alpha^2(x-1)^2 = (2n+3/2)$, $n=0, \pm 1, \pm 2, \dots$ they are equal in size and opposite in sign, causing a null in $S(\omega)$. Thus $S(\omega)$ has nulls approximately at

$$x_n = 1 \pm \frac{1}{\gamma} \sqrt{2n+3/2} \quad (F-17)$$

APPENDIX G

1. Proof that A and C are Maximum for White Noise Alone

Consider noise spectra of the general form

$$N(\omega) = N_0 + LN_r(\omega) \quad (G-1)$$

For any positive function, say $G^2(\omega)$, the inequality is obvious:

$$\int \frac{G^2(\omega)}{N_0 + LN_r(\omega)} \frac{d\omega}{2\pi} < \int \frac{G^2(\omega)}{N_0} \frac{d\omega}{2\pi} \quad (G-2)$$

For the ellipse parameter A, (see 2-41), $G^2(\omega) = (\omega - \bar{\omega})^2 |S(\omega)|^2$; for parameter C, $G^2(\omega) = [(a - \bar{a})^2 + (\dot{\psi} - \bar{\dot{\psi}})^2] |S(\omega)|^2$; and for SNR, $G^2(\omega) = |S(\omega)|^2$. Consequently each of these is maximized when $L=0$. This is not so for B, since the function $(\omega - \bar{\omega}) \cdot (\dot{\psi} - \bar{\dot{\psi}}) |S(\omega)|^2$ is not always positive.

2. The Uncertainty Principle for Δ in White Noise

Helstrom (7) (p.20) uses Schwartz's inequality to show:

$$\frac{1}{(2E)^2} \left[\int t^2 m^2(t) dt \int \omega^2 |S(\omega)|^2 \frac{d\omega}{2\pi} - \left[\int M^2(t) t \phi(t) dt \right]^2 \right] \geq \frac{1}{4} \quad (G-3)$$

But from (2-34) - (2-36) A, B, and C are proportional to these quantities when center frequency and epoch are zero, so that when the constants are included, one has $\Delta = AC - B^2 \geq \frac{1}{4} (kQ WSNR)^2$.

Helstrom has shown (p. 21) that the equality holds only for gaussian signals

$$s(t) \propto e^{-(a+jb)t^2} \quad a>0 \quad (G-4)$$

which exist for all time. Now from (3-20) $\rho^2 = B^2/AC$ so that the uncertainty principle asserts

$$1 - \rho^2 \geq \frac{1}{4}(kQWSNR)^2/AC \quad (G-5)$$

Using the definitions of dispersion bandwidth and duration of (2-34) and (2-36) we then have

$$\rho^2 < 1 - \frac{1}{(2 \text{ bandwidth} \cdot \text{duration})^2} \quad (G-6)$$

Hence for large values of the bandwidth-duration product the upper limit approaches one. This limit can be attained by using the signal of (G-4).

Appendix H

Approximate Calculation of C for a Motionless Target

We assume that the signal has the form

$$s(t) = m_0 \frac{1}{\sqrt{2\pi d}} e^{-1/2(t/d)^2} \quad (H-1)$$

so that

$$S(\omega) = m_0 e^{-1/2(\omega d)^2} \quad (H-2)$$

If the probability density function of scatterer doppler shifts is also gaussian

$$p_w(w) = \frac{1}{\sqrt{2\pi B}} e^{-1/2(w/B)^2} \quad (H-3)$$

then using (4-10) we have

$$\begin{aligned} |S(\omega)|_p^2 &= m_0^2 \frac{1}{\sqrt{2\pi B}} \int_{-\infty}^{\infty} e^{-1/2(x/B)^2 - d^2(\omega-x)^2} dx \\ &= m_0^2 \sqrt{\gamma} e^{-(\omega d)^2/\gamma} \end{aligned} \quad (H-4)$$

where

$$\gamma = 1 + 2(\beta d)^2$$

We note that for the motionless target case $w_0 = 0$ the function

$$\frac{S(\omega) \dot{S}(\omega)}{N(\omega)}$$

is odd, so that the second term of C in (2-33) vanishes, leaving only

$$C = kQ^2 \sigma_o^2 \int \frac{m_o^2 d^4 \omega^2 e^{-\omega^2 d^2}}{\Lambda m_o^2 / \sqrt{\gamma} e^{-\omega^2 d^2 / \gamma + N_o}} \frac{d\omega}{2\pi} \quad (H-5)$$

Now if the reverberation level is much larger than N_o over all frequencies for which $|S(\omega)|^2$ is significant then we may find an approximation to the value for C by deleting the N_o term.

$$C = k Q^2 \sigma_o^2 \sqrt{\gamma} / \Lambda d^4 \int \omega^2 e^{-(\omega d)^2 (1-1/\gamma)} \frac{d\omega}{2\pi}$$

$$= \frac{kQ^2 \sigma_o^2}{\sqrt{2\pi} \Lambda \beta} \left[\frac{1+2(\beta d)^2}{2\beta d} \right]^2 \quad (H-6)$$

APPENDIX I

Form of J

To find the form of J we analyze B'^2/Δ' . Using (3-14) we have for $\Delta' = A'C' - B'^2$:

$$\Delta' = A' \left[\frac{\Delta_1}{A_1} + \frac{\Delta_2}{A_2} \right] + A_1 A_2 \left[t_i - \frac{B_1}{A_1} + \frac{B_2}{A_2} \right]^2 \quad (I-1)$$

where $\Delta_1 = A_1 C_1 - B_1^2 > 0$ and similarly for Δ_2 . Hence $\Delta' > 0$.

To form J we simplify B'^2 :

$$\begin{aligned} B'^2 &= \left[(B_1 - A_1 t_t) + (B_2 - A_2 t_w) \right]^2 \\ &= \left[A' t_w + A_1 t_i - B_1 - B_2 \right]^2 \\ &= A'^2 \left[t_w + R_1 t_i - R_1 \rho_1 \gamma_1 - R_2 \rho_2 \gamma_2 \right]^2 \\ &= A'^2 \left[(t_w - \rho_2 \gamma_2) + R_1 (t_i - \rho_1 \gamma_1 + \rho_2 \gamma_2) \right]^2 \end{aligned} \quad (I-2)$$

using (3-19b), (3-20), and $-R_2 = R_1 - 1$. Similarly from (I-1)

$$\Delta'/A'^2 = \left[R_1 \gamma_1^2 (1 - \rho_1^2) + R_2 \gamma_2^2 (1 - \rho_2^2) + R_1 R_2 (t_i + \rho_2 \gamma_2 - \rho_1 \gamma_1) \right]^2 \quad (I-3)$$

Combining these to form B'^2/Δ' we have J as in (3-22).

The shape of J as a function of t_1 is simply discovered by considering B'^2/Δ' as a function of $x \equiv t_1 - \rho_1 \gamma_1 + \rho_2 \gamma_2$.

$$B'^2/\Delta' = \frac{[(t_w - \rho_2 \gamma_2) + R_1 x]^2}{\Delta_s + R_1 R_2 x^2} \quad (I-4)$$

where $\Delta_s = R_1 \gamma_1^2 (1 - \rho_1^2) + R_2 \gamma_2^2 (1 - \rho_2^2)$. B'^2/Δ' clearly has a minimum value of zero when $R_1 x = -(t_w - \rho_2 \gamma_2)$. It has a single maximum when $x = \Delta_s / R_2 (t_w - \rho_2 \gamma_2)$ since

$$\frac{\partial}{\partial x} \frac{B'^2}{\Delta'} = \frac{2 [(t_w - \rho_2 \gamma_2) + R_1 x] [\Delta_s - (t_w - \rho_2 \gamma_2) R_2 x]}{[\Delta_s + R_1 R_2 x^2]^2} \quad (I-5)$$

(The second derivative is negative at the x given above.)

APPENDIX J

Demonstration that A, C are attainable in White Noise Case

claim: Given bandwidth and duration constraints, W and D, respectively, using the definitions

$$\begin{aligned}(\text{bw})^2 &= \frac{1}{2E} \int \left[\dot{m}^2(t) + m^2(t) \dot{\phi}^2(t) \right] dt \\ (\text{dur})^2 &= \frac{1}{2E} \int t^2 m^2(t) dt\end{aligned}\tag{J-1}$$

signals may always be found having bandwidth and duration allowed by the constraints.

.....

Consider the class G_1 of signals with gaussian envelope:

$$s(t) = m(t)e^{j\phi(t)} \in G_1 \quad \text{if } m(t) = e^{-at^2} \quad \text{for some } a > 0. \tag{J-2}$$

It is easy to see that

$$(\text{dur})^2 = \frac{1}{4a\sqrt{2}}\tag{J-3}$$

and

$$\frac{1}{2E} \int \dot{m}^2(t) dt = \frac{a}{\sqrt{2}}\tag{J-4}$$

One can always adjust $m(t)$ so that $(dur)^2 = D^2$ just by making $m(t)$ of sufficient width. This condition is

$$a = \frac{1}{4D^2\sqrt{2}} \quad (J-5)$$

from which the contribution to the bandwidth from the $\dot{m}^2(t)$ integral is $1/8D^2$. Now if this contribution is less than the allowed W^2 , one can always adjust $\phi(t)$ to make up the difference, simply by increasing $\dot{\phi}^2(t)$ until the contribution it makes in (J-1) to $(bw)^2$ yields W^2 . Thus the only question is whether the integral of $\dot{m}^2(t)$ can ever exceed W^2 . The answer is no, and follows immediately from the uncertainty principle (see Appendix G) which gives $W^2 D^2 \geq \frac{1}{4}$. For if the $\dot{m}^2(t)$ integral component were greater than W^2 , then we would have $W^2 D^2 < 1/8$, which is impossible. Consequently one can always find a signal, having a gaussian shaped envelope, which meets any W, D with $WD > 1/2$. qed

.

APPENDIX K

Determine ρ_2 For Minimum J in Single Ping Case

From (3-25) we have immediately

$$\frac{\partial J}{\partial \rho_2} = \frac{2}{\gamma_2^2} \frac{(t_w - \rho_2 \gamma_2)(\rho_2 t_w - \gamma_2)}{(1 - \rho_2^2)^2} \quad (K-1)$$

and

$$\left. \frac{\partial^2 J}{\partial \rho_2^2} \right|_{\rho_2 = \gamma_2 / t_w} = 2 \left(\frac{t_w}{\gamma_2} \right)^2 > 0 \quad (K-2)$$

Now by inspection of (3-25) J has a minimum of one at $\rho_2 = t_w / \gamma_2$. This is attainable if $t_w / \gamma_2 < 1$. If on the other hand $t_w / \gamma_2 > 1$, then we can set $\rho_2 = \gamma_2 / t_w$, which is then a minimum for J, with value

$$J_{\min} = 1 + t_w^2 (1 - \gamma_2^2 / t_w^2) / \gamma_2^2 = (t_w / \gamma_2)^2.$$

APPENDIX L

Clutter Elimination under Dispersion Bandwidth Constraint

If we assume no target or scatterer motion for simplicity, and choose $|S(\omega)|^2$ summetrical, then from (4-7) and (4-14)

$$A = k\sigma_o^2 \int \frac{\omega^2 |S(\omega)|^2}{\Lambda |S(\omega)|^2 + N_o} \frac{d\omega}{2\pi} \quad (L-1)$$

Under a dispersion bandwidth constraint we have some preset value W_1^2 [see definition (2-34)] :

$$W_1^2 = \frac{1}{2E} \int \omega^2 |S(\omega)|^2 \frac{d\omega}{2\pi}, \text{ where } 2E = \int |S(\omega)|^2 \frac{d\omega}{2\pi} \quad (L-2)$$

To show that an $|S(\omega)|^2$ is always possible that satisfies (L-2) and eliminates the effect of clutter, consider the class of spectra shown in Figure L-1. All but a fraction ϵ of the signal energy is put in a very narrow region about $\omega=0$, while the fraction ϵ of $2E$ is distributed evenly over a large band of width $2W$. Then to satisfy (L-2):

$$W_1^2 = \frac{1}{3} \left[\frac{\epsilon}{W-b} (W^3 - b^3) + \frac{1-\epsilon}{b} b^3 \right] = \frac{1}{3} \left[\epsilon W^2 + (1-\epsilon)b^2 \right] \text{ for } b \ll W. \quad (L-3)$$

We need only choose W such that

$$W^2 = \frac{1}{\epsilon} \left[3W_1^2 - (1-\epsilon)b^2 \right] \quad (L-4)$$

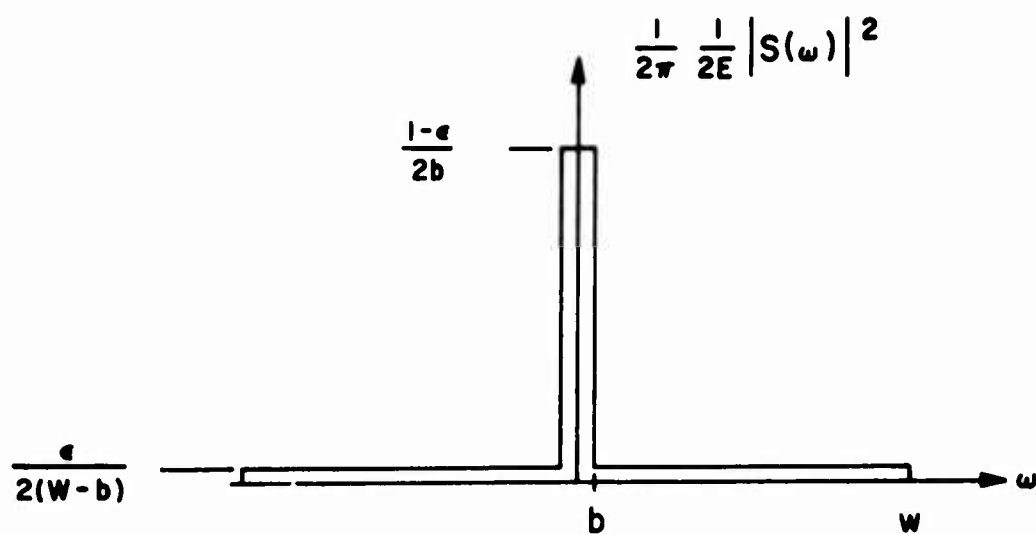


FIGURE L-1 SPECTRUM FOR REVERBERATION ELIMINATION

Now the ellipse parameter A becomes (using (L-1) and (L-5)), as well as $WSNR = 2E\sigma_o^2/N_o$,

$$A = k WSNR \left[\frac{\epsilon W^2}{\Lambda \epsilon / W + 2} + \frac{(1-\epsilon)b^3}{\Lambda(1-\epsilon) + 2b} \right] \quad (L-6)$$

$$= k WSNR \frac{2}{3} \left[\frac{3W_1^2 - (1-\epsilon)b^2}{\Lambda \epsilon^{3/2} [3W_1^2 - (1-\epsilon)b^2]^{-1/2} + 2} + \frac{(1-\epsilon)b^3}{\Lambda(1-\epsilon) + 2b} \right]$$

If ϵ is now chosen very small so that $\Lambda \epsilon^{3/2} \ll 2 \sqrt{3W_1^2 - (1-\epsilon)b^2}$, then

$$A \approx k WSNR \frac{1}{3} \left[\Lambda(3W_1^2 - b^2) + 6bW_1^2 \right] / (\Lambda + 2b) \quad (L-7)$$

Finally, if b is chosen small so that $2b \ll \Lambda$, $b^2 \ll 3W_1^2$, then

$$A \approx k WSNR W_1^2 \quad (L-8)$$

It is clear that this is the same value as would have been obtained if no clutter were present ($\Lambda=0$). Consequently the clutter has been entirely eliminated by using this peculiar distribution of signal energy. Very large processing bands W must be used however.

If the target and scatterers were moving, the same kind of argument would apply, since the basic stance of this argument is that the signal energy is spread so thinly over the band that $\Lambda |S(\omega + \omega_o)|_p^2 \ll N_o$ in (L-1).

APPENDIX M

Optimum $g(x)$ for no Target or Scatterer Motion

We wish to maximize A_g given by (4-26) by selecting $g(x)$ under the constraint that $g(x)$ is positive and has unit area. We first show that $g(x)$ should be symmetrical.

1. Show that the optimum $g(x)$ is symmetrical about $x=0$.

$$\text{Define } P(x) = g(x)/(Rg(x)+1) = P_e(x) + P_o(x) \quad (M-1)$$

where P_e and P_o are the even and odd parts of P respectively.

Then

$$A_g = \int_{-1}^1 x^2 P_e(x) dx - \left[\int_{-1}^1 P_e(x) dx \right]^{-1} \left[\int_{-1}^1 x P_o(x) dx \right]^2 \quad (M-2)$$

which is maximized when $P_o(x) = 0$. qed

2. Maximize A_g for symmetric $g(x)$.

We now wish to choose a unit area symmetrical $g(x)$ to maximize:

$$A_g = \int_{-1}^1 \frac{x^2 g(x)}{Rg(x)+1} dx \quad (M-3)$$

Using Lagrange Multipliers (J. Tou, (19) p. 151), define

$$L = A_g - \lambda \int_{-1}^1 g(x) dx, \quad |x| \leq 1 \quad (M-4)$$

Then $\partial L / \partial g = 0$ yields

$$\frac{x^2}{(Rg(x)+1)^2} - \lambda = 0 \quad (M-5)$$

or

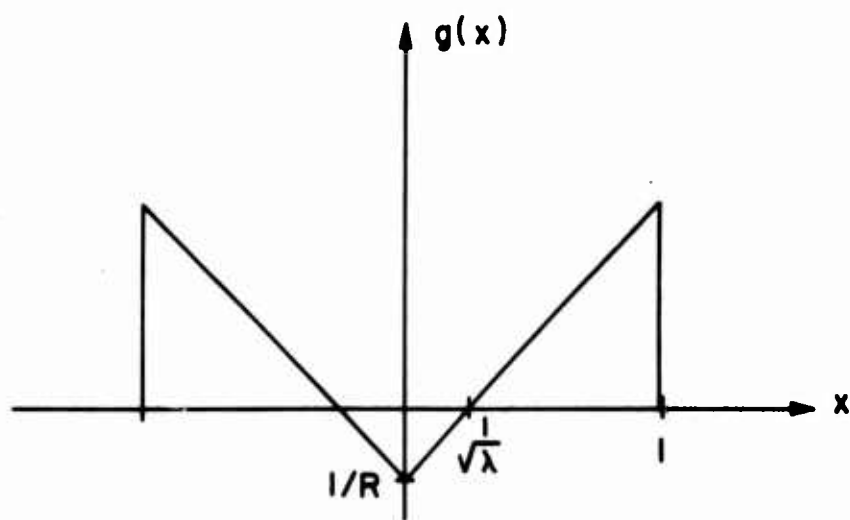
$$g(x) = \frac{1}{R} \left[\frac{|x|}{\sqrt{\lambda}} - 1 \right], \quad |x| \leq 1$$

as sketched in Figure M-1a. The difficulty with this solution is that it goes negative for $|x| \leq 1/\sqrt{\lambda}$, which is not permitted.

To determine the actual optimum $g(x)$, a dynamic programming technique was used on a computer. The problem here is equivalent to the "allocation problem" (Bellman (20), Chapter 1) if we partition the interval $|x| \leq 1$ into, say $2n$ equal subintervals, and select n quantities g_i as the level of $g(x)$ in the i^{th} subinterval. Then we rephrase the question as: Given a total resource $n/2$, allocate amounts g_i to maximize

$$A_g = \frac{2}{n^3} \sum_{i=1}^n \frac{g_i}{Rg_i+1} \left[i^{2-i} + \frac{1}{3} \right] \quad (M-6)$$

a).



b).

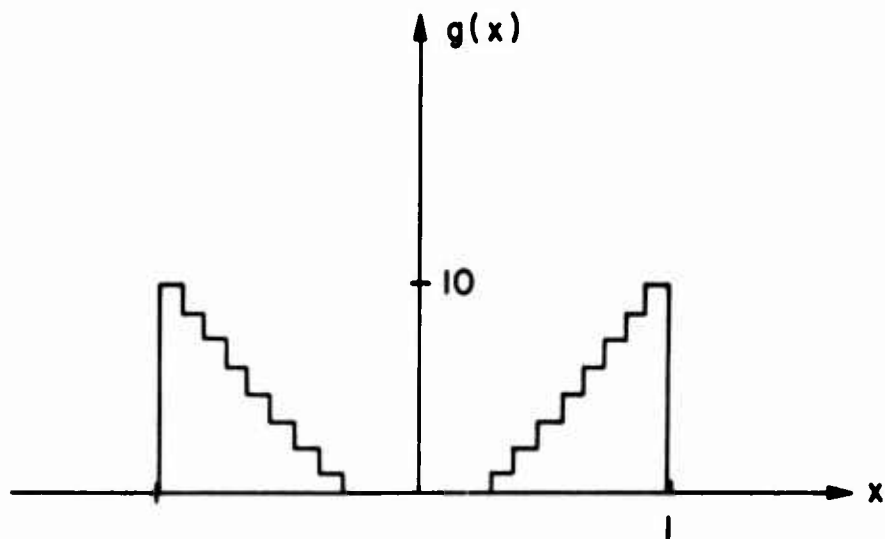


FIGURE M-1 LAGRANGE MULTIPLIER
AND DYNAMIC PROGRAMMING RESULTS

under the constraint

$$\sum_{i=1}^n g_i = n/2, \quad g_i \geq 0 \quad (M-7)$$

The algorithm for this class of problems is given by Bellman, and is easily applied to a computer program. The result for $R=10$ is shown in Figure M-1b.

In retrospect one can see that the Lagrange parameter solution was very nearly optimum. In fact, if the solution in (M-5) is simply altered so that $g(x)=0$ for $|x| < 1/\sqrt{\lambda}$, and if λ is now found according to the area constraint on $g(x)$, the result is

$$g(x) = \begin{cases} \frac{1}{R}|x| / \left[1+R/2 - \sqrt{R+R^2/4} \right] & \text{if } |x| \geq 1+R/2 - \sqrt{R+R^2/4} \\ 0 & \text{otherwise} \end{cases} \quad (M-8)$$

This matches the computer solution within the resolution of the program, and is thus a satisfactory result.

REFERENCES

1. See sequence of papers by T. Usher, Jr., and R. A. MacDonald, "Processing of Data from Sonar Systems," Vol. II, Dunham Lab., Yale University., G./D. Electric Boat, Groton, Connecticut, contract 53-00-10-0231, July, 1964.
2. M. N. Hill, The Sea, Wiley (Interscience), N. Y., N. Y., 1963.
3. Woodward, P. M. & Davies, I. L., "A Theory of Radar Information," Philosophical Magazine, 41, 1001, 1950.
4. Woodward, P. M., Probability and Information Theory, with Applications to Radar, Pergamon Press, Oxford, 1953.
5. Cook, C. E. & Bernfeld, M., Radar Signals, Academic Press, N. Y., N. Y., 1967.
6. Kelly, E. J., Reed, I. S. & Root, W. L., "The Detection of Radar Echoes in Noise," J. Soc. Indust. Applied Math., 8, 309-341, 481-507, 1960.
7. Helstrom, C. W., Statistical Theory of Signal Detection, Pergamon Press, Oxford, 1960.
8. Cahlander, D. A., "Echolocation with Wide band Waveforms: Bat Sonar Signals," MIT Lincoln Labs, Tech. Rept. 271, May, 1964, Lexington, Mass.
9. Siebert, W. M., "A Radar Detection Philosophy," IRE Trans on Information Theory, IT-2, 204-219, 1956.
10. W. B. Davenport & W. L. Root, An Introduction to the Theory of Random Signals, Mc-Graw Hill Book Co., N. Y., N. Y., 1958.

References - 2

11. Wainstein, L. A. & Zubakov, V. D., Extraction of Signals from Noise, trans. R. A. Silverman, Prentice-Hall, Englewood Cliffs, N. J., 1962.
12. Handbook of Mathematical Functions, U. S. Dept. of Commerce, National Bur. of Standards, Applied Math Series #55, 1964, U. S. Govt. Printing Office, Washington, D.C.
13. Papoulis, A., The Fourier Integral and Its Applications, McGraw-Hill Book Co., N. Y., N. Y., 1962.
14. Ramp, H. O. & Wingrove, E. R., "Principles of Pulse Compression," IRE Trans Military Electronics, MIL-5, 109-116, 1961.
15. Rihaczek, A. W., "Range Accuracy of Chirp Signals," Proc. IEEE (Corr.) 53, 412-413 (1965).
16. H. L. Van Trees, "Optimum Signal Design and Processing for Reverberation Limited Environments," IEEE Trans. on Military Electronics, MIL-9, 212-229, 1965.
17. Cramer, H., Mathematical Methods of Statistics, Princeton Univ. Press, Princeton, N. J., 1946.
18. Halmos, P. R., Naive Set Theory, D. Van Nostrand Co., Princeton, N. J., 1960.
19. Tou, J. T., Modern Control Theory, McGraw Hill, N. Y., 1964.
20. Bellman, R., Dynamic Programming, Princeton, N. J., 1957.
21. Guillemin, E. A., The Mathematics of Circuit Analysis, J. Wiley & Sons, Inc., N. Y., 1949.



OPTIMUM PASSIVE BEARING ESTIMATION
IN A SPATIALLY INCOHERENT NOISE ENVIRONMENT

by

Verne H. MacDonald
and
Peter M. Schultheiss

Progress Report No. 37

General Dynamics/Electric Boat Research

(8050-31-55001)

June 1968

DEPARTMENT OF ENGINEERING
AND APPLIED SCIENCE

YALE UNIVERSITY

Summary

This report investigates the minimum bearing error attainable with a linear passive array. Signal and noise are stationary Gaussian processes and the noise is assumed to be statistically independent from hydrophone to hydrophone. The Cramér-Rao technique is used to set a lower bound on the rms bearing error for linear arrays with an arbitrary number of arbitrarily spaced hydrophones. In order to obtain meaningful comparisons with the performance of a conventional split beam tracker the results are then specialized to the case of equally spaced hydrophones. One finds

- 1) For a two hydrophone array (arbitrary signal and noise spectra) the split beam tracker reaches the Cramér-Rao lower bound (and is therefore optimal) if each hydrophone output is passed through an appropriate linear filter prior to further processing. The required filter is a generalized version of the Eckart filter.
- 2) For arrays with M equally spaced hydrophones the split beam tracker accuracy comes very close to the Cramér-Rao lower bound if the combined output of each array half is passed through a generalized Eckart filter prior to further processing. Under these conditions the split beam tracker rms error exceeds the lower bound by a factor depending only on the number of hydrophones and increasing monotonically from unity at $M = 2$ to $\sqrt{4/3}$ at $M \rightarrow \infty$.
- 3) The dependence of the rms error on signal-to-noise ratio is the same for the split beam tracker and for the Cramér-Rao lower bound. If the post beam forming signal-to-noise ratio is much smaller than unity throughout the processed frequency band the rms error

varies as the inverse first power of the signal-to-noise ratio.

If the post beam forming signal-to-noise ratio is much larger than unity throughout the processed frequency band the rms error varies inversely with the half power of the signal-to-noise ratio.

I. Introduction

The present report treats the case of a linear array with an arbitrary number of hydrophones and arbitrary spacing. The Cram r-Rao lower bound on rms bearing estimation error is derived in terms of samples of the Fourier transforms of the hydrophone outputs over a finite observation time. We assume a plane wavefront, emanating from a distant target. The bearing angle θ is measured from an axis perpendicular to the array axis. (See Figure 1).

Noise is assumed independent from hydrophone to hydrophone. Hydrophone outputs due to signal and due to noise are assumed to be zero-mean Gaussian variables.

For arbitrary spacing, the lower bound is obtained in a cumbersome form, but for uniform spacing, the result is relatively simple.

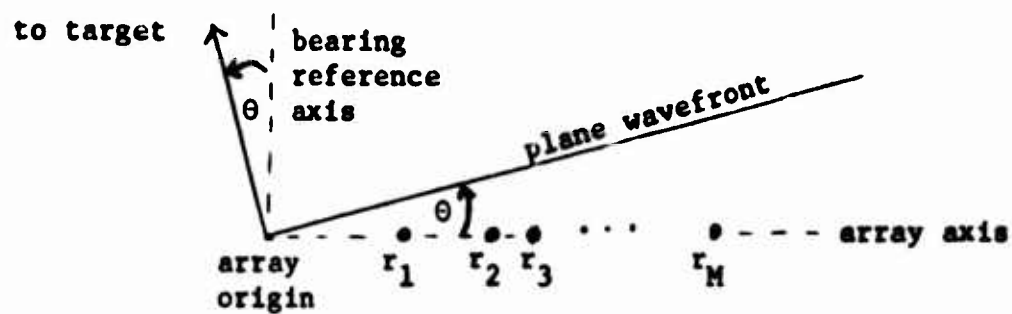


Figure 1
Array Geometry

II. Fourier Transforms of Hydrophone Outputs

The voltage waveform $f_i(t)$ produced by each of the M hydrophones in the assumed linear array may be written as the superposition of a signal component $s_i(t)$ and a noise component $n_i(t)$. If the voltage induced by the signal plane wavefront in a hypothetical hydrophone at the arbitrary array axis origin is written as $s(t)$, then the signal waveform at the i th hydrophone is $s(t-\Delta_i)$, where Δ_i is the wavefront delay between the origin and the i th hydrophone. We shall use the following expression frequently, with c representing sound velocity:

$$(1) \quad \Delta_i = r_i/c \sin \theta . \quad (i = 1, \dots, M)$$

The hydrophone outputs are expressed as

$$(2) \quad f_i(t) = s(t-\Delta_i) + n_i(t) \quad (i = 1, \dots, M)$$

Note that attenuation of signal amplitude and nonuniformity of velocity along the array are neglected.

We shall soon require an expression for the correlation between hydrophone outputs. Let $R_s(\tau)$ represent the signal autocorrelation, and let $R_{ni}(\tau)$ represent noise autocorrelation at the i th hydrophone. Assume that the noise is white, with the same power level at all hydrophones; then $R_{ni}(\tau) = N\delta(\tau)$ for all i .

This assumption is actually not at all restrictive: One can think of each hydrophone output as having been passed through a filter which prewhitens the noise prior to further processing. Such an operation clearly does not alter the minimum rms error for, if necessary, it could always be reversed by the optimum processor. It follows that the results are quite general with regard to signal and noise spectral properties, if

one interprets the signal spectrum as the actual signal spectrum modified by a linear filter which prewhitens the noise.

Assume also that noise is independent from hydrophone to hydrophone and independent of the signal process. Then,

$$(3) \quad \overline{f_i(t+\tau) f_j(t)} = \overline{[s(t+\tau-\Delta_i) + n_i(t+\tau)] [s(t-\Delta_j) + n_j(t)]} \\ = R_s(\tau-\Delta_i+\Delta_j) + N\delta(\tau) \delta_{ij}, \text{ where}$$

$$\delta_{ij} = \begin{cases} 1 & i = j \\ 0 & i \neq j \end{cases}$$

The Fourier transforms of the hydrophone outputs over an observation time T may be written as

$$(4) \quad F_i(w) = \int_{-T/2}^{T/2} f_i(t) e^{-jwt} dt. \quad (i = 1, \dots, M)$$

Henceforth we shall consider a hypothetical processor which samples these Fourier transforms at frequencies $f_k = k / T$, or

$$(5) \quad w_k = k \frac{2\pi}{T}.$$

Note that if $s(t)$ and all $n_i(t)$ are assumed to be zero-mean Gaussian variables, then all $f_i(t)$ are zero-mean Gaussian variables. The real and imaginary parts of all the $F_i(w)$, being the result of linear operations on the $f_i(t)$, are likewise zero-mean Gaussian variables.

The likelihood function, which depends on bearing θ , is the joint probability density of all the frequency samples of the Fourier transforms of all the hydrophone outputs; we write the likelihood function as¹

¹_T - transpose; * - complex conjugate.

$$(6) \quad T(\theta) = \frac{1}{(2\pi)^{nM} \det \underline{R}} e^{-\frac{1}{2} \underline{F}^T \underline{R}^{-1}(\theta) \underline{F}^*},$$

where \underline{F} is the vector of all samples, arrayed in the form

$$(7) \quad \underline{F} = F_1(w_1), \dots, F_M(w_1); F_1(w_2), \dots, F_M(w_2); \dots; F_1(w_n), \dots, F_M(w_n).$$

The corresponding $Mn \times Mn$ correlation matrix is \underline{R} , whose elements, in terms of hydrophone indices i, j and frequency indices k, l , are

$$(8) \quad R_{i, k; j, l} = \frac{1}{2} \overline{F_i^*(w_k) F_j(w_l)} \quad \begin{matrix} (i, j = 1, \dots, M) \\ (k, l = 1, \dots, n) \end{matrix}$$

In Appendix A, certain conditions are shown to be necessary to permit the writing of the joint probability density of Gaussian complex variables in the form (6). Presently we shall verify that these conditions are fulfilled for the variables \underline{F} .

First we derive an expression for the correlation $\overline{F_i^*(w) F_j(\sigma)}$, making use of the fundamental relationship between the autocorrelation function and spectrum of any real stationary random process.

$$(9) \quad S(w) = \int_{-\infty}^{\infty} R(\tau) e^{-jw\tau} d\tau \quad R(\tau) = \frac{1}{2\pi} \int_{-\infty}^{\infty} S(w) e^{jw\tau} dw$$

On the basis of (3) and (4), substituting (9), we obtain

$$\begin{aligned} (10) \quad \overline{F_i^*(w) F_j(\sigma)} &= \iint_{-T/2}^{T/2} \overline{f_i(t) f_j(u)} e^{j(wt - \sigma u)} dt du \\ &= \iint_{-T/2}^{T/2} [R_s(t - \Delta_1 - u + \Delta_j) + N\delta(t - u)\delta_{ij}] e^{j(wt - \sigma u)} dt du \\ &= \iint_{-T/2}^{T/2} dt du \frac{1}{2\pi} \int_{-\infty}^{\infty} d\alpha [S_s(\alpha) + N\delta_{ij}] e^{j\alpha(t - u + \Delta_j - \Delta_1)} e^{j(wt - \sigma u)} \\ &= \frac{1}{2\pi} \int_{-\infty}^{\infty} d\alpha [S_s(\alpha) + N\delta_{ij}] e^{j\alpha(\Delta_j - \Delta_1)} \int_{-T/2}^{T/2} dt e^{j(\alpha + w)t} \int_{-T/2}^{T/2} du e^{-j(\alpha + \sigma)u} \end{aligned}$$

In the above expressions, $S_s(\alpha)$ represents the signal spectrum, and N is the white noise spectral density. Consider the type of integral which appears in the last line of (10).

$$(11) \quad \int_{-T/2}^{T/2} du e^{-j(\alpha+\sigma)u} = \frac{e^{-j(\alpha+\sigma)T/2} - e^{j(\alpha+\sigma)T/2}}{-j(\alpha+\sigma)} = \frac{2 \sin(\alpha+\sigma)T/2}{\alpha+\sigma}$$

In the limit as $T \rightarrow \infty$, the above expression approaches $2\pi \delta(\alpha+\sigma)$, where $\delta(\cdot)$ is the Dirac delta function. If $\alpha = -\sigma$, the value of the expression is T . The limiting form of the correlation for large T is

$$(12) \quad \begin{aligned} & \lim_{T \rightarrow \infty} \overline{F_1^*(w) F_j(\sigma)} \\ &= \lim_{T \rightarrow \infty} \frac{1}{2\pi} \int_{-\infty}^{\infty} d\alpha [S_s(\alpha) + N\delta_{1j}] e^{j\alpha(\Delta_j - \Delta_1)} \frac{2 \sin(\alpha+w)T/2}{\alpha+w} \cdot \frac{2 \sin(\alpha+\sigma)T/2}{\alpha+\sigma} \\ &= 2\pi \int_{-\infty}^{\infty} d\alpha [S_s(\alpha) + N\delta_{1j}] e^{j\alpha(\Delta_j - \Delta_1)} \delta(\alpha+w) \delta(\alpha+\sigma) \end{aligned}$$

It is clear that for infinite observation time, samples at different frequencies w and σ are uncorrelated. We shall assume that the actual observation time is sufficiently large so that the correlation of samples at different frequencies is negligible compared with the correlation of samples at the same frequency. At a single frequency, the correlation, with the assumption of large T , is

$$(13) \quad \begin{aligned} \overline{F_1^*(w) F_j(w)} &= \frac{1}{2\pi} \int_{-\infty}^{\infty} d\alpha [S_s(\alpha) + N\delta_{1j}] e^{j\alpha(\Delta_j - \Delta_1)} \left[\frac{2 \sin(\alpha+w)T/2}{\alpha+w} \right]^2 \\ &= \int_{-\infty}^{\infty} d\alpha [S_s(\alpha) + N\delta_{1j}] e^{j\alpha(\Delta_j - \Delta_1)} \left[\frac{2 \sin(\alpha+w)T/2}{\alpha+w} \right] \delta(\alpha+w) \\ &= [S_s(-w) + N\delta_{1j}] e^{-jw(\Delta_j - \Delta_1)} T = T [S_s(w) + N\delta_{1j}] e^{jw(\Delta_1 - \Delta_j)} \end{aligned}$$

The conditions (A-14) which must be satisfied in order for the formulation (6) to be valid may be expressed for the present case as

$$(14a) \quad \overline{F_{c1}(w) F_{cj}(\sigma)} = \overline{F_{s1}(w) F_{sj}(\sigma)}$$

$$(14b) \quad \overline{F_{c1}(w) F_{s1}(w)} = 0$$

$$(14c) \quad \overline{F_{c1}(w) F_{sj}(\sigma)} = -\overline{F_{s1}(w) F_{cj}(\sigma)},$$

where $F_{c1}(w)$ and $F_{s1}(w)$ represent the real and imaginary parts of $F_1(w)$, obeying the relations

$$(15) \quad F_1(w) = F_{c1}(w) + j F_{s1}(w)$$

$$F_{c1}(w) = \int_{-T/2}^{T/2} f_1(t) \cos wt \, dt \quad F_{s1}(w) = \int_{-T/2}^{T/2} f_1(t) \sin wt \, dt .$$

In Appendix B it is proved that these conditions are asymptotically satisfied as the observation time approaches infinity, so long as all sample frequencies have the same sign. We shall arbitrarily deal with positive frequencies only. No information is discarded, since the Fourier transform of a real variable obeys the relation $F(-w) = F^*(w)$.

III. The Correlation Matrix, Its Determinant, and Its Inverse

In the previous section, it was established that samples at different frequencies are asymptotically uncorrelated as the observation time approaches infinity. The elements of the correlation matrix, by (8) and (13), are

$$(16) \quad \begin{aligned} R_{1,k;j,l} &= \delta_{kl} \frac{T}{2} e^{-j\omega_k(\Delta_j - \Delta_1)} [S_s(\omega_k) + N\delta_{1j}] \\ &= \delta_{kl} \frac{T}{2} a_{1j}^k (S^k + N\delta_{1j}), \end{aligned} \quad \begin{aligned} (1,j=1,\dots,M) \\ (k,l=1,\dots,n) \end{aligned}$$

where the following notation is implicitly defined for convenience.

$$(17) \quad a_{1j}^k = e^{j\omega_k(\Delta_1 - \Delta_j)} \quad S^k = S_s(\omega_k).$$

We are now ready to write out the correlation matrix in detail. For reference, the \underline{F} vector is written at the edges. Note that the matrix is composed of n^2 submatrices of dimension $M \times M$, each of which correlates samples from all hydrophones at two sample frequencies. Only the diagonal submatrices are nonzero.

$$(18) \quad \underline{R} = \frac{T}{2} \begin{bmatrix} \begin{array}{ccc|c|c} S^{1+N} & a_{12}^1 S^1 & \dots & a_{1M}^1 S^1 & F_1(\omega_1) \\ a_{21}^1 S^1 & S^{1+N} & \dots & a_{2M}^1 S^1 & F_2(\omega_1) \\ \vdots & \vdots & \ddots & \vdots & \vdots \\ a_{M1}^1 S^1 & a_{M2}^1 S^1 & \dots & S^{1+N} & F_M(\omega_1) \end{array} & \dots & \begin{array}{c} \text{all elements} \\ \text{zero} \end{array} \\ \hline \begin{array}{c} \vdots \\ \vdots \\ \vdots \end{array} & \begin{array}{c} \vdots \\ \vdots \\ \vdots \end{array} & \begin{array}{c} \vdots \\ \vdots \\ \vdots \end{array} \\ \hline \begin{array}{c} \vdots \\ \vdots \\ \vdots \end{array} & \begin{array}{c} \vdots \\ \vdots \\ \vdots \end{array} & \begin{array}{ccc|c|c} S^{n+N} & a_{12}^n S^n & \dots & a_{1M}^n S^n & F_1(\omega_n) \\ a_{21}^n S^n & S^{n+N} & \dots & a_{2M}^n S^n & F_2(\omega_n) \\ \vdots & \vdots & \ddots & \vdots & \vdots \\ a_{M1}^n S^n & a_{M2}^n S^n & \dots & S^{n+N} & F_M(\omega_n) \end{array} \end{array}$$

$F_1(\omega_1), F_2(\omega_1), \dots, F_M(\omega_1); \dots; F_1(\omega_n), F_2(\omega_n), \dots, F_M(\omega_n)$

Appendix C furnishes verification of the results given here for the determinant and inverse of \underline{Q} . The determinant is found to be independent of bearing angle. The inverse, like \underline{Q} itself, contains nonzero elements only in the n diagonal $M \times M$ submatrices. Each diagonal submatrix of \underline{Q}^{-1} is the inverse of the corresponding submatrix of \underline{Q} . The determinant and inverse follow.

$$(19) \quad \det \underline{Q} = (T/2)^{Mn} N^{(M-1)n} \prod_{k=1}^n (N + MS^k)$$

$$(20) \quad \underline{Q}^{-1} = \frac{2}{T} \begin{bmatrix} \frac{(M-1)S^{1+N}}{MS^{1N+N^2}} & \frac{-a_{12}^1 S^1}{MS^{1N+N^2}} & \dots & \frac{-a_{1M}^1 S^1}{MS^{1N+N^2}} & & \\ \frac{-a_{21}^1 S^1}{MS^{1N+N^2}} & \frac{(M-1)S^{1+N}}{MS^{1N+N^2}} & \dots & \frac{-a_{2M}^1 S^1}{MS^{1N+N^2}} & & \\ \vdots & \vdots & \ddots & \vdots & & \\ \frac{-a_{M1}^1 S^1}{MS^{1N+N^2}} & \frac{-a_{M2}^1 S^1}{MS^{1N+N^2}} & \dots & \frac{(M-1)S^{1+N}}{MS^{1N+N^2}} & & \\ & \vdots & & & \ddots & \\ & \vdots & & & & \ddots \end{bmatrix} \dots \begin{bmatrix} \text{all elements} \\ \text{zero} \end{bmatrix}$$

$$\begin{bmatrix} \vdots & & & & & \\ \vdots & & & & & \\ \vdots & & & & & \end{bmatrix}$$

$$\begin{bmatrix} \text{all elements} \\ \text{zero} \end{bmatrix} \dots \begin{bmatrix} \frac{(M-1)S^{n+N}}{MS^{nN+N^2}} & \frac{-a_{12}^n S^n}{MS^{nN+N^2}} & \dots & \frac{-a_{1M}^n S^n}{MS^{nN+N^2}} \\ \frac{-a_{21}^n S^n}{MS^{nN+N^2}} & \frac{(M-1)S^{n+N}}{MS^{nN+N^2}} & \dots & \frac{-a_{2M}^n S^n}{MS^{nN+N^2}} \\ \vdots & \vdots & & \vdots \\ \frac{-a_{M1}^n S^n}{MS^{nN+N^2}} & \frac{-a_{M2}^n S^n}{MS^{nN+N^2}} & \dots & \frac{(M-1)S^{n+N}}{MS^{nN+N^2}} \end{bmatrix}$$

IV. The Likelihood Function

We are now in a position to write out a detailed expression for the likelihood function $L(\theta)$ in the form (6). \underline{F} , $\det \underline{Q}$ and \underline{Q}^{-1} are taken from (7), (19), and (20), respectively; i and j are the hydrophone indices; k and l are frequency indices.

$$\begin{aligned}
 (21) \quad L(\theta) &= \frac{1}{(2\pi)^{n_{\det \underline{Q}}}} e^{-\frac{1}{2} \underline{F}^T \underline{Q}^{-1}(\theta) \underline{F}} \\
 &= \frac{1}{(2\pi)^{n_{\det \underline{Q}}}} \exp \left\{ -\frac{1}{2} \sum_{k=1}^n \sum_{l=1}^n \sum_{i=1}^M \sum_{j=1}^M F_i^k Q_{i,k;j,l}^{-1} F_j^{l*} \right\} \\
 &= \frac{1}{(2\pi)^{n_{\det \underline{Q}}}} \exp \left\{ -\frac{1}{2} \sum_{k=1}^n \sum_{i=1}^M \sum_{j=1}^M F_i^k Q_{i,k;j,k}^{-1} F_j^{k*} \right\} \\
 &= \frac{1}{(2\pi)^n (T/2)^{Mn} N^{(M-1)n} \prod_{k=1}^n (N+MS^k)} \times \\
 &\quad \exp \left\{ -\frac{1}{2} \sum_{k=1}^n \sum_{i=1}^M \sum_{j=1}^M F_i^k \frac{2}{T} \frac{-a_{ij}^k S^k}{MS^k N+N^2} F_j^{k*} \right. \\
 &\quad \left. - \frac{1}{2} \sum_{k=1}^n \sum_{i=1}^M F_i^k \frac{2}{T} \frac{(M-1) S_{N+N}^k}{MS^k N+N^2} F_i^{k*} \right\}
 \end{aligned}$$

V. General Results for the Lower Bound on Bearing Estimation Error

The variable θ , bearing, which in a practical situation has a fixed but unknown value, appears as a parameter in the probability density (the likelihood function $L(\theta)$) of the set \underline{F} of random variables. When an estimate of θ is derived from a set of measured values of \underline{F} , a method is known¹ for computing the lower bound on the variance of the estimate $\hat{\theta}$ of θ . According to this method,

$$(22) \quad D^2(\hat{\theta}) \geq \left[\overline{\left| \frac{\partial \log L}{\partial \theta} \right|^2} \right]^{-1},$$

where the average is taken over the random variables \underline{F} .

In the final form of (21), note that $L(\theta)$ depends on θ only through the terms a_{ij}^k . By (1) and (17),

$$(23) \quad a_{ij}^k = e^{jw_k \frac{r_i - r_j}{c} \sin \theta} \quad a_{ij}^k = a_{ji}^{k*} = 1/a_{ji}^k$$

Now we differentiate the logarithm of the likelihood function

$$(24) \quad \frac{\partial \log L}{\partial \theta} = \frac{\partial}{\partial \theta} \left\{ -\frac{1}{2} \sum_{k=1}^n \sum_{i=1}^M \sum_{j=1}^M F_i^k \frac{2}{T} \frac{-a_{ij}^k S^k}{MS^k N+N^2} F_j^{k*} \right\}$$

$$= \sum_{k=1}^n \sum_{i=1}^M \sum_{j=1}^M F_i^k \frac{1}{T} \frac{(\partial a_{ij}^k / \partial \theta) S^k}{MS^k N+N^2} F_j^{k*}$$

$i \neq j$

¹Harold Cramér, Mathematical Methods of Statistics, Princeton, 1963, §32.8

$$= \frac{1}{T} \sum_{k=1}^n \sum_{i=1}^M \sum_{j=1}^M \underset{i \neq j}{F_i^k} \frac{j w_k \frac{r_i - r_j}{c} \cos \theta a_{ij}^k S^k}{MS^k N + N^2} F_j^{k*}$$

$$= \frac{1 \cos \theta}{Tc} \sum_{k=1}^n \sum_{i=1}^M \sum_{j=1}^M F_i^k \frac{w_k (r_i - r_j) a_{ij}^k S^k}{MS^k N + N^2} F_j^{k*} \quad 1$$

Now, for the next step toward the lower bound, with k and l frequency indices, and i, j, p , and q hydrophone indices,

$$(25) \quad \overline{\left| \frac{\partial \log L}{\partial \theta} \right|^2} = \left\langle \left\{ \frac{1 \cos \theta}{Tc} \sum_{k=1}^n \sum_{i=1}^M \sum_{j=1}^M \underset{i \neq j}{F_i^k} \frac{w_k (r_i - r_j) a_{ij}^k S^k}{MS^k N + N^2} F_j^{k*} \right\} \times \right. \\ \left. \left\{ \frac{-1 \cos \theta}{Tc} \sum_{l=1}^n \sum_{p=1}^M \sum_{q=1}^M F_p^{l*} \frac{w_l (r_p - r_q) a_{pq}^l S^l}{MS^l N + N^2} F_q^l \right\} \right\rangle \\ = \frac{\cos^2 \theta}{T^2 c^2} \sum_{k=1}^n \sum_{l=1}^n \sum_{i=1}^M \sum_{j=1}^M \sum_{p=1}^M \sum_{q=1}^M \overline{F_i^k F_j^{k*} F_p^{l*} F_q^l} \frac{w_k w_l (r_i - r_j) (r_p - r_q) a_{ij}^k a_{pq}^l S^k S^l}{[MS^k N + N^2] [MS^l N + N^2]}$$

In Appendix D we demonstrate that the following expansion is valid for complex variables with zero-mean real and imaginary parts, all jointly Gaussian:

$$(26) \quad \overline{F_i^k F_j^{k*} F_p^{l*} F_q^l} = \overline{F_i^k F_j^{k*}} \cdot \overline{F_p^{l*} F_q^l} + \overline{F_i^k F_p^{l*}} \cdot \overline{F_j^{k*} F_q^l} + \overline{F_i^k F_q^l} \cdot \overline{F_j^{k*} F_p^{l*}}$$

The above correlations may be deduced from Section II. Correlations between

¹We discontinue writing " $i \neq j$," since the factor $(r_i - r_j)$ cancels terms in which $i = j$ anyway.

samples at different frequencies are essentially zero. Terms of the form

$\overline{F_1^k F_q^l} = \overline{F_1(w_k) F_q(w_l)}$ require special attention. When this term is

developed as in (12), the result is

$$(27) \quad \overline{F_1(w_k) F_q(w_l)} = 2\pi \int_{-\infty}^{\infty} d\alpha [S_s(\alpha) + N\delta_{1q}] e^{j\alpha(\Delta_1 - \Delta_q)} \delta(\alpha - w_k) \delta(\alpha + w_l).$$

Since we are considering only positive sample frequencies, this expression

must equal zero; $\overline{F_j^{k*} F_p^{l*}}$ also equals zero. Returning to (26), substituting

the correlations (13), we have

$$(26) \quad \overline{F_1^k F_j^{k*} F_p^{l*} F_q^l} = (a_{j1}^k TS^k) (a_{pq}^l TS^l) \\ + [a_{p1}^k T(S^{k+N\delta_{p1}})] [a_{jq}^l T(S^{l+N\delta_{jq}})] \delta_{kl}$$

This result is now substituted into (25).

$$(29) \quad \left| \frac{\partial \log L}{\partial \theta} \right|^2 = \frac{\cos^2 \theta}{T^2 c^2} \sum_{k=1}^n \sum_{l=1}^n \sum_{i=1}^M \sum_{j=1}^M \sum_{p=1}^M \sum_{q=1}^M \frac{w_k w_l (r_i - r_j) (r_p - r_q) a_{ij}^k a_{qp}^l S^k S^l}{[MS^{k+N^2}] [MS^{l+N^2}]} \times \\ T^2 [a_{j1}^k a_{pq}^l S^k S^l + a_{p1}^k a_{jq}^l (S^{k+N\delta_{p1}}) (S^{l+N\delta_{jq}}) \delta_{kl}] \\ = \frac{\cos^2 \theta}{c^2} \sum_{k=1}^n \sum_{l=1}^n \sum_{i=1}^M \sum_{j=1}^M \sum_{p=1}^M \sum_{q=1}^M \frac{w_k w_l (r_i - r_j) (r_p - r_q) a_{ij}^k a_{ij}^k a_{qp}^l a_{qp}^l (S^k)^2 (S^l)^2}{[MS^{k+N^2}] [MS^{l+N^2}]} \\ + \frac{\cos^2 \theta}{c^2} \sum_{k=1}^n \sum_{i=1}^M \sum_{j=1}^M \sum_{p=1}^M \sum_{q=1}^M \left\{ \frac{(w_k)^2 (r_i - r_j) (r_p - r_q) a_{ij}^k a_{qp}^k a_{p1}^k a_{jq}^k (S^k)^2}{(MS^{k+N^2})^2} \times \right. \\ \left. [(S^k)^2 + S^{k(N\delta_{p1} + \delta_{jq})} + N^2 \delta_{p1} \delta_{jq}] \right\}$$

$$\begin{aligned}
&= \frac{\cos^2 \theta}{c^2} \sum_{k=1}^n \sum_{l=1}^n \sum_{i=1}^K \sum_{j=1}^H \sum_{p=1}^M \sum_{q=p+1}^M \frac{w_k w_l (r_i - r_j) \overbrace{(r_p - r_q + r_q - r_p)}^{\equiv 0} (s^k s^l)^2}{[MS^k N + N^2] [MS^l N + N^2]} \\
&+ \frac{\cos^2 \theta}{c^2} \sum_{k=1}^n \sum_{i=1}^M \sum_{j=1}^M \sum_{p=1}^M \sum_{q=1}^M \frac{(w_k)^2 (r_i - r_j) (r_p - r_q) (s^k)^2}{(MS^k N + N^2)^2} \times \\
&\quad e^{j w_k (\Delta_i - \Delta_j + \Delta_q - \Delta_p - \Delta_i + \Delta_j - \Delta_q)} [(s^k)^2 + 2s^k N \delta_{pi} + N^2 \delta_{pi} \delta_{jq}]^1 \\
&= \frac{\cos^2 \theta}{c^2} \sum_{k=1}^n \sum_{i=1}^M \sum_{j=1}^M \sum_{p=1}^M \sum_{q=p+1}^M \frac{(w_k)^2 (r_i - r_j) \overbrace{(r_p - r_q + r_q - r_p)}^{\equiv 0} (s^k)^4}{(MS^k N + N^2)^2} \\
&\quad + \sum_{k=1}^n \sum_{i=1}^M \sum_{j=1}^M \sum_{q=1}^M \frac{(w_k)^2 (r_i - r_j) (r_i - r_q) 2(s^k)^3 N}{(MS^k N + N^2)^2} \\
&\quad + \sum_{k=1}^n \sum_{i=1}^M \sum_{j=1}^M \frac{(w_k)^2 (r_i - r_j)^2 (s^k)^2 N^2}{(MS^k N + N^2)^2} \\
&= \frac{\cos^2 \theta}{c^2} \sum_{k=1}^n \sum_{i=1}^M \sum_{j=i+1}^M \sum_{q=1}^M \frac{(w_k)^2 (r_i - r_j)^2 2(s^k)^3 N}{(MS^k N + N^2)^2} \\
&\quad + \sum_{k=1}^n \sum_{i=1}^M \sum_{j=i+1}^M \frac{(w_k)^2 2(r_i - r_j)^2 (s^k)^2 N^2}{(MS^k N + N^2)^2} \\
&= \frac{2 \cos^2 \theta}{c^2} \sum_{k=1}^n \frac{(w_k s^k)^2}{(MS^k N + N^2)^2} \sum_{i=1}^M \sum_{j=i+1}^M (r_i - r_j)^2 (MS^k N + N^2)
\end{aligned}$$

¹We replace $(\delta_{pi} + \delta_{jq})$ with $2\delta_{pi}$, which is equivalent because of symmetries in the expression.

For computational convenience, we use an integral with respect to frequency to replace the summation on the frequency index k . By (5), the interval between sample frequencies is $\Delta\omega = 2\pi/T$. We multiply and divide the final result in (29) by $\Delta\omega$, then replace the summation by an integral and $\Delta\omega$ by $d\omega$. We assume that the observation time T is large enough so that this approximation introduces little error, and that the signal spectrum is essentially zero for frequencies above the highest sample frequency, ω_{\max} . From (22) and (29),

$$(30) \quad D^2(\hat{\theta}) \geq \left\{ \frac{T}{2\pi} \cdot \frac{2 \cos^2 \theta}{c^2} \int_0^{\omega_{\max}} \frac{\omega^2 S^2(\omega) d\omega}{MS(\omega)N+N^2} \left[\sum_{i=1}^M \sum_{j=i+1}^M (r_i - r_j)^2 \right] \right\}^{-1}$$

This result is entirely general for any signal spectrum and any hydrophone spacing in a linear array. Equation (30) assumes a particularly simple form when the elements of the array are uniformly spaced. In that case

$$(31) \quad r_i = id, \quad (i = 1, \dots, M)$$

where d is the distance between hydrophones. Substituting (31) into (30) and taking the square root of the result, we have

$$(32) \quad D(\hat{\theta}) \geq \frac{c\sqrt{\pi}}{d \sqrt{T} \cos \theta} \left[\int_0^{\omega_{\max}} \frac{\omega^2 S^2(\omega) d\omega}{MS(\omega)N+N^2} \sum_{i=1}^M \sum_{j=i+1}^M (i-j)^2 \right]^{-1/2}$$

We show in Appendix F that

$$(33) \quad \sum_{i=1}^M \sum_{j=i+1}^M (i-j)^2 = \frac{M^4 - M^2}{12} = \frac{M^2(M+1)(M-1)}{12}$$

Substituting (33) into (32) we have

$$\begin{aligned}
 (34) \quad D(\hat{\theta}) &\geq \frac{2\sqrt{3\pi} c}{d\sqrt{T} \cos\theta M\sqrt{(M+1)(M-1)}} \left[\int_0^{w_{\max}} \frac{w^2 S^2(w) dw}{MS(w)N+N^2} \right]^{-1/2} \\
 &= \frac{2\sqrt{3\pi} c}{d\sqrt{T} \cos\theta M\sqrt{M^2-1}} \left[\int_0^{w_{\max}} dw w^2 \frac{\frac{S^2(w)}{N^2}}{1 + M \frac{S(w)}{N}} \right]^{-1/2}
 \end{aligned}$$

Finally, invoking the fact that the signal spectrum of our derivation may be regarded as the actual signal spectrum modified by passage through a filter which prewhitens the noise (see p. 4), one obtains

$$(35) \quad D(\hat{\theta}) \geq \frac{2\sqrt{3\pi} c}{d\sqrt{T} \cos\theta M\sqrt{M^2-1}} \left[\int_0^{w_{\max}} dw w^2 \frac{\frac{S^2(w)}{N^2(w)}}{1 + M \frac{S(w)}{N(w)}} \right]^{-1/2}$$

where $S(w)$ and $N(w)$ now stand for the actual signal and noise spectra.

VI. Comparison with Split Beam Tracker

We now compare the lower bound on rms error given by Equation (35) with the rms error of the conventional split beam tracker (linear equally spaced array) whose idealized block diagram is shown in Figure 2. The basic theory of this tracker is developed in Report No. 29. Adapting¹ the results obtained there to our present purposes and nomenclature we obtain:

The average output \bar{z} is given by

$$(36) \quad \bar{z} = \frac{2}{2\pi} \sum_{l=1}^{M/2} \sum_{k=1}^{M/2} \int_0^{w_{\max}} dw \, w \, S(w) |H(jw)|^2 \sin[w(k-l + \frac{M}{2}) \frac{d}{c} (\sin \theta - \sin \phi)]$$

θ is the target bearing, as before, while ϕ is the direction in which the tracker is steered. An elementary computation now yields the on target slope of the average tracker output curve.

$$(37) \quad \left. \frac{\partial \bar{z}}{\partial \phi} \right|_{\phi=\theta} = - \frac{2}{2\pi} \int_0^{w_{\max}} dw \, w^2 \, S(w) |H(jw)|^2 \frac{d}{c} \cos \theta \sum_{l=1}^{M/2} \sum_{k=1}^{M/2} (k-l + \frac{M}{2})$$

With the change of variable $k-l = r$ one can readily evaluate the double sum.

¹Note: In Report No. 29 the total number of hydrophones is $2M$, here it is M . In Report No. 29 the 90° phase shift is obtained by an element with transfer function $jw/|w|$, a prime phase shift, here it is obtained by a differentiator with transfer function jw . Furthermore, $S(w)$ is here defined such that total power is

$$\frac{1}{2\pi} \int_{-\infty}^{\infty} S(w) \, dw.$$

$$\begin{aligned}
 (38) \quad \sum_{l=1}^{M/2} \sum_{k=1}^{M/2} (k-l + \frac{M}{2}) &= \sum_{r=-(\frac{M}{2}-1)}^{\frac{M}{2}-1} (\frac{M}{2}+r) (\frac{M}{2} - |r|) \\
 &= \frac{M^2}{4} (M-1) + \frac{M}{2} \sum_{r=-(\frac{M}{2}-1)}^{\frac{M}{2}-1} r - \frac{M}{2} \sum_{r=-(\frac{M}{2}-1)}^{\frac{M}{2}-1} |r| - \sum_{r=-(\frac{M}{2}-1)}^{\frac{M}{2}-1} r|r| \\
 &= \frac{M^3}{8}
 \end{aligned}$$

Hence, using the fact that $S(w)$ is even,

$$(39) \quad \left. \frac{\partial z}{\partial \phi} \right|_{\phi=0} = -\frac{1}{2\pi} \frac{d}{c} \cos \theta \frac{M^3}{8} \int_{-w_{\max}}^{w_{\max}} dw w^2 S(w) |H(jw)|^2$$

The on target tracker output variance σ_z^2 is (by similar adaptation of results in Report No. 29)

$$(40) \quad \sigma_z^2 = \frac{1}{8\pi T} \int_{-\infty}^{\infty} dw w^2 |H(jw)|^4 \{M^3 S(w) N(w) + M^2 N(w)\}$$

It follows that the rms error is given by

$$(41) \quad D(\theta) = \frac{\sigma_z}{\left| \frac{\partial z}{\partial \theta} \right|_{\phi=0}} = \frac{\sqrt{2\pi} \times 4 c \sqrt{\int_{-w_{\max}}^{w_{\max}} dw w^2 |H(jw)|^4 \{MS(w) N(w) + N^2(w)\}}}{\sqrt{T} d \cos \theta M^2 \int_{-w_{\max}}^{w_{\max}} dw w^2 |H(w)|^2 S(w)}$$

There remains the adjustment of the spectrum shaping filter $H(jw)$.

Taking a clue from optimum detection theory one suspects that a good

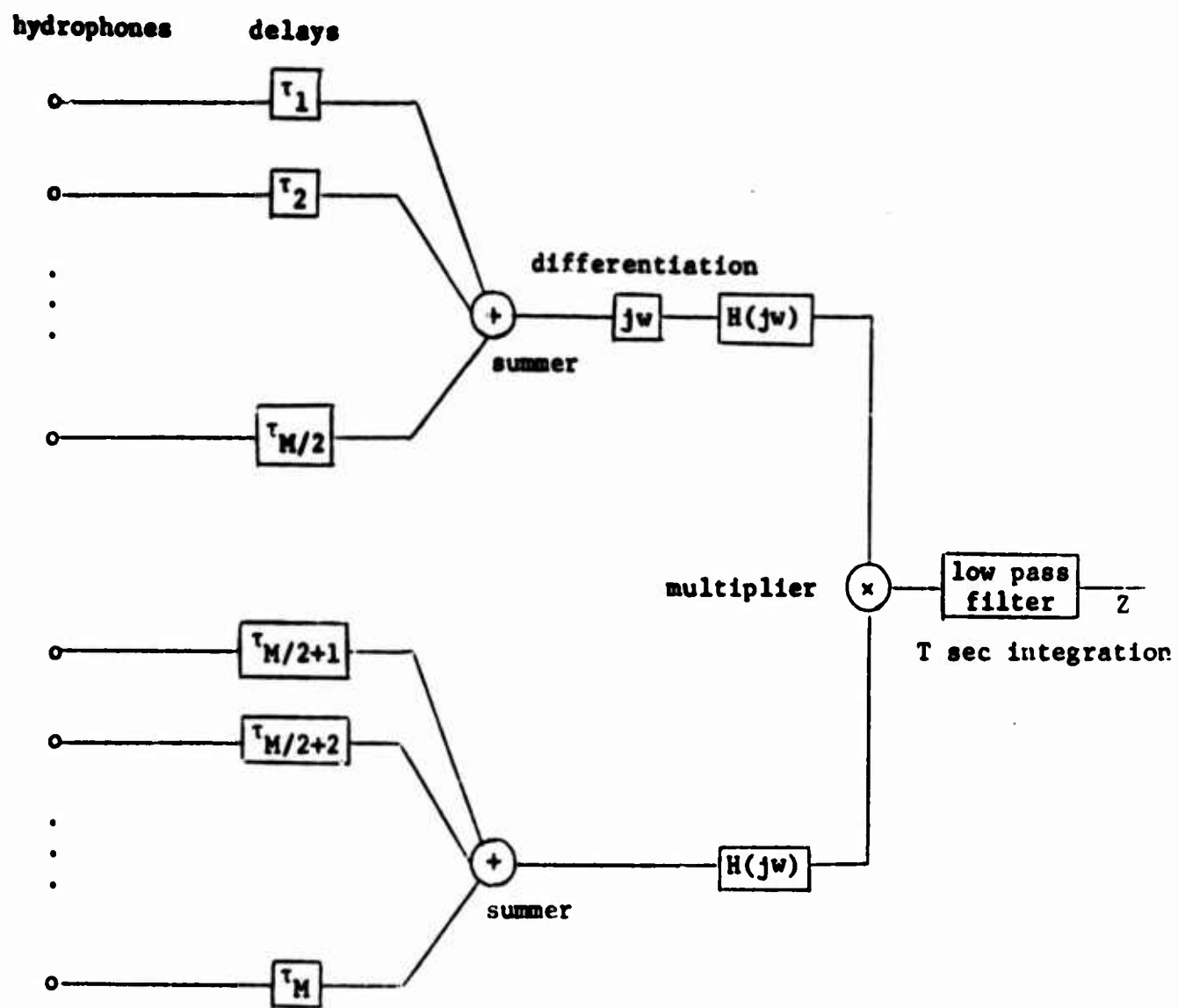


Figure 2

candidate for $H(jw)$ would be the generalized Eckart filter

$$(42) \quad |H(jw)|^2 = \frac{\frac{S(w)}{N^2(w)}}{1 + M \frac{S(w)}{N(w)}} = \frac{S(w)}{M S(w) N(w) + N^2(w)}$$

Substituting Equation (42) into Equation (41) one finds

$$(43) \quad D(\theta) = \frac{\sqrt{2\pi} \cdot 4 c}{\sqrt{T} d \cos \theta M^2} \left[\int_{-w_{\max}}^{w_{\max}} dw w^2 \frac{\frac{S^2(w)}{N^2(w)}}{1 + M \frac{S(w)}{N(w)}} \right]^{-1/2}$$

Comparing Equation (43) and Equation (35) and using once more the fact that $S(w)$ and $N(w)$ are even functions of w

$$(44) \quad \frac{D(\theta)}{D(\hat{\theta})} = \sqrt{\frac{4}{3}} \sqrt{1 - \frac{1}{M^2}}$$

Equation (44) equals unity for $M=2$ and increases steadily to an asymptotic value of $\sqrt{4/3}$ for large M . Thus the split beam tracker reaches the Cramér-Rao lower bound for $M=2$, a fact which had already been observed in Report No. 32 for the special case of $S(w) = N(w)$. For $M=2$, therefore, the split beam tracker is the absolute optimum instrumentation in the sense that it yields the minimum rms error. For $M > 2$ some improvement may be possible, although one cannot assert in general that the Cramér-Rao lower bound is attainable. The important point to observe, however, is the small factor by which $D(\theta)$ can exceed $D(\hat{\theta})$ [Equation (44)]. One can therefore reasonably conclude that the conventional split beam tracker operating in a noise environment independent from hydrophone to hydrophone is so close to the optimum that a search for better instrumentations would

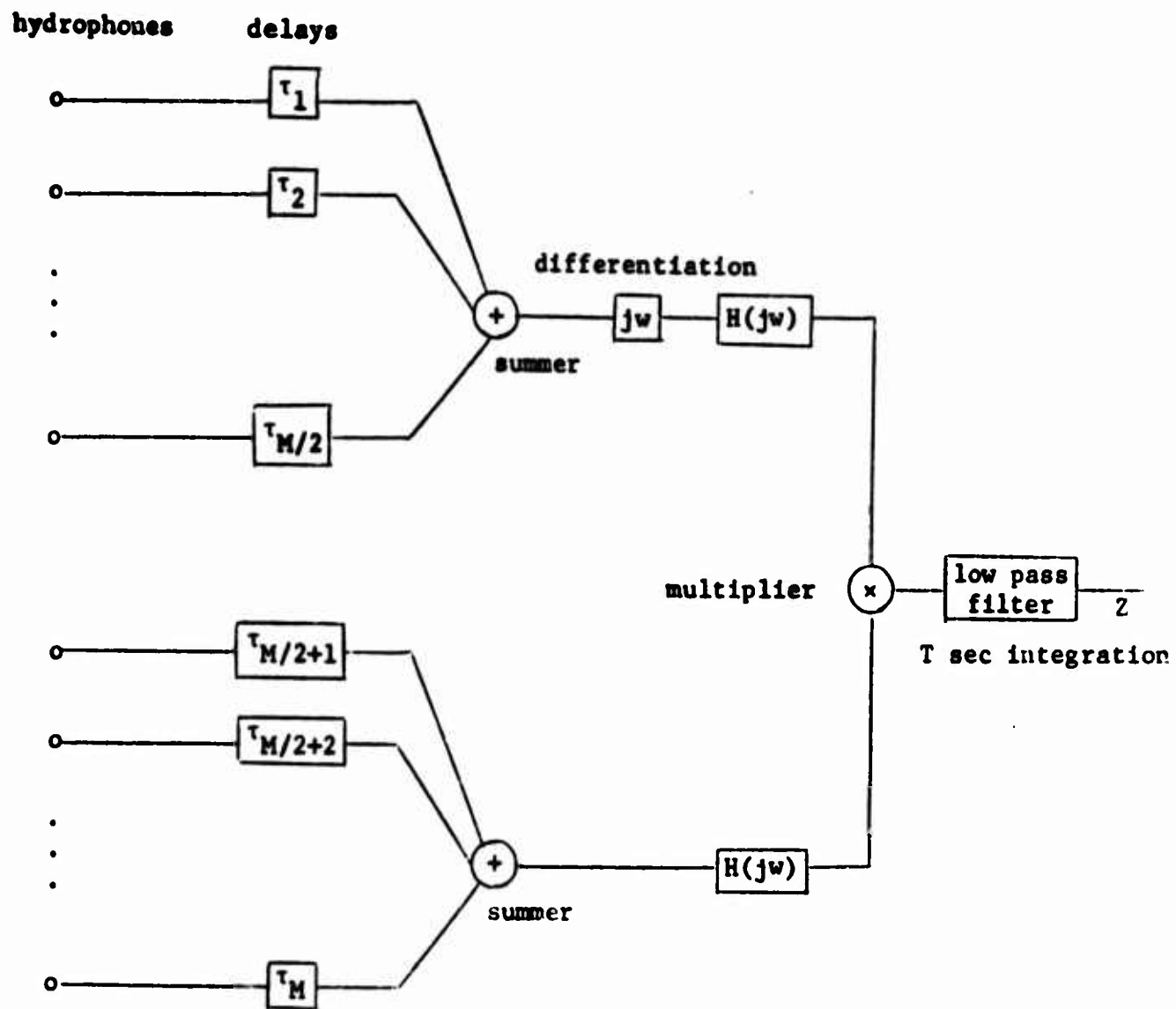


Figure 2

candidate for $H(jw)$ would be the generalized Eckart filter

$$(42) \quad |H(jw)|^2 = \frac{\frac{S(w)}{N^2(w)}}{1 + M \frac{S(w)}{N(w)}} = \frac{S(w)}{M S(w) N(w) + N^2(w)}$$

Substituting Equation (42) into Equation (41) one finds

$$(43) \quad D(\theta) = \frac{\sqrt{2\pi} \cdot 4 c}{\sqrt{T} d \cos \theta M^2} \left[\int_{-w_{\max}}^{w_{\max}} dw w^2 \frac{\frac{S^2(w)}{N^2(w)}}{1 + M \frac{S(w)}{N(w)}} \right]^{-1/2}$$

Comparing Equation (43) and Equation (35) and using once more the fact that $S(w)$ and $N(w)$ are even functions of w

$$(44) \quad \frac{D(\theta)}{D(\hat{\theta})} = \sqrt{\frac{4}{3}} \sqrt{1 - \frac{1}{M^2}}$$

Equation (44) equals unity for $M=2$ and increases steadily to an asymptotic value of $\sqrt{4/3}$ for large M . Thus the split beam tracker reaches the Cramér-Rao lower bound for $M=2$, a fact which had already been observed in Report No. 32 for the special case of $S(w) = N(w)$. For $M=2$, therefore, the split beam tracker is the absolute optimum instrumentation in the sense that it yields the minimum rms error. For $M > 2$ some improvement may be possible, although one cannot assert in general that the Cramér-Rao lower bound is attainable. The important point to observe, however, is the small factor by which $D(\theta)$ can exceed $D(\hat{\theta})$ [Equation (44)]. One can therefore reasonably conclude that the conventional split beam tracker operating in a noise environment independent from hydrophone to hydrophone is so close to the optimum that a search for better instrumentations would

be very difficult to justify.

The dependence of $D(\theta)$ and $D(\hat{\theta})$ on signal-to-noise ratio is precisely the same as that observed in Report No. 32. For low input signal-to-noise ratios the rms error varies as $(S/N)^{-1}$, whereas for large input signal-to-noise ratios it varies as $(S/N)^{-1/2}$.

Appendix A

Joint Probability Density for n Complex Gaussian Variables

We assume that every member of the n -dimensional vector \underline{x} is a complex Gaussian variable; i.e., when x_k is written $x_k = a_k + jb_k$ ($k=1, \dots, n$), the real variables a_k and b_k are Gaussian variables. For convenience, assume $\bar{a}_k = \bar{b}_k = 0$. We wish to establish the conditions on all the variables $\{a_k, b_k\}$ which are necessary to permit writing the joint probability density of the n complex Gaussian variables in the following form,¹ analogous to the joint probability density for real Gaussian variables:

$$(A-1) \quad p(\underline{x}) = \frac{1}{(2\pi)^n \det \underline{P}} e^{-\frac{1}{2} \underline{x}^T \underline{P}^{-1} \underline{x}^*},$$

where \underline{P} is the $n \times n$ correlation matrix with elements

$$(A-2) \quad P_{kl} = 1/2 \overline{x_k^* x_l} \quad (k=1, \dots, n)$$

As a first step, we derive the characteristic function corresponding to the above probability density. The procedure parallels that used by Cramér² for real variables. The characteristic function $\phi(\underline{r})$ is related to the probability density as follows, with $d\underline{x} = da_1 db_1 \dots da_n db_n$ and $\underline{r} = \{r_k\} = \{y_k + jz_k\}$:

¹Notation: T - transpose; $*$ - complex conjugate

²Harald Cramér, op. cit., §11.12

$$\begin{aligned}
 (A-3) \quad \phi(\underline{r}) &= \int_{-\infty}^{\infty} \cdots \int_{-\infty}^{\infty} e^{j \operatorname{Re}\{\underline{r}^{*T} \underline{x}\}} p(\underline{x}) d\underline{x} \\
 &= \int_{-\infty}^{\infty} \cdots \int_{-\infty}^{\infty} \frac{1}{(2\pi)^n \det \underline{P}} e^{j \operatorname{Re}\{\underline{r}^{*T} \underline{x}\} - \frac{1}{2} \underline{x}^T \underline{P}^{-1} \underline{x}}
 \end{aligned}$$

Let \underline{C} designate the unitary matrix which transforms \underline{P}^{-1} into the diagonal matrix \underline{D} as follows:

$$(A-4) \quad \underline{D} = \underline{C}^{*T} \underline{P}^{-1} \underline{C}$$

Let \underline{D} and \underline{D}^{-1} be represented as

$$(A-5) \quad \underline{D} = \begin{bmatrix} d_1 & 0 & \cdots & 0 \\ 0 & d_2 & \cdots & 0 \\ \vdots & \vdots & \ddots & \vdots \\ 0 & 0 & \cdots & d_n \end{bmatrix} \quad \underline{D}^{-1} = \begin{bmatrix} d_1^{-1} & 0 & \cdots & 0 \\ 0 & d_2^{-1} & \cdots & 0 \\ \vdots & \vdots & \ddots & \vdots \\ 0 & 0 & \cdots & d_n^{-1} \end{bmatrix}$$

Note the following relations:

$$(A-6) \quad \underline{D}^{-1} = \underline{C}^{*T} \underline{P} \underline{C} \qquad \underline{C}^{*T} \underline{C} = \underline{I}$$

$$\det \underline{P} = \det \underline{D}^{-1} = \prod_{k=1}^n d_k^{-1}$$

Let the n -dimensional vectors \underline{v} and $\underline{\psi}$ be defined as follows:

$$\begin{aligned}
 (A-7) \quad \underline{r} &= \underline{C}^{*} \underline{v} & v_k &= u_k + jv_k \\
 \underline{x} &= \underline{C}^{*} \underline{\psi} & \psi_k &= p_k + jq_k
 \end{aligned}$$

We shall use the following results:

$$\begin{aligned}
 (A-8) \quad \underline{r}^{*T} \underline{x} &= \underline{v}^{*T} \underline{C}^T \underline{C}^{*} \underline{\psi} = \underline{v}^{*T} \underline{\psi} \\
 d\underline{x} &= |\det \underline{C}^{*}| d\underline{\psi} = 1 \cdot dp_1 dq_1 \cdots dp_n dq_n
 \end{aligned}$$

Substitute (A-7) and (A-8) into (A-3):

$$\begin{aligned}
 (A-9) \quad \phi(\underline{r}) &= \int_{-\infty}^{\infty} \int_{-\infty}^{\infty} \frac{1}{(2\pi)^n \det \underline{D}^{-1}} e^{j \operatorname{Re}(\underline{v}^* \underline{\psi}) - \frac{1}{2} \underline{\psi}^T \underline{C}^* \underline{P}^{-1} \underline{C} \underline{\psi}} d\underline{\psi} \\
 &= \int_{-\infty}^{\infty} \int_{-\infty}^{\infty} \frac{1}{(2\pi)^n \det \underline{D}^{-1}} e^{j \operatorname{Re}(\underline{v}^* \underline{\psi}) - \frac{1}{2} \underline{\psi}^T \underline{D} \underline{\psi}} d\underline{\psi} \\
 &= \prod_{k=1}^n \int_{-\infty}^{\infty} \int_{-\infty}^{\infty} \frac{d_k}{2\pi} e^{j(u_k p_k + v_k q_k) - \frac{1}{2} (p_k + j q_k) d_k (p_k - j q_k)} dp_k dq_k \\
 &= \prod_{k=1}^n \frac{d_k}{2\pi} \int_{-\infty}^{\infty} e^{j u_k p_k - \frac{1}{2} d_k p_k^2} dp_k \int_{-\infty}^{\infty} e^{j v_k q_k - \frac{1}{2} d_k q_k^2} dq_k \\
 &= \prod_{k=1}^n \frac{d_k}{2\pi} \sqrt{\frac{2\pi}{d_k}} e^{-\frac{1}{2} d_k^{-1} u_k^2} \sqrt{\frac{2\pi}{d_k}} e^{-\frac{1}{2} d_k^{-1} v_k^2} \\
 &= \prod_{k=1}^n e^{-\frac{1}{2} (u_k + j v_k) d_k^{-1} (u_k - j v_k)} \\
 &= e^{-\frac{1}{2} \underline{v}^T \underline{D}^{-1} \underline{v}} = e^{-\frac{1}{2} \underline{v}^T \underline{C}^* \underline{P} \underline{C} \underline{v}} \\
 &= e^{-\frac{1}{2} \underline{r}^T \underline{P} \underline{r}}
 \end{aligned}$$

The next step is to set the above characteristic function equal to the characteristic function for the $2n$ real variables $\{a_k, b_k\}$ to ascertain the necessary conditions on these variables. The $2n$ real variables may be arrayed in the vector $\underline{x} = (a_1, b_1, \dots, a_n, b_n)$. Let \underline{R} designate the corresponding $2n \times 2n$ correlation matrix, and let the argument of the characteristic function be the vector $\underline{t} = (y_1, z_1, \dots, y_n, z_n)$. The characteristic function is

$$(A-10) \quad \phi(t) = e^{-\frac{1}{2} t^T R t}$$

We shall now write out the logarithms of $\phi(t)$ and $\phi(\tau)$ in detail and compare them.

$$\begin{aligned}
 (A-11) \quad -2 \log \phi(t) &= \sum_{k=1}^n \sum_{l=1}^n [y_k z_k] \begin{bmatrix} \overline{a_k a_l} & \overline{a_k b_l} \\ \overline{b_k a_l} & \overline{b_k b_l} \end{bmatrix} \begin{bmatrix} y_l \\ z_l \end{bmatrix} \\
 &= \sum_{k=1}^n [y_k z_k] \begin{bmatrix} \overline{a_k^2} & \overline{a_k b_k} \\ \overline{b_k a_k} & \overline{b_k^2} \end{bmatrix} \begin{bmatrix} y_k \\ z_k \end{bmatrix} \\
 &+ \sum_{k=1}^n \sum_{l=k+1}^n \left\{ [y_k z_k] \begin{bmatrix} \overline{a_k a_l} & \overline{a_k b_l} \\ \overline{b_k a_l} & \overline{b_k b_l} \end{bmatrix} \begin{bmatrix} y_l \\ z_l \end{bmatrix} + [y_l z_l] \begin{bmatrix} \overline{a_l a_k} & \overline{a_l b_k} \\ \overline{b_l a_k} & \overline{b_l b_k} \end{bmatrix} \begin{bmatrix} y_k \\ z_k \end{bmatrix} \right\} \\
 &= \sum_{k=1}^n y_k^2 \overline{a_k^2} + 2 y_k z_k \overline{a_k b_k} + z_k^2 \overline{b_k^2} \\
 &+ \sum_{k=1}^n \sum_{l=k+1}^n y_k y_l (2 \overline{a_k a_l}) + y_k z_l (2 \overline{a_k b_l}) + z_k y_l (2 \overline{a_l b_k}) + z_k z_l (2 \overline{b_k b_l})
 \end{aligned}$$

By the result (A-9) and definitions (A-2) and (A-7),

$$\begin{aligned}
 (A-12) \quad -2 \log \phi(\tau) &= \sum_{k=1}^n \sum_{l=1}^n (y_k + j z_k) \{ \frac{1}{2} (\overline{a_k - j b_k} (a_l + j b_l)) \} (y_l - j z_l) \\
 &= \sum_{k=1}^n \frac{1}{2} (y_k^2 + z_k^2) (\overline{a_k^2} + \overline{b_k^2}) \\
 &+ \sum_{k=1}^n \sum_{l=1}^n \frac{1}{2} [(y_k + j z_k) (\overline{a_k - j b_k} (a_l + j b_l)) (y_l - j z_l)] \\
 &\quad k \neq l
 \end{aligned}$$

$$\begin{aligned}
&= \frac{1}{2} \sum_{k=1}^n (y_k^2 + z_k^2) (\overline{a_k^2 + b_k^2}) \\
&+ \frac{1}{2} \sum_{k=1}^n \sum_{\ell=k+1}^n \left\{ [(y_k y_\ell + z_k z_\ell) + j(z_k y_\ell - y_k z_\ell)] [(\overline{a_k a_\ell + b_k b_\ell}) + j(\overline{a_k b_\ell - b_k a_\ell})] \right. \\
&\quad \left. + [(y_\ell y_k + z_\ell z_k) + j(z_\ell y_k - y_\ell z_k)] [(\overline{a_\ell a_k + b_\ell b_k}) + j(\overline{a_\ell b_k - b_\ell a_k})] \right\} \\
&= \frac{1}{2} \sum_{k=1}^n (y_k^2 + z_k^2) (\overline{a_k^2 + b_k^2}) \\
&+ \frac{1}{2} \sum_{k=1}^n \sum_{\ell=k+1}^n [(A_k + jB_k)(C_k + jD_k) + (A_k - jB_k)(C_k - jD_k)] \\
&= \frac{1}{2} \sum_{k=1}^n (y_k^2 + z_k^2) (\overline{a_k^2 + b_k^2}) + \frac{1}{2} \sum_{k=1}^n \sum_{\ell=k+1}^n 2(A_k C_k - B_k D_k),
\end{aligned}$$

where the following definitions are implied:

$$\begin{bmatrix} A_k \\ B_k \\ C_k \\ D_k \end{bmatrix} = \begin{bmatrix} y_k y_\ell + z_k z_\ell \\ z_k y_\ell - y_k z_\ell \\ \overline{a_k a_\ell + b_k b_\ell} \\ \overline{a_k b_\ell - b_k a_\ell} \end{bmatrix}$$

To continue,

$$\begin{aligned}
(A-13) \quad \phi(\underline{r}) &= \frac{1}{2} \sum_{k=1}^n (y_k^2 + z_k^2) (\overline{a_k^2 + b_k^2}) \\
&+ \sum_{k=1}^n \sum_{\ell=k+1}^n [(y_k y_\ell + z_k z_\ell) (\overline{a_k a_\ell + b_k b_\ell}) - (z_k y_\ell - y_k z_\ell) (\overline{a_k b_\ell - b_k a_\ell})]
\end{aligned}$$

We now compare (A-11) and (A-13), equating coefficients of like variable products.

$$\begin{array}{ccc}
 & \overline{\phi(t)} & \overline{\phi(t)} \\
 y_k^2 & \overline{a_k^2} & \frac{1}{2}(\overline{a_k^2} + \overline{b_k^2}) \\
 y_k z_k & 2 \overline{a_k b_k} & 0 \\
 z_k^2 & \overline{b_k^2} & \frac{1}{2}(\overline{a_k^2} + \overline{b_k^2}) \\
 y_k y_l & 2 \overline{a_k a_l} & \overline{a_k a_l} + \overline{b_k b_l} \\
 y_k z_l & 2 \overline{a_k b_l} & \overline{a_k b_l} - \overline{b_k a_l} \\
 z_k y_l & 2 \overline{a_l b_k} & \overline{b_k a_l} - \overline{a_k b_l} \\
 z_k z_l & 2 \overline{b_k b_l} & \overline{a_k a_l} + \overline{b_k b_l}
 \end{array}
 =$$

The following conditions result from solving the above set of equations:

$$\begin{aligned}
 (A-14) \quad \overline{a_k a_l} &= \overline{b_k b_l} \\
 \overline{a_k b_k} &= 0 & (k, l = 1, \dots, n) \\
 \overline{a_k b_l} &= -\overline{a_l b_k}
 \end{aligned}$$

When these conditions are satisfied, the joint probability density of the n complex Gaussian variables may be written as in (A-1).

Appendix B

Verification of Requirements on Fourier Cosine and Sine Transforms

The conditions (14) to be verified are

$$(B-1) \quad \overline{F_{c1}(w) F_{cj}(\sigma)} = \overline{F_{s1}(w) F_{sj}(\sigma)}$$

$$(B-2) \quad \overline{F_{c1}(w) F_{s1}(w)} = 0$$

$$(B-3) \quad \overline{F_{c1}(w) F_{sj}(\sigma)} = - \overline{F_{s1}(w) F_{cj}(\sigma)},$$

where, by (5), sample frequencies w and σ are multiples of $2\pi/T$.

To verify (B-1) we use a trigonometric expansion of both sides of this equation, taking the definitions of F_{c1} and F_{s1} from (10).

$$(B-4a) \quad \overline{F_{c1}(w) F_{cj}(\sigma)} = \iint_{-T/2}^{T/2} \overline{f_1(t) f_j(u)} \cos wt \cos \sigma u \, dt \, du$$

$$= \frac{1}{2} \iint_{-T/2}^{T/2} \overline{f_1(t) f_j(u)} [\cos(wt - \sigma u) + \cos(wt + \sigma u)]$$

$$(B-4b) \quad \overline{F_{s1}(w) F_{sj}(\sigma)} = \iint_{-T/2}^{T/2} \overline{f_1(t) f_j(u)} \sin wt \sin \sigma u \, dt \, du$$

$$= \frac{1}{2} \iint_{-T/2}^{T/2} \overline{f_1(t) f_j(u)} [\cos(wt - \sigma u) - \cos(wt + \sigma u)]$$

Evidently the two sides of (B-1) are equal if the following relation is true:

$$(B-5) \quad \iint_{-T/2}^{T/2} \overline{f_1(t) f_j(u)} \cos(wt + \sigma u) = 0$$

To verify (B-5), we employ the mathematical procedure which is explained in detail in Section II.

$$\begin{aligned}
 (B-6) \quad & \iint_{-T/2}^{T/2} \overline{f_1(t) f_j(u)} \cos(wt + \sigma u) dt du \\
 &= \iint_{-T/2}^{T/2} [R_s(t-u-\Delta_1+\Delta_j) + N\delta(t-u)] \cos(wt + \sigma u) dt du \\
 &= \frac{1}{2} \iint_{-T/2}^{T/2} dt du \frac{1}{2\pi} \int_{-\infty}^{\infty} d\alpha [S_s(\alpha) + N\delta_{1j}] e^{j\alpha(t-u+\Delta_j-\Delta_1)} [e^{j(wt+\sigma u)} + e^{-j(wt+\sigma u)}] \\
 &= \frac{1}{4\pi} \int_{-\infty}^{\infty} d\alpha [S_s(\alpha) + N\delta_{1j}] e^{j\alpha(\Delta_j-\Delta_1)} \iint_{-T/2}^{T/2} dt du [e^{j(\alpha+w)t} e^{-j(\alpha-\sigma)u} \\
 &\quad + e^{j(\alpha-w)t} e^{-j(\alpha+\sigma)u}] \\
 &= \frac{1}{4\pi} \int_{-\infty}^{\infty} d\alpha [S_s(\alpha) + N\delta_{1j}] e^{j\alpha(\Delta_j-\Delta_1)} \left[\frac{2 \sin(\alpha+w)T/2}{\alpha+w} \cdot \frac{2 \sin(\alpha-\sigma)T/2}{\alpha-\sigma} \right. \\
 &\quad \left. + \frac{2 \sin(\alpha-w)T/2}{\alpha-w} \cdot \frac{2 \sin(\alpha+\sigma)T/2}{\alpha+\sigma} \right] \\
 &= \pi \int_{-\infty}^{\infty} d\alpha [S_s(\alpha) + N\delta_{1j}] e^{j\alpha(\Delta_j-\Delta_1)} [\delta(\alpha+w)\delta(\alpha-\sigma) + \delta(\alpha-w)\delta(\alpha+\sigma)]
 \end{aligned}$$

We are assuming that the observation time T is sufficiently large so that the last line above is a good approximation. Unless $w = -\sigma$, the above expression must equal zero (or nearly zero in actual practice). By restricting sample frequencies to be of one sign only, so that the relation $w = -\sigma$ is impossible, we can force the expression to be zero, so that (B-1) is satisfied.

To test (B-2) and (B-3), we next derive $\overline{F_{c1}(w) F_{sj}(\sigma)}$.

$$\begin{aligned}
(B-7) \quad \overline{F_{c1}(w) F_{sj}(\sigma)} &= \iint_{-T/2}^{T/2} \overline{f_1(t) f_j(u)} \cos wt \sin \sigma u \, dt \, du \\
&= \frac{1}{2\pi} \int_{-\infty}^{\infty} d\alpha [S_s(\alpha) + N\delta_{1j}] e^{j\alpha(\Delta_j - \Delta_1)} \int_{-T/2}^{T/2} dt e^{j\alpha t} \cos wt \int_{-T/2}^{T/2} du e^{-j\alpha u} \sin \sigma u \\
&= \frac{1}{8\pi} \int_{-\infty}^{\infty} d\alpha [S_s(\alpha) + N\delta_{1j}] e^{j\alpha(\Delta_j - \Delta_1)} \int_{-T/2}^{T/2} dt e^{j\alpha t} (e^{j\omega t} + e^{-j\omega t}) \times \\
&\quad \int_{-T/2}^{T/2} \frac{du e^{-j\alpha u} (e^{j\sigma u} - e^{-j\sigma u})}{j} \\
&= \frac{1}{8\pi} \int_{-\infty}^{\infty} d\alpha [S_s(\alpha) + N\delta_{1j}] e^{j\alpha(\Delta_j - \Delta_1)} \left[\frac{2 \sin(\alpha - \omega)T/2}{\alpha - \omega} + \frac{2 \sin(\alpha + \omega)T/2}{\alpha + \omega} \right] \times \\
&\quad \frac{1}{j} \left[\frac{2 \sin(\alpha - \sigma)T/2}{\alpha - \sigma} - \frac{2 \sin(\alpha + \sigma)T/2}{\alpha + \sigma} \right] \\
&= \frac{1}{4} \int_{-\infty}^{\infty} d\alpha [S_s(\alpha) + N\delta_{1j}] e^{j\alpha(\Delta_j - \Delta_1)} [\delta(\alpha - \omega) + \delta(\alpha + \omega)] \times \\
&\quad \frac{1}{j} \left[\frac{2 \sin(\alpha - \sigma)T/2}{\alpha - \sigma} - \frac{2 \sin(\alpha + \sigma)T/2}{\alpha + \sigma} \right] \\
&= \frac{1}{4j} \left\{ [S_s(\omega) + N\delta_{1j}] e^{j\omega(\Delta_j - \Delta_1)} \left[\frac{2 \sin(\omega - \sigma)T/2}{\omega - \sigma} - \frac{2 \sin(\omega + \sigma)T/2}{\omega + \sigma} \right] \right. \\
&\quad \left. + [S_s(-\omega) + N\delta_{1j}] e^{-j\omega(\Delta_j - \Delta_1)} \left[\frac{2 \sin(-\omega - \sigma)T/2}{-\omega - \sigma} - \frac{2 \sin(-\omega + \sigma)T/2}{-\omega + \sigma} \right] \right\}
\end{aligned}$$

Again, a long observation time is assumed to justify the approximation.

Using the fact that sample frequencies w and σ are multiples of $2\pi/T$, the fact that all sample frequencies have the same sign, and the fact that $S_s(w) = S_s(-w)$, we conclude that

$$(B-8) \quad \overline{F_{c1}(w) F_{sj}(\sigma)} = 0 \quad w \neq \sigma$$

$$= \frac{1}{4_j} [S_s(w) + N\delta_{1j}] [e^{jw(\Delta_j - \Delta_1)} T + e^{-jw(\Delta_j - \Delta_1)} (-T)]$$

$$= \frac{1}{2} [S_s(w) + N\delta_{1j}] T \sin w(\Delta_j - \Delta_1) \quad w = \sigma$$

Simply by interchanging i and j , w and σ , we have

$$(B-9) \quad \overline{F_{s1}(w) F_{cj}(\sigma)} = 0 \quad w \neq \sigma$$

$$= \frac{1}{2} [S_s(\sigma) + N\delta_{1j}] T \sin \sigma(\Delta_1 - \Delta_j) \quad w = \sigma$$

Comparison of (B-8) and (B-9) reveals that (B-2) and (B-3) are verified.

Appendix C

Determinant and Inverse of the Correlation Matrix

The correlation matrix \underline{R} (18) is composed of n^2 submatrices of dimension $M \times M$. Only the n diagonal submatrices, each of which corresponds to a particular sample frequency, are nonzero. Hence, the determinant of \underline{R} is the product of the determinants of the diagonal submatrices. Each submatrix has the form

$$(C-1) \quad \underline{A}_M^k = \frac{TS^k}{2} \begin{bmatrix} 1+\chi^k & a_{12}^k & a_{13}^k & \dots & a_{1M}^k \\ a_{21}^k & 1+\chi^k & a_{23}^k & \dots & a_{2M}^k \\ \vdots & \vdots & \vdots & \ddots & \vdots \\ a_{M1}^k & a_{M2}^k & a_{M3}^k & \dots & 1+\chi^k \end{bmatrix}$$

where

$$(C-2) \quad a_{ij}^k = e^{-jw_k(\Delta_j - \Delta_i)} \quad \chi^k = N/S^k$$

We use an inductive method to establish the determinant of the following matrix:

$$(C-3) \quad \underline{K}_M = \begin{bmatrix} 1+\chi & a_{12} & a_{13} & \dots & a_{1M} \\ a_{21} & 1+\chi & a_{23} & \dots & a_{2M} \\ \vdots & \vdots & \vdots & \ddots & \vdots \\ a_{M1} & a_{M2} & a_{M3} & \dots & 1+\chi \end{bmatrix}$$

We now expand the determinant of \underline{K}_M along the last column, for arbitrary M ; we shall expand $\det \underline{K}_4$ simultaneously for a concrete illustration.

For reference,

$$(C-4) \quad \underline{K}_4 = \begin{bmatrix} 1+\chi & a_{12} & a_{13} & a_{14} \\ a_{21} & 1+\chi & a_{23} & a_{24} \\ a_{31} & a_{32} & 1+\chi & a_{34} \\ a_{41} & a_{42} & a_{43} & 1+\chi \end{bmatrix}$$

The notation $|K_M^{ij}|$ will be used to signify the (i,j) th minor of K_M .

$$(C-5a) \quad |K_M| = (1+\chi) |K_{M-1}| + \sum_{i=1}^{M-1} (-1)^{1+M} a_{iM} |K_M^{iM}|$$

$$(C-5b) \quad |K_4| = (1+\chi) |K_3| - a_{14} \begin{vmatrix} a_{21} & 1+\chi & a_{23} \\ a_{31} & a_{32} & 1+\chi \\ a_{41} & a_{42} & a_{43} \end{vmatrix} \\ + a_{24} \begin{vmatrix} 1+\chi & a_{12} & a_{13} \\ a_{31} & a_{32} & 1+\chi \\ a_{41} & a_{42} & a_{43} \end{vmatrix} - a_{34} \begin{vmatrix} 1+\chi & a_{12} & a_{13} \\ a_{21} & 1+\chi & a_{23} \\ a_{41} & a_{42} & a_{43} \end{vmatrix}$$

The last row of each $(M-1) \times (M-1)$ matrix \underline{K}_M^{iM} is

$$[a_{M1} \ a_{M2} \ a_{M3} \ \dots \ a_{M,M-1}] = a_{M1} [a_{11} \ a_{12} \ a_{13} \ \dots \ a_{1,M-1}]^1$$

Let $\hat{\underline{K}}_M^{iM}$ represent the matrix obtained by changing the last row of \underline{K}_M^{iM} to $[a_{11}, a_{12}, a_{13}, \dots, a_{1,M-1}]$. Then $|K_M^{iM}| = a_{M1} |\hat{\underline{K}}_M^{iM}|$

$$(C-6a) \quad |K_M| = (1+\chi) |K_{M-1}| + \sum_{i=1}^{M-1} (-1)^{1+M} a_{iM} a_{M1} |\hat{\underline{K}}_M^{iM}| \\ = (1+\chi) |K_{M-1}| + \sum_{i=1}^{M-1} (-1)^{1+M} |\hat{\underline{K}}_M^{iM}|$$

¹Note that $a_{11} = 1$

$$\begin{aligned}
 (C-6b) \quad |K_4| &= (1+\chi) |K_3| - \begin{vmatrix} a_{21} & 1+\chi & a_{23} \\ a_{31} & a_{32} & 1+\chi \\ 1 & a_{12} & a_{13} \end{vmatrix} \\
 &+ \begin{vmatrix} 1+\chi & a_{12} & a_{13} \\ a_{31} & a_{32} & 1+\chi \\ a_{21} & 1 & a_{23} \end{vmatrix} - \begin{vmatrix} 1+\chi & a_{12} & a_{13} \\ a_{21} & 1+\chi & a_{23} \\ a_{31} & a_{32} & 1 \end{vmatrix}
 \end{aligned}$$

Now let \hat{K}_M^{1M} designate the matrix obtained by moving the last row of \underline{K}_M^{1M} into the i th position. \underline{K}_M^{1M} is converted into \hat{K}_M^{1M} by $(M-1-i)$ interchanges of rows; hence $|\hat{K}_M^{1M}| = (-1)^{M-1-i} |\underline{K}_M^{1M}|$

$$\begin{aligned}
 (C-7a) \quad |K_M| &= (1+\chi) |K_{M-1}| + \sum_{i=1}^{M-1} (-1)^{1+i} (-1)^{M-1-i} \hat{K}_{M,i}^{1M} \\
 &= (1+\chi) |K_{M-1}| - \sum_{i=1}^{M-1} \hat{K}_M^{1M}
 \end{aligned}$$

$$\begin{aligned}
 (C-7b) \quad |K_4| &= (1+\chi) |K_3| - \begin{vmatrix} 1 & a_{12} & a_{13} \\ a_{21} & 1+\chi & a_{23} \\ a_{31} & a_{32} & 1+\chi \end{vmatrix} \\
 &- \begin{vmatrix} 1+\chi & a_{12} & a_{13} \\ a_{21} & 1 & a_{23} \\ a_{31} & a_{32} & 1+\chi \end{vmatrix} - \begin{vmatrix} 1+\chi & a_{12} & a_{13} \\ a_{21} & 1+\chi & a_{23} \\ a_{31} & a_{32} & 1 \end{vmatrix}
 \end{aligned}$$

The $(M-1) \times (M-1)$ matrices \hat{K}_M^{1M} differ from \underline{K}_{M-1} only in that the $(1,1)$ th term is 1 instead of $1+\chi$. If \hat{K}_M^{1M} is expanded along the i th column, the minor corresponding to the $(1,1)$ th element is equal or equivalent to $|\underline{K}_{M-2}|$. If the same expansion is made of $|\underline{K}_{M-1}|$, the

coefficient of this same minor is $(1+x)$. It follows that $|\hat{K}_M^{1M}| = |\underline{K}_{M-1}| - x |\underline{K}_{M-2}|$, for all i .

$$(C-8a) \quad \begin{aligned} |\underline{K}_M| &= (1+x) |\underline{K}_{M-1}| - (M-1) [|\underline{K}_{M-1}| - x |\underline{K}_{M-2}|] \\ &= (2+x-M) |\underline{K}_{M-1}| + (M-1)x |\underline{K}_{M-2}| \end{aligned}$$

$$(C-8b) \quad |\underline{K}_4| = (1+x) |\underline{K}_3| - 3 \left[\begin{vmatrix} 1+x & a_{12} & a_{13} \\ a_{21} & 1+x & a_{23} \\ a_{31} & a_{32} & 1+x \end{vmatrix} - x \begin{vmatrix} 1+x & a_{23} \\ a_{32} & 1+x \end{vmatrix} \right]$$

We assert that

$$(C-9) \quad |\underline{K}_M| = x^{M-1} (x+M).$$

We verify this formula by substitution into (C-8a):

$$(C-10) \quad \begin{aligned} x^{M-1}(x+M) &= (2+x-M) x^{M-2}(x+M-1) + (M-1)x \cdot x^{M-3}(x+M-2) \\ &= x^{M-2} [x^2 + x(M-1+2-M) + (M-1)(2-M)] \\ &\quad + x^{M-2} [(M-1)x + (M-1)(M-2)] \\ &= x^{M-2} [x^2 + x + (M-1)(2-M) + (M-1)x + (M-1)(M-2)] \\ &= x^{M-2} [x^2 + Mx] \\ &= x^{M-1}(x+M) \end{aligned}$$

By reference to (18), (C-1) - (C-3), and (C-9), we obtain the final result

$$(C-11) \quad \begin{aligned} \det \underline{R} &= \prod_{k=1}^n \left[\frac{TS^k}{2} \right]^M x^{M-1}(x+M) = \prod_{k=1}^n \left[\frac{T}{2} \right]^M S_N^{kM-1} \left[\frac{N}{S^k} + M \right] \\ &= (T/2)^{Mn} \prod_{k=1}^n N^{M-1} (N+MS^k) \end{aligned}$$

We now verify that \underline{R}^{-1} in (20) is the correct inverse of \underline{R} . If each diagonal submatrix of \underline{R}^{-1} is the inverse of the corresponding submatrix of \underline{R} , then \underline{R}^{-1} is the inverse of \underline{R} . In notation like that of (C-1), we write each submatrix of \underline{R}^{-1} as

$$(C-12) \quad \underline{B}_M^k = \frac{2}{TS^k} \cdot \frac{1}{\chi^k (M+\chi^k)} \begin{bmatrix} (M-1)+\chi^k & -a_{12}^k & -a_{13}^k & \dots & -a_{1M}^k \\ -a_{21}^k & (M-1)+\chi^k & -a_{23}^k & \dots & -a_{2M}^k \\ \vdots & \vdots & \vdots & \ddots & \vdots \\ -a_{M1}^k & -a_{M2}^k & -a_{M3}^k & \dots & (M-1)+\chi^k \end{bmatrix}.$$

The matrices \underline{B}_M^k are the inverses of the matrices \underline{A}_M^k in (C-1) if the following matrix \underline{K}_M^{-1} is the inverse of \underline{K}_M in (C-3).

$$(C-13) \quad \underline{K}_M^{-1} = \frac{1}{\chi(M+\chi)} \begin{bmatrix} (M-1)+\chi & -a_{12} & -a_{13} & \dots & -a_{1M} \\ -a_{21} & (M-1)+\chi & -a_{23} & \dots & -a_{2M} \\ \vdots & \vdots & \vdots & \ddots & \vdots \\ -a_{M1} & -a_{M2} & -a_{M3} & \dots & (M-1)+\chi \end{bmatrix}$$

We now show that $\underline{K}_M \underline{K}_M^{-1}$ equals the identity matrix.

$$(C-14) \quad \underline{K}_{Mij} = \begin{cases} 1+\chi & i=j \\ a_{ij} & i \neq j \end{cases}$$

$$\underline{K}_{Mij}^{-1} = \begin{cases} \frac{(M-1)+\chi}{\chi(M+\chi)} & i=j \\ \frac{-a_{ij}}{\chi(M+\chi)} & i \neq j \end{cases}$$

$$\begin{aligned}
 \text{(C-15)} \quad (\underline{K} \underline{K}^{-1})_{ij} &= \sum_{k=1}^M K_{Mik} K_{ikj}^{-1} \\
 &= \begin{cases} \sum_{\substack{k=1 \\ k \neq i}}^M a_{ik} \cdot \frac{-a_{ki}}{\chi(M+\chi)} + (1+\chi) \cdot \frac{(M-1)+\chi}{\chi(M+\chi)} & i=j \\ \sum_{\substack{k=1 \\ k \neq i, j}}^M a_{ik} \cdot \frac{-a_{kj}}{\chi(M+\chi)} + (1+\chi) \frac{-a_{ij}}{\chi(M+\chi)} + a_{ij} \frac{(M-1)+\chi}{\chi(M+\chi)} & i \neq j \end{cases} \\
 &\quad \quad \quad (k=i) \quad \quad \quad (k=i) \quad \quad \quad (k=j) \\
 &= \begin{cases} \sum_{\substack{k=1 \\ k \neq i}}^M \frac{-1}{\chi(M+\chi)} + \frac{(M-1)+M\chi+\chi^2}{\chi(M+\chi)} & i=j \\ \sum_{\substack{k=1 \\ k \neq i, j}}^M \frac{-a_{ij}}{\chi(M+\chi)} + a_{ij} \frac{-(1+\chi)+(M-1)+\chi}{\chi(M+\chi)} & i \neq j \end{cases} \\
 &= \begin{cases} \frac{-(M-1)}{\chi(M+\chi)} + \frac{(M-1)+M\chi+\chi^2}{\chi(M+\chi)} & i=j \\ \frac{-a_{ij}(M-2)}{\chi(M+\chi)} + \frac{a_{ij}(M-2)}{\chi(M+\chi)} & i \neq j \end{cases} \\
 &= \begin{cases} 1 & i=j \\ 0 & i \neq j \end{cases}
 \end{aligned}$$

It follows that the expression for \underline{Q}^{-1} in (20) is correct.

Appendix D

Mean of a Fourfold Product

For four zero-mean jointly Gaussian real variables, the following relation is known to be valid.

$$(D-1) \quad \overline{abcd} = \overline{ab} \cdot \overline{cd} + \overline{ac} \cdot \overline{bd} + \overline{ad} \cdot \overline{bc}$$

We propose to prove that for four complex variables, whose real and imaginary parts are all zero-mean jointly Gaussian,

$$(D-2) \quad \overline{ABCD} = \overline{AB} \cdot \overline{CD} + \overline{AC} \cdot \overline{BD} + \overline{AD} \cdot \overline{BC}$$

We use a strictly "brute force" technique of expanding the left side of (D-2), using (D-1), and recombining to obtain the right side of (D-2). We define

$$(D-3) \quad \begin{aligned} A &= a + ja' \\ B &= b + jb' \\ C &= c + jc' \\ D &= d + jd' \end{aligned}$$

$$\begin{aligned} (D-4) \quad \overline{ABCD} &= \overline{\langle (a+ja')(b+jb')(c+jc')(d+jd') \rangle} \\ &= \overline{\langle [ab-a'b'+j(a'b+ab')] [cd-c'd'+j(c'd+cd')] \rangle} \\ &= \overline{\langle abcd+a'b'c'd'-abc'd'-a'b'cd-(a'bc'd+a'bcd'+ab'c'd+ab'cd') \\ &\quad +j(a'bcd+ab'cd-a'bc'd'-ab'c'd'+abc'd+abcd'-a'b'c'd-a'b'cd') \rangle} \\ &= \overline{\langle abcd+a'b'c'd'-(a'b'cd+a'bc'd+a'bcd'+ab'c'd+ab'cd'+abc'd') \\ &\quad +j[a'bcd+ab'cd+abc'd+abcd'-(ab'c'd'+a'bc'd'+a'b'cd'+a'b'c'd)] \rangle} \\ &= \{ (\overline{ab \cdot cd} + \overline{ac \cdot bd} + \overline{ad \cdot bc}) + (\overline{a'b' \cdot c'd'} + \overline{a'c' \cdot b'd'} + \overline{a'd' \cdot b'c'}) \\ &\quad - [(\overline{a'b' \cdot cd} + \overline{a'c' \cdot b'd} + \overline{a'd' \cdot b'c}) + (\overline{a'b \cdot c'd'} + \overline{a'c' \cdot bd} + \overline{a'd \cdot bc'}) \\ &\quad + (\overline{a'b \cdot cd'} + \overline{a'c \cdot bd'} + \overline{a'd' \cdot bc}) + (\overline{ab' \cdot c'd} + \overline{ac' \cdot b'd} + \overline{ad \cdot b'c'}) \\ &\quad + (\overline{ab' \cdot cd'} + \overline{ac \cdot b'd'} + \overline{ad' \cdot b'c}) + (\overline{ab \cdot c'd'} + \overline{ac' \cdot bd'} + \overline{ad \cdot bc'})] \} \end{aligned}$$

$$\begin{aligned}
& +j\{(\overline{a'b \cdot cd + a'c \cdot bd + a'd \cdot bc}) + (\overline{ab' \cdot cd + ac \cdot b'd + ad \cdot b'c}) \\
& + \overline{ab \cdot c'd + ac' \cdot bd + ad \cdot bc'}) + (\overline{ab \cdot cd' + ac \cdot bd' + ad' \cdot bc}) \\
& - [(\overline{ab' \cdot c'd' + ac' \cdot b'd' + ad' \cdot b'c'}) + (\overline{a'b \cdot c'd' + a'c' \cdot bd' + a'd' \cdot bc'}) \\
& + (\overline{a'b' \cdot cd' + a'c \cdot b'd' + a'd' \cdot b'c}) + \overline{a'b' \cdot c'd + a'c' \cdot b'd + a'd \cdot b'c'})]\} \\
= & \{ \overline{ab \cdot cd + a'b' \cdot c'd'} - (\overline{a'b' \cdot cd + ab \cdot c'd' + a'b \cdot c'd + a'b \cdot cd' + ab' \cdot c'd + ab' \cdot cd'}) \\
& + j[\overline{ab \cdot c'd + ab \cdot cd' + a'b \cdot cd + ab' \cdot cd} - (\overline{a'b' \cdot c'd + a'b' \cdot cd' + a'b \cdot c'd' \\
& + \overline{ab' \cdot c'd'})]\} \\
& + \{ \overline{ac \cdot bd + a'c' \cdot b'd'} - (\overline{ac \cdot b'd' + a'c' \cdot bd + ac' \cdot bd' + ac' \cdot b'd + a'c \cdot bd' + a'c \cdot b'd}) \\
& + j[\overline{ac \cdot bd' + ac \cdot b'd + ac' \cdot bd + a'c \cdot bd} - (\overline{a'c' \cdot bd' + a'c' \cdot b'd + ac' \cdot b'd' \\
& + \overline{a'c \cdot b'd'})]\} \\
& + \{ \overline{ad \cdot bc + a'd' \cdot b'c'} - (\overline{ad \cdot b'c' + a'd' \cdot bc + ad' \cdot b'c + ad' \cdot b'c + a'd \cdot b'c + a'd \cdot bc'}) \\
& + j[\overline{ad \cdot b'c + ad \cdot bc' + ad' \cdot bc + a'd \cdot bc} - (\overline{a'd' \cdot b'c + a'd' \cdot bc' + ad' \cdot b'c' \\
& + \overline{a'd \cdot b'c'})]\} \\
= & \langle ab - a'b' + j(a'b + ab') \rangle \langle cd - c'd' + j(c'd + cd') \rangle \\
& + \langle ac - a'c' + j(a'c + ac') \rangle \langle bd - b'd' + j(b'd + bd') \rangle \\
& + \langle ad - a'd' + j(a'd + ad') \rangle \langle bc - b'c' + j(b'c + bc') \rangle \\
= & \langle (a + ja') (b + jb') \rangle \langle (c + jc') (d + jd') \rangle \\
& + \langle (a + ja') (c + jc') \rangle \langle (b + jb') (d + jd') \rangle \\
& + \langle (a + ja') (d + jd') \rangle \langle (b + jb') (c + jc') \rangle \\
= & \overline{AB \cdot CD + AC \cdot BD + AD \cdot BC}
\end{aligned}$$

Appendix E

An Integral

(E-1)

$$\begin{aligned}
 \int_{2\pi(f_0 - B/2)}^{2\pi(f_0 + B/2)} w^2 dw &= \frac{(2\pi)^3}{3} \left[(f_0 + B/2)^3 - (f_0 - B/2)^3 \right] \\
 &= \frac{(2\pi)^3}{3} \left[f_0^3 + 3f_0^2 B/2 + 3f_0 B^2/4 + B^3/8 \right. \\
 &\quad \left. - (f_0^3 - 3f_0^2 B/2 + 3f_0 B^2/4 - B^3/8) \right] \\
 &= \frac{(2\pi)^3}{3} (3f_0^2 B + B^3/4) = (2\pi)^3 (f_0^2 B + B^3/12)
 \end{aligned}$$

Appendix F

A Double Summation

Make the change of variable $k = i - j$. Then

$$\begin{aligned}
 (F-1) \quad & \sum_{i=1}^M \sum_{j=i+1}^M (i-j)^2 = \sum_{k=1}^{M-1} k^2 (M-k) = M \sum_{k=1}^{M-1} k^2 - \sum_{k=1}^{M-1} k^3 \\
 & = M \frac{(M-1) M(2M-1)}{6} - \frac{(M-1)^2 M^2}{4} \\
 & = \frac{2M^2(M-1)(2M-1)}{12} - \frac{3M^2(M-1)^2}{12} = \frac{M^2(M-1)}{12} [2(2M-1) - 3(M-1)] \\
 & = \frac{M^2(M-1)(M+1)}{12}
 \end{aligned}$$

¹H. B. Dwight, Tables of Integrals and Other Mathematical Data, Macmillan, 1964, §29.

Unclassified

Security Classification

DOCUMENT CONTROL DATA - R & D

(Security classification of title, body of abstract and indexing annotation must be entered when the overall report is classified)

1. ORIGINATING ACTIVITY (Corporate author) General Dynamics Corporation Electric Boat division Groton, Conn.		2a. REPORT SECURITY CLASSIFICATION Unclassified	
		2b. GROUP	
3. REPORT TITLE PROCESSING OF DATA FROM SONAR SYSTEMS, VOLUME VI			
4. DESCRIPTIVE NOTES (Type of report and inclusive dates)			
5. AUTHOR(S) (First name, middle initial, last name) Francis S. Hill, Jr., John B. Lewis, Verne H. McDonald, and Peter M. Schultheiss			
6. REPORT DATE September 1, 1968		7a. TOTAL NO. OF PAGES 442	7b. NO. OF REFS ---
8a. CONTRACT OR GRANT NO NOnr 2512(00)		9a. ORIGINATOR'S REPORT NUMBER(S) U417-68-80	
b. PROJECT NO			
c.		9b. OTHER REPORT NO(S) (Any other numbers that may be assigned this report)	
d.			
10. DISTRIBUTION STATEMENT Each transmittal of this document outside the agencies of the U.S. Government must have prior approval of the Office of Naval Research.			
11. SUPPLEMENTARY NOTES		12. SPONSORING MILITARY ACTIVITY Office of Naval Research Washington, D. C.	
13. ABSTRACT Volume VI deals with passive detection and target location, signal design, and optimum passive bearing estimation. Using a linear array, the problem of passive detection and target location was analyzed for the case of stationary Gaussian signals and noises with known statistical properties. A comprehensive treatment of this problem is presented. The problem of sonar signal design is considered, with primary interest centered on redesign of the pulse waveshape based on information gained from an earlier return. Results indicate that, in principle, some improvements are possible. In the problem of target location, an arbitrary number of hydrophones, arbitrarily spaced on a linear array, were studied in this report, as compared to an earlier report which studied a two-element array. Lower bounds are set on the rms bearing error attainable with a linear array and the results compared with the rms error of a split beam tracker which is modified by the insertion of an appropriate spectrum-shaping filter into each array half. Under the given circumstances, the split beam tracker is very nearly optimal instrumentation.			

DD FORM 1473

1 NOV 65

(PAGE 1)

S/N 0101-807-6801

Unclassified

Security Classification

Security Classification

14.

KEY WORDS

LINK A

LINK B

LINK C

NAME	ROLE
1. [Name]	[Role]
2. [Name]	[Role]
3. [Name]	[Role]
4. [Name]	[Role]
5. [Name]	[Role]
6. [Name]	[Role]
7. [Name]	[Role]
8. [Name]	[Role]
9. [Name]	[Role]
10. [Name]	[Role]
11. [Name]	[Role]
12. [Name]	[Role]
13. [Name]	[Role]
14. [Name]	[Role]
15. [Name]	[Role]
16. [Name]	[Role]
17. [Name]	[Role]
18. [Name]	[Role]
19. [Name]	[Role]
20. [Name]	[Role]
21. [Name]	[Role]
22. [Name]	[Role]
23. [Name]	[Role]
24. [Name]	[Role]
25. [Name]	[Role]
26. [Name]	[Role]
27. [Name]	[Role]
28. [Name]	[Role]
29. [Name]	[Role]
30. [Name]	[Role]
31. [Name]	[Role]
32. [Name]	[Role]
33. [Name]	[Role]
34. [Name]	[Role]
35. [Name]	[Role]
36. [Name]	[Role]
37. [Name]	[Role]
38. [Name]	[Role]
39. [Name]	[Role]
40. [Name]	[Role]
41. [Name]	[Role]
42. [Name]	[Role]
43. [Name]	[Role]
44. [Name]	[Role]
45. [Name]	[Role]
46. [Name]	[Role]
47. [Name]	[Role]
48. [Name]	[Role]
49. [Name]	[Role]
50. [Name]	[Role]
51. [Name]	[Role]
52. [Name]	[Role]
53. [Name]	[Role]
54. [Name]	[Role]
55. [Name]	[Role]
56. [Name]	[Role]
57. [Name]	[Role]
58. [Name]	[Role]
59. [Name]	[Role]
60. [Name]	[Role]
61. [Name]	[Role]
62. [Name]	[Role]
63. [Name]	[Role]
64. [Name]	[Role]
65. [Name]	[Role]
66. [Name]	[Role]
67. [Name]	[Role]
68. [Name]	[Role]
69. [Name]	[Role]
70. [Name]	[Role]
71. [Name]	[Role]
72. [Name]	[Role]
73. [Name]	[Role]
74. [Name]	[Role]
75. [Name]	[Role]
76. [Name]	[Role]
77. [Name]	[Role]
78. [Name]	[Role]
79. [Name]	[Role]
80. [Name]	[Role]
81. [Name]	[Role]
82. [Name]	[Role]
83. [Name]	[Role]
84. [Name]	[Role]
85. [Name]	[Role]
86. [Name]	[Role]
87. [Name]	[Role]
88. [Name]	[Role]
89. [Name]	[Role]
90. [Name]	[Role]
91. [Name]	[Role]
92. [Name]	[Role]
93. [Name]	[Role]
94. [Name]	[Role]
95. [Name]	[Role]
96. [Name]	[Role]
97. [Name]	[Role]
98. [Name]	[Role]
99. [Name]	[Role]
100. [Name]	[Role]

WT

NAME	ROLE
Mr. J. Edgar Hoover	Director
Mr. Clegg	Chief of Bureau
Mr. Glavin	Chief of Bureau
Mr. Ladd	Chief of Bureau
Mr. Nichols	Chief of Bureau
Mr. Rosen	Chief of Bureau
Mr. Tracy	Chief of Bureau
Mr. Carson	Chief of Bureau
Mr. Egan	Chief of Bureau
Mr. Gurnea	Chief of Bureau
Mr. Hendon	Chief of Bureau
Mr. Pennington	Chief of Bureau
Mr. Quinn	Chief of Bureau
Mr. Nease	Chief of Bureau
Mr. Gandy	Chief of Bureau

WT

NAME	ROLE
Mr. J. Edgar Hoover	Director
Mr. Clegg	Chief Clerk
Mr. Glavin	Chief of Bureau
Mr. Ladd	Chief of Bureau
Mr. Nichols	Chief of Bureau
Mr. Rosen	Chief of Bureau
Mr. Tracy	Chief of Bureau
Mr. Egan	Chief of Bureau
Mr. Gurnea	Chief of Bureau
Mr. Harbo	Chief of Bureau
Mr. Hendon	Chief of Bureau
Mr. Pennington	Chief of Bureau
Mr. Quinn	Chief of Bureau
Mr. Nease	Chief of Bureau
Mr. Gandy	Chief of Bureau

WT

Unclassified

Security Classification